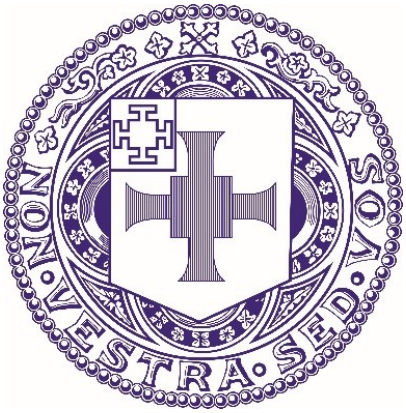

Realising the CO_2 sequestration potential of steel and iron making slags.

Andrew Jan Dobrzański

Department of Earth Science

Durham University

One volume

Thesis submitted in accordance with the regulations for the degree of Master of Philosophy at the University of Durham

Department of Earth Sciences

March 2016

Abstract

Climate change is now recognised as being a serious threat to the current structures of advanced human societies, however, technological innovations can help remove CO_2 from the atmosphere and one such innovation which shows promise is carbon capture and storage (CCS). Metallurgical slag products have been shown to readily carbonate thereby creating an uncharacterised carbon sink. This sink could help the UK attain its net CO_2 targets and reducing the net amount of carbon emitted by the industrial blast and basic-oxygen furnaces. This thesis argues that metallurgical slag products provide an economic way of sequestering significant amounts of CO_2 and provides data to show that approximately 6,434 to 10,127 tonnes of CO_2 was being passively sequestered at the Lafarge-Tarmac Redcar site by the volume of slag products located there in 2015. This thesis also reports results of experimental studies that aim to actively react metallurgical slag with CO_2 under pressure conditions of 10 bar or 100 bar CO_2 pressure, temperatures of 25 ˚C or 125 ˚C as well as under differing water availabilities. Further experiments investigated the effect upon the material carbonation due to the pre-treatment of samples with 1M HCl or 1M NaOH. A field trial investigating the potential to carbonate metallurgical slag samples under environmental pressures and temperatures using a gas line delivering 2 dm^3 min^{-1} CO_2 was also undertaken. This thesis also shows the economics of combining the net-CO_2 uptake with different energy sources used to power and recommends that further reduction in net-CO_2 emissions can be achieved by switching to 'green' energy sources. Comparing the %-metal-cation content of each material, conversion of 0.55% to 1.76% was achieved by steel slags and 0.3% to 4.89% for blast furnace slags. Further work needs to focus on the mineralogy of the samples and the carbonate mineral growth processes in order to create the optimum conditions needed to realise further untapped carbonation potential.

Declaration and Copyright

I confirm that no part of the material presented in this thesis has previously been submitted by me or any other person for a degree in this or any other university. Where relevant, material from the work of others has been acknowledged.

Signed:

Date:

Acknowledgements

I sincerely thank Professor Fred Worrall for his time and patience with the project. I sincerely thank you for giving me the opportunity to do this work. It has been a positively life-changing experience and has helped me to see materials science in a new light.

I thank Lafarge-Tarmac for generously sponsoring the work and in particular Alan Moffett for helping with access to the Redcar site and for additional samples.

I also thank Professor Jon Gluyas for additional help and supervision during the project. I thank Professor Chris Greenwell and Professor David Manning for their suggestions which have greatly improved this manuscript.

Thanks also go to the XRD section at Durham University Chemistry Dept., the XRCT section at Durham University Engineering and Computer Science Dept., the Durham University Geography Dept. for weather data, Durham University Aracheology Dept. for SEM time and to Ian Chaplin for producing such excellent quality thin sections.

Thanks to all at Durham Earth Sciences who helped me feel at home in particular Ben Maunder and Adam Sproson for the post-Formal hilarity, Matthew Funnell and Adam Robinson of 'Geophysics Corner' for the great conversations, Finke Nanne for getting me to Sweden, Blanca Raionero-Gomez and Josie Mahoney for bringing joy wherever they went and of course to Sam Clark for being the best desk-mate ever. Thanks to Kate Horan for organising the equestrian trips and Zhuoli Zhang for all the entertainment during those parties in the Castle. Of course thanks go to Jack Hardwick, Helena Kelly, Dimitrios Michelioudakis, Bansri Raithatha, Rebecca Hayes, Hongliang Wang, Jing Zhang and others for brightening up the department as well.

Thanks to everyone at DUDT for further brightening up my time at Durham particularly Jenny Ferris, Richard Root, Emily Horsburgh, Emma Budenberg, Alysia Davies, Christopher Darvill, Lydia Powell, Sarah Taylor and Sarah McMullan. It's been a pleasure competing for Durham with you and I've learnt a lot about Latin and Ballroom dancing from all of you. Of course the biggest thanks go to Sarah Tutton for being a wonderful dance partner. It was a sincere pleasure to dance with you and to reach the Northern Finals with you.

Finally I'd like to thank everyone at St Chad's College. You filled my days and nights with fun hilarity and gave me a true home; I'm very grateful to all of you and am proud to call myself a Chadsman. I am eternally grateful to the Rev. Michael Sadgrove for your advice and insight into many matters and for your tours around that very fine cathedral that so gathers its fair city of Durham around it. My unending gratitude goes to Megumi Chou for being dragged to an endless number of Formals and for giving me a new appreciation of the humanities, James Lewis for your insights into politics and Freudian psychology, Joe Gustar-Russell for your unique philosophical outlook and to Rebecca Bristow (and Neil Riley), Curtis Runstedler, Brian Williamson, Jess Moore and Xiao Lei et al. for being the finest M.C.R. a College could wish for.

Contents

List of Figures

List of Tables

Chapter 1:

Carbon Capture and Storage – A Global Issue

1.1 Introduction

Climate change, on anthropogenic timescales, is now recognised as being a serious threat to the current structures of advanced human societies (IPCC 2013). Tackling this issue will require a variety of social and technological innovations. One such innovation which shows promise is carbon capture and storage (CCS). CCS involves the permanent storage of CO_2 either within porous geological strata or as a mineral phase – typically as a carbonate mineral. The iron and steel industry is one of the largest emitters of CO_2 (IPCC 2005). However, studies have shown that the slag by-product produced as a result of the industrial iron and steel making process has the potential to sequester CO_2 as mineral carbonates, due to its high cation content (Huijgen et al. 2005). This thesis will investigate the potential of using iron and steelmaking slags as feedstocks to produce carbonates and to calculate the magnitude of the potential carbon sink. This thesis also seeks to outline the best method for carbonating each slag material studied. The sequestration methods described in this thesis will include: Passive weathering and active reaction of slag products, together with chemical-treatment options and a mock field trial.

1.2 IPCC Executive Findings

The Intergovernmental Panel on Climate Change (IPCC) is the leading international body for the assessment of climate change. In its 2013 report entitled Climate Change 2013 – The Physical Science Basis (IPCC 2013) the IPCC stated that, based on the latest published compilation of physical climate observations, 'warming of the climate system is unequivocal and many of the observed changes since the 1950s are unprecedented when compared to the previous decades or millennia.' Each of the last three decades has been successively warmer at the Earth's surface than any preceding decade since 1850. This has resulted in atmospheric and oceanic temperatures rising, the amounts of snow and ice diminishing and concentrations of greenhouse gases increasing. The rising levels of greenhouse gases are cited as reasons for climate change, with atmospheric concentrations of carbon dioxide, methane and nitrous oxides increasing to levels which are thought to be unprecedented in the last 800,000 years. The only likely process causing this unprecedented rise in the concentrations of greenhouse gases is anthropogenic activity. Significantly, as a result of the growth of industrialization, atmospheric concentrations of carbon dioxide (CO_2), methane (CH_4), and nitrous oxide (N_2O) have all increased since 1750. In 2011, the concentrations of these greenhouse gases were 391 ppm, 1803 ppb, and 324

ppb respectively. These concentrations exceed pre-industrial levels by approximately 40%, 150%, and 20%, respectively. By far the greatest contributor to the greenhouse effect is CO_2 and in order to limit the warming caused by anthropogenic CO_2 emissions alone to lower than 2°C since 1861-1880 will require cumulative CO_2 emissions from all anthropogenic sources to stay below 1210 GtC (4440 $GtCO_2$). Currently, the amount emitted up to 2011 was 515 ±70 GtC. (IPCC 2013). The global surface temperature rise for the end of the 21st century is predicted to exceed 1.5°C when compared to the period between 1850 and 1900. Any further warming will begin to seriously disrupt ecosystems and consequently human food sources as well as resulting in higher sea-levels due to sea ice reduction and oceanic thermal expansion. This has the potential to have a dramatic effect on human settlements in coastal areas. It is anticipated that the effects of climate change will persist for many centuries, even after emissions of CO_2 are stopped. Therefore, a multi-century approach to dealing with the effects and consequences of climate change will be required (IPCC 2013) with anthropogenic intervention in the carbon system to actively reduce the amount of CO_2 in the atmosphere being required. This action is being taken in a number of different ways. Table 1.1 shows the current CO_2 emissions from a range of industrial sectors which produce CO_2 emissions.

Process	**Emissions ($MtCO_2\ yr^{-1}$)**
Power	10,537
Cement Production	932
Oil Refineries	789
Iron and Steel	646
Petrochemical	379
Oil and Gas Processing	50
Other Fossil Fuels	33
Bioethanol and bioenergy	91
Total	**13,466**

Table 1.1: Processes or industrial activity which produce CO_2 emissions greater than 0.1 $MtCO_2\ yr^{-1}$ (after IPCC 2005).

The largest sector is power generation (of which coal is responsible for the most significant part of the CO_2 emissions). However, renewable energy projects are steadily reducing emissions in this sector. Iron and steel production is the fourth largest CO_2 emitter, but it is also the sector which has the most potential to offset its emissions due to the production of approximately 163,700 to 245,550 tonnes (in 2014) of cation rich steel slag per year (World Steel Association 2015), which can sequester CO_2 as carbonate minerals. This is a currently poorly understood carbon sink which can be used to offset emissions from the industry and help to meet UK emissions reduction targets.

1.3 Current Emissions Targets

In 2008 the United Kingdom passed the Climate Change Act which established the world's first legally binding climate change target (UK Government - Policy Paper 2015) via the establishment of a series of legally binding carbon budgets (Table 1.2). This aimed to cut UK greenhouse gas emissions by at least 80% from 1990 levels by 2050. UK emissions in 2014 were 497 $MtCO_2e$ (c.f. 597.9 Mt CO_2e in 1990 - Bates 2015) of which 1.66 Mt were due to iron and steel production making the sector the joint second highest emitter in the UK (Table 1.3).

Budget	% reduction below base year
1st Carbon budget (2008-12)	23%
2nd Carbon budget (2013-17)	29%
3rd Carbon budget (2018-22)	35% by 2020
4th Carbon budget (2023-27)	50% by 2025
5th Carbon budget (2027-30)	57% by 2030

Table 1.2: UK carbon budgets 2008 – 2030 (CCC 2016)

Sector	% UK Emissions	Mt CO_2e
Refineries	17	86.21
Chemicals	14	71.00
Iron and Steel	14	71.00
Constriction	10	50.71
Cement and Lime	9	45.64
Food, Drink and Tobacco	8	40.57
Paper Pulp and Printing	4	20.29
Mechanical Engineering	4	20.29
Water and Waste Management	3	15.21
Non-Ferrous Metals	3	15.21
Glass and Ceramics	3	15.21
Vehicles	2	10.14
Rubber and Plastics	2	10.14
Wood	2	10.14
Textiles	2	10.14
Other	1	5.07
Total		**497 Mt**

Table 1.3: UK carbon emissions by sector (CCC 2016)

Given that climate change, as a consequence of CO_2 emissions, is considered to be irreversible on a multi-century to millennial time scale, the development of technologies which can rapidly remove CO_2 from the atmosphere are an essential prerequisite in mitigating the effects of CO_2 emissions. Therefore, a well-planned slag management scheme which capitalises on the CCS potential of the slags through mineral sequestration could help to dramatically offset CO_2 emissions across the iron and steel sector and will help the UK meet its emissions reduction targets.

1.4 Climate Change Mitigation through Carbon Capture and Storage (CCS)

There are several avenues by which climate change can be tackled, but one of the most promising methods is Carbon Capture and Storage (CCS). This has the potential to store carbon on geological timescales through the direct storage of CO_2, such as the In-Salah CCS project (Ringrose 2013), or by the precipitation of geologically stable minerals containing carbon, usually as carbonate minerals (Huijgen 2007). Geological storage of CO_2 presents several geotechnical problems. While the infrastructure for CO_2 injection can be rapidly created through the repurposing of hydrocarbon extraction infrastructure which is already present at potential reservoir sites. However, the reservoirs into which the CO_2 is injected need to be continuously monitored for leaks. The leaks occur due to degradation of the porosity and permeability of the reservoir and importantly of the cap rock (typically through the desiccation and volume reduction of clays) (Kaszuba 2005). A further factor is that the mineralogy of traditional oil and gas reservoirs (i.e. sandstones) do not promote the precipitation of significant amounts of carbonate minerals, unlike basaltic rock types which do, as a result of their higher divalent cation content. This has led to the establishment of the *Hellisheiði* project in Iceland in which CO_2 is injected into basaltic formations in order to precipitate carbon bearing minerals – a permanent and stable mineral carbonation storage solution rather than problematic CO_2 gas/liquid storage in reservoirs (Alfredsson et al. 2008).

During CO_2 mineral sequestration the CO_2 is sequestered in the form of carbonate minerals. The carbonate minerals are formed when materials rich in soluble metallic cations dissolve in water. The dissolved metallic cations react with $CO_{2(aq)}$ to precipitate carbonate. The fundamental carbonation equation for carbon sequestration via mineral carbonation is:

$$M^{2+}_{(aq)} + CO_3^{2-}{}_{(aq)} \rightarrow MCO_{3(aq/s)}$$

Reaction 1.1

Any material which can supply M^+ ions can produce carbonate minerals in the presence of CO_3^{2-} ions under stable conditions. However, materials with high metal-cation components are particularly

effective. The advantages of mineral sequestration are that it provides a stable method of sequestering CO_2 in a way which does not require constant monitoring and there is a vast quantity of material, which is readily available for reaction. In contrast, reservoir storage requires constant monitoring for CO_2 leaks and can only be undertaken in certain geological environments. Mineral sequestration may be performed not only by using a naturally occurring metal-cation rich material, but can also be accomplished by using industrial man-made materials such as metal-rich slag products. If this technique were to be applied to industrial materials, then a new carbon sink would be characterised and understood, the use of which could make a significant contribution towards reducing the impact of CO_2 emissions.

1.5 Slag Production and CO_2 Offsetting

Slag is produced at Redcar and other integrated iron and steel works as a by-product of two processes. Within a blast furnace a slag is produced to remove impurities from a reduced Fe-melt. This slag is then either air cooled, granulated or pellitiesed to form a range of different products. Within a Basic Oxygen Furnace (BOF) a slag is also produced to remove impurities from a melt, but this slag has a slightly different composition to blast furnace slag as it is formed from a melt with a different starting composition. The slag is then typically air cooled. As the slags are formed to remove impurities they become enriched in metals such as Ca, Mg and Mn (along with Fe) and there are a number of advantages to using these waste materials over natural materials for mineral carbonation. Firstly, the waste slags have a lower silica content compared to natural rocks and so contain a higher proportion of carbonateable cations within the material and secondly, the slags are in plentiful supply in the UK with 1.375 Mt of this low value material being produced each year. The slags must be weathered before they can be used as building materials to reduce their reactivity. Hence, by adding further carbonate onto their surfaces their value is increased both in terms of their usefulness and by the price they command per kg due to a small weight addition. Another advantage is that, apart from the environmental impact of the iron-ore and limestone flux mining, no further environmental impact occurs once the slags have been produced and their use in carbonation would prevent natural analogues (such as basic igneous rocks) being mined to supply the material for carbonation projects.

Despite the many advantages to using waste iron and steel slags there have been little to no studies documenting their passive weathering characteristics or any live-field trials of active carbonation. There has been substantially more work carried out on the active reaction of slags (e.g. Huijgen et al. 2005) but little work on granulated or pellitised slag or larger grain sizes of steel slags. Within those studies there has been some attempt at using chemical treatments to enhance carbonation, but these have been carried out on very fine grain sizes and only on a limited number of slag products. This

thesis will aim to fill the gaps in literature regarding both passive and active carbonation, test the effectiveness of a field trial and research the effect of chemical additives during active carbonation on a wider range of commercially available slag products.

1.6 Aims, Objectives and Thesis Layout

The aims of this study are:

- To characterise the different slag products and their physical attributes and properties. This analysis is required to fully understand the materials within the study and to allow the results from each experiment to be correctly interpreted in the appropriate context.

- To measure the extent to which the different slag products 'passively' form mineral carbonates under environmental conditions and under conditions of enhanced pressure and temperature. This analysis will allow the current weathering rates at Redcar to be understood and a baseline for carbonation to be established.

- To understand how pressure and temperature affect the carbonation rate of the different slag products. This understanding is essential to describing the most efficient and effective pressure and temperature conditions for carbonating the slag products studied. The data produced can be compared to the current 'passive' baseline to assess the effectiveness of using enhanced conditions to react the slag.

- To expand the data set for materials which have the potential to sequester carbon into carbonate minerals. The data currently available for slag products is limited to the finer grain sizes of steel slag and the behaviour of coarser grain sizes has not been investigated. This aspect of the study will generate new data regarding the weathering of slag products at both Redcar and their reactivity to CO_2 in general.

- To assess the applicability and economics of each sequestration method in order to present the best option for carbonating each type of slag product.

The outline of this thesis is as follows:

- Chapter 2 will detail the physical and chemical properties of the slag products used in this study. These properties will be deduced by analytical and petrographical means. The data from this chapter will be used in subsequent chapters to aid the understanding of the behaviour of the slag products when they are placed under different experimental conditions.

- Chapter 3 will outline a predicted chemical model for the H_2CO_3 concentrations present in the experiments carried out in Chapters 4 and 5. The carbonation potential under each set of conditions will be predicted.

- Chapter 4 will report the results of a study of the passive carbonation of slag materials under the environmental conditions present in the City of Durham and will present new data relating to the weathering characteristics of the different slag products.

- Chapter 5 will describe the experimental process used for actively reacting slag products with CO_2 under varying conditions of pressure, temperature and water availability. In particular, new data relating to the carbonation of steel slag with a grain size of 20mm will be presented, alongside the results obtained for other grain sizes of different slag products under novel P/T conditions.

- Chapter 6 will report the results from a small-scale field trial in which the slag products were actively reacted, under environmental conditions with CO_2 at a constant flow rate of 2 dm^3 min^{-1}, but with a controlled amount of water. The experiments were conducted in order to assess the applicability of actively carbonating slag products under environmental conditions.

- Chapter 7 will report the results of the active reaction of slag products, which have previously been reacted with either 1M HCl or 1M NaOH solutions. The slag products were then further reacted with CO_2 under varying conditions of pressure and temperature.

- Chapter 8 will conclude the findings of this thesis and will suggest the most economic carbon sequestration method.

Chapter 2:

Characterising the Study Materials

2.1 Introduction

Iron and steel-making slags are produced as a by-product of iron smelting and by the refining of hot liquid iron into steel. The slags formed by these processes have been shown to have the potential to sequestrate CO_2 through the formation of stable, carbon bearing minerals. This occurs to such an extent that slags have found use in building cements as a replacement for Portland lime, which suggests that the slags can offer a credible option for mineral CCS. In this chapter the chemical and physical properties of the materials used within this study will be characterised in order to understand and explain their behaviour in subsequent experiments. The textural characteristics of the slag were observed through petrography and SEM analysis, while the chemical composition of the slag was determined by XRF and the phases present characterised by XRD.

2.1.1 Iron and Steel Production at Redcar

Slag is produced at the Redcar works via two processes. Either as a by-product of blast-furnace iron production through the removal of impurities from a reduced-Fe metallic melt (BFS or Blast Furnace Slag) or as a by-product of a Basic Oxygen Furnace (BOF or Steel Slag) reaction via the Bessemer Process. Blast furnace slag (iron making slag) is produced as a by-product within the Redcar blast furnace owned by Sahaviriya Steel Industries (SSI). Within this furnace, a combination of a reducing agent (coke and/or metallurgical coal), a source of Fe (lump iron ore, sintered iron nodules, iron pellets) and a flux (limestone, dolomite, other additions) are added and heated to >1500°C. This produces liquid iron or 'hot metal' which is siphoned into a 'torpedo' for storage and transportation, molten blast furnace slag and off-gas from the furnace. The blast furnace slag is then treated in one of three ways;

Granulation: Liquid slag is poured onto a water-covered rotating metal drum to quickly vitrify it into thin shards. This slag is known as GBFS (Granulated Blast Furnace Slag) and has a texture similar to the long glassy strands of 'Pele's hair' produced at volcanic vents.

Pelletisation: Pellite is produced via quick cooling with air to produce glassy/finely crystalline pellets. The material formed is similar to pumice in texture.

Air-Cooling: Air-cooling produces a fine-grained crystalline material which can be crushed to varying sizes for use as aggregate. This slag has a texture similar to basalt.

Basic oxygen furnace slag (steelmaking slag) is produced within a basic oxygen furnace (BOF) owned by TATA STEEL. The BOF furnace is filled with a combination of flux (lime and additions), scrap metal (steel, iron) and hot iron metal tapped from the Redcar blast furnace and transported within a 'torpedo' to the BOF. While in the BOF, the mixture of reactants has pure (99%) oxygen blown through the melt igniting the carbon content of the melt and raising the temperature to >1700°C. Fluxes are then added to the furnace to form the steelmaking slag which is then tapped off from the furnace and left to air-cool outside the plant. This air-cooled slag is subsequently ground into 20, 14, 10 and 6 mm aggregate with a 'Dust' fraction being produced during the crushing process, which is <4 mm. During the crushing stage any metallic 'blebs' liberated from the slags are removed via an electromagnet and returned as scrap steel to the BOF for the next batch process.

2.1.2 Study Site

Samples of GBFS, Pellite and air cooled steelmaking slag were collected from windrow heaps located on an industrial site at Redcar in North East England. The site is owned by Lafarge-Tarmac, Sahaviriya Steel Industries and TATA STEEL. The sampling sites (Fig. 2.1) are located on the south shore of the River Tees and comprise an approximately 12 km^2 area of made ground that is a mixture of glacial drift deposits and slag heaps underlain by carboniferous sandstones.

Figure 2.1: Satellite photo of the Redcar industrial site, localities marked by a star (Google Earth).

The steel slag heaps were located on the Lafarge-Tarmac site and approximately average 80 m in length, 11 m in width and up to 2-3 m in height. Heap volumes average 1800 m^3 and have a mass of approximately 3000 tonnes. Steel slag blocks are crushed to typical grain sizes of 20 mm, 10 mm and 6 mm and are then stockpiled to form the heaps. Occasionally 14 mm and 3 mm heaps are present. The heaps were well-sorted, with the grains grey-to-black in colour and of angular and spherical shape. Approximately 1 kg of sample was taken from each heap.

It should be noted that the applicability of the results reported is relevant to the slags produced at the Redcar site. No comparison with other slags has been undertaken or made with Al-slags or Pb-Zn slags (Warchulski et al. 2015) for example. However, the results are likely comparable with other iron and steel slags from UK based integrated-steelworks and potentially European wide integrated-steelworks as well.

2.2 Grain Size of Material Descriptions

2.2.1 Methods

The sampled material was observed visually in the field area, in the laboratory and during crushing. A 1 kg sample of each slag type was sieved using standard Endecott's sieves (ϕ sizes between 8mm and <32μm) to ascertain the grain size distribution. The variations between each fraction caught by the sieves was described as required. Each material was observed by eye and using an x10 hand lens at each stage.

2.2.2 Results

Steel slag aggregate had been mechanically graded prior to being left in heaps at Redcar. All other slag products were a mixture of grain sizes. The grain-size distributions of these materials are reported below.

20 mm and 6 mm Steel Slag Aggregate **-** Mechanically graded steel slag aggregate is of a uniform grain size (predominantly of either 20 mm or 6 mm grain size). The grains are sub-angular and display low sphericity. The grains are dull to light grey in colour and can display small (≈1 mm) specks of white on their surfaces due to the growth of carbonate minerals. Red streaks or flecks of iron (III) oxide may be present due to the inclusion of metallic blebs within the grains.

Dust **-** Dust is the by-product formed when steel-slag blocks are crushed to produce lower aggregate grain sizes. Dust displays a grain size of below 4 mm with a predominant grain size range from 2 mm to 125μm (Fig. 2.2). The visibly observable grain size fractions consist of sub-angular to rounded grains with low to high sphericity. There are occasional 0.5 mm to 4 mm sized metallic blebs within the dust.

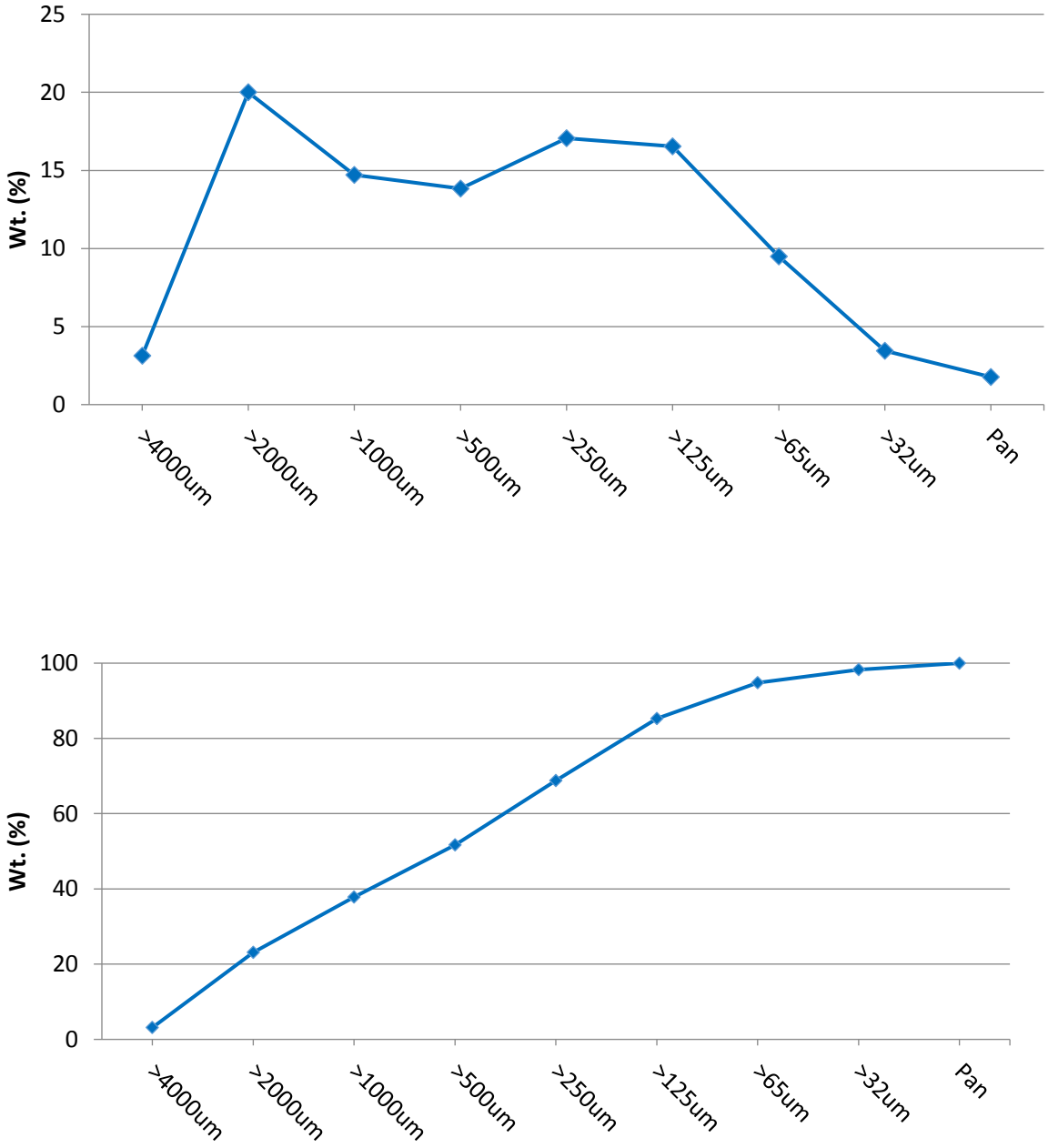

Figure 2.2: Grain size distribution profiles of Dust from sieve analysis: Top – Grain size distribution for each mesh size. Bottom – Cumulative grain size distribution

Pellite

Pellite was collected from a heap approximately 70-150 m in length, 40-50m wide and 5m in height. Overall, the grains displayed a well-rounded, highly spherical shape and a pumicious texture. The grains were typically of a cream to golden-yellow colour. A strongly sulphurous smell was detected when the grains were damp. The >8 mm grain size fraction contained pellite grains no larger than 2 cm in size. These grains were sub-angular to sub-rounded with medium to high sphericity. They were

heaviliy vesicular and displayed a 'pitted' surface texture to to the smooth cuspate walls of the vesicles. The 4-0.5 mm grain size fraction was sub-rounded to well rounded with medium to high sphericity. They commonly displayed a texture similar to the long glassy strands of 'Pele's hair' with many droplets displaying very thin ends from which the glassy strands had snapped off. Many grains were almost perfect spheres. The visibly observable grains below the 0.5 mm grain size fraction were rounded to well rounded with low to high sphericity. There were two roughly evenly disributed groups of grains; the first were near perfect spheres, the second were of more irregular shape consisting of bubble wall shards and long and thin fragments which were likely the thin ends of necks (formed by the necking of the slag) that had broken off from the larger grains (Fig. 2.3).

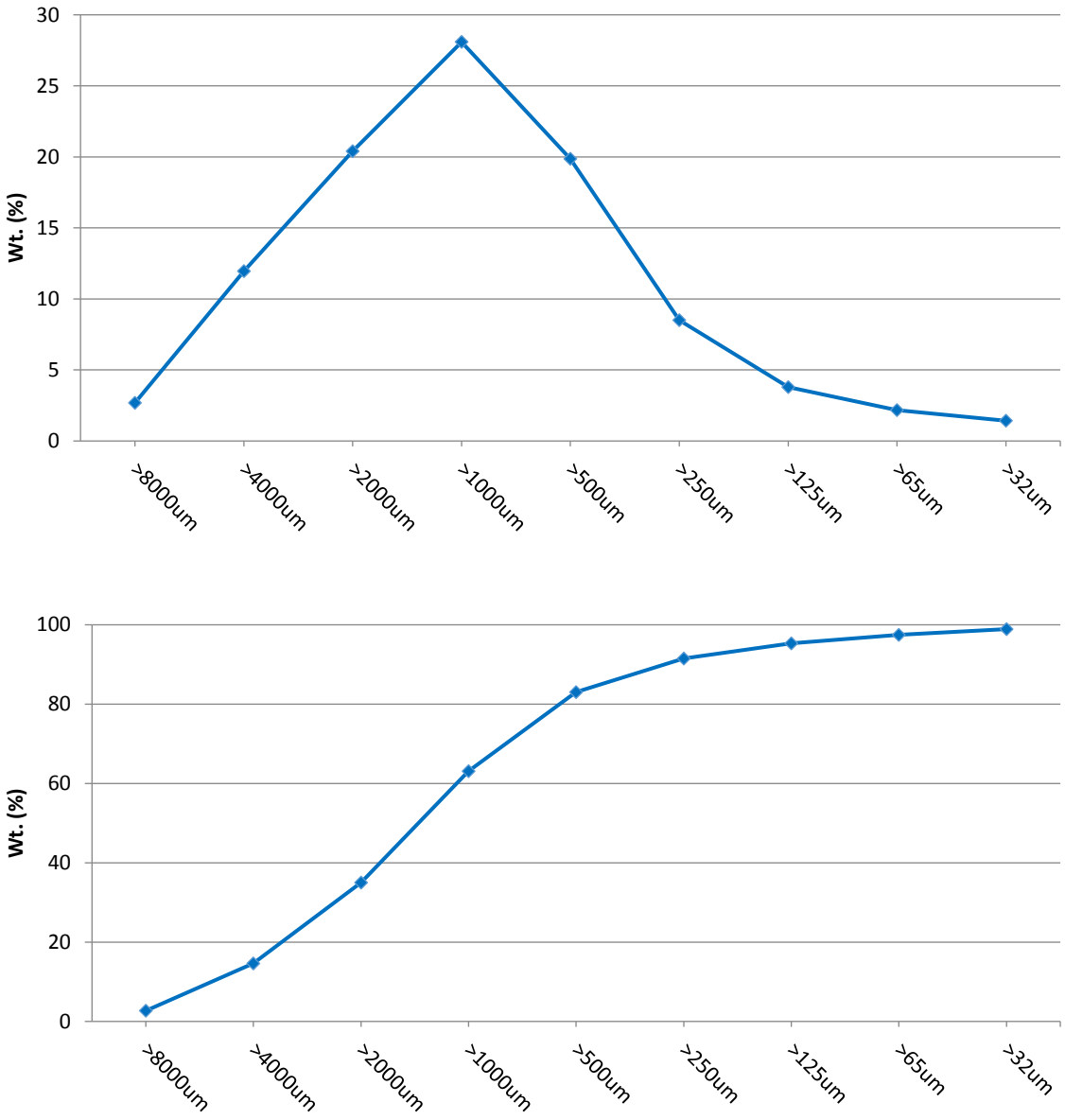

Figure 2.3: Grain size distribution profiles of Pellite from sieve analysis: Top – Grain size distribution for each mesh size. Bottom – Cumulative grain size distribution

Granulated Blast Furnace Slag

Granulated blast furnace slag was collected from a heap approximately 3 m in length by 3 m in width and 3m high, located at the end of a granulation conveyer belt. The grains predominantly displayed a shard like morphology. The grains were golden in colour and were vitreous in texture. They contained abundant mm-scale vesicles (the remnant shape of a gas bubble). The >4 mm grain size fraction contained glassy shards no bigger than 1 cm. The 4-1 mm grain size fraction was very angular to sub-angular and displayed a high sphericity. The visibly observable grains below the 1 mm grain size fraction displayed two separate grain fractions: The predominant fraction was very angular to sub-angular and displayed a low to high sphericity, while the other fraction consisted of long elongate well rounded fragments with low sphericity. The ratio of elongate-shards vs spherical-grains increased with decreasing grain size with elongate grains becoming highly needle-like below the 64 µm size (Fig. 2.4).

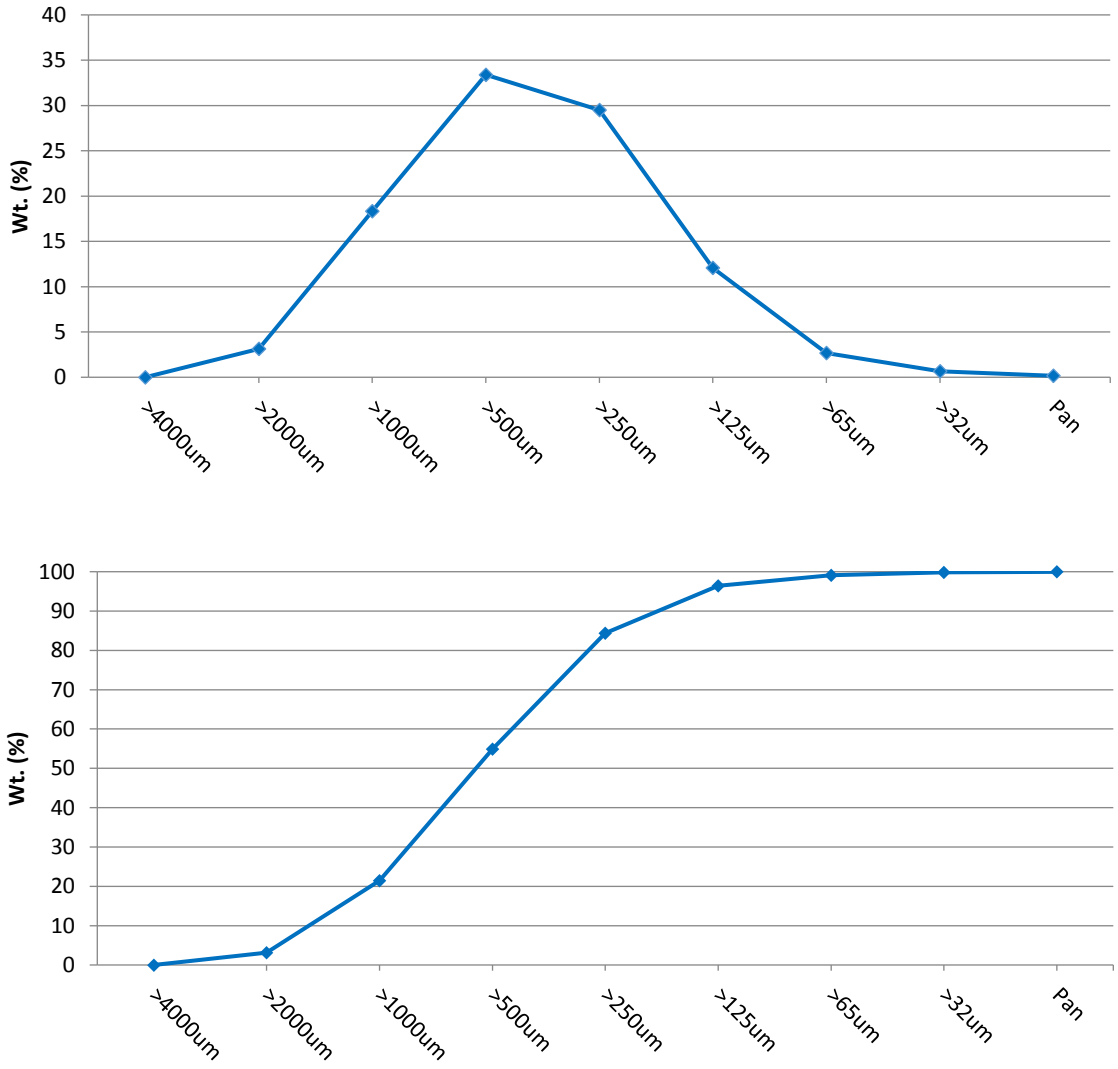

Figure 2.4: Grain size distribution profiles of GBFS from sieve analysis: Top – Grain size distribution for each mesh size. Bottom – Cumulative grain size distribution

2.3 Porosity and Hydraulic Conductivity

2.3.1 Methods

Porosity **-** An estimated porosity of the samples was ascertained by the immersion of a weighed sample of each material in a 250 cm^3 beaker filled to the 200 cm^3 level with material. The beaker and its contents were subsequently weighed and the original weight deducted from this. Given that 1 cm^3 (ml) of water is equal to 1 g the porosity was calculated using Equation 2.1:

$$\Phi_T = \frac{\text{Volume of Water Added}}{200\ \text{cm3}}$$

Equation 2.1

A more quantified measurement of porosity for blocks of steel and blast furnace slag was undertaken though X-Ray Computed Tomography (XRCT) (See2.4.7 XRCT Analysis for method).

Hydraulic Conductivity **-** An estimated permeability for each material was derived by using a modified version of Darcy's Law for a vertical pipe (Equation 2.2) using the apparatus shown in Figure 2.5:

$$Q = K\,A\,\frac{h_1 - h_2}{L} \qquad \text{when } h_1\text{-}h_2 = L \Rightarrow \qquad Q = K\,A$$

Q – Rate of flow ($dm^3\,s^{-1}$)

K – Hydraulic Conductivity ($m\,s^{-1}$)

A – Cross sectional area of the pipe (m^2)

L – Vertical length of the pipe (m)

Equation 2.2

Figure 2.5: Simple apparatus for determining vertical permeability.

The apparatus was designed to maintain a constant pressure head of water, just above a 50 cm tall column of sample material. Water was added to the pipe via a hose connected to a mains water supply. The water column was kept at a constant height – and therefore pressure – via a water-escape hole at the top of the material column. Water exited the pipe from the base and was collected into containers with a volume of 500 cm^3, 700 cm^3 or 1000 cm^3. The time taken to fill a given container used was measured and converted into a flow rate. From this flow rate the hydraulic conductivity of the material was calculated. The cross-sectional area of the pipe and the vertical height of the material were kept constant for each experiment. It is acknowledged, however, that the errors involved in using this method were considerable due to the lack of control over the flow of water.

To convert hydraulic conductivity to permeability Equation 2.3 is used:

$$K = \frac{\rho g}{\mu K}$$

k – permeability (Darcy's)

ρ – density of fluid (Kg m^{-3})

g – gravitational acceleration

μ – dynamic viscosity

K – hydraulic conductivity (m s^{-1})

Equation 2.3

2.3.2 Results

The porosity and hydraulic conductivity properties of the materials used are reported below.

20 mm **-** The measured porosity of 20 mm aggregate was 53.7% (± 1%). The calculated vertical hydraulic conductivity for 20 mm aggregate slag was 42.3 L s^{-1} m^{-2}. This classified the 20 mm aggregate as pervious.

6 mm **-** The measured porosity of 6mm aggregate was 48.2% (± 1%). The calculated vertical hydraulic conductivity for 6mm aggregate slag was 14.4 L s^{-1} m^{-2}. This classified the 6 mm aggregate as pervious. The hydraulic conductivity of a column of weathered and cemented 6 mm aggregate was also measured. The calculated vertical hydraulic conductivity for this column was 7.5 L s^{-1} m^{-2} which was also classified as pervious.

Dust The measured porosity of Dust was 36.1% (± 1%). Hydraulic conductivity could not be calculated as the sample turned to an impermeable paste upon the addition of water.

Pellite The measured porosity of Pellite was 15.3% (± 1%). Hydraulic conductivity was not calculated for this material as further samples could not be obtained due to site closure.

GBFS The measured porosity of GBFS was 49.2% (± 1%). Hydraulic conductivity was not calculated for this material as further sample could not be obtained due to site closure.

Of all the slag products 20 mm was the most porous, followed by GBFS and 6 mm aggregate slag. Pellite displayed the lowest porosity (Table 2.1).

Material	ϕ (%)	K (L s^{-1} m^{-2})
20 mm	53.7	42.3
6 mm	48.2	14.4
Dust	36.1	-
Pellite	15.3	-
GBFS	49.2	-

Table 2.1: Values for porosity and hydraulic conductivity for different slag products

2.4 Material Saturation Points

2.4.1 Methods

The saturation potential of the samples was measured in order to understand the maximum amount of water available to each material (if not immersed) for the dissolution of CO_2. The maximum saturation potential of each material was calculated by saturating 110-115 g of each sample of slag product with water within 100 cm^3 volume plastic pots which had been initially weighed. These filled pots were drained of any excess water and weighed. The samples were then placed into an oven at 105±1 °C overnight until dry. The samples were then removed from the oven, left to cool and then reweighed. The final weight was deducted from the initial weight. The resulting value was taken as the wt. % saturation of the material.

2.4.2 Results

The moisture retained by each sample depended both on the grain size and the type of sample measured. The average point of saturation for each material is shown in Table 2.2.

	20 mm	10 mm	6 mm	Dust	Pellite	GBF Slag
Wt.%	0.228	0.176	0.394	12.843	10.213	7.318

Table 2.2: Average saturations for each material type

Aggregate slags displayed similar points of saturation, with Dust displaying a saturation point two orders of magnitude greater than that of the aggregate slags. Pellite and GBF Slag displayed similar saturation points.

If a material can retain water and remain damp over a period of time then this can allow for a longer carbonation period to occur in comparison with a material which dries out quickly. As such, the saturation point of each material is hypothesised to affect carbonation values. In light of this hypothesis an interpretation for the effect of each materials saturation point under atmospheric conditions is provided below.

Aggregate Slag and Dust - The surfaces of aggregate slags became saturated at a lower point than Dust. In general, there was a trend which showed that as grain size decreased the saturation point increased. Given that Dust holds more water, it may be able to sequester more CO_2 than aggregate slags as it will dry out more slowly.

Pellite **-** Pellite became saturated at a similar point to Dust. This may be because it also displays a medium to fine grain size fraction and, as it is pumicious in texture, Pellite displays a large internal surface area (despite its low effective porosity) which may be able to store water.

GBFS **-** GBFS displayed the lowest saturation point of the medium to fine grained slags (Pellite, Dust, GBFS) despite displaying a similar grain size distribution to Pellite. This may be due to the shape of the grains as they lacked any internal porosity and had smoother surfaces in comparison to Pellite and Dust.

2.5 Grain Size of Material Descriptions

X-Ray Fluorescence (XRF) analysis was carried out in order to derive the bulk chemistry of a suite of slag samples representing a year of production.

2.5.1 Methods

The XRF data was collected at the Department of Geology at the University of Leicester using a PANalytical Axios Advanced XRF spectrometer with WROXI analytical package. Samples were provided as <250 µm crushed powders. The sample powders were dried overnight at 105^{o}C and then ignited for 90 minutes at 950^{o}C in an air ventilated electric muffle furnace. The prepared powders were then fused into glass beads using Lithium tetraborate flux (Fluxana FX-X100) with a sample to flux ratio 1:10, 100%. All concentrations were accurate to 3σ, concentrations below this were reported as below the detection limit. Twenty three samples of slag have had their major element compositions analysed (% oxide). Twenty samples of steel slag of various grain sizes and ages (February 2013 – October 2013) were analysed using XRF. Three samples of blast furnace slag were analysed; fresh block blast furnace slag, granulated blast furnace slag (September 2013) and Pellite.

2.5.2 Results

The results of the XRF analysis of each slag product is shown in Table 2.3.

Element Oxide (%)	Fresh BF Block (n=1)	Pellite (n=1)	GBFS (n=1)	Average Steel Slag (n=18)	Dust (n=1)
CaO	**39.792**	**39.758**	**38.866**	**37.647**	**42.170**
SiO_2	**36.574**	**35.733**	**37.890**	**12.704**	**7.700**
Fe_2O_3	0.508	0.358	0.370	**31.673**	**24.068**
Al_2O_3	**12.572**	**12.538**	**12.606**	**2.394**	**1.451**
MgO	**8.159**	**8.607**	**7.222**	**9.164**	**6.311**
Mn_3O_4	0.369	0.405	0.403	**3.211**	**2.303**
P_2O_5	0.024	0.020	0.021	**1.547**	**1.220**
TiO_2	0.560	0.537	0.563	0.600	0.427
K_2O	0.606	0.532	0.796	0.000	b.d.l. (<0.003)
SO_3	0.255	0.225	0.266	0.138	0.219
Na_2O	0.255	0.225	0.278	0.022	0.009
Cr_2O_3	b.d.l. (<0.004)	b.d.l. (<0.004)	b.d.l. (<0.004)	0.223	0.146
BaO	0.113	0.102	0.114	0.031	b.d.l. (<0.006)
V_2O_5	0.005	0.002	0.002	0.197	0.100
LOI	-0.414	0.127	0.163	-	12.278
Total	99.379	99.170	99.562	99.551	98.402

Table 2.3: XRF data for five different types of slag product produced at Redcar. Results quoted as component oxide weight percent re-calculated to include LOI (except in cases of negative LOI). Samples were also analysed for SrO, ZrO_2, ZnO, PbO, HfO_2, NiO, CuO and were all either below detection limits (3σ on background levels) or present <0.1% and were not included in this table. Numbers in bold are >1% and were taken as the major element components for EVA-DIFFRAC peak-search/match function as part of the XRD analysis.

Blast Furnace Slags

The XRF data showed that the composition of the blast furnace slag was constant across the different products. This was due to a standardised slag melt being produced from the SSI blast furnace used in the production of block slag, Pellite and granulated slag. Hence, the initial composition of blast furnace slag products may be assumed to be constant and independent of their physical morphology. The silica content of the slag ranged from 35.7 -37.9%, the alumna content ranged from 12.5-12.6%. The main divalent cations present within the slag were Ca, Mg and Fe, each an order of magnitude lower than the former successively. CaO had the highest concentrations 38.9-39.8%, MgO moderate concentrations 7.2-8.6% and Fe_2O_3 the lowest concentration 0.4-0.5%. The cations with lower concentration were K_2O, SrO and P_2O_5 successively. This is shown graphically in Fig. 2.6.

Basic Oxygen Furnace Slags

The XRF data in Figure 2.6 showed that the chemical composition of the steel slag could be considered as being consistent over time. This is likely due to the industrial standardisation of the blast furnace melt which is tapped from the furnace and stored in the torpedoes for use within the basic oxygen furnaces at the TATA plant. The silica content of the slag ranged from 11.7-14.5%, the alumna content ranged from 1.9-3.0%. The main divalent cations present within the slag were Ca, Fe and Mg. However, in contrast with blast furnace slag the concentration of Fe_2O_3 was far higher than MgO. CaO had the highest concentration at 36.4-39.8%, Fe_2O_3 the moderate at 30.1-35.1% and MgO the lowest at 8.3-10.99%. The cations with lower concentration were P_2O_5, SrO and Na_2O successively. K_2O was now below detection (<0.003) unlike in Blast furnace slag. Na_2O concentrations were below 0.022%.

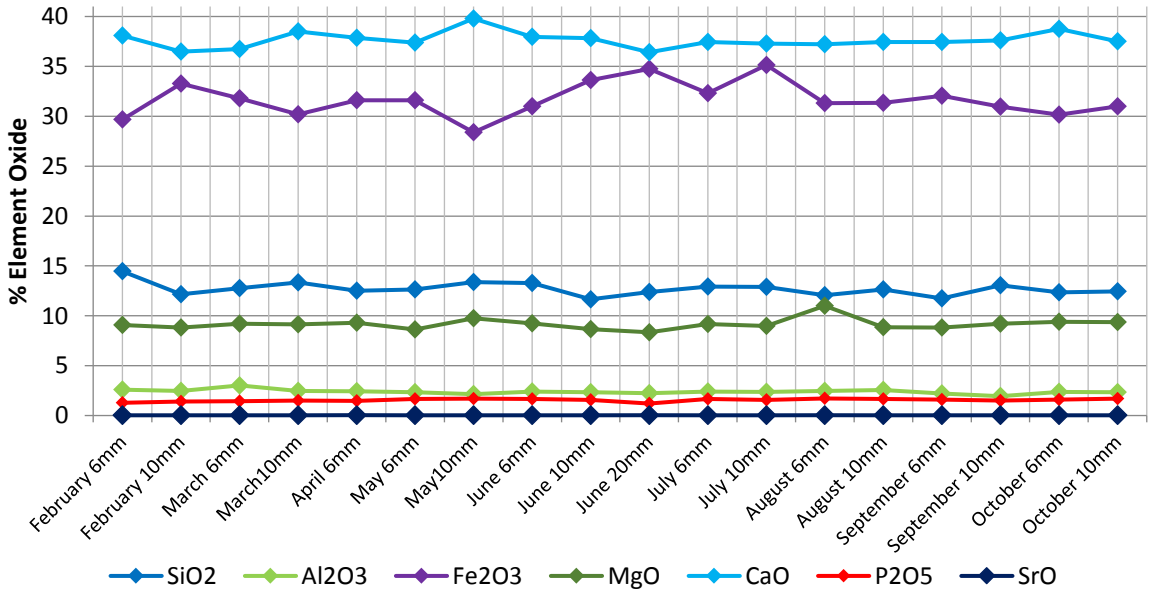

Figure 2.6: Major element compositions of TATA BOF slags through time (Redcar site).

2.5.3 Interpretation

Overall, the quantity of elements capable of forming +2 cations (by oxide mass) available for carbonation in blast furnace slag was 47.5% to 49.7% compared to 82.3% for steel slag block (75.3% for Dust). Both slags shared similar MgO contents (BFS – 7.996, STS – 9.1638) and CaO contents (BFS – 39.472, STS – 37.647) (Table 2.3). However, there were variations in other components often on at least an order of magnitude. Significantly, steel slag displayed Fe_2O_3 concentrations 76.8 times that of blast furnace slag. Steel slag was also enriched in Mn_3O_4 (by 8.2 times that of BFS) and P_2O_5 (by 71.3 times that of BFS). However, blast furnace slags displayed higher concentration of Al_2O_3 (by 5.3 times that of STS) and also displayed 2.89 times the SiO_2 content. From these results it is apparent that during smelting in a basic oxygen furnace more Fe separates into the slags than during smelting in a blast furnace (Fig. 2.7).

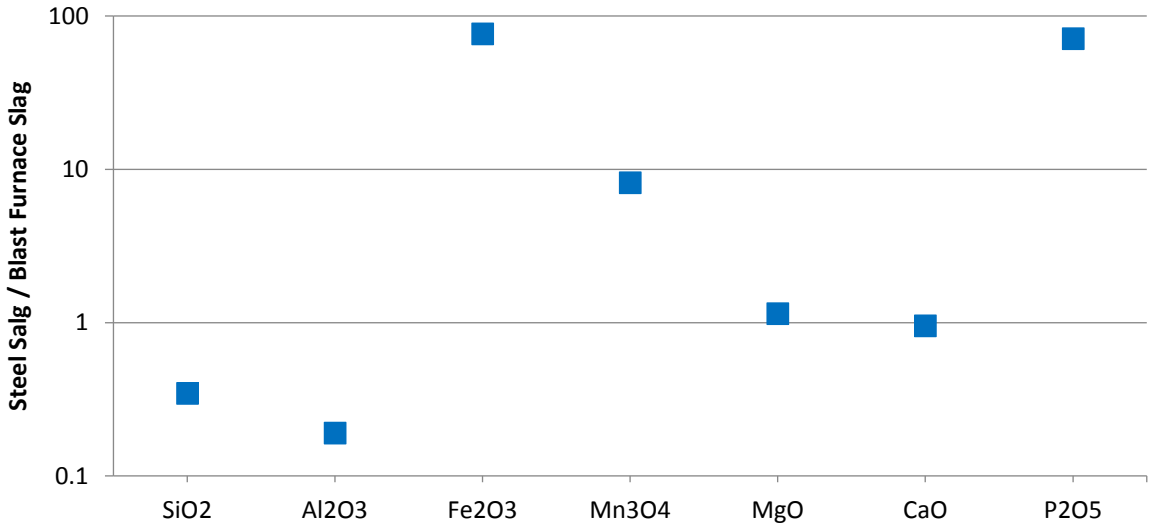

Figure 2.7: Cation ratio of average steel slag (STS) relative to average blast furnace slag (BF).

Variations in Major Carbonate Cation Ratios

There appears to be no significant internal variation in the ratios of Ca, Mg or Fe across different blast furnace slag products with Ca being the most abundant cation available for carbonation as is has an average ratio of 0.825 of the total major cations (Ca:Mg:Fe = 83:17:01) (Table 2.4,Fig. 2.8).

Steel slags contain greater concentrations of Fe which results in a lower Ca/T-Cation ratio of 0.48 for steel slag block. The average Ca:Mg:Fe ratio is 53:10:37. Notably, Dust displays a slightly higher Ca/T-Cation ratio (by 0.102) than block steel slag. This may be due to the removal of iron blebs, via an electromagnet for industrial recycling, during the grinding process to produce aggregate. This reduces the Fe content and raises the Ca-ratio due to the mass loss of iron removal.

	BF Block	Pellite	GBFS	STS Agg.	Dust
Fe_2O_3	0.508	0.358	0.370	31.673	24.068
MgO	8.159	8.607	7.222	9.164	6.311
CaO	39.792	39.758	38.866	37.647	42.170
Total	48.459	48.723	46.458	78.484	72.549
Fe/ (Fe+Mg+Ca)	0.010	0.007	0.008	0.404	0.332
Mg/ (Fe+Mg+Ca)	0.168	0.177	0.155	0.117	0.087
Ca/ (Fe+Mg+Ca)	0.821	0.816	0.837	0.480	0.581

Table 2.4: Ratios of the major cations within each slag product against each other.

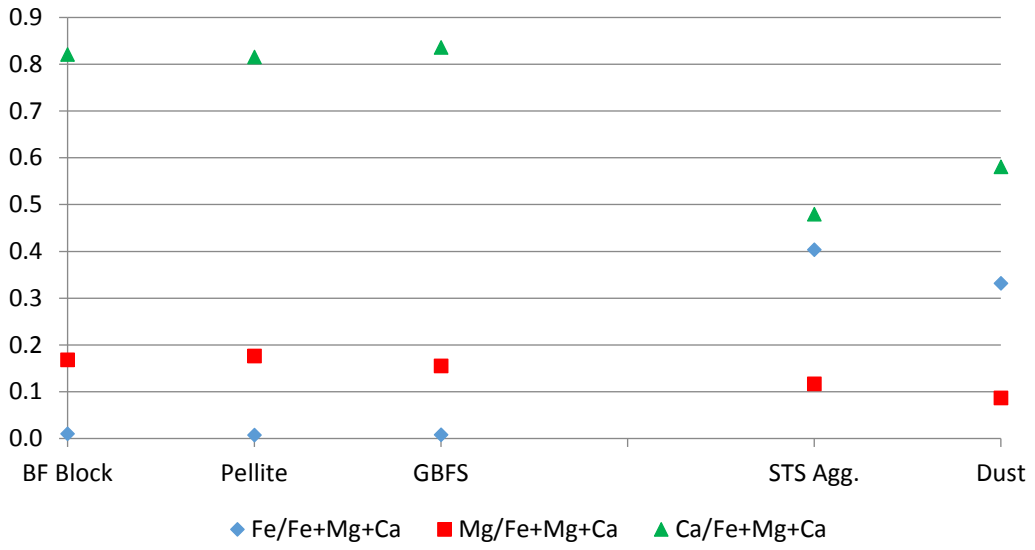

Figure 2.8: Fe, Mg and Ca ratios over total Fe+Mg+Ca contents ratios of slag products

2.6 XRD Analysis

Bulk XRD was undertaken on fresh samples of Pellite, Granulated slag, 20 mm - and 6 mm- slag aggregate and Dust in order to identify the mineral phases present.

2.6.1 Methods

Slag samples were crushed using an agate pestle and mortar and sieved through a 125µm mesh sieve. Powder X-Ray Diffraction (PXRD) data was collected from a sub-sample of the <125µm powdered sample. Samples were analysed with CuKα1 radiation using a BRUKER D8 ADVANCE X-Ray

Diffractometer (XRD) equipped with a BRUKER LYNXEYE Detector within a 10-90 2θ range with a step size of 0.02 over a period of 25 minutes in a BB-Slit, V6-incident slit configuration.

All PXRD data were processed using EVA DIFFRAC. The identification of individual phases was achieved using the 'search/match' function of EVA DIFFRAC utilising the main (>1%) elements identified using XRF analysis to narrow the search parameters. The interpretation of the data is shown in section 2.4.4.

2.6.2 Results

The XRD traces obtained for each material used within the study are shown below. The initial EVA-DIFFRAC matches obtained using the XRF data [see 2.3.4] are also shown.

Steel Slag

The elements with oxide concentrations >1% were CaO (37.65%), SiO_2 (12.70%), Fe_2O_3 (31.67%), Al_2O_3 (2.39%), MgO (9.16%), Mn_3O_4 (3.21%) and P_2O_5 (1.55%). EVA-DIFFRAC selected 300 of 2000 possible matches to display. The following trace was produced (Fig. 2.9).

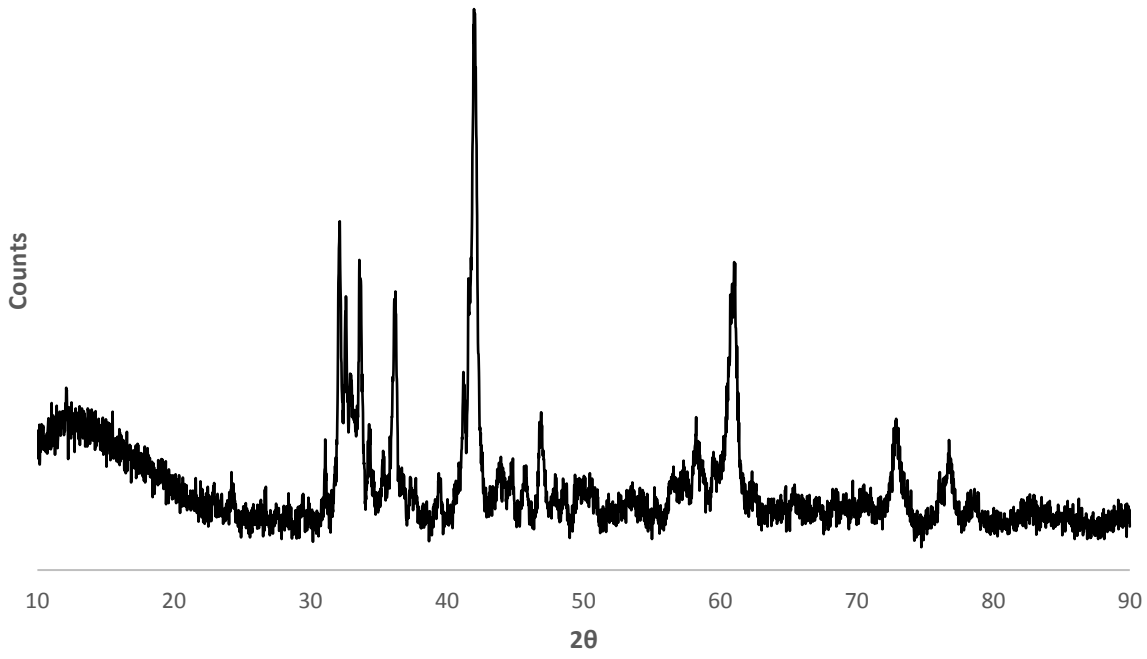

Figure 2.9: XRD-trace for fresh steel slag

Pellite

The elements with oxide concentrations >1% were SiO_2 (35.733%), Al_2O_3 (12.538%), MgO (8.607%), CaO (39.758%). EVA-DIFFRAC selected 156 of 1310 possible matches to display. The following trace was produced (Fig. 2.10).

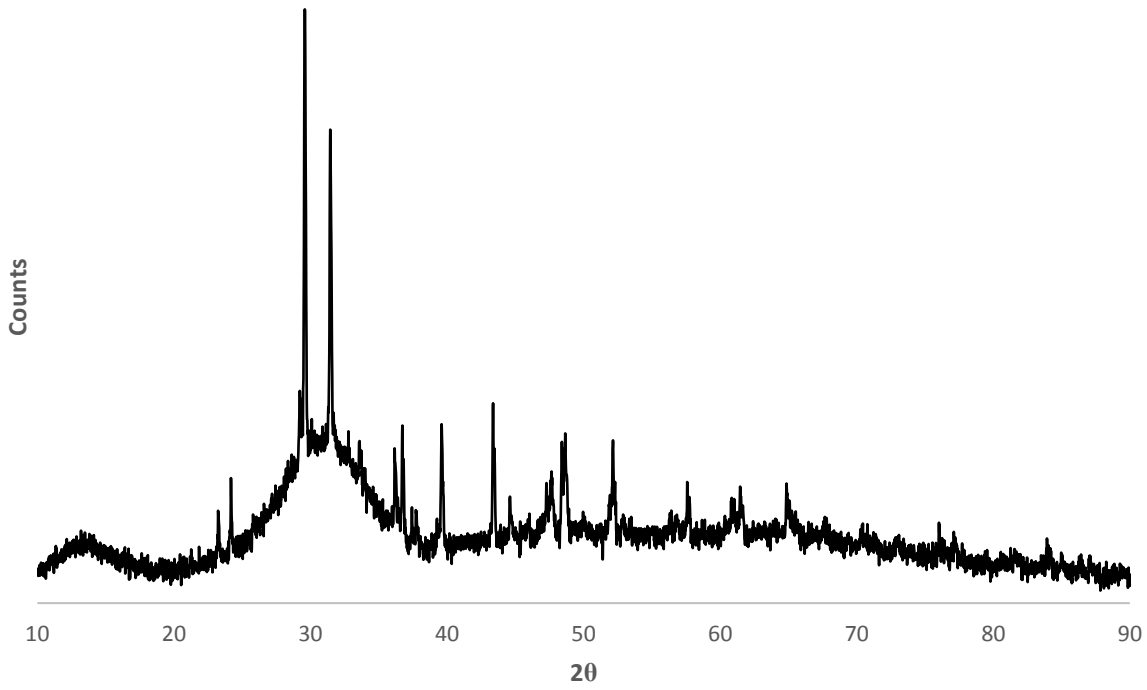

Figure 2.10: XRD-trace for fresh Pellite

Granulated Blast Furnace Slag

The elements with oxide concentrations >1% are SiO_2 (37.890%), Al_2O_3 (12.606%), MgO (7.222%), CaO (38.866%). EVA-DIFFRAC selected 79 of 3094 possible matches to display. The following trace was produced (Fig. 2.11):

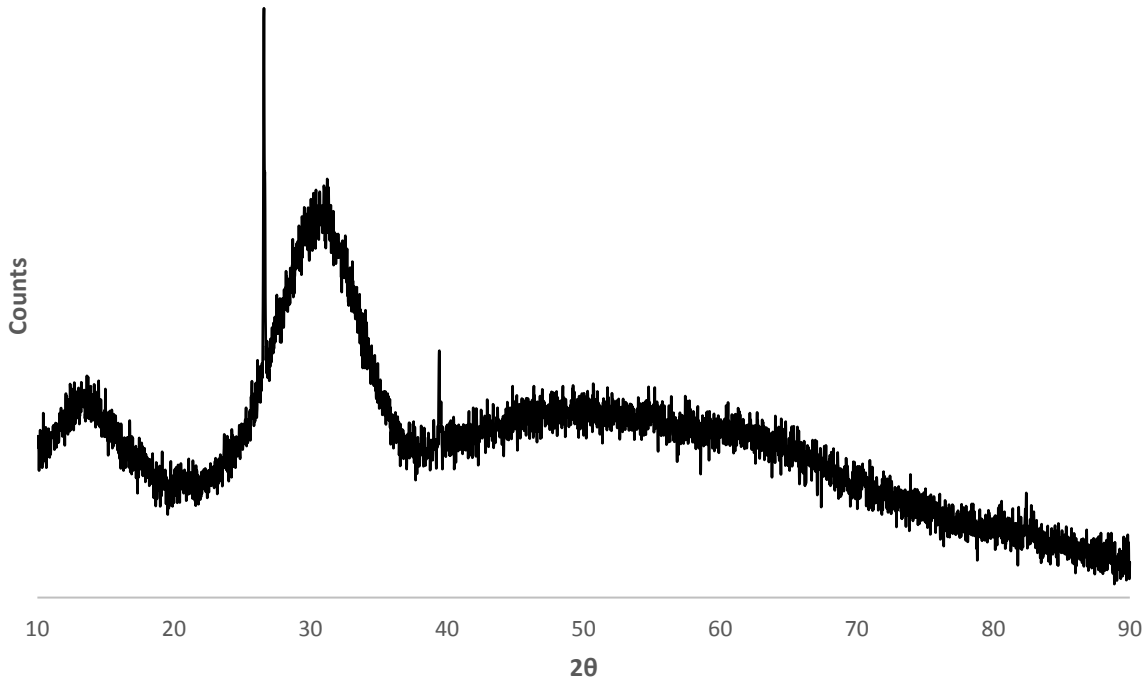

Figure 2.11: XRD-trace for fresh GBFS

2.6.3 Interpretation

Steel Slag

EVA-DIFFRAC selected 250 individual matches of 2000 possible matches to display. Of these results a total of 96 were present as selectable matches. The author then sorted these 96 matches to remove chemical duplicates. This left a total of 82 individual chemical matches. The author then removed those matches that did not fully match the XRD trace to leave a total of 57 matches which fitted into 8 different groups. The remaining matches are reported below in Appendix 1 (XRD Matches). The main metals and minerals present are metals, metal oxides, metal-alumnide-oxides, olivines, assorted silicates, phosphides, hydroxides and carbonates.

Pellite

EVA-DIFFRAC selected 156 individual matches of 1310 possible matches to display. Of these results a total of 96 were present as selectable matches. The author then sorted these 96 matches to remove chemical duplicates. This left a total of 43 individual chemical matches. The author then removed those matches that did not fully match the XRD trace to leave a total of 26 matches. The remaining matches are reported below in Appendix 1 (XRD Matches). The main metals and minerals present are Mg, Ca, aluminium oxides, Pyroxene-group minerals, Alumnide-minerals and Feldspathide-esq minerals.

Granulated Blast Furnace Slag

EVA-DIFFRAC selected 144 individual matches of 1254 possible matches to display. Of these results a total of 63 were present as selectable matches. The author then sorted these 63 matches to remove chemical duplicates. This left a total of 27 individual chemical matches. The author then removed those matches that did not fully match the XRD trace to leave a total of 10 matches. The remaining matches are reported below in Appendix 1 (XRD Matches). The main metals and minerals present are metal oxides, Al- Mg- Ca-pyroxenes, and hydroxide minerals.

2.7 Petrography

2.7.1 Methods

Polished 30µm thin sections of air-cooled iron-making and steel-making slags were produced and analysed using a Zeiss microscope with a Zeiss camera system.

2.7.2 Results

Blast furnace slag **-** Blast Furnace Slag was observed to be composed of three different minerals and a vesicle phase (Fig. 2.12). The minerals can be observed as:

1. A colourless mineral with an abundance of 50-60% present as euhedral crystals. Under XPL the mineral displayed 1st order to lower 2nd order purple-blue interference colours and hour-glass zoning. The crystals contain occasional metallic blebs.
2. A brown coloured ‘spinifex’ textured mineral with an abundance of 30-40%. Under reflected light the mineral displays reflective cores and abundant metallic blebs.
3. Metallic blebs are common throughout the sample and are up to 0.3 mm in dimension however they are commonly far smaller at <0.05 mm in dimension. The inclusions displayed a dendritic texture under reflected light.

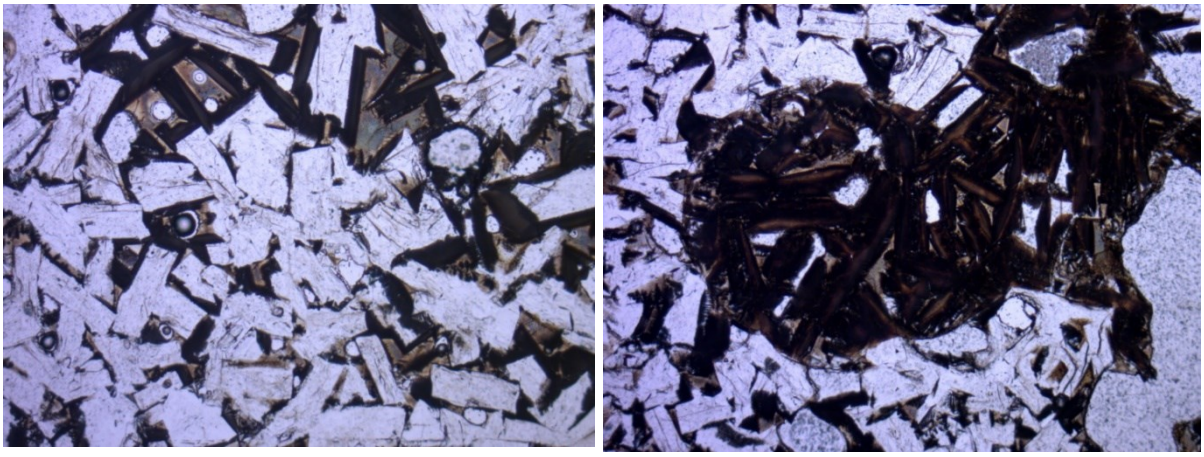

***F**igure 2.12: Thin section photomicrographs of blast furnace slag samples when viewed in Plane Polarised Light. Field of view = 2 mm.*

These minerals are interpreted as:

1. Melilite (Ca, Mg, Fe, Al – sillicates ±Na, K),
2. Metal rich interstitial glass,
3. Fe-metallic blebs,

The reactivity of the material will be dictated by the combined reactivity of all of the minerals present. In this case the (Ca, Mg, Fe, Al – silicates ±Na, K) silicate minerals.

Basic Oxygen Furnace Slag - Basic Oxygen Furnace Slag was observed to be composed of two different metals, a mineral phase and a minor vesicle phase (Fig. 2.13). The metals observed are:

1. Light grey metal with an abundance of 35% which is light grey in reflected light.
2. Dark grey metal with an abundance of 30%. This metal displayed a coarser texture than the lighter grey metal and is slightly dark grey under reflected light.

The mineral observed displayed 2nd order birefringence colours in XPL and displays an abundance of up to 35%.

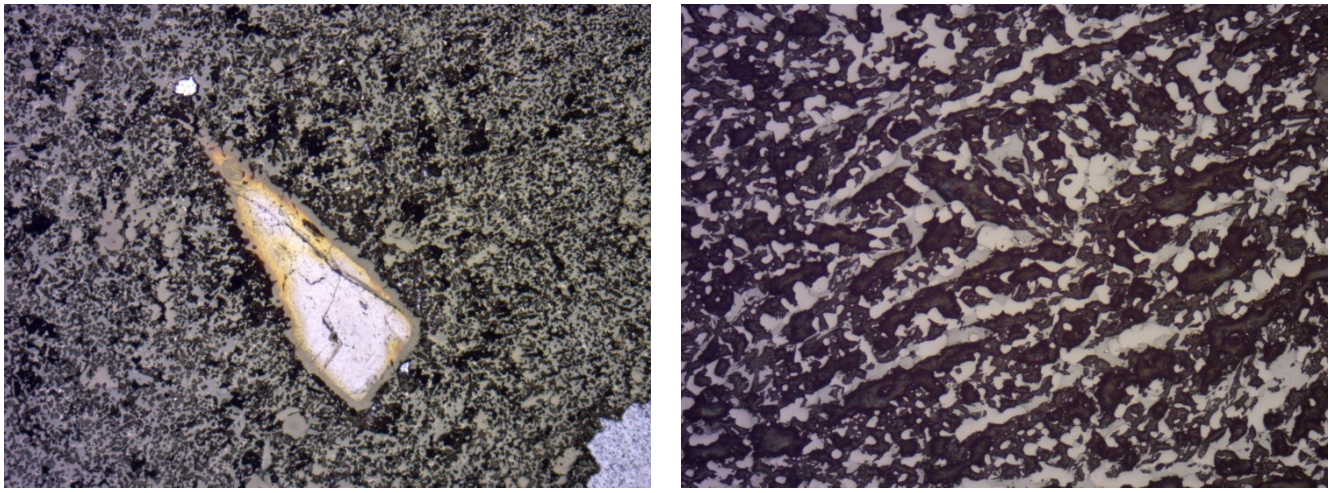

***F**igure 2.13: Thin section photomicrographs of basic oxygen furnace slag samples when viewed in Reflected Light. Field of view, left image = 2 mm, right image = 1 mm.*

These metals are interpreted as Fe and varying compositions of metal-oxides. The mineral displaying 2nd order birefringence will be a silicate mineral.

The reactivity of the material will be dictated by the combined reactivity of all of the mineral present. In this case the nesosilicate / pyroxene-group minerals and the metallic phases.

2.8 X-Ray Computer Tomography (XRCT)

2.8.1 Methods

XRCT 3D analysis of a 7 x 2 x 2 cm drill core of air-cooled steelmaking slag was carried out using an Xradia/Zeiss VersaXRM 410 providing 1 µm resolution x-ray tomography in the School of Engineering and Computing Sciences, University of Durham. This sample was chosen as air-cooled slag is broken up and crushed to produce aggregate sized slags. Therefore, the porosity characteristics of the final aggregate are dependent upon that of the original air-cooled material. The score was analysed with a 150kV 10W microfocus x-ray source, 2k x 2k 16bit CCD x-ray camera MACRO-70 (0.4X) large field of view camera assembly and 3 high contrast detectors. Data was visualised in 3D and analysed for the volume of each phase using a high performance workstation running Avizo Fire software at the Department of Earth Sciences, University of Durham.

The data shows the three different phases (metallic blebs, groundmass and vesicle content) of the slag as identified by optical petrography. The data was then analysed to produce 3D models of the metallic blebs and vesicles and %-content based upon voxel size was calculated [2.4.7].

2.8.2 Interpretation

The volume composition of the slag was calculated to be 13% metallic blebs, 41% vesicles and 46% slag material. The connectivity of the vesicle phase was highly variable. In areas where there were larger vesicles the connectivity was greater and in areas where the vesicles were smaller the connectivity was almost non-existent. This leads to the aggregate steel-slag showing a range of surface areas available for carbonation, though it is likely that only the top surface of each grain will carbonate (Fig. 2.14).

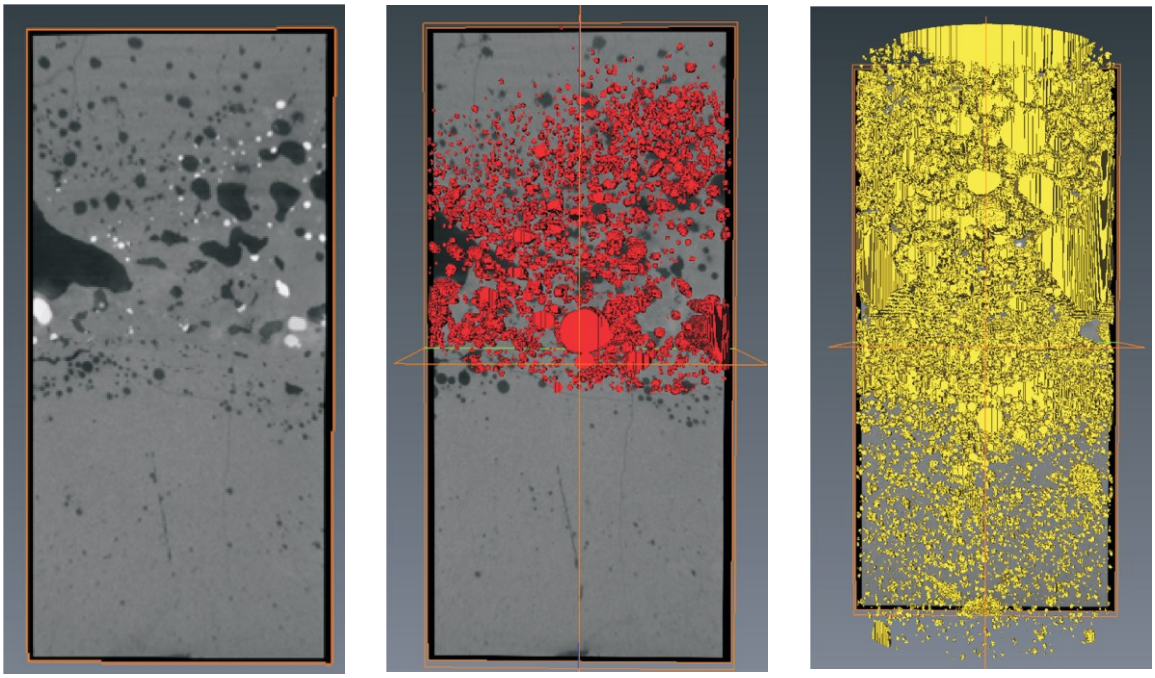

XRCT Steel Slag Core | Metallic Fe-Blebs | Vesicles

Figure 2.14: XRCT images of an unprocessed core, and a 3D visualisation of the metallic-Fe bleb content and the vesicle content

2.9 Overall Characteristics of Each Material

2.9.1 Steel Slag

Steel slag displayed high CaO (37.7%) and Fe_2O_3 (32.7%) contents with significant amounts of SiO_2 (12.7%) and MgO (9.2%). Dust displayed slightly different concentrations with slightly higher CaO (42.2%) and slightly lower Fe_2O_3 (24.1%) contents with less SiO_2 (7.7%) and MgO (6.3%)

20 mm The 20 mm aggregate slag used in this study was a dark to light grey material. It had been mechanically sorted to only include the 20 mm grain size fraction and was very well sorted. The aggregate was sub-angular and displayed a low sphericity with individual grains being variable in their internal porosity. As an aggregate heap displays a porosity of 53.7%. A 50cm high column of 20 mm

aggregate slag displayed a vertical hydraulic conductivity of 42.3 L s^{-1} m^{-2} and was therefore considered to be pervious. 20 mm aggregate became saturated at 0.228 wt%. Steel slag was composed of neosilicate / pyroxene-group minerals and the metallic phases.

6 mm The 6 mm aggregate slag used in this study was a dark to light grey material. It had been mechanically sorted to only include the 6 mm grain size fraction and was therefore very well sorted. The aggregate was sub-angular and displayed a low sphericity and varied in internal porosity. As an aggregate heap, the material displayed a porosity of 48.2%. A 50 cm high column of 6 mm aggregate slag displayed a vertical hydraulic conductivity of 14.2 L s^{-1} m^{-2} and was therefore considered to be pervious. When weathered, this was reduced to 7.5 L s^{-1} m^{-2} which was therefore also considered to be pervious. 6 mm aggregate became saturated at 0.394wt%. Steel slag is composed of nesosilicate / pyroxene-group minerals and the metallic phases.

Dust -Dust is a dark to light brown fine grained material. It displayed a porosity of 36.1%. Dust became saturated at 12.84wt%. Dust was predominately composed of neosilicate and pyroxene-group minerals with a minor proportion of metallic phases.

Overall Reactivity of the Steel Slag Products The aggregate slags displayed coarser grain sizes and higher contents of metallic iron and are likely to be less reactive than the Dust which has a smaller grain size and a higher content of neosilicate and pyroxene-group minerals.

2.9.2 Pellite

The Pellite used in this study was a white to creamy-yellow pumicious material. It gave off a sulphurous smell when damp. The grains ranged from 20 mm to sub-32µm size and the material was poorly-sorted. The grains were heavily vesicular and displayed a porosity of 15.3%. Pellite became saturated at 10.21 wt%, indicating that the material was able to hold water thus allowing carbonation over a large surface area. Pellite displayed high CaO (39.76%), SiO_2 (35.73%) contents with significant amounts of Al_2O_3 (12.54%) and MgO (8.6%). Its mineralogy is dominated by pyroxene group minerals, metallic-alumnides and feldspar affinity minerals. Due to the presence of pyroxenes and a low metallic content Pellite may be readily carbonateable.

2.9.3 GBFS

GBFS used in this study was a glassy golden-coloured material. It was fine to very fine grained and poorly sorted. GBFS was dominantly composed of glassy shards and displayed a porosity of 49.2%. GBFS became saturated at 7.32 wt%. GBFS displayed high CaO (39.87%), SiO_2 (37.89%) contents with significant amounts of Al_2O_3 (12.61%) and MgO (7.22%). Its mineralogy is dominated by quartz and alumno-silicate minerals. The mineralogy and physical texture of GBFS would suggest that it may not be easily carbonateable.

Chapter 3:

The Chemical Basis for the Carbonation Potential of Slag and a Theoretical Chemical Model to predict how this may occur

3.1 Introduction

Efficient carbonation of materials depends upon two physical processes: Firstly, the reactant material must be energetically unstable under the conditions into which it has been placed and therefore is 'carbonateable' and secondly, the CO_2 present in the reaction environment must be in a form which makes it available for reaction with the material.

Throughout this chapter the following abbreviations for later experimental conditions are used:

Pressure: Lp – 10 bar CO_2 pressure, Hp – 100 bar CO_2 pressure.

Temperature: Lt – 25˚C, Ht – 125˚C.

Water Availability: Ls – 15 wt. % saturated, Hs – excess water used.

3.1.1 Reactant Materials

A wide variety of minerals display negative Gibbs free energies (ΔGf [kJ mol^{-1}]) upon carbonation. This indicates that the carbonation reaction is 'spontaneous' which means that the reaction will take place without any external 'forcing' being required. A negative Gibbs free energy value not only gives an indication of the potential reactivity of the mineral, but also shows that the reaction will be exothermic. The heat given off may well play a part in the reaction - most likely through increasing the reaction rate. The Gibbs free energy values for the carbonation of several selected minerals present within the slag products described in Chapter 2 are shown in Table 3.1:

Mineral	Formula	Occurrence	Carbonation Reaction	ΔGf (kJ mol^{-1})
Larnite	Ca_2SiO_4	cement clinker	$Ca_2SiO_4 + 2H_2CO_3 \rightarrow 2CaCO_3 + H_4SiO_4$	-127.2
Forsterite	Mg_2SiO_4	basic rocks; slag	$Mg_2SiO_4 + 2H_2CO_3 \rightarrow 2MgCO_3 + H_4SiO_4$	-66.8
Wollastonite	$CaSiO_3$	metamorphic rocks	$CaSiO_3 + H_2CO_3 + H_2O \rightarrow CaCO_3 + H_4SiO_4$	-27.0
Diopside	$CaMgSi_2O_6$	basic rocks	$CaMgSi_2O_6 + 2H_2CO_3 + 2H_2O \leftrightarrows CaCO_3 + MgCO_3 + 2H_4SiO_4$	-26.2
Enstatite	$MgSiO_3$	basic rocks	$MgSiO_3 + H_2CO_3 + H_2O \rightarrow MgCO_3 + H_4SiO_4$	0.14
Portlandite	$Ca(OH)_2$	Portland cement	$Ca(OH)_2 + H_2CO_3 \rightarrow CaCO_3 + 2H_2O$	-81.5

Table 3.1 – Gibbs free energies of carbonation, after Renforth et al. (2011)

The minerals in Table 3.1 represent three of the major minerals present within the slag products: **Olivine** (larnite, forsterite), **Pyroxene** (wollastionite, diopside, enstatite) and **Hydroxide** minerals (portlandite). As observed in Chapter 2, there can be departures from these pure mineral formulae in

the form of solid solutions. However, the ΔGf values can be taken as being representative of the wider mineral family.

3.1.2 Carbonation Source

The intention of this project is to sequester CO_2 in mineral form by utilising the reactivity of aqueous carbonate ions. These ions are formed when $CO_{2(g)}$ dissolves into $H_2O_{(l)}$ and subsequently disassociates along the following reaction pathways (Reaction 3.1):

$$CO_{2\ (g)} + H_2O_{\ (l)} \leftrightarrows CO_{2\ (aq)} + H_2O_{\ (l)}$$

$$CO_{2\ (aq)} + H_2O_{\ (l)} \leftrightarrows H^+_{\ (aq)}) + HCO_3^-{}_{\ (aq)}$$

$$H_2CO_{3\ (aq)}) \leftrightarrows H^+_{\ (aq)} + HCO_3^-{}_{\ (aq)}$$

$$HCO_3^-{}_{\ (aq)} \leftrightarrows H^+_{\ (aq)} + CO_3^{2-}{}_{\ (aq)}$$

Reaction 3.1

This reaction can be simplified as shown in Reaction 3.2:

$$CO_{2(g/l/sc)}) + H_2O_{(l)} \leftrightarrows H_2CO_{3(aq)} \leftrightarrows 2H^+_{\ (aq)} + CO_3^{2-}{}_{\ (aq)}$$

Reaction 3.2

The position of the equilibrium in Reaction 3.2 is moved to the right by an amount dependent upon the partial pressure of CO_2 available in the reaction. The molar concentration of CO_2 present under the different experimental conditions can be theoretically modelled by calculating the partial pressure of CO_2 in each experiment and then dividing this by the appropriate Henry's Constant.

3.1.3 Reaction Pathways

The next stage in the carbonation of the samples after CO_2 dissolution and the production of $HCO_3^-{}_{(aq)}$ or $CO_3^{-2}{}_{(aq)}$ ions is the reaction of these ions with a suitable metal cation (M^+) to produce a stable carbonate phase. These metal cations are made available by the metals or minerals present within the slag samples either by their dissolution into the water which surrounds them (Reaction 3.3) or via a surface reaction between the HCO_3^- ions and the mineral (Reaction 3.4).

$$M_{(s)} \leftrightarrows M^+_{(aq)} + HCO_3^-{}_{\ (aq)} + H^+_{(aq)} \leftrightarrows MCO_{3(aq/s)} + 2H^+_{\ (aq)}$$

Reaction 3.3

$$M_{(s)} + HCO_3^-{}_{\ (aq)} + H^+_{(aq)} \leftrightarrows MCO_{3(aq/s)} + 2H^+_{(aq)}$$

Reaction 3.4

It may be assumed that if carbonate is produced via reaction 3.2, then a greater amount of carbonate could be produced by this reaction than via reaction 3.3. This is because in surface reactions, the surface area available for reaction is reduced as insoluble carbonate is precipitated onto mineral surface thereby terminating the reaction unless a stable reaction front with sufficient porosity can be created (Pollok et al. 2011). If an unstable reaction front is produced, then it is preferable to remove the carbonate-saturated fluid or precipitate the carbonate elsewhere in order to preserve the dissolution surface as opposed to allowing the sample surfaces to become covered by the precipitated carbonate minerals.

3.1.3 Modelling Method

Initial Conditions

The conditions investigated by this study ranged from 1 bar to 100 bar CO_2 pressure and utilised temperatures of 25˚C to 125˚C (Table 3.2), under controlled experimental conditions. The lower end of this temperature range (25˚C) was used as the standard temperature at atmospheric conditions. Realistically, the environmental temperature at the Redcar site fluctuated between a minimum of -8˚C and a maximum of 28˚C. Chapter 4 will detail a passive weathering study where the sample material was left to react at environmental conditions of 1 bar atmospheric pressure (atmospheric CO_2 is currently ≈400ppm concentration – NOAA 2015) and temperatures between -8˚C to 28˚C. Chapter 5 and 7 will detail active reaction of sample material with CO_2 at set pressures of 10 bar to 100 bar CO_2 pressure and temperatures of 25˚C to 125˚C. Additionally, Chapter 5 will investigate the importance of water in the carbonation system by varying the amount of water available to the reactions. This will also inform the water availabilities used in Chapter 7.

P – bar	T (˚C)	*Chapter*	*Code*	P (Pa)	V (m^3)	T (K)
1	25	*4*	*r.t.p.*	100,000	NA	297.15
10	25	*5*	*LpLt*	1,000,000	0.00375	297.15
10	125	*5*	*LpHt*	1,000,000	0.00375	397.15
100	25	*5*	*HpLt*	10,000,000	0.00375	297.15
100	125	*5*	*HpHt*	10,000,000	0.00375	397.15

Table 3.2: Reaction conditions for the studies in Chapters 4-5.

Partial Pressure Calculations

Partial pressure for each set of conditions was calculated using Equation 3.1:

$$P_{P\,CO_2} = \frac{Mol\ of\ CO_2}{Total\ Mol\ of\ Gas} \times Total\ Pressure$$

Equation 3.1

For atmospheric pressure, a value of 400ppm (NOAA 2015) was used for the concentration of CO_2 within the 100 M of theoretical atmosphere used to calculate the partial pressure. For all other conditions, industrial-grade CO_2 will be the only gas present within the active reaction vessel and the effects of steam will be suppressed due to the higher than atmospheric pressure retaining H_2O as a liquid phase. Therefore, the partial pressure of CO_2 will be equal to the pressure conditions of the experiment. This is shown in Table 3.3:

	P (Pa)	p CO_2 (Pa)
r.t.p.	100,000	40
LpLt	1,000,000	1,000,000
LpHt	1,000,000	1,000,000
HpLt	10,000,000	10,000,000
HpHt	10,000,000	10,000,000

Table 3.3: Partial pressure of CO_2 under each set of experimental conditions.

Henry's Constant (K)

Henry's Constant is found within Henry's Law (Equation 3.2) which describes the equilibrium between vapour and liquid:

$$Pp_{CO2} = K \cdot XCO_2$$

Pp_{CO2} – Partial pressure of CO_2 (Pa)
K – Henry's Constant (Pa)
XCO_2 – Equilibrium Mole fraction in the liquid phase

Equation 3.2

The solubility of CO_2 is temperature dependent. However, this factor can be taken into account by using the Krichevsky-Kasarnovsky Equation, a modified version of Henry's Law. This can be used to model the CO_2-H_2O system below 100˚C (Carroll et al. 1992). The range of Henry's Constant with varying temperature and pressure is shown in Figure 3.1. The values above 100˚C are still applicable to liquid water as H_2O remains within the liquid phase at these pressures.

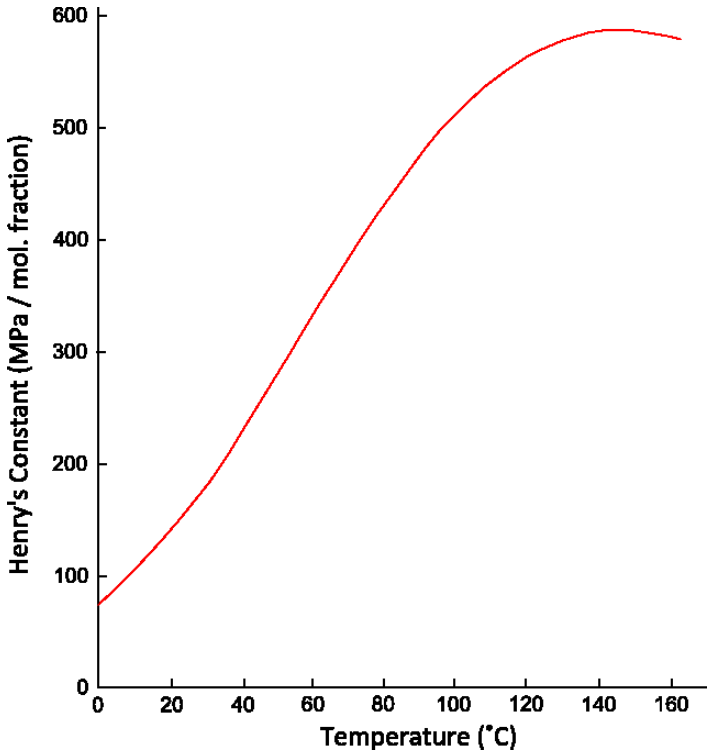

Figure 3.1: Henry's Constant for Carbon Dioxide in Water - from Carroll et al. (1992) and references therein.

From the data from Carroll et al. (1992) the following Henrys Constants were derived (Table 3.4).

	P (Pa)	T (˚K)	Henry's K (MPa)
r.t.p.	100,000	297.15	164.5
LpLt	1,000,000	297.15	164.5
LpHt	1,000,000	397.15	558.1
HpLt	10,000,000	297.15	164.5
HpHt	10,000,000	397.15	558.1

Table 3.4: Henry's Constants for each set of experimental conditions.

CO_2 Mole Fraction

The CO_2 Mole fraction present within the water is calculated using Equation 3.3.

$$\mathrm{CO_2 Mole\ Fraction} = \frac{\mathrm{P_{pCO2}}}{\mathrm{K}}$$

CO_2 Mole Fraction (Mpa)
Pp_{CO2} – Partial pressure of CO_2 (MPa)
K – Henry's Constant (MPa)

Equation 3.3

The calculated results of Equation 3.3 are listed in Table 3.5.

	p CO_2 (MPa)	Henry's K	CO_2 Mole fraction
r.t.p.	$3.14x10^{-5}$	164.5	$2.43x10^{-7}$
LpLt	1	164.5	0.00608
LpHt	1	558.1	0.00179
HpLt	10	164.5	0.06079
HpHt	10	558.1	0.01792

Table 3.5: CO_2 Mole fraction within $H_2O_{(l)}$ for each set of experimental conditions considered in this thesis.

Molar Concentration of CO_2

To calculate the molar concentration of CO_2 the molar density of H_2O must also be calculated (Equation 3.4). This is because the molar CO_2 concentration is dependent upon the temperature conditions due to the expansion of H_2O. The expansion coefficient of H_2O at 25˚C is $2.57\ x10^{-4}\ K^{-1}$ and at 125˚C is $8.60x10^{-4}\ K^{-1}$ (engineeringtoolbox.com).

$$\rho = \rho_0 \div (1 + \beta\,(t_1 - t_0)) \div (1 - \frac{(P_1 - P_{0)}}{E})$$

ρ = Density of H_20 at conditions P/T (Kg m^{-3})
ρ0 = Density of water at 0°C (i.e. 999.8 Kg m^{-3})
β = Expansion coefficient of H_2O at a given temperature
T1 = Temperature of experimental conditions
T0 = Temperature at 0°C (i.e. 0°C)
P1 = Pressure of experimental conditions
P0 = Atmospheric Pressure (i.e. 100000 Pa)
E = Bulk Modulus of Water

Equation 3.4

The values obtained are reported in Table 3.6.

	CO_2 Mole fraction	Density of H_2O (kg m^{-3})	Molar Density of H_20 (mol dm^{-3})
r.t.p.	$2.43x10^{-7}$	993.417	55.129
LpLt	0.00608	993.833	55.152
LpHt	0.00179	903.132	50.118
HpLt	0.06079	998.013	55.384
HpHt	0.01792	906.930	50.329

Table 3.6 – Density of H_2O and Molar Density of H_2O at different conditions

Using the molar density of H_2O, the CO_2 concentration can now be calculated using Equation 3.5. The results are reported in Table 3.7.

$$\mathrm{CO_2\ Concentration} = \mathrm{XCO_2} \times \boldsymbol{\rho}_{\mathrm{H_2O}}$$

CO_2 Concentration (mol dm^{-3})
XCO_2 – CO_2 Mole Fraction (MPa)
ρ_{H2O} – Molar density of H_2O

Equation 3.5

	CO_2 mol fraction	Molar Density of H_20	CO_2 Concentration	
r.t.p.	$2.43x10^{-7}$	55.1286	$1.34x10^{-5}$	mol dm^{-3}
LpLt	0.00608	55.1517	0.3352	mol dm^{-3}
LpHt	0.00179	50.1183	0.0898	mol dm^{-3}
HpLt	0.06079	55.3836	3.3678	mol dm^{-3}
HpHt	0.01792	50.3291	0.9018	mol dm^{-3}

Table 3.7: Calculation of CO_2 concentration within the reaction fluid

The theoretical capacity for CO_2 concentration within the fluid surrounding the samples is subject to two physical laws. As the p_{CO2} increases, so does the CO_2 concentration within water, but as temperature increases the capacity for the water to hold dissolved gasses decreases resulting in a decrease in CO_2 concentrations. In both cases the fluid within the batch experiments will display a CO_2 concentration many times higher than that possible during passive atmospheric weathering.

3.1.4 Theoretical Determination of pH

The pH of the solution is determined by the extent of both the formation of and the disassociation of $H_2CO_{3(aq)}$ into $2H^+_{(aq)}$ and $CO_3^{2-}{}_{(aq)}$ (Reaction 3.2). The extent of this disassociation, and hence the pH of the liquid distilled-$H_2O_{(l)}$ (which is assumed to be the only phase present), can be calculated via Equations 3.6, 3.7, 3.8 and 3.9. When CO_2 dissolves into H_2O it produces $H_2CO_{3(aq)}$. The concentrations of this species can be calculated using Equation 3.6 using the value of K_a as 1.7 x 10^{-3} mol dm^{-3}:

$$K_a = \frac{[H_2CO_3]}{[CO_2]}$$

K_a – Acid dissociation constant
$[H_2CO_3]$ - Concentration of H_2CO_3 (mol dm^{-3})
$[CO_2]$ - Concentration of CO_2 (mol dm^{-3})

Equation 3.6

When H_2CO_3 dissociates it produces H^+ and HCO_3^-. The concentrations of these species can be calculated using Equation 3.6 using the K_a of 2.5 x 10^{-4} mol dm^{-3}:

$$K_a = \frac{[H^+]\,[HCO_3^-]}{[H_2CO_3]}$$

K_a – Acid dissociation constant
$[H^+]$ – Concentration of H^+ (mol dm^{-3})
$[HCO_3^-]$ - Concentration of HCO_3^- (mol dm^{-3})
$[H_2CO_3]$ - Concentration of H_2CO_3 (mol dm^{-3})

Equation 3.7

As H^+ and CO_2 are related Equation 3.6 becomes Equation 3.8 using a disassociation constant of 4.47 x 10^{-7}:

$$K_a = \frac{[H^+]^2}{[CO_2]}$$

K_a – Acid dissociation constant
$[H^+]$ – Concentration of H^+ (mol dm^{-3})
$[CO_2]$ - Concentration of CO_2 (mol dm^{-3})

Equation 3.8

These disassociations result in a change in the pH of the distilled-water surrounding the sample, which can be calculated using Equation 3.9 using the results from Equation 3.8:

$$pH = -\log_{10} [H^+]$$

$[H^+]$ – Concentration of H^+ (mol dm^{-3})

Equation 3.9

These calculations allow the behaviour of the elements within the solution to be predicated using Eh-pH diagrams (section 3.2). The pH values and theoretical dissolved carbonate ions are also of use for understanding the extent of reaction which may occur under the various conditions (Table 3.8). These values can also be used to understand the percentage of each carbonate species present within the solution by using a Bjerrum plot of the stability of each carbonate species.

	CO_2 Concentration (mol dm^{-3})	$[H_2CO_3(aq)]$ mol dm^{-3}	$[HCO_3^-]$ mol dm^{-3}	pH
r.t.p.	1.34×10^{-5}	2.28×10^{-8}	5.70×10^{-12}	5.61
LpLt	0.335	5.70×10^{-4}	1.42×10^{-7}	3.41
LpHt	0.097	1.66×10^{-4}	4.14×10^{-8}	3.68
HpLt	3.367	5.72×10^{-3}	1.43×10^{-6}	2.91
HpHt	0.978	1.66×10^{-3}	4.16×10^{-7}	3.18

Table 3.8: Calculated pH of the reaction fluid.

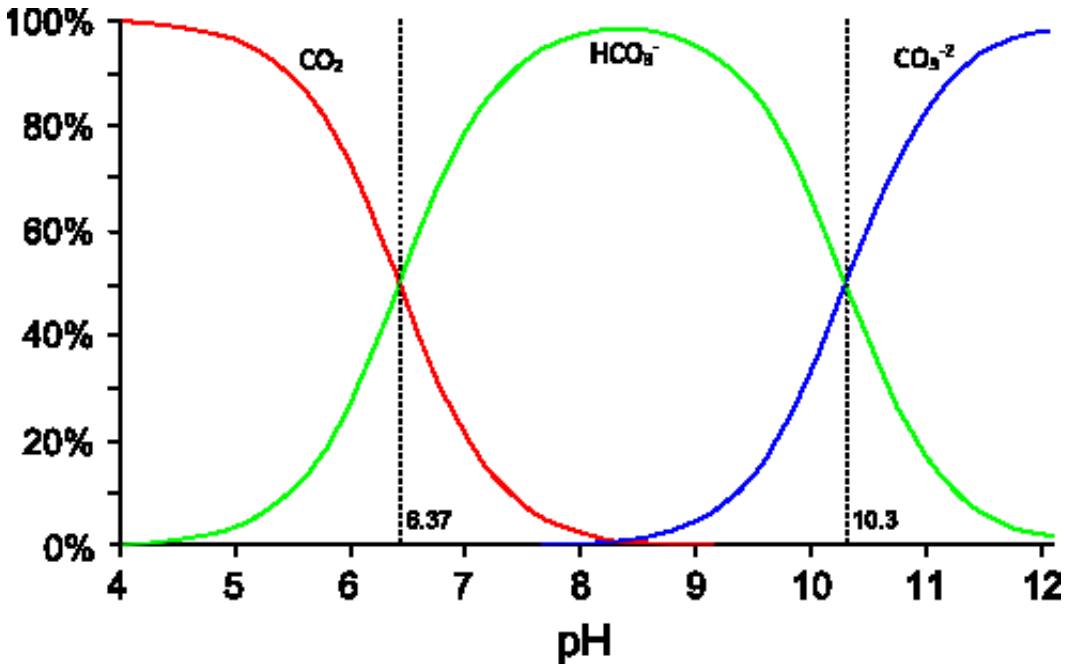

Figure 3.2: Bjerrum plot of the distribution of each carbonate species within a solution of a given pH.

Plotting the calculated pH values for each experiment onto Figure 3.2 enables the proportions of each carbonate species within the fluid surrounding the samples to be estimated. These proportions are reported in Table 3.9.

		% Species		
	pH	CO_2	HCO_3^-	CO_3^{-2}
LpLt	3.41	100	0	0
LpHt	3.68	100	0	0
HpLt	2.91	100	0	0
HpHt	3.18	100	0	0
r.t.p.	5.61	83	17	0

Table 3.9: Proportions of each carbonate species available to react at equilibrium conditions.

3.2 Dissolution of Reaction Material and Activity Diagrams

In terms of chemical reactions, the whole system can be visualised as an electro chemical cell (Fig. 3.3). The anode consists of the sample of slag which provides positive ions to the system for carbonation. The cathode is created through the dissolution of CO_2 into the H_2O surrounding the sample. This process disassociates the water to provide not only the CO_3^{2-} ions (the electron donors in this system) but also the pH conditions (as calculated above) which determine the stability of CO_2-HCO_3—CO_3^{2-} within the solution. The H_2O is treated as a medium into which all available ions can diffuse.

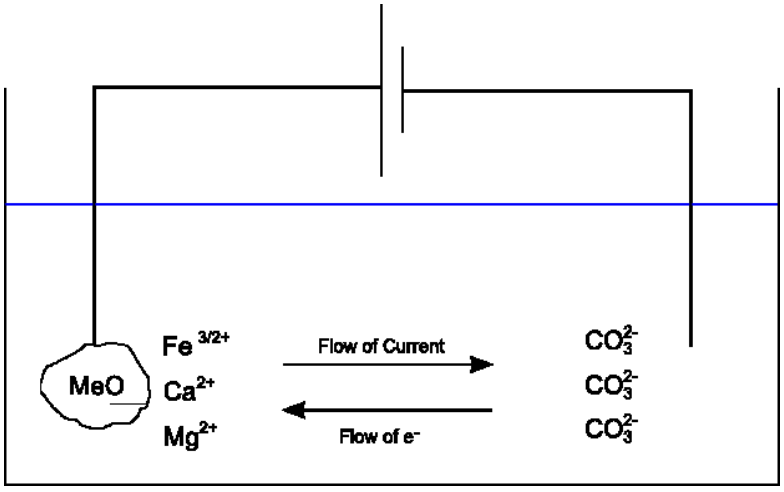

Figure 3.3: Electro-chemical cell model of carbonation.

Individual elements and minerals will dissolve into the fluid surrounding the samples if they are unstable in relation to the Eh-pH conditions of the fluid. However, while the reaction rate of a monophase-material with CO_3^{2-} ions is easily predicted, the overall reactivity within polyphase systems is dictated not only by the dissolution of the different minerals, but also by the ratios of the different minerals present within the system along with other factors such as the physical shape of the material (including its grain size) and the porosity and permeability characteristics of the material. The combination of these factors is complex to model. However, a brief chemical model will be outlined below in the form of Eh-Ph diagrams. These diagrams were calculated using Geochmists Workbench V11 with each element modelled (Ca, Fe, Mg, Mn, P, S) using an activity of 1, H_2O activity as 1, $CO_{2(g)}$ ⇆ HCO_3^- fugacity as 1 and the temperature and pressure conditions of each experiment in ˚C and bars respectively.

3.2.1 Calcium

The speciation of dissolved calcium within the system of Ca-C-O-H is shown in Figure 3.4. There is little difference between the phase diagrams, with organic Ca-compounds potentially being stable across a wider field at lower temperatures. Depending on the pH of the reaction liquid $CaCO_3$ can be considered stable even under acidic conditions.

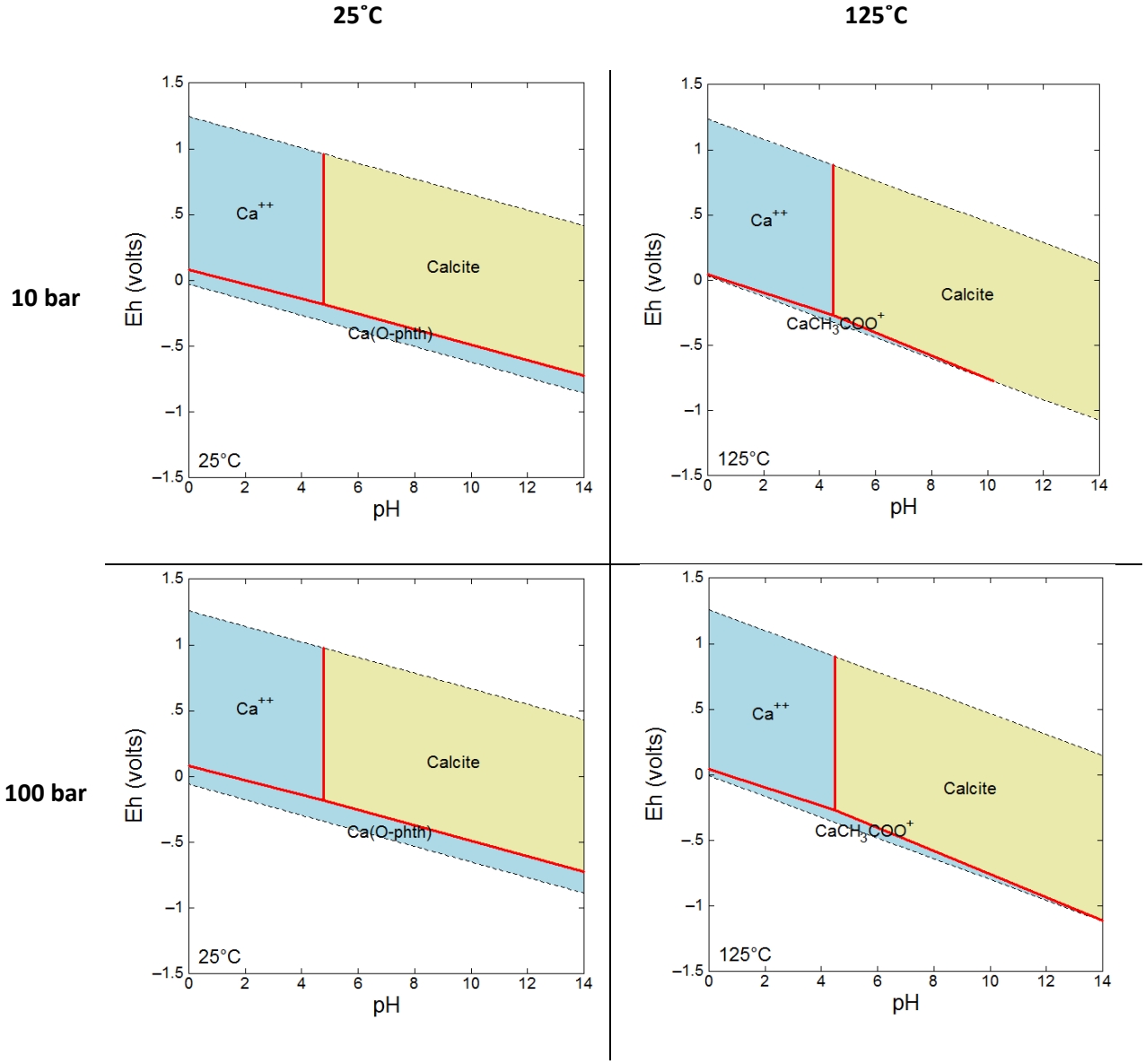

Figure 3.4: Eh-pH diagram for the system Ca-C-O-H

3.2.2 Iron

The speciation of dissolved iron within the system of Fe-C-O-H is shown in Figure 3.5. Iron within the system is capable of forming siderite, but the majority of the field is taken up by haematite. Under higher temperatures siderite will form at a lower Eh than at lower temperatures, but there is the possibility of forming organic Fe-compounds which may trap carbon within them.

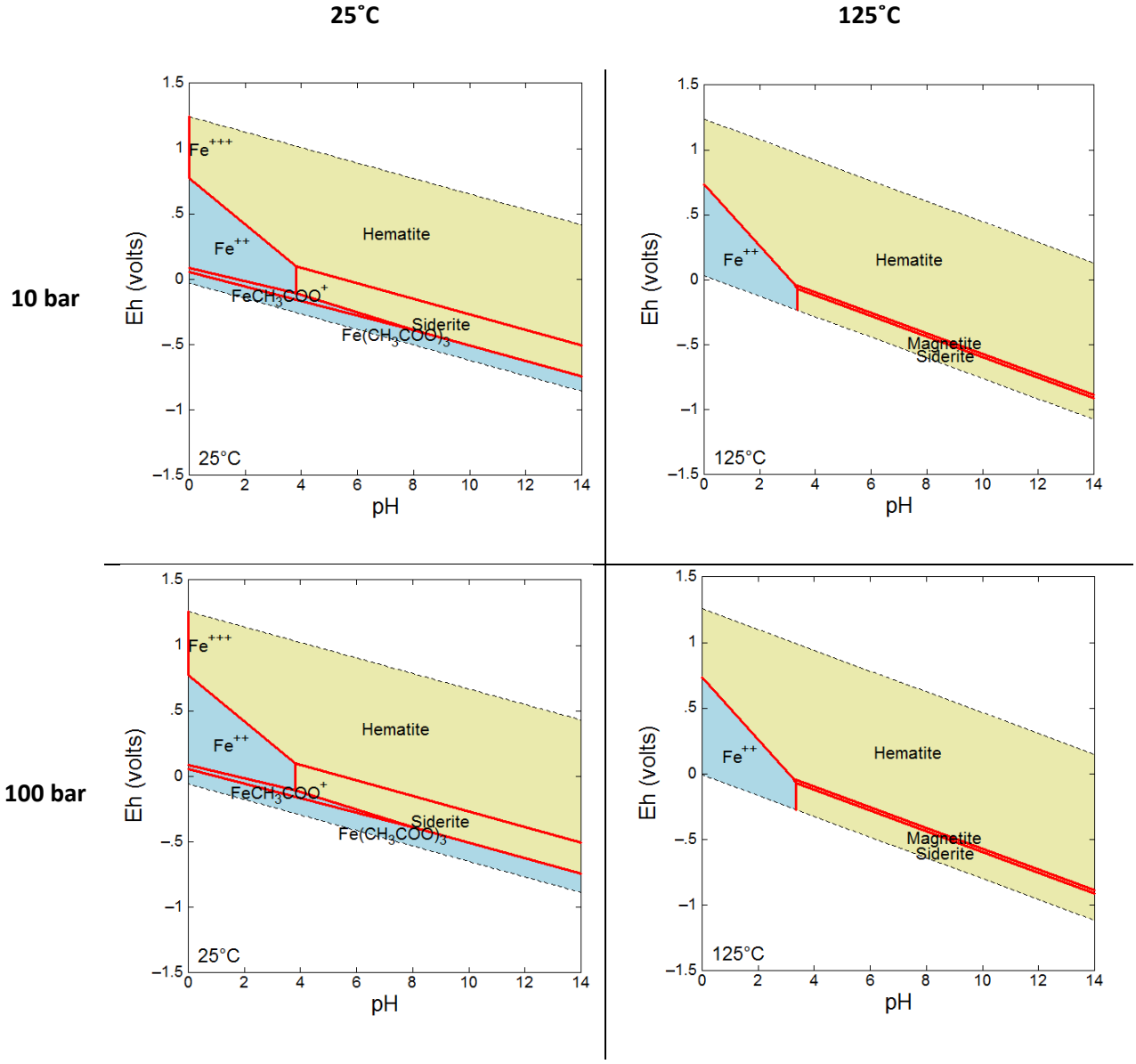

Figure 3.5: Eh-pH diagram for the system Fe-C-O-H

3.2.3 Magnesium

The speciation of dissolved magnesium within the system of Mg-C-O-H is shown in Figure 3.6. Magnesium within the system is capable of forming either Mg^{2+} ions or $MgCO_3$ (magnesite). There is a limited field for organic Mg-bearing compounds to form at low Eh values at low temperature.

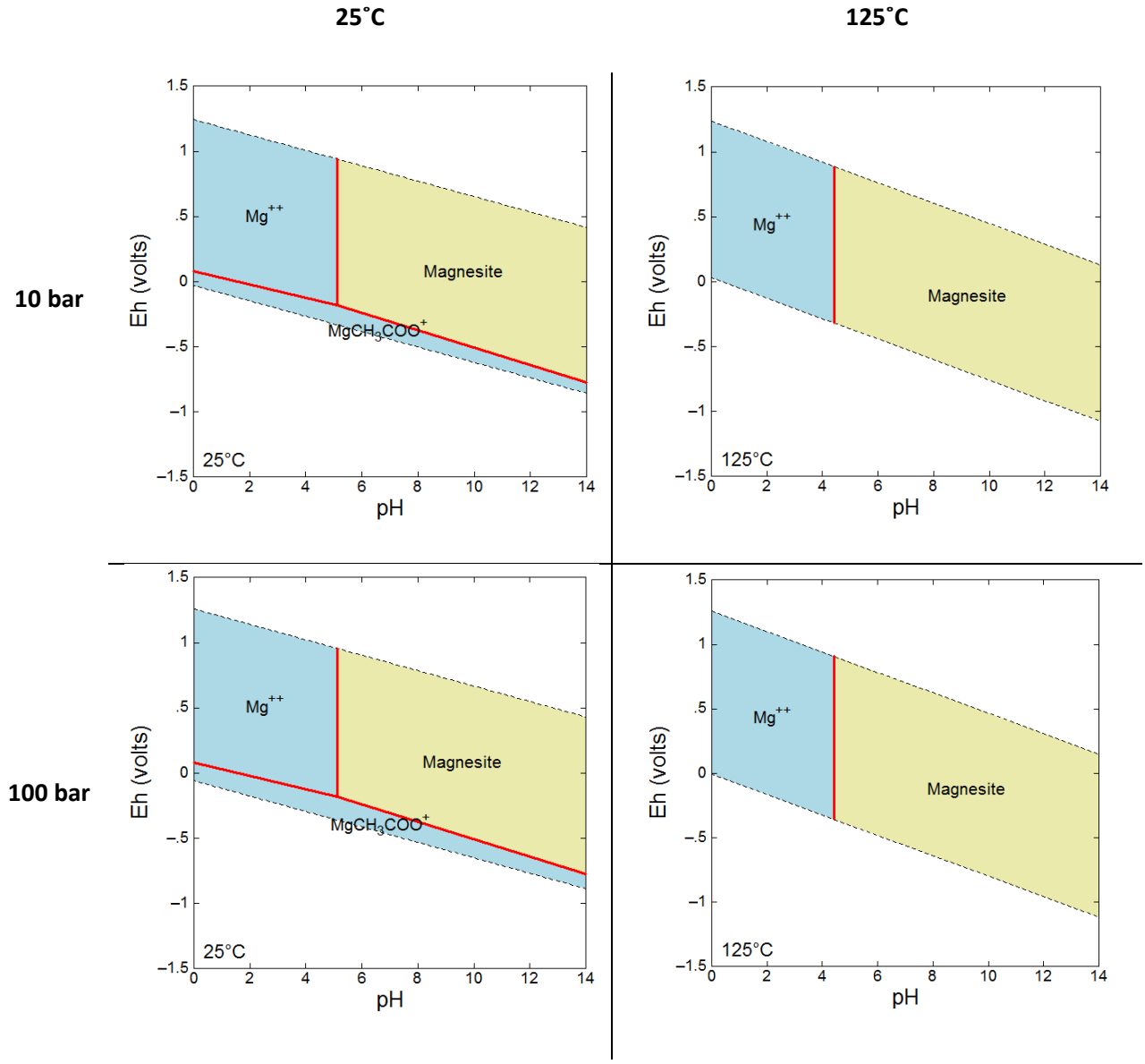

Figure 3.6: Eh-pH diagram for the system Mg-C-O-H

3.2.4 Manganese

Dissolved manganese within the system of Mn-C-O-H is shown in Figure 3.7. Manganese within the system will readily form $MnCO_3$ (rhodochrosite) across a large range of Eh and pH. At higher temperatures Mn_2O_3 (bixbyite) will form. Mn is present within the samples at concentrations of less than 4% and may take part in the fluid reactions to produce minor amounts of rhodochrosite.

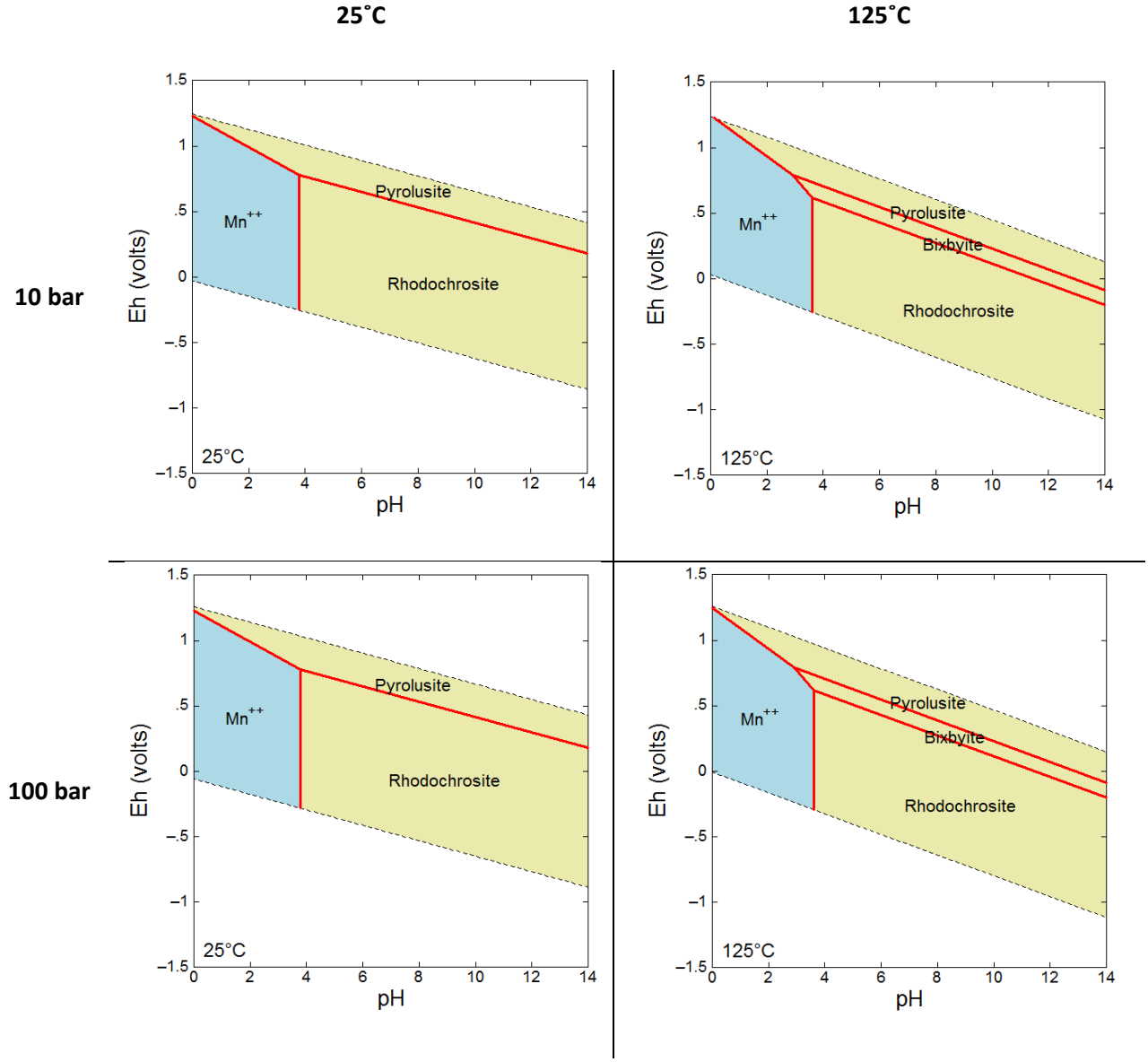

Figure 3.7: Eh-pH diagram for the system Mn-C-O-H

3.2.5 Phosphorus

The speciation of dissolved phosphorus within the system P-C-O-H is shown in Figure 3.8. Phosphorus is present within the samples at concentrations of less than 2% (Chapter 2.3.4) and may take part in the fluid reactions. Hydroxy-apatite may well be able to precipitate in conjunction with the high Ca^{2+} concentrations.

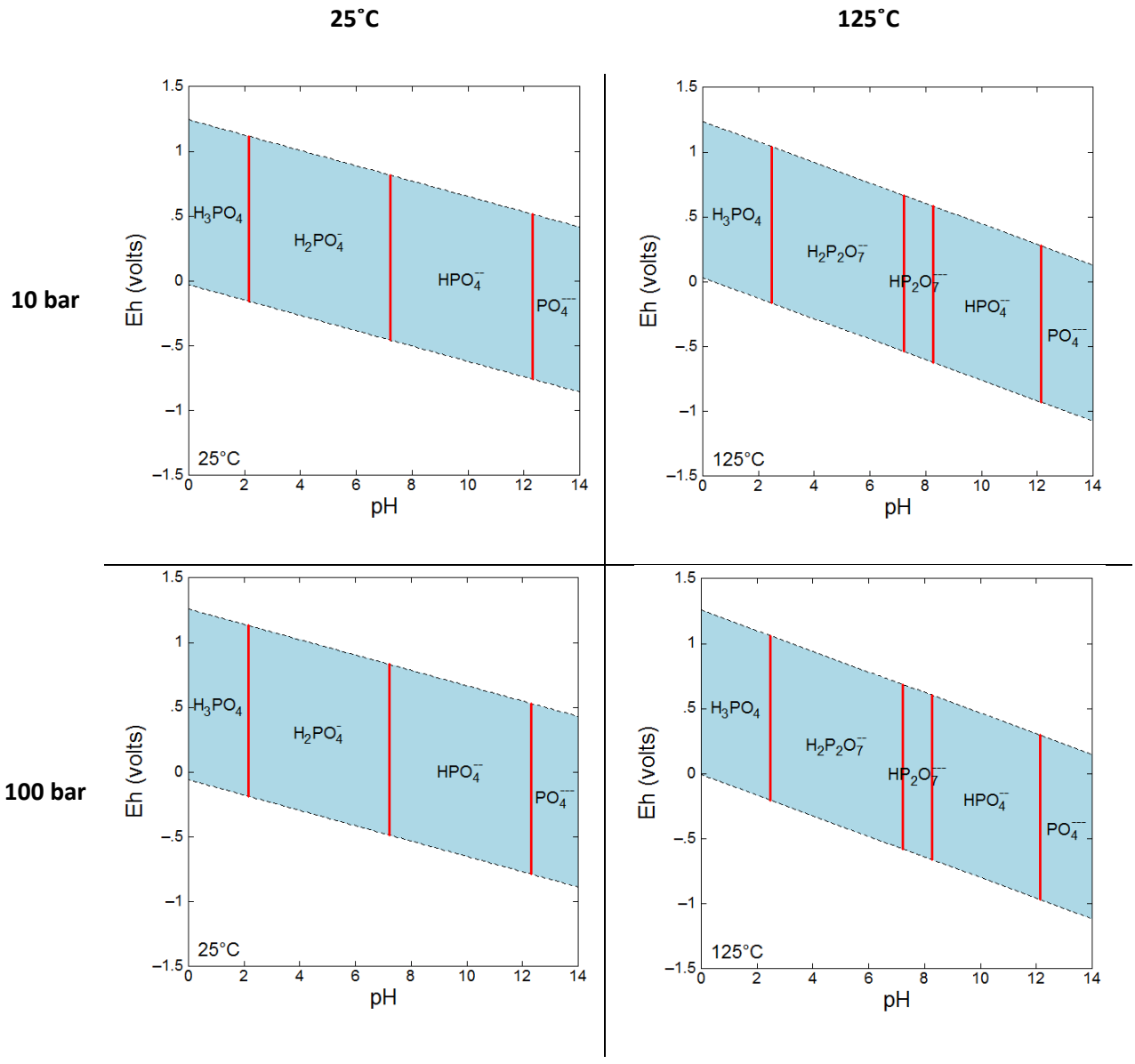

Figure 3.8: Eh-pH diagram for the system P-C-O-H

3.2.6 Sulphur

The speciation of dissolved sulphur within the system P-C-O-H is shown in Figure 3.9. Sulphur is present within the samples at concentrations of less than 0.14% in steel slag and less than 0.26% in blast furnace slag. It may take part in the fluid reactions as the SO_4^{2-} ion is stable. The behaviour of sulphur may be significant as it has the potential to 'mop up' cations to form minerals such as gypsum thus reducing the availability of Ca^{2+} to form carbonate.

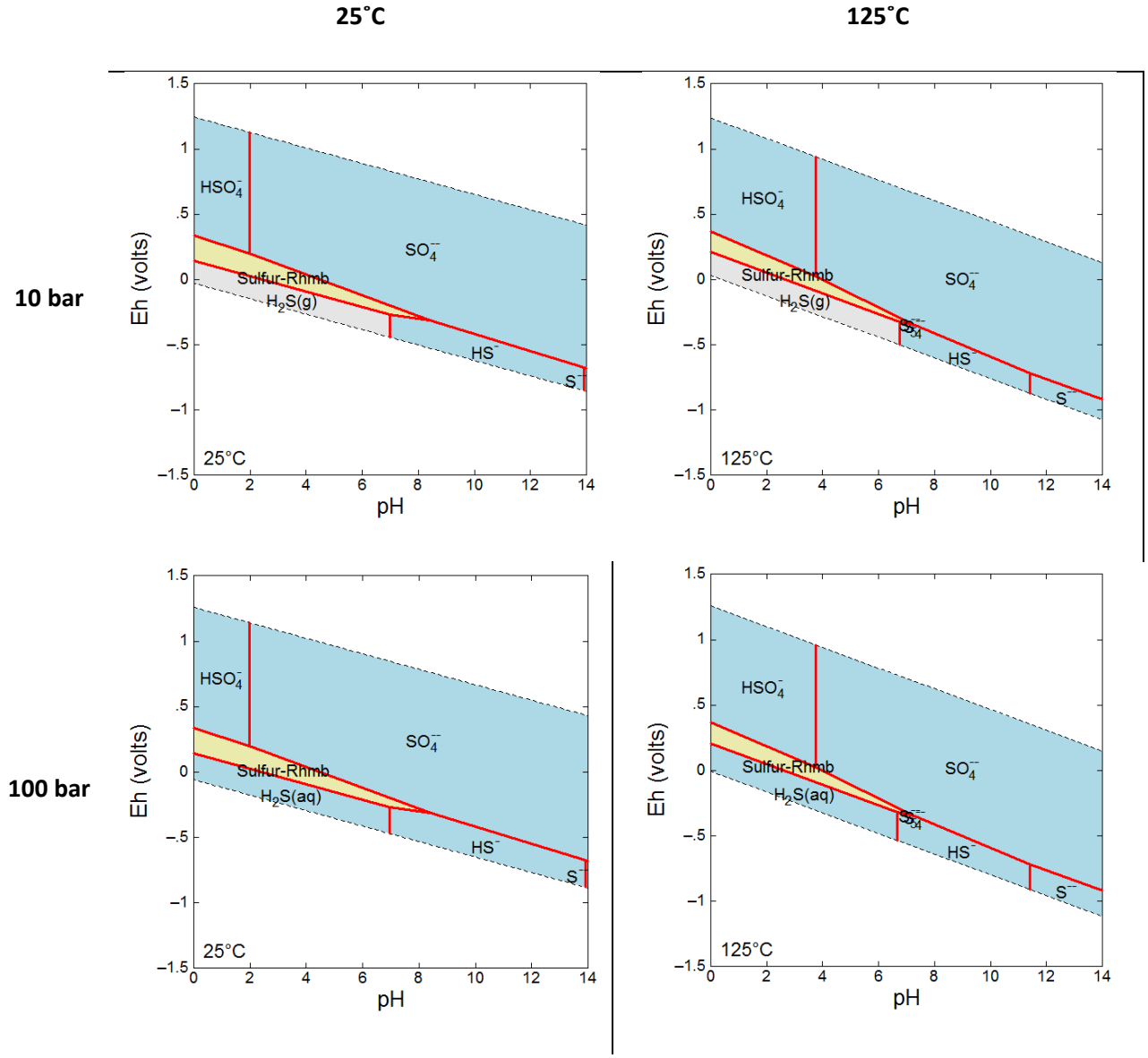

Figure 3.9: Eh-pH diagram for the system S-C-O-H

3.3 Predictions

Given an understanding of the calculated pH conditions and the Eh-pH diagrams it is possible to predict the availability of each ion to the system. Predictions about the form of each ion within each of the experiments undertaken in Chapters 4 and 5 are made below and will be used to comment upon the likely carbonate products of each experiment.

3.3.1 Passive Experiments [Chapter 4]

The calculated pH under the passive weathering conditions is 5.61 at 25°C. Under these conditions the following species are stable:

Passive	Ca	Fe	Mg	Mn	P	S
Present as:	$CaCO_3$ Ca-Carboxyl	Fe_2O_3 $FeCO_3$ Fe-Carboxyl	$MgCO_3$ Mg-Carboxyl	MnO_2 $MnCO_3$	$H_2PO_4^-$	SO_4^{2-} S $H_2S_{(g)}$

The predicted behaviour of this system is that $CaCO_3$ and $MgCO_3$ will form directly on the surface of the slag. $FeCO_3$ and $MnCO_3$ may form but it is more likely that under oxidising atmospheric conditions Fe_2O_3 and MnO_2 will be prevalent. Some phosphates and sulphides may be precipitated.

3.3.2 Active Reaction Experiments [Chapter 5]

Low Pressure - Low Temperature (10 bar / 25°C)

The calculated pH under low pressure low temperature (10 bar / 25°C) conditions is 3.41. Under these conditions the following species are stable:

LL	Ca	Fe	Mg	Mn	P	S
Present as:	Ca^{2+} Ca-Carboxyl	Fe_2O_3 Fe^{2+} Fe-Carboxyl	Mg^{2+} Mg-Carboxyl	MnO_2 Mn^{2+}	$H_2PO_4^-$	SO_4^{2-} S $H_2S_{(g)}$

The predicted behaviour of this system is that Ca, Mg, Fe and Mn carbonates may form via the disassociated metal ions reacting with carbonate species. These will be precipitated if the pH of the system is increased by the alkalinity of the slag sample. However, Fe-carbonate may form if there is a low Eh otherwise it is more likely that Fe_2O_3 will form instead. Mn-carbonate is likely to form, but MnO_2 will precipitate at high Eh. Phosphorus will be present as hydrogen phosphate ions while sulphur will still be present as sulphate ions.

Low Pressure – High Temperature (10 bar / 125°C)

The calculated pH under low pressure high temperature (10 bar / 125°C) conditions is 3.68. Under these conditions the following species are stable:

LH	Ca	Fe	Mg	Mn	P	S
Present as:	Ca^{2+} Ca-Carboxyl	Fe_2O_3 Fe_3O_4 $FeCO_3$	Mg^{2+}	MnO_2 Mn_2O_3 $MnCO_3$ Mn^{2+}	$H_2P_2O_7^-$	HSO_4^- S $H_2S_{(g)}$

The predicted behaviour of this system is that Ca and Mg carbonates may form via the disassociated metal ions reacting with carbonate species. These will be precipitated if the pH of the system is increased by the alkalinity of the slag sample. Fe_2O_3 is the most likely Fe-mineral to form, though $FeCO_3$ may form at a low Eh. Mn is close to the Mn^{2+} boundary and may form MnO_2, Mn_2O_3, $MnCO_3$ or Mn^{2+} depending upon the Eh conditions. Phosphorus will be present as dihydrogen phosphate ions while sulphur will still be present as hydrogen sulphate ions.

High Pressure - Low Temperature (100 bar / 25°C)

The calculated pH under high pressure low temperature (100 bar / 25°C) conditions is 2.91. Under these conditions the following species are stable:

HL	Ca	Fe	Mg	Mn	P	S
Present as:	Ca^{2+} Ca-Carboxyl	Fe_2O_3 Fe^{2+} Fe-Carboxyl	Mg^{2+} Mg-Carboxyl	MnO_2 Mn^{2+}	$H_2PO_4^-$	SO_4^{2-} S $H_2S_{(aq)}$

The predicted behaviour of this system is that Ca, Mg, Fe and Mn carbonates may form via the disassociated metal ions reacting with carbonate species. These will be precipitated if the pH of the system is increased by the alkalinity of the slag sample. However, Fe-carbonate may form if there is a low Eh otherwise it is more likely that Fe_2O_3 will form instead. Mn-carbonate is likely to form but MnO_2 will precipitate at high Eh. Phosphorus will be present as hydrogen phosphate ions while sulphur will still be present as sulphate ions.

High Pressure – High Temperature (100bar / 125°C)

The calculated pH under high pressure, high temperature (100bar / 125°C) conditions is 3.18. Under these conditions the following species are stable:

HH	Ca	Fe	Mg	Mn	P	S
Present as:	Ca^{2+} Ca-Carboxyl	Fe_2O_3 Fe_3O_4 $FeCO_3$	Mg^{2+}	MnO_2 Mn_2O_3 $MnCO_3$ Mn^{2+}	$H_2P_2O_7^-$	HSO_4^- S $H_2S_{(aq)}$

The predicted behaviour of this system is that Ca and Mg carbonates may form via the disassociated metal ions reacting with carbonate species. These will be precipitated if the pH of the system is increased by the alkalinity of the slag sample. Fe_2O_3 is the most likely Fe-mineral to form though $FeCO_3$ may form at a low Eh. Mn is close to the Mn^{2+} boundary and may form MnO_2, Mn_2O_3, $MnCO_3$ or Mn^{2+} depending upon the Eh conditions. Phosphorus will be present as dihydrogen phosphate ions while sulphur will still be present as hydrogen sulphate ions.

3.4 Conclusions

The concentrations of disassociated carbonate species within a reaction fluid under different experimental conditions have been calculated, together with the accompanying pH conditions within the reaction liquid which will surround the samples. These results were then used, in combination with the Eh-pH diagrams of the major elements present within the reaction system, to predict whether carbonate minerals would be formed. The conclusions of this study are briefly outlined below.

3.4.2 Carbonate Species Availability

As CO_2 displays decreasing solubility with increasing water temperature, the concentration of HCO_3^- is dependent upon both the reaction pressure conditions and the temperature of the water in which the reaction is taking place. As shown in Figure 3.10 the HCO_3^- concentration is highly variable by several orders of magnitude across the experimental conditions.

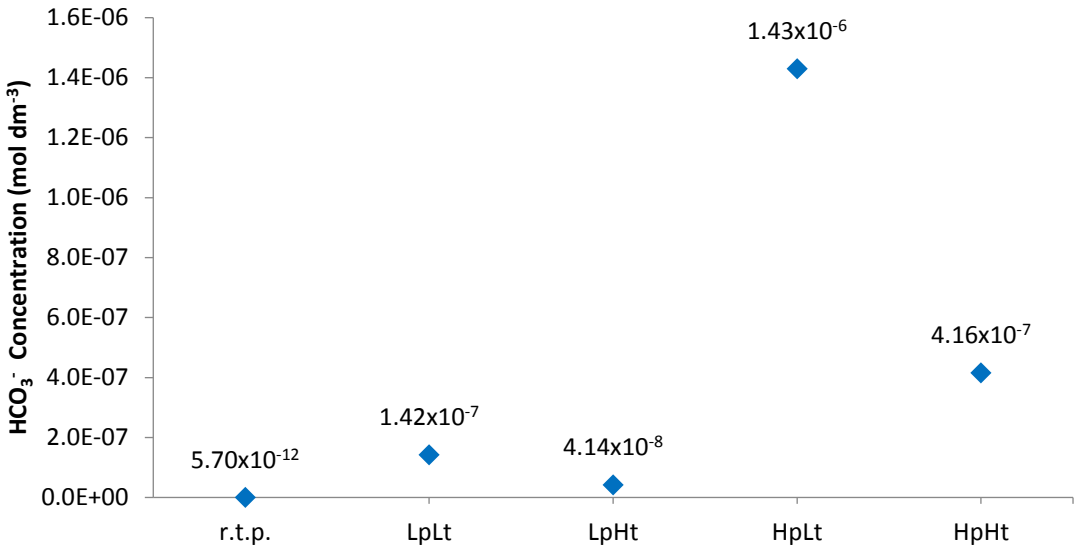

Figure 3.10: HCO_3^- (mol dm^{-3}) Concentrations under different experimental conditions.

Though passive weathering at r.t.p. appears to show the least potential for reaction due to the low concentration of HCO_3^- present, it is likely that other factors will be important in the carbonation process e.g. the length of reaction. Passive weathering experiments will be carried out over timescales three-to-four orders of magnitude greater than those of the active reaction experiments. Therefore, despite their lower reactivity they may ultimately be able to achieve higher carbonation values over the longer time period.

While it is possible that higher concentrations of HCO_3^- will result in a greater degree of material carbonation, there is also the possibility that the active reaction experiments may not reach an equilibrium point during the allotted 19 hours of reaction time. However, despite the HCO_3^- concentrations being lower at higher temperatures, the enhanced kinetics of the system may result in these lower HCO_3^- concentrations not being a reaction-limiting factor.

3.4.2 Chemical Modelling

Chemical modelling produced the following conclusions:

- While $CaCO_3$ will directly precipitate under passive conditions the pH of the active reaction experiments is too low for this to occur. However, the dissolved Ca^{2+} ions will form carbonates if the alkalinity of the reacting slag product raises the pH of the reaction liquid. Due to the presence of phosphorus and sulphur anions there is the possibility of minor amounts of gypsum forming, thereby removing Ca-ions from the system.

- Fe may form carbonate minerals. However, it is far more likely that Fe_2O_3 (haematite) will precipitate instead due to the large Eh stability field.

- While Mg will directly precipitate under passive conditions the pH of the active reaction experiments is too low for this to occur. However, the dissolved Mg^{2+} ions will form carbonates if the alkalinity of the reacting slag product raises the pH of the reaction liquid.

- Mn may form carbonate minerals via dissolved Mn^{2+} ions reacting with carbonate ion, but only if the alkalinity of the reacting slag product raises the pH of the reaction liquid. Otherwise the formation of MnO_2 is likely especially under oxidising conditions.

- P will form $H_2PO_4^-$ ions at low temperatures and $H_2P_2O_7^-$ ions at high temperatures.

- S will be predominantly present as SO_4^{2-} at low temperatures and HSO_4^- at high temperatures. At lower Eh, sulphur may precipitate as a solid or form H_2S as a gas at low pressure or as an aqueous species at high pressure.

Chapter 4:

Passive carbonation experiments – assessing the extent of carbonation within the environment

4.1 Introduction

In this chapter, the carbonation sequestration potential of different slag products will be characterised in relation to the degree of weathering achieved under the climatic conditions present at the City of Durham. Original data relating to the weathering rates of Steel Slag Aggregate of varying grain size viz. Pellite and Granulated Blast Furnace Slag (GBFS) will be presented and the differences between the various products and grain sizes assessed. The results of this study will also establish a baseline carbonation potential with which the results of future studies (Chapters 5, 6, 7) will be compared.

Weathering is a natural process involving the disintegration and breakdown of minerals which are unstable at the pressures, temperatures and oxidation states of the Earth's surface (Waugh 2000). Considering that the mineralogy of the slag samples used in this study were formed at temperatures >1000°C and under the redox conditions of a reducing blast furnace, they are likely to be unstable under the oxidising climatic conditions present at the Redcar industrial site.

The degree of weathering a material will undergo will depend upon the structure and mineral composition of the slag product; the local climate; the presence of vegetation or other organic influences and the length of time these processes have had to operate upon the material (Waugh 2000).

- Biological weathering can be ruled out for the samples used in this study as no vegetation or mosses were observed on the surface of the samples or were present on the sampled windrow heaps at the Redcar site. Only one slag-heap appeared to be covered in vegetation (a moss species). However, this heap was created pre-2011 and was not part of the study.
- Mechanical weathering is unlikely to operate in any form other than frost shattering during the period between November and February at the Redcar site due to the mild winters in the area. The main factor affecting the grain size of the material available for weathering is the mechanical grinding and sorting of the different aggregate products prior to their stockpiling into appropriate heaps.
- Chemical weathering is the factor which will be investigated in this study. As outlined in Chapter 3, CO_2 will dissolve into H_2O to produce carbonic acid. Reaction with carbonic acid

results in the breakdown of minerals within the slag and the formation of carbonate minerals. These minerals are stable in neutral to alkaline conditions over geological timescales and can, therefore, act as a viable long term carbon sink. Lafarge-Tarmac are required to weather their slag products in order to reduce their reactivity before they can be used as construction materials. The weathering is typically carried out for around six months in windrows (slag heaps). These heaps act as currently uncharacterised carbon sinks.

4.1.1 Factors effecting passive weathering

The factors which control reaction rates of the slag products are: The availability of reactants (concentration of CO_2 in the atmosphere and the reactivity of the minerals within the slag), the temperature (as determined by the environmental conditions in which the slag is present) and the physical size and morphology of the reacting materials - the majority of these factors cannot be altered in this study. The concentration of CO_2 in the atmosphere was taken to be the current mean CO_2 concentration at Mauna Loa as recorded by NOAA and, though this value is likely to fluctuate in an urban setting such as Teesside, CO_2 concentration was not considered a variable in this study. This is because it was reasonable to assume a constant concentration over time, due to the constant mixing of the atmosphere. The temperature is dependent upon the variations in the weather conditions which occurred over time at the City of Durham and at the Redcar site. Other factors, i.e. the concentration of dissociated carbonate species available for reaction with the slags, were dependent upon the uncontrolled variable of rainfall, as the reactive carbonate species are not formed under dry conditions. The main questions this study were left with were: How do different chemical and physical characteristics, as well as the grain sizes of each slag product, behave under these environmental conditions and is there a link between the variations in weather and the behaviours of the slags? These were the main variables against which the results of the study were interpreted.

Interpretation of the weathering rates demonstrated for each slag product material can be understood in terms of the factors affecting reaction rates in general. Processes which are taken to be constant, are the phases in which the reactants are present and the dissolution of CO_2 into the solvating-water. CO_2 concentration and temperature are acknowledged to be variable, but will be taken to be effectively constant. The variables taken into account for this study are the surface area effects and the mineralogy, physical morphology and crystallinity of each material that is reacting. Catalytic agents were not used in this study.

Phase Effects

The phases in which the reactants exist in, affects the ability of chemical species to react. As outlined in Chapter 2 there are two ways in which this occurs; either through aqueous carbonate species reacting with aqueous components of the slag which have dissolved into the moisture layer surrounding the slag (Reaction 3.3) or aqueous carbonate species reacting with the solid mineral surface of the slag products (Reaction 3.4). This second factor will not be dealt with during the interpretation due to a lack of data.

Solvent Effects

CO_2 dissolves into the moisture layer surrounding the slag at a constant rate, in accordance with the disassociation constants outlined in Chapter 3. The dissolution of CO_2 is inferred to occur constantly, thus maintaining the equilibrium dissolution conditions. However, no reaction can occur if the slag is dry as there is no moisture layer for the CO_2 to dissolve and disassociate into - as such the availability of moisture (via rainfall) will be taken into account at the end of the chapter.

CO_2 Concentration

The concentration of CO_2 and carbonation was calculated for 40 Pa CO_2 pressure and 25°C conditions in Chapter 3. The values for the concentrations of carbonate species and the pH under these conditions were reported in Table 4.1.

Temperature

The temperature at which a reaction occurs affects the kinetics of the reaction. The temperatures under which the study was performed varied between -1°C to 19.5°C and as such were lower than the 25°C temperature-conditions used for theoretical modelling of carbonate concentration and pH. Calculations using the method outlined in Chapter 3 were carried out to additionally model the carbonate concentrations and pH at 1°C and 20°C and were reported in Table 4.1. This shows only a slight decrease in the pH by 0.4 units. Therefore, the pH of the reactive moisture layer will be assumed to be effectively constant.

Surface Area Effects

Reactions proceed to completion at quicker rates when there is a large surface area available for reaction as opposed to a smaller surface area. Therefore, grain size was considered to be a major factor in controlling the rate of carbonation.

Materials

The mineral compositions of each material, as determined from the data acquired in Chapter 2, will be taken into account. The mineral nature of each material (glassy or fine-grained) will also be taken into consideration.

					% Species		
Temperature (°C)	CO_2 Concentration	$[H_2CO_{3(aq)}]$ mol dm^{-3}	$[HCO_3^-{}_{(aq)}]$ mol dm^{-3}	pH	$CO_{2(aq)}$	$HCO_3^-{}_{(aq)}$	$CO_3^{-2}{}_{(aq)}$
25	$1.34x10^{-5}$	$2.28x10^{-8}$	$5.70x\ 10^{-12}$	5.61	87	17	0
20	$1.58x10^{-5}$	$2.69x10^{-8}$	$6.72x10^{-12}$	5.58	87	17	0
1	$3.07x10^{-5}$	$5.22x10^{-8}$	$1.30x10^{-11}$	5.43	87	17	0

Table 4.1: Values for the carbonate concentration and the pH of the moisture layer surrounding the slag under the theoretical conditions of 25°C, and under the range of environmental conditions (1°C - 20°C)

4.1.2 Predicted Carbonation Potential

As stated in Chapter 3 [3.3.1] the calculated pH of the water surrounding the samples of slag was predicted to be pH 5.61 at 25°C. Given the nature of the oxidizing environment present the following species were predicted to be stable.

Passive	Ca	Fe	Mg	Mn	P	S
Present as:	$CaCO_3$ Ca-Carboxyl	Fe_2O_3 $FeCO_3$ Fe-Carboxyl	$MgCO_3$ Mg-Carboxyl	MnO_2 $MnCO_3$	$H_2PO_4^-$	SO_4^{2-} S $H_2S_{(g)}$

Ca, Fe, Mg, and Mn carbonates are all able to form under the pH conditions of passive weathering. As such, the materials should be carbonateable as along as metals ion are available. The concentrations of P and S in the steel slag samples used were between 1.2% to 1.6% and 0.14% to 0.22% respectively. The concentrations of P and S in the blast furnace slag samples were even lower at 0.02% to 0.24% and 0.23% to 0.27% respectively. Therefore, apatite and gypsum were unlikely to be major phases, allowing the metal ions to form carbonate rather than P- or S- minerals. Physically, all slags will allow rainwater to enter and percolate through them. Therefore, access to water should not be a limiting factor for reaction. However, GBFS was predicted to be the least reactive (due to the major presence of non-carbonateable amorphous quartz) and Dust was predicted to be the most reactive due to the range of minerals present and the small grain size of the material.

4.2 Methods

The objective of the study was to observe the passive weathering characteristics of different slag materials. To accomplish this, samples of slag were collected and left to weather under the environmental conditions at the City of Durham. Lafarge-Tarmac do not control the environmental conditions of their slag heaps and so an uncontrolled environmental experiment was chosen rather than a lab controlled study, as this would allow observations of the 'natural' weathering behaviour of the samples under normal industrial conditions.

4.2.1 Experimental Setup and Sampling

100-200 g of each sample was spread to a depth of 2 cm within plastic seed-trays (24cm by 18cm in dimension). The holes in the bottom of the trays were covered by paper-towel to allow rainwater to drain away while keeping the sample material contained within the tray. The trays were left in a semi-sheltered area outside the Department of Earth Sciences, University of Durham, City of Durham (Fig 4.1). This location was selected over Redcar due to the ease of access to the samples and also to avoid the samples being removed for industrial purposes. Durham and Redcar also have near identical environmental conditions and so the experiment would still be relevant to the Redcar site. Given that some of the steel slag aggregates had been left to weather for up to seven months before the sampling for this project was carried out, any further weathering which took place during these experiments was in addition to that which had already occurred. This would, therefore, allow the data from the experiments to be used to show a longer period of weathering and to better show the effects of weathering over time. The Pellite and GBFS had not been pre-weathered before sampling.

Figure 4.1: Samples weathering in trays under environmental conditions.

The trays were inspected twice a week and any plant material that had fallen into the trays was removed. 3-4 g of material was sampled from each of the trays on a weekly basis. Each sample was dried in a 100 cm^3 size plastic pot, which was placed into an oven at 99°C overnight. Once cooled to room-temperature, each sample was then crushed to <250 µm in size using an agate pestle and mortar

and a 250 µm-mesh-sieve with pan. Acetone was added to the Pellite and GBFS samples during crushing to reduce the sample loss via fine powder elutriation.

4.2.2 Thermo-Gravimetric Analysis

All samples were analysed using a SciMed STA i 1200 TGA with data collection carried out using Infinity Pro Software v.4.2.194 from Instrument Specialists Incorporated. A crushed sample of 350 mg (±5mg) was placed into a platinum bucket, which was suspended within the TGA on a hook attached to an electronically monitored counterbalance. The counterbalance had a nominal instrument error of ±1 µg. The sample was heated from 25˚C to 100˚C at a heating rate of 25˚C per minute in a 100 % nitrogen atmosphere within the water-cooled STA-furnace. As the temperature increased, minerals may break down resulting in the loss of H_2O or CO_2 leading to a detectable change in weight (measured in wt. %) relative to the original weight of the sample. The data was recorded via the TGA Acquire programme [4.0.1072] as a wt. % and the first derivative of the data was automatically calculated via Infinity Pro Software [Instrument Specialists Inc. v2.2.194]. Typical TGA patterns collected for each material analysed are shown in Fig. 4.2.

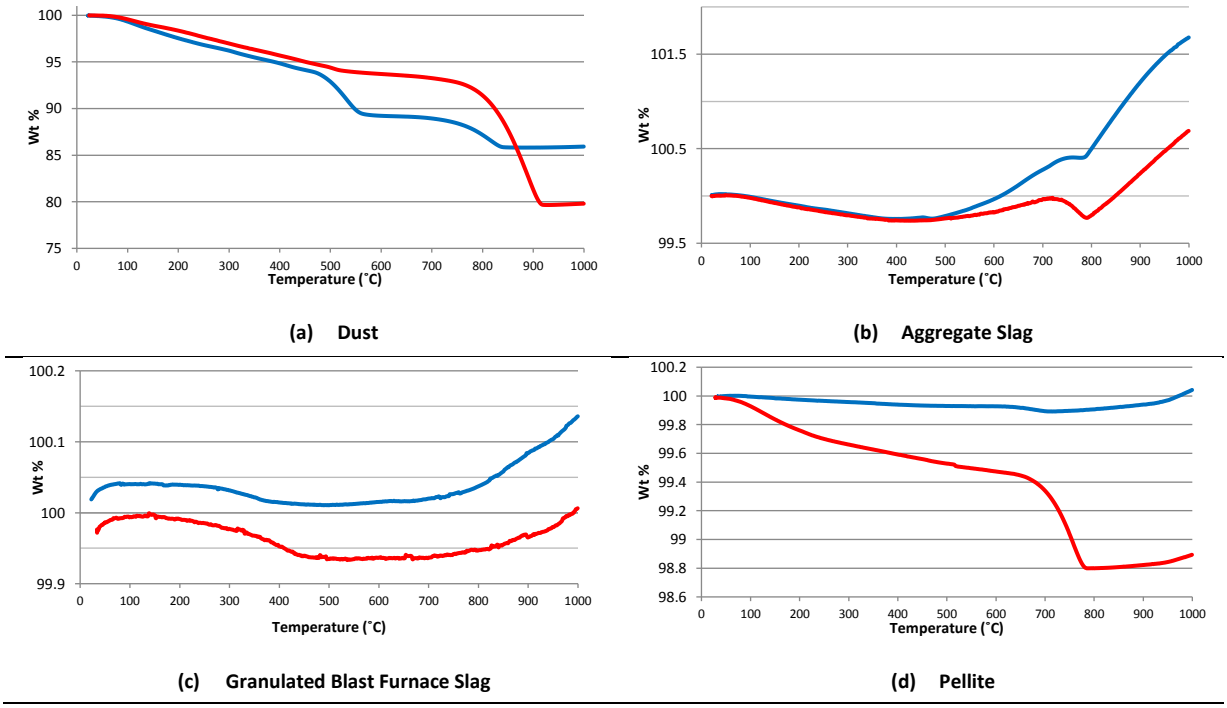

Figure 4.2: TGA graphs showing the typical profiles for the changes in weight during a TGA-run for each material examined in this study. Note differing scales on the y-axes. Weight loss at ≈500˚C is due to the breakdown of OH-bearing minerals; weight loss >700˚C is due to the breakdown of carbonate minerals. Red line – the typical profile of the greatest weight change measured. Blue line – the typical profile of the least weight change measured. a) Dust, b) Aggregate Slag (6 mm aggregate shown, but the profile is identical in shape to that of 20 mm aggregate), c) Granulated Blast Furnace Slag, d) Pellite.

Processing of TGA DATA

In order to calculate the weight loss for a sample, each TGA trace was handpicked to identify the weight loss signal from the start of the reaction beyond 625°C (Brown 1999) and the end of the reaction. The END weight was subtracted from the START weight to acquire the final weight loss in wt. %.

4.2.3 Environmental Data

An environmental data set (temperature and rainfall) was obtained from the Department of Geography, Durham University. The data were collected via an automated weather station at the Durham University Observatory, City of Durham.

4.3 Results

The general wt. % change trend of all samples involved a loss in weight up to 450˚C. Past this point different materials showed different curves. The Granulated Blast Furnace Slag (GBFS) started to show a gentle upwards curve with little to no sign of any weight loss. Pellite continued on a downward trend until ≈650˚C whereupon there was a steep weight loss followed by a gentle upwards gradient in weight gain, which then further steepened upwards past ≈950˚C. The samples of 6 mm, 10 mm and 20 mm steel slag showed a steady increase in weight up until ≈700˚C, past which there was a period of weight loss until ≈800˚C after which there was a steep weight gain. The Dust fraction, however, may or may not exhibit a weight loss at ≈500˚C depending upon the sample, followed by a typically large (on the order of several wt. %) weight loss at ≈800˚C. Above ≈900˚C there was only a minor weight increase. The final total weight loss was observed by manually picking the start and end points of the weight loss curve between ≈700-900˚C. All data are reported in Appendix 2 as wt. % loss. The plots of the data take into account the different production dates of the steel slag aggregate, by taking the date when the heap was originally created as time = 0. This allowed the weathering data collected at Durham to be plotted in relation to this time in order to give an accurate representation of the weathering achieved through time. The errors for all plots are within the size of the plotted symbol.

4.3.1 Crushed Steel Slag

Overall crushed steel slag appeared to display increasing carbonation values with time and with decreasing grain size.

20 mm Steel Slag Aggregate

The 20 mm grain size fraction of crushed steel slag aggregate consistently showed null values for carbonation (Figs. 4.3, 4.4). The highest value achieved was 0.060 wt. % showing that the material did achieve a very low level of carbonation. Over time the carbonation appeared to increase but overall still remained low.

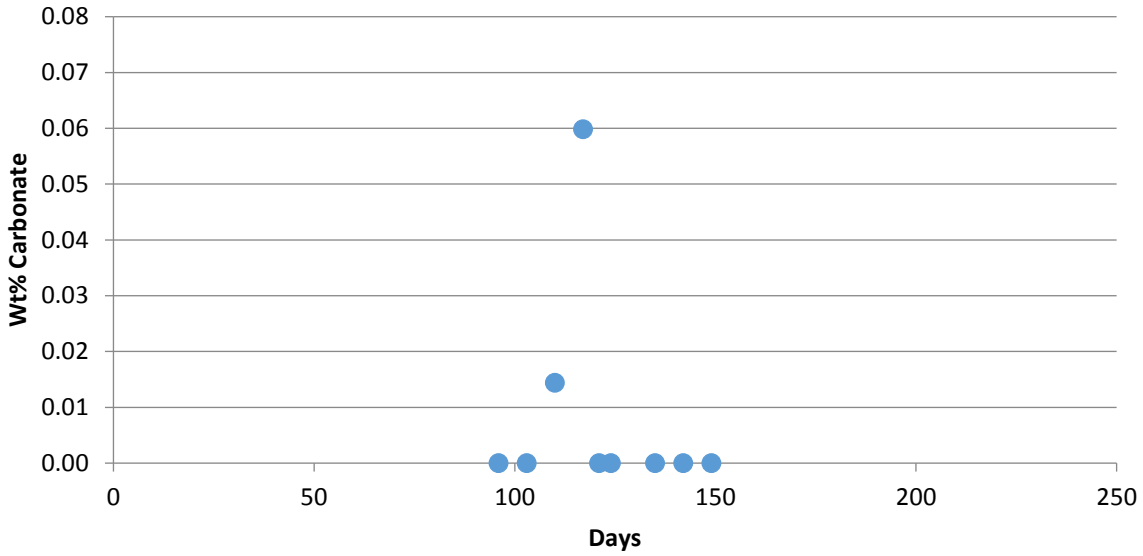

Figure 4.3: Wt. % carbonation of 20 mm aggregate slag over 149 days.

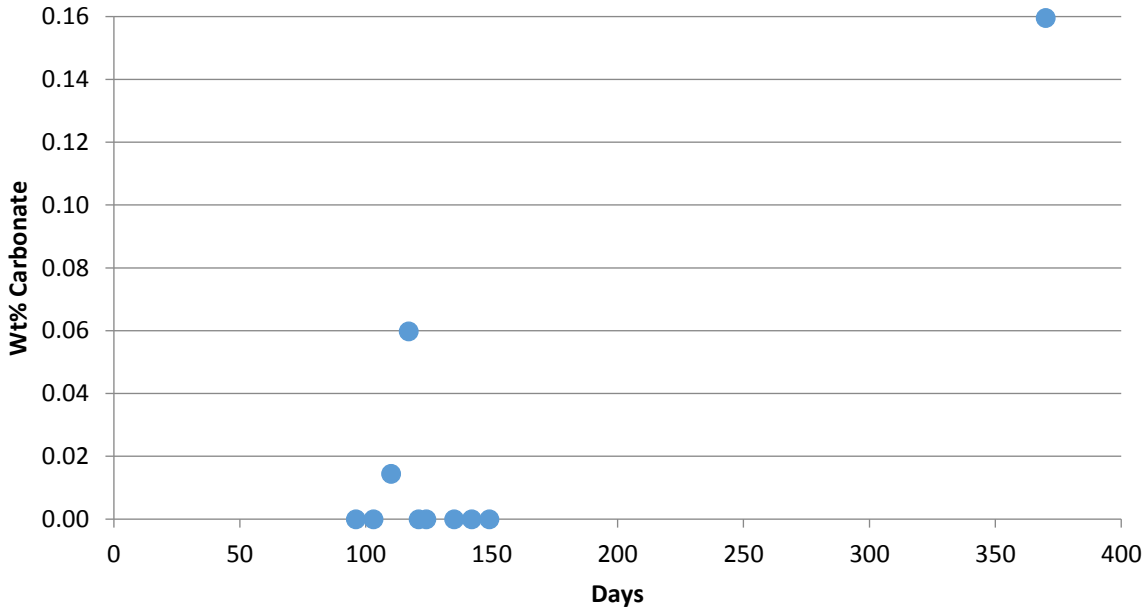

Figure 4.4: Wt. % carbonation of 20 mm aggregate slag over 370 days.

10 mm Steel Slag Aggregate

The 10 mm grain size fraction of crushed steel slag aggregate showed an upwards trend towards carbonation values of 0.1-0.2 wt. %, with samples regularly displaying values of 0.05 wt. % (Fig. 4.5). The highest value attained was 0.158 wt. %. The material appeared to show a weathering rate of 0.0003 wt. % per day.

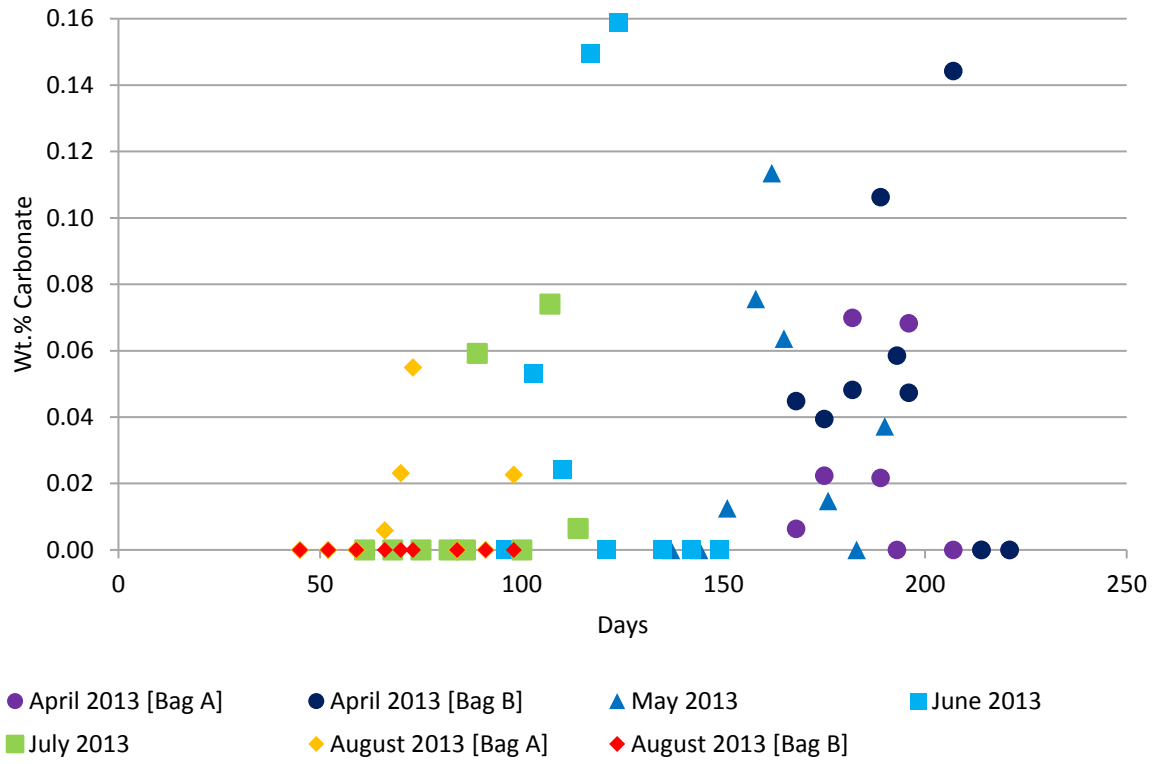

Figure 4.5: Wt. % carbonation of 10 mm aggregate slag over 221 days. The sample names relate to the month the aggregate heap was created.

6 mm

The 6mm grain size fraction of crushed steel slag aggregate showed an upwards trend towards carbonation values >0.15 wt. %, with samples regularly displaying carbonation values between 0.05 to 0.15 wt. %. The highest value attained was 0.462 wt. %. The material appeared to show a weathering rate of 0.0001 wt. % per day (Fig. 4.6).

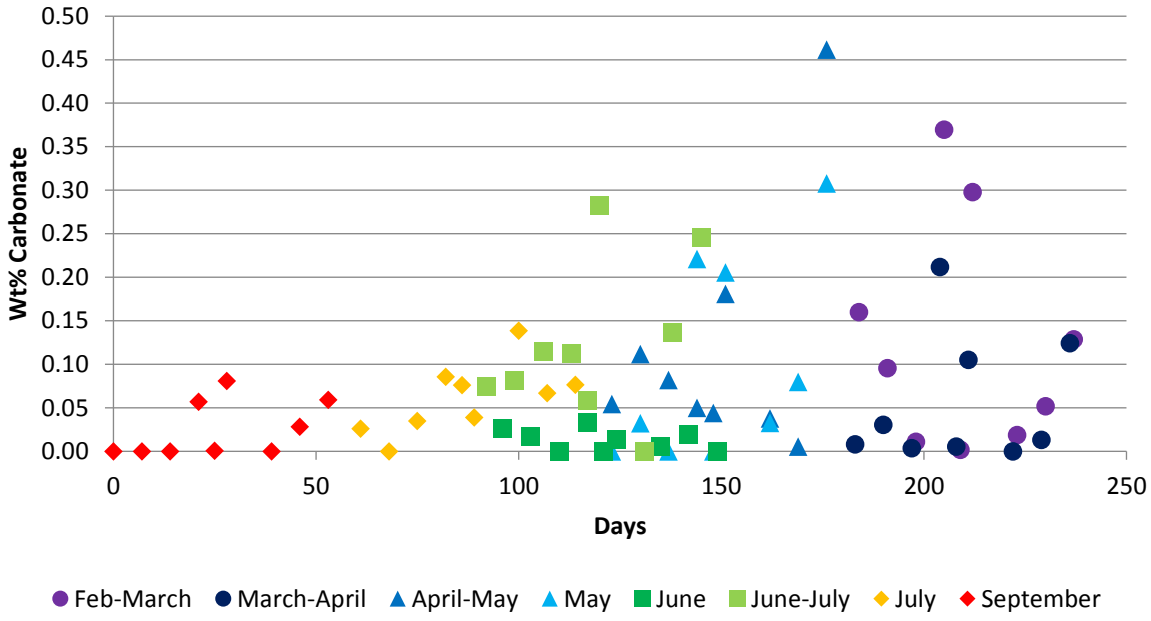

Figure 4.6: Wt. % carbonation of 6 mm aggregate slag over 236 days. The sample names relate to the month the aggregate heap was created.

Dust

Dust displayed the highest passive carbonation values of any slag product, consistently displaying carbonation values over 8 wt. % (Figs. 4.7, 4.8). Dust also appear to carbonate rapidly gaining an additional 1 wt% in carbonate within seven days. The high initial values (T=0) is likely due the have been allowed to preweather before the start of the experiment (within a month of the sampling date). The maximum value recorded was 14.054 wt. %. The material appeared to show a rapid weathering rate towards 14 wt. % within 50 days (approximately 0.28 wt. % per day).

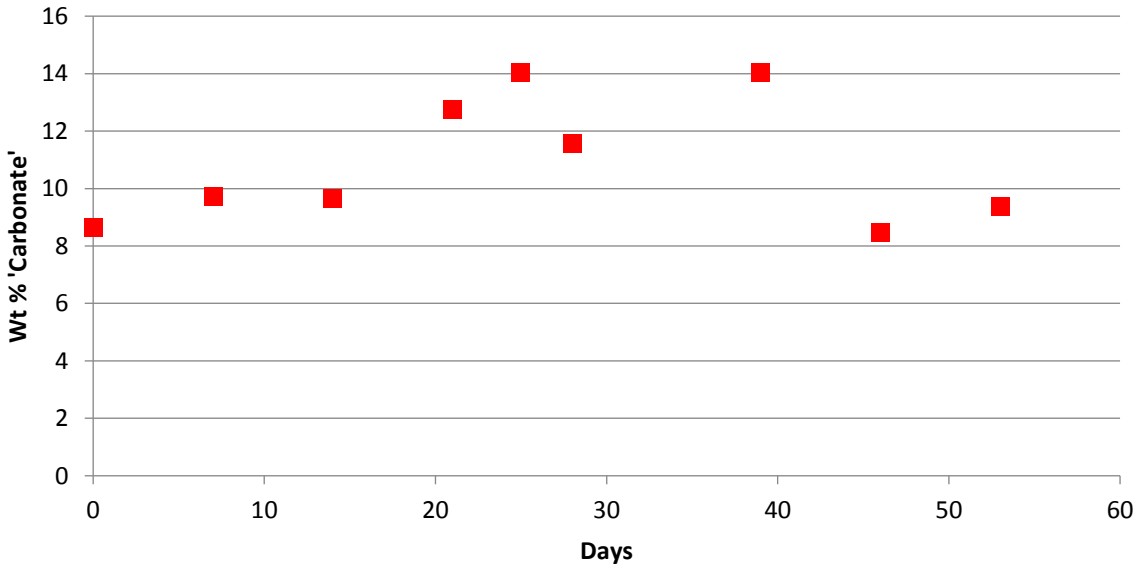

Figure 4.7: Wt. % carbonation of slag 'dust' over 53 days.

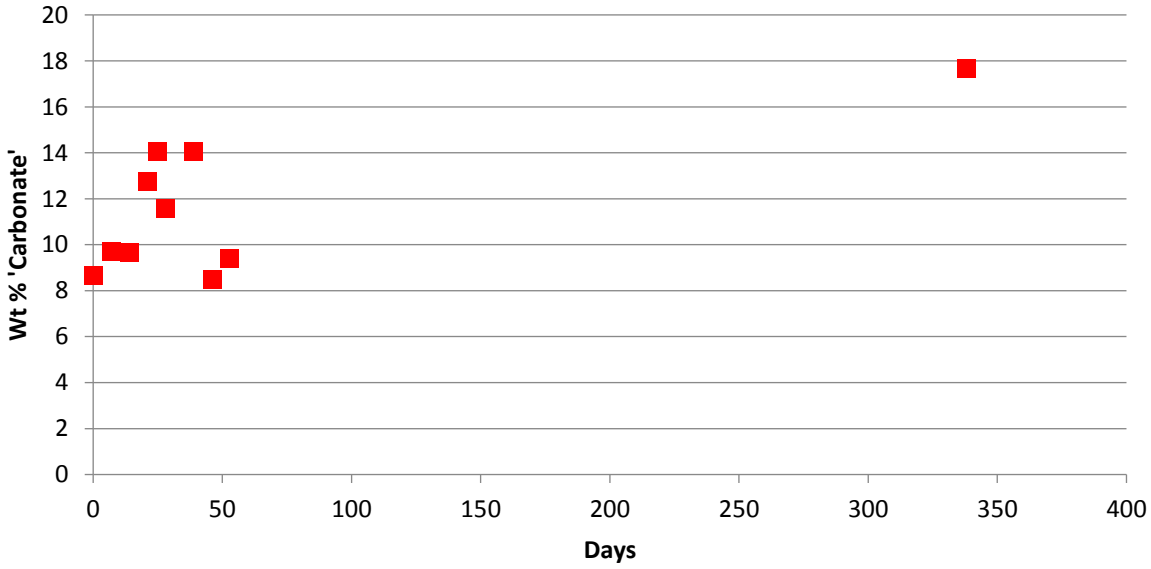

Figure 4.8: Wt. % carbonation of slag 'dust' over 338 days.

4.3.2 Pellite

Pellite displayed a consistent upwards trend in carbonation towards 0.2-0.3 wt. %. A maximum value of 0.696 wt. % was recorded in one sample (Fig. 4.9). Over time, the carbonation did appear to increase (Fig. 4.10).

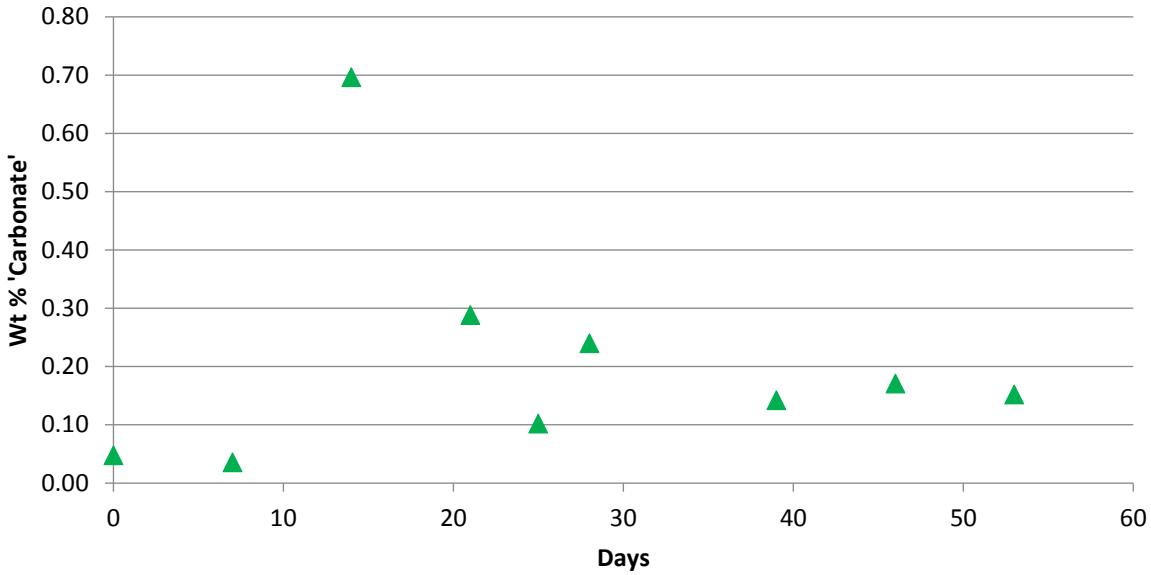

Figure 4.9: Wt. % carbonation of Pellitised Slag over 53 days.

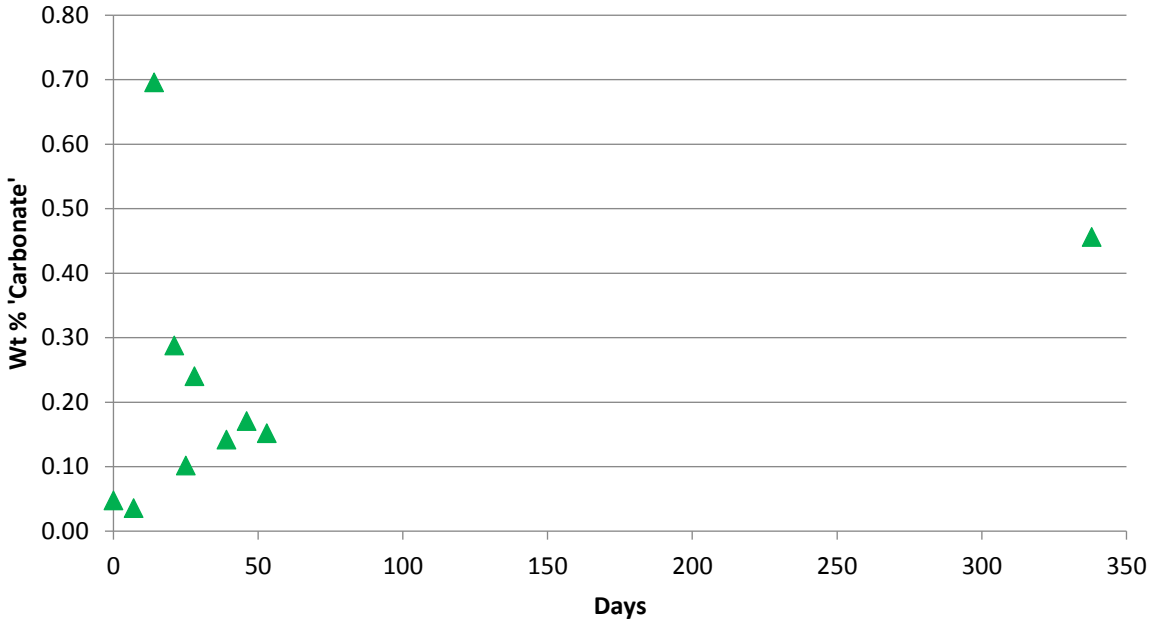

Figure 4.10: Wt. % carbonation of Pellitised Slag over 338 days.

4.3.3 Granulated Blast-Furnace Slag (GBFS)

Granulated Blast Furnace Slag displayed no real carbonation above 0 wt. %. The material showed no appreciable passive carbonation over time (Figs. 4.11, 4.12).

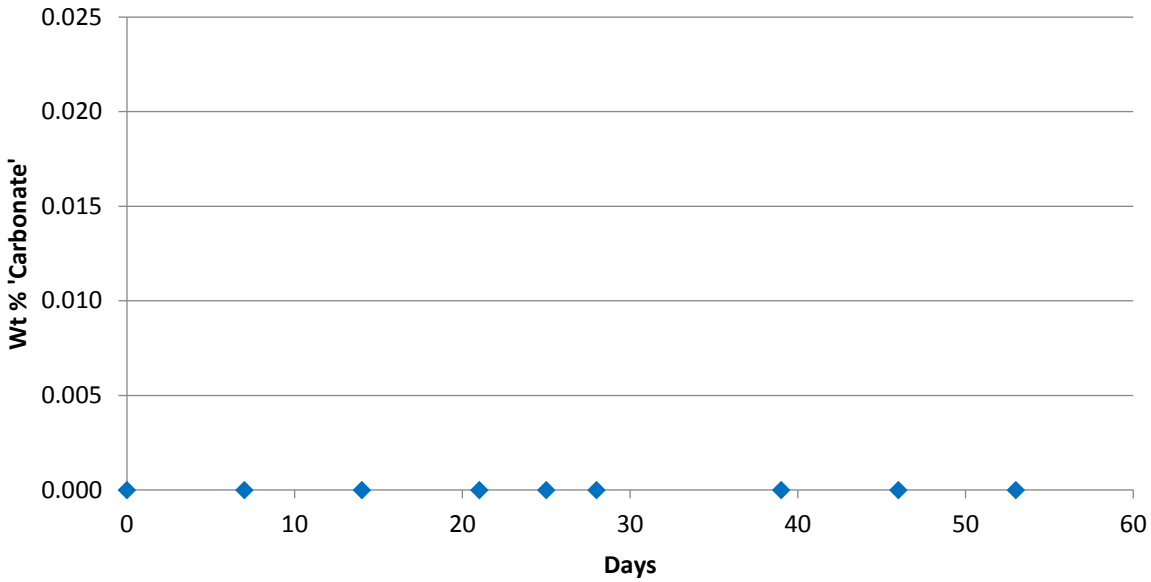

Figure 4.11: Wt. % carbonation of Granulated Blast Furnace Slag over 53 days.

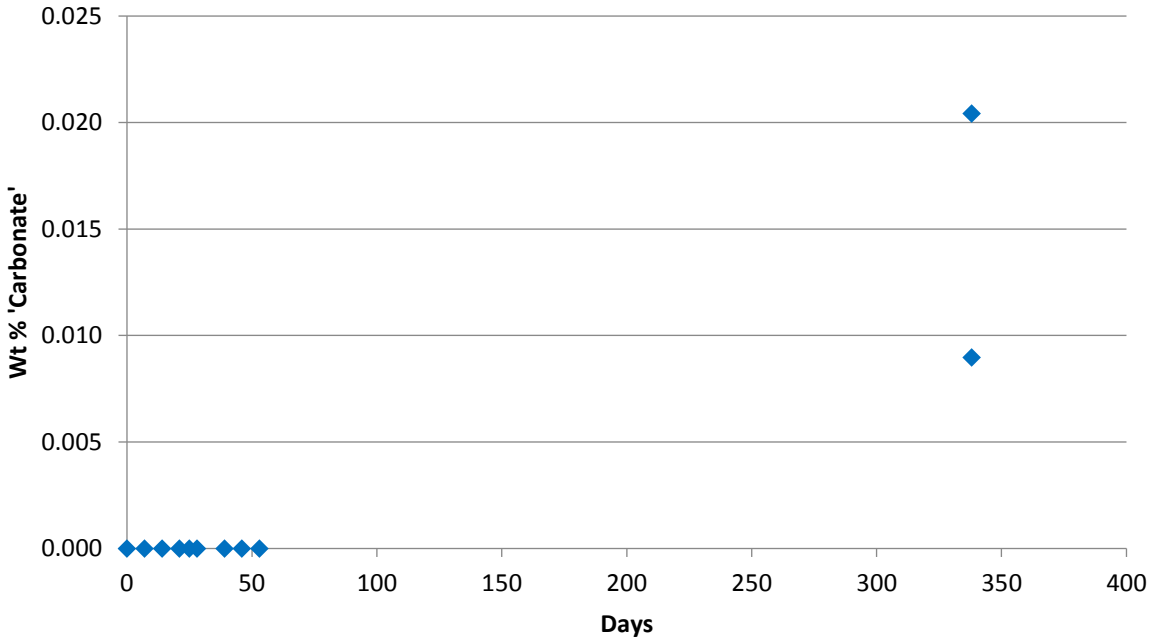

Figure 4.12: Wt. % carbonation of Granulated Blast Furnace Slag over 338 days.

4.3.5 Environmental Data

The environmental conditions during the passive weathering study are presented in Fig. 4.13. The data were recorded at the Durham University Observatory by the Department of Geography, Durham University. Temperatures during the three-month study varied between -1°C and 19.5°C. The maximum daily rainfall recorded was 21.4mm.

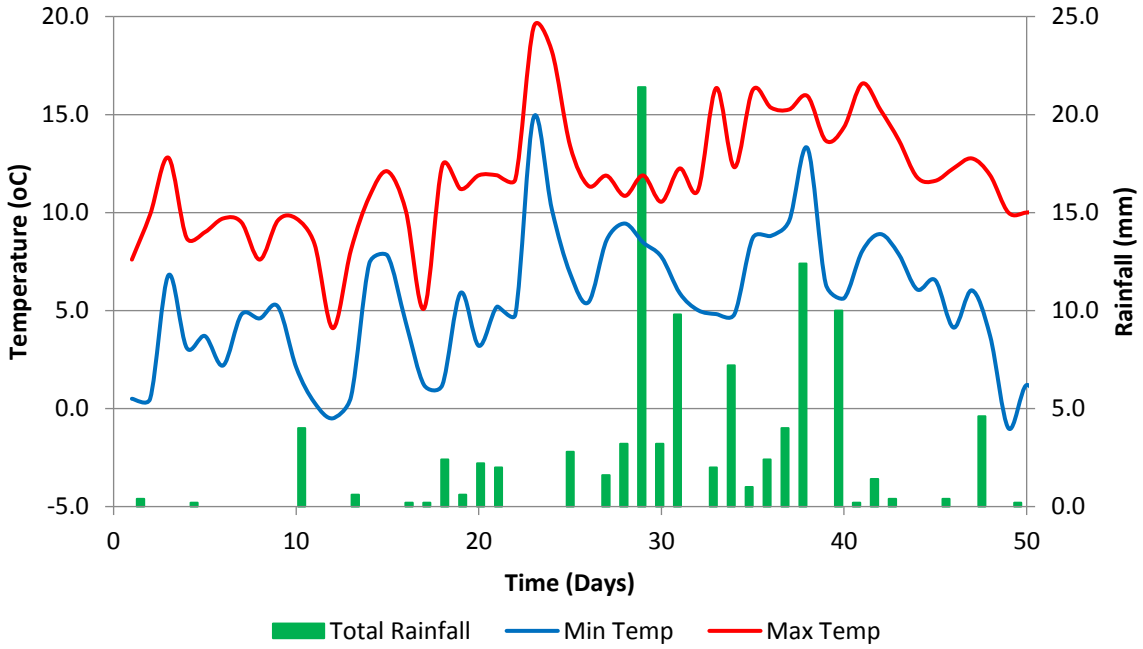

Fig 4.13: Environmental conditions at the city of Durham during the three-month weathering study conducted at the City of Durham.

The material used within the study was already passively being weathered while it was part of a slag heap prior to sampling. A dataset for the weather conditions for Redcar was not available. As such, the data set recorded in Durham at Durham University Observatory (33.64 km NW of Redcar) was used as a local record. Temperatures between the months February 2013 – December 2013 varied between -3.93°C and 28.43°C. The maximum rainfall recorded was 63 mm (Fig. 4.14).

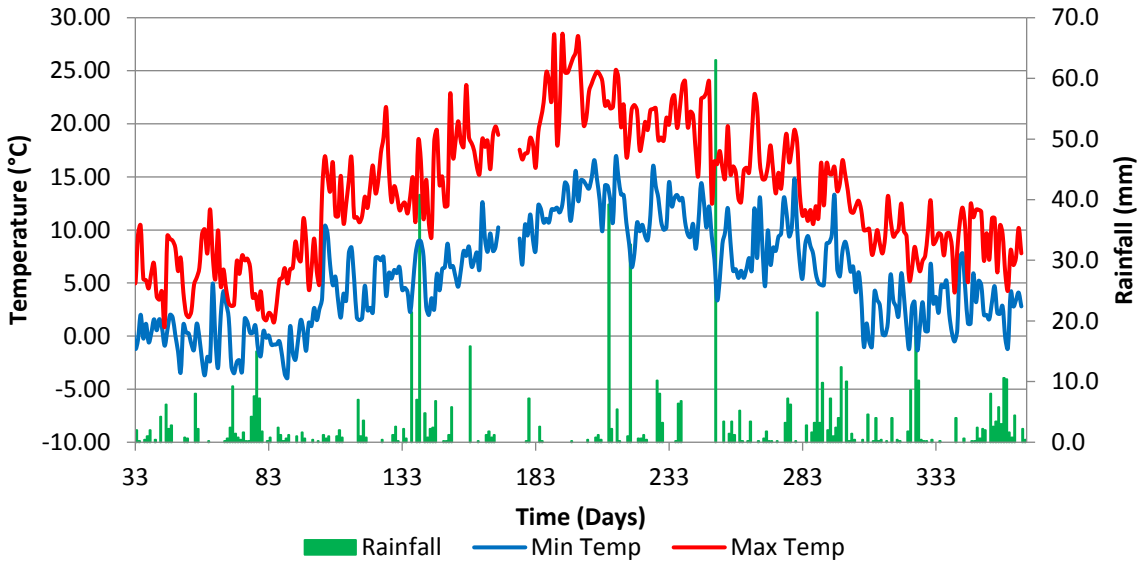

Fig 4.14: Environmental conditions at the City of Durham (taken as similar to Redcar) between February 2013 – December 2013 during which time the weathering of the slag heaps at Redcar site occurred.

4.5 Interpretation

The maximum weight-percent carbonate gain achieved for each type of material is shown in Table 4.2. All data has been rounded above the limits for analysis detection errors by the TGA equipment.

	Highest wt. % Carbonate achieved	Days
Dust	14.054	25/39
6mm	0.462	176
10mm	0.158	124
20mm	0.060	117
Pellite	0.696	14
GBFS	0.0204	338

Table 4.2: Maximum carbonation achieved for each weathered material and the reaction time taken to achieve the carbonation.

4.5.1 General Trends within the data

Of the materials studied, granulated blast-furnace slag (GBFS) achieved the least carbonation with little above 0 wt. % realistically achieved over the course of three months. A value of 0.2 wt. % was achieved after 338 days. Pellite achieved a maximum of 0.7 wt. % after 14 days. Dust achieved 17.7 wt. % and consistently achieved greater than 10 wt. %. The data for the 6 mm and 10 mm grain sizes displayed a broadly similar trend, where the material showed relatively little carbonate formation before relatively rapidly (within 10-20 days) displaying increasingly higher amounts of carbonation.

The carbonation values show a large internal spread. The 20 mm carbonation data was limited, but showed a significantly lower carbonation value to that of the 6 mm and 10 mm material.

4.5.2 Crushed Steel Slag

The crushed steel slag in this study was represented by samples of 20 mm, 10 mm and 6 mm aggregate slag and Dust. The increase in carbonation rate with decreasing grain size is shown in Table 4.3.

Material	20 mm (117 days)	10 mm (124 days)	6 mm (176 days)	Dust (25 days)
Max Carbonation (wt. %)	0.06	0.158	0.462	14.054
Av. Rate per Day (wt. %)	0.000513	0.00127	0.00263	0.562
Increase Factor	2.48	2.06	214.16	-

Table 4.3: Increase in carbonation and carbonation rate with decrease in grain size.

Between 20 mm and 10 mm and 10 mm and 6 mm grain sizes, the maximum carbonation achieved more than doubled. However, between 6 mm and Dust (<2mm) there was over a 214 fold increase in the carbonation rate. It was observed that there was an evident grain size dependency upon the extent of carbonation and this may partly be due to the physical conditions present as a result of the shape of the aggregates. The coarser grains were too large to retain the thick moisture film needed to enable the carbonation reaction to occur, when there was a lower water input from rain. However, Dust formed a 'mud' like substance when wet, which appeared capable of retaining moisture and, therefore, allowed a greater amount of mineral dissolution compared to that of the aggregates.

In addition, the higher carbonation values displayed by the Dust may partly be due to the fractionation of Ca-rich minerals into the Dust during its production by the grinding process. During the process of crushing steel slag 'block' into different sized aggregates, blebs of metallic-iron are removed as part of the metal reclamation process. This enriches the residual 'dust' into a Ca-rich fraction as the Fe content is reduced. During the crushing process, materials with a lower hardness are also preferentially broken up. Therefore, Dust becomes comprised of the 'softer' mineral fragments which have preferentially fractured during the crushing process and this may well enhance the reactivity of the material.

4.5.3 Pellite

The highest carbonation value achieved for Pellite was 0.696 wt. % after 14 days. These comparatively small values of carbonation were achieved despite Pellite displaying a similar grain size range (albeit

shifted one phi coarser) to Dust (which displayed a carbonation rate ≈20 times that of Pellite). There was no observable 'crusting' of the material and hence, despite a slightly lower porosity due to poor grain sorting, there was no barrier to the infiltration of water through the material. Therefore, the limiting carbonation factor was likely to be determined by the composition. XRD analysis determined that the likely minerals present (Chapter 2.4.5.2) within Pellite were metals and alumnide-minerals, but significantly pyroxenes were also present. The pyroxenes were likely to be the main minerals being carbonated and as Pellite was more reactive than GBFS this is likely due to its mineralogy. However, Pellite is a pumicious material which displays a larger internal grain surface area when compared to GBFS and this factor may be responsible for its increased carbonation.

4.5.4 Granulated Blast Furnace Slag

The highest carbonation value achieved for GBFS was 0.0204 wt. % after 338 days. For the first three months there was no appreciable carbonation. No samples were collected between 53 days to 338 days, therefore the pattern of increase in carbonation was unknown during this period. GBFS is finer grained and better sorted than Dust and Pellite and yet displayed no significant carbonation. In addition, its permeability allowed it to maintain its moisture content in much the same way as Dust. Therefore, its mineralogy must be the limiting factor. GBFS essentially comprises of amorphous-quartz and alumno-silicate minerals (Chapter 2.4.5.3). Therefore, despite showing a high Ca content GBFS may simply be inert due to its vitreous internal structure.

4.5.5 Environmental Conditions

Though temperature and the availability of water were assumed to be constant this cannot be true due to the natural variability of any temperate climate. As shown in Fig. 4.15 the temperature and rainfall were variable and both played a part in the carbonation of the samples. Fig. 4.15 also shows the difference in carbonation between each sample (exaggerated x 10 for clarity) and there was a clear reduction in carbonation values during a warmer period accompanied by higher rainfall. It is possible that the higher temperatures resulted in the materials drying out, thereby stopping the reaction. However, as the temperature range during this time was 6˚C to 17˚C and there was high rainfall, this was unlikely. Indeed, these temperatures may have been expected to increase the kinetics of the system, despite CO_2 being less soluble with increases in temperature, and result in higher carbonation values.

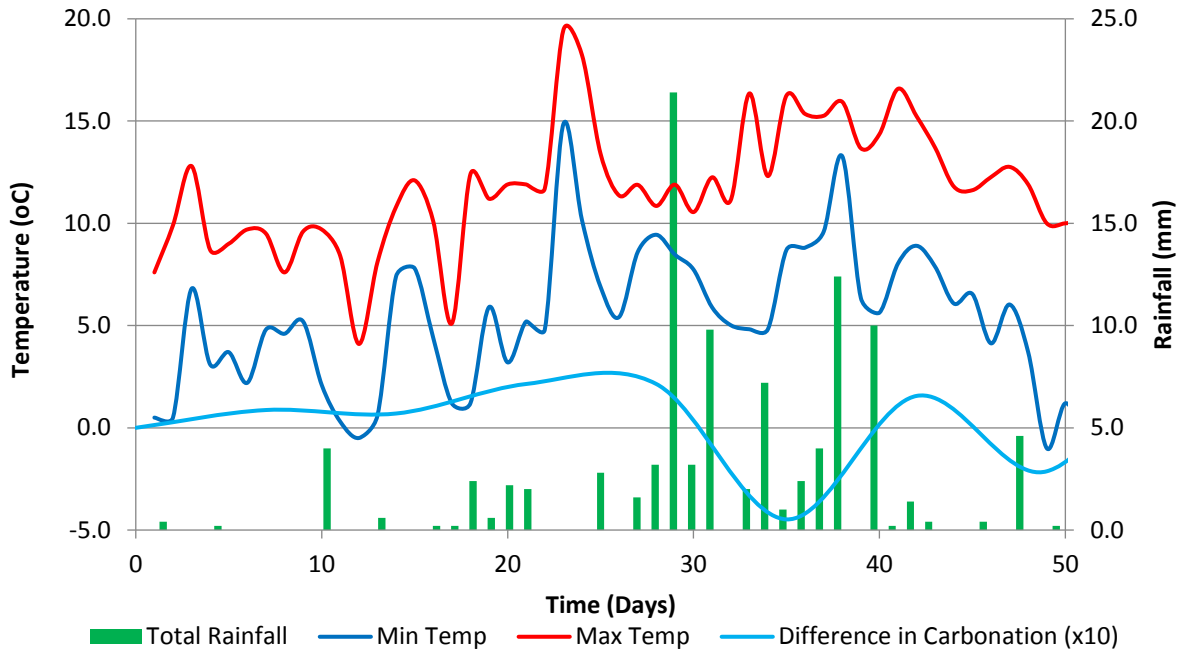

Fig 4.15: [Difference in carbonation across each sample has been exaggerated x 10 and is read from the same scale as Temperature] (Sample number = 16)

The alternative option is that the higher period of rainfall washed the carbonate from the grains resulting in an inaccurate measurement of the carbonation being recorded. This is possible as the paper that lined the bottom of each weathering tray did display some minor traces of carbonate minerals forming upon them.

Therefore, should the sum total of all carbonate measurements be taken as a more accurate record of material carbonation? An examination of a cross section of a heap showed a white cemented layer towards the centre of the heap. As the hydraulic conductivity data [Chapter 2.3.2.1] showed the conductivity was approximately halved by the presence of cemented material. Layers such as these could act as carbonate 'traps' within heaps. Analysis of the samples from the white layer in Fig. 4.16 yielded wt. % carbonate values of 7.51 to 8.99 (n=2). This is unlikely to be as a result of increasing carbonation through the heap and rather due to the movements of carbonate downwards through the heap.

Figure 4.16: Photo of weathering within a sectioned 6 mm aggregate slag heap. Weathered layer is approximately 2.66 % of the heap volume. (Heap height approximately 2 m – gold disk is £1 coin)

If such carbonate mobility occurs within each tray, then the carbonation achieved by each material, assuming that each week the carbonate upon the surface of the slag is completely removed and then renewed, is significantly higher than expected and is almost equivalent to the carbonation achieved by Dust (Table 4.4). These figures should, however, be treated with caution.

	Av.	Max.	Min.	Range
6 mm	9.79	12.57	6.71	5.86
10 mm	6.51	8.50	3.89	4.62
20 mm	4.86	4.86	4.86	0.00

Table 4.4: The total sum of carbonate formed upon different aggregate products during the three month passive weathering study.

4.6 Discussion

The factors affecting the passive weathering of the slag are; the mineralogy of the samples, solvent, temperature, pressure, concentration of carbonate ions present, water availability, the effect of surface area and the material composition. Of the above factors, the physical factors of the phases, solvents, CO_2 pressure and carbonate concentrations were fixed. Environmentally, the temperature and water availability are considered constant. So, material type and grain size are the only factors which significantly affect the carbonation value.

4.6.1.1 Material Type

Out of all the materials used in this study the material which achieved the highest carbonation (based upon a grain size <2 mm) was Dust, followed by Pellite, with GBFS achieving the lowest carbonation value.

Dust is composed of metals, metal oxides, olivine-structure minerals, longer mixed silicates, phosphides and hydroxides. It is this combination of minerals which may be responsible for the reactivity of Dust and, in particular, allowing the formation of hydroxide phases which could be an initial step towards carbonation.

Pellite, however, is mainly comprised of metals, metal oxides, pyroxenes, alumnides and feldspathoidal minerals. The aluminides and feldspars are not expected to readily undergo carbonation. Therefore, the material expected to be controlling the extent of carbonation would be the pyroxene phases.

As shown by XRD, GBFS is composed mainly of metal oxides and pyroxenes with a significant amorphous phase. As shown above, pyroxenes are capable of undergoing carbonation. The reason attributed to the lower carbonation values of the GBFS is therefore the amorphous nature of the material which may not readily release cations for carbonation.

4.6.1.2 Grain Size

The only material studied which varied in grain size was the steel slag aggregate. The carbonation rate of which, approximately doubled between 6 mm to 10 mm, and 10 mm to 20 mm (Table 4.3). However, there was an increase in the carbonation rate of 214 times between 6 mm and Dust. Therefore, it is evident that grain size plays an important part in the carbonation rate of a material and in turn the extent to which its carbonation potential is achieved over a set timeframe.

4.6.2 Comparison of Tray Scale Experiments to Heap Scales

The applicability of this study is important if the results are to be applied in an industrial setting. The dimensions and volumes of the sample trays used in the study were dramatically different from the dimensions, morphologies and volumes of the slag heaps present within the field area. Furthermore, samples from each slag heap were only taken from the top section of the heap. The results in the study are therefore only applicable to only the top part of a heap. The samples of material were not packed into each tray but were left with ample space around them. This further restricted the applicability to only the top layer of each heap and provided no data as to the behaviour of water flowing through the heap material. Additionally, only up to 350 mg of sample was analysed for each data point and, as such, the data may not be wholly representative of the heap material. The applicability of the results of this study are further explored below.

Steel Slag

The steel slag heaps at the Redcar site were located on the Lafarge-Tarmac site and approximately averaged 80 m in length, 11 m in width and up to 2 m in height. Heap volumes averaged 1800 m^3 with a mass of approximately 3000 tonnes. Steel slag blocks were crushed and screened to typical grain sizes of 20 mm, 10 mm and 6 mm and are used to form the heaps. Occasionally, heaps of 14 mm and 3mm material were present. The heaps were well graded, with the grains grey to black in colour and of angular and spherical shape.

Within the tray experiments the ratio of the thickness of the samples of crushed steel slag to the maximum slag heap thickness was approximately 1:100. The thickness of the sample in the tray was not great enough to allow the formation of efflorescent layers such as those seen in Fig 4.16.

The extent to which this modified the reaction conditions is debatable between two models. Either the top layer of heap material only carbonates slightly or the carbonate formed at the top of the heap is washed continuously into the lower parts of the slag heap – the latter model would, however, result in the lower parts of the heap being coated with carbonate thereby restricting the production of further carbonate lower in the heap.

Dust

Heaps of 'Dust' (crushed steel averaging a grain size of 2 mm to 125 μm) were on a similar scale to those of the steel slag. Typically, these heaps were covered by a 5 cm thick layer of cemented, weathered material indicating that weathering did not penetrate deeply into the heap.

For the dust samples, the ratio of thickness within a sample tray to maximum slag heap thickness was approximately 1:100. In addition, the thickness of sample was not great enough to produce the ≈5cm thick weathered layer observed in the field. This potentially allowed for a greater degree of weathering of the sample material to take place in contrast to a >5 cm thick heap of dust which may develop a relatively impermeable surface layer. Therefore, the total carbonation of the heap was restricted to that of the top 5 cm of any heap size. It is likely, however, that regular working of 'dust' heaps could provide almost complete weathering of the available material and would be the preferable method for enhancing the passive weathering of the material.

Pellite

Pellite heaps were approximately 70-150 m in length, 40-50 m width and 5 m in height. Grain size varied from 1 mm to 150 µm with grains displaying a well-rounded, highly spherical shape and a pumicious texture. The grains were typically a cream to golden yellow colour. A strongly sulphurous smell was detected when the grains were damp.

Within the tray experiments, the ratio of the thickness of the samples of Pellite to the maximum slag heap thickness was approximately 1:250. The thickness in the tray was not sufficient to produce the reducing conditions that may be formed within the centre of the heaps. Therefore, this study is applicable only to areas of the heap where there were oxic conditions. Pellite also 'crusts' in a similar way to Dust producing areas of lower hydraulic conductivity, which could restrict the movement of water (and therefore carbonate of free cations) around the heap. Regular working of Pellite heaps may help to improve the carbonation achieved by the whole of the heap in the same way as for dust.

GBFS

Granulated blast furnace slag was collected from a heap approximately 3 m in length by 3 m in width and 3 m high, located at the end of a granulation conveyer belt. On average, the grain size was between 1 mm to 125 µm, with grains displaying a shard like morphology. The grains were golden in colour and vitreous in texture.

Within the tray experiments the ratio of the thickness of the samples of GBFS to the maximum slag heap thickness was approximately 1:150. No crusting or strong smell was detected at the GBFS heap. Based upon the results of this study no further limitations may apply particularly as GBFD is so inert.

4.6.3 Total % of Sequestration Occurring

The total amount of slag produced per year at the Redcar site is 1.396 million tonnes. The total tonnes of GBFS, Pellite and Steel Slag aggregate produced each year are shown in Table 4.5.

Annual T. BFS		980000	tonnes
of which			
40%	GBFS	392000	tonnes
25%	Pellite	245000	tonnes
35%	Air cooled	343000	tonnes
Annual T. Steel Slag		416000	tonnes
	De-Sulphurised Slag	62000	tonnes
	Debris	59000	tonnes
of which	Crushed Aggregates	295000	tonnes
10%	20mm	29500	tonnes
10%	14mm	29500	tonnes
30%	10mm	88500	tonnes
30%	6mm	88500	tonnes
20%	DUST	59000	tonnes

Table 4.5: Total slag products produced per year.

Based upon the carbonation factors presented in this study the total tonnage of CO_2 theoretically sequestered by the different materials within this study was calculated and is shown in Table 4.6. The total amount of CO_2 that is being sequestered at the Redcar site is likely to be between 6,434 and 10,127 tonnes per year. The vast majority of this is through the carbonation of Dust followed by that of Pellite.

Inter-Quartile Range	0%	25%	50%	75%	100%
20 mm	0.00	0.00	0.00	4.25	47.14
14 mm	*0.00*	*0.00*	*0.00*	*10.06*	*47.00*
10 mm	0.00	0.00	0.00	41.90	140.74
6 mm	0.00	5.35	41.77	5.35	605.51
Dust	2046.58	6153.98	7025.80	9386.35	12663.59
Pellite	88.55	275.11	397.04	678.86	1718.16
GBFS	0.00	0.00	0.00	0.00	80.05
Tonnes of CO_2	**2135.13**	**6434.43**	**7464.60**	**10126.78**	**15302.18**

Table 4.6: Total tonnes of CO_2 sequestered by each material per year based upon the tonnes of material produced at Redcar. (14 mm has been extrapolated from the trend of the other data points).

4.7 Conclusions

This study has shown that:

- Dust achieved the highest wt. % carbonation values out of both the steel-slag aggregates and of all the materials included within this study. The carbonation rate of steel-slag aggregate roughly doubled as grain size was halved up until the creation of Dust (<2 mm fraction) when carbonation rate rapidly exceeded this.

- Pellite achieved the highest carbonation values out of the two types of blast furnace slag used in this study. The carbonation values achieved by Pellite were approximately comparable to that of 6 mm steel-slag aggregate.

- GBFS has been shown to achieve little to no carbonation. However, if the highest carbonation value measured for GBFS was typical, the material would be sequestering approximately 80 tonnes of CO_2 at the Redcar site per year.

- Overall the amount of CO_2 sequestered by each material is highly dependent upon the composition of each material.

- Grain size is a controlling factor in the carbonation rate and therefore the degree of carbonation of the material. As grain size decreased the carbonation value achieved increased.

- These results are applicable only to the top surface of an industrial slag heap. However, the values achieved can be considered typical of the whole heap, if there is suitable heap management such as the reworking of the heaps in order to avoid the material crusting.

- The effect of the possible removal of carbonate from the surfaces slag grains at the top of a heap into the centre and bottom of the heap via water percolation (and therefore the effect on the carbonation potential of a heap of material) is, as yet, not understood.

- This study has shown that approximately 6,434 to 10,127 tonnes of CO_2 is being passively sequestered at the Redcar site by the total volume of slag products per year. Over the three sites owned by Lafarge-Tarmac across the UK (all of which are of similar size and have similar production rates) the total passive CO_2 sequestration was between 19,302 to 30,381 tonnes of CO_2 per year.

Chapter 5:

Active carbonation experiments – assessing the carbonation potential

5.1 Introduction

A series of Experiments were conducted in order to determine the degree of carbonation which different slag products and pure minerals would undergo, when placed under conditions of enhanced pressure, temperature and varying water availability. The pressure and temperature variation showed how the materials responded under these variables and how this affected the eventual degree of carbonation. Throughout this chapter the following abbreviations have been used to describe the experimental conditions:

Pressure: Lp – 10 bar CO_2 pressure, Hp – 100 bar CO_2 pressure.

Temperature: Lt – 25˚C, Ht – 125˚C.

Water Availability: Ls – 15 wt. % saturated, Hs – excess water used.

5.1.1 Previous Experiments

The main variables used in previous carbonation studies (Table 5.1) were:

- Reaction material.
- Reaction time.
- Reaction temperature.
- The partial pressure of CO_2.
- The grain size.
- Liquid to Solid ratio.
- Agitation.

This study used a reaction time of 19 hours. This was a long reaction time when compared to the times used in other studies (e.g. Huijgen PhD Thesis 2007) where the experiments were run for less than 1 hour. The liquid to solid ratio in this study is expressed as conditions of either HIGH or LOW water availability. Agitation of the reaction material was not possible with the equipment used at the Department of Earth Sciences, University of Durham. Therefore, all experiments were conducted under static conditions. The effects of the reaction material used, the grain sizes and the temperature and pressure conditions of the experimental runs are shown below:

5.1.2 Reaction Material

A range of materials have been studied in previous carbonation experiments as shown in Fig. 5.1. These materials ranged from calcium and magnesium hydroxides, wollastonite, olivine (fayalite – forstetite) to Dutch steel slags. Most of the values achieved were below 40% conversion to carbonate (Fig. 5.1). However, it should be noted that each data point represents a wide variation in experimental conditions, both in relation to each other and to the experimental conditions used. The results from this study will be compared to those values obtained from earlier studies, in an attempt to compare different experimental methodologies and to direct research towards a preferential method.

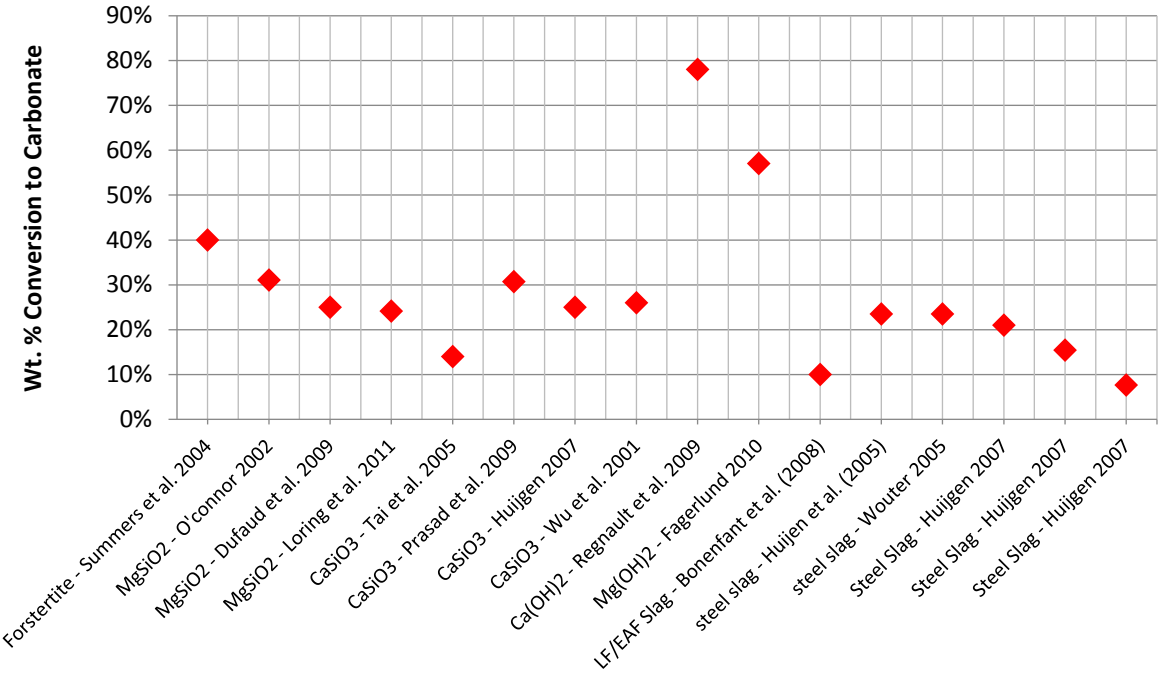

Figure 5.1: Carbonation values for different materials as reported in the literature

The materials used in this study all had very different geological or anthropogenic origins and may or may not be suited to industrial scale carbonation. Some cases are considered below:

Hydroxides are found in a range of geological environments, as is Wollastonite (a pyroxene mineral). However, without there being a significant economic gain in actively carbonating the materials found in geological deposits, the minerals will continue to remain unexploited.

Olivine, however, is abundant in a range of geological environments and exists in large volumes (e.g. the Oman Ophiolite and the Lizard Peninsular) and is commonly associated with large economic ore deposits (e.g. the PGE mines of Bushveld and Sudbury). Olivine, associated with economically important ore deposits, is mined as a gangue mineral and left in spoil heaps. Although natural

weathering is likely to occur in these heaps, active carbonation of the material may increase the CO_2 uptake and, in the right economic environment (e.g. carbon pricing of on-site electricity/fuel consumption or stricter environmental mining legislation), would go to some way to alleviate the CO_2 emissions produced as a result of the mining activity. Such a method would be economically preferable to mining olivine rich deposits purely for carbonation purposes, as the energy used and environmental impact would be such as to restrict the method to locations which were already providing societal gain within an existing economic framework.

Chapter 2 showed that both of these minerals were present within metallurgical slags and metallurgical slag is readily available without having to be mined. The material already exists as a sizeable resource as between 163,700 and 245,550 tonnes of steel slag was produced in 2014 (World Steel Association 2015). Passive weathering of these products occurs naturally. If active carbonation was successful for any of these materials and the process could be further optimised, then this would open up new avenues for capturing and storing CO_2 and in the case of metallurgical slag would provide a method of decarbonising the iron and steel industry.

5.1.3 Grain Size

The grain size of material is an important factor in chemical reactions. Smaller grain sizes result in larger surface areas being available for reaction. The grain size range and the sorting of a material also dictates the porosity which in turn impacts on the ability of reacting fluids to move through or around the material. The smaller grain sizes used in this study are not the smallest to be reported in the literature (Fig. 5.2). However, the 20 mm steel slag aggregate is the largest grain-size of steel slag that has been reported to date.

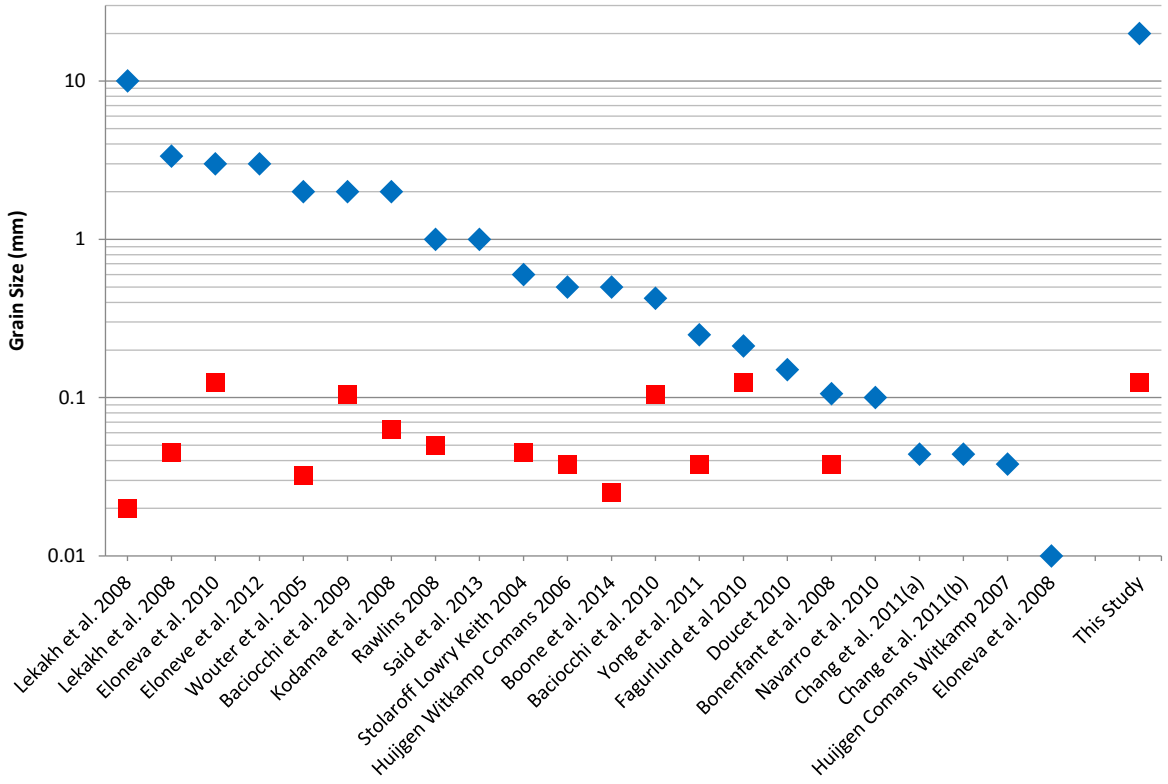

Figure 5.2: Grain sizes used within carbonation experiments from a sample of the literature. Diamonds indicate the maximum grain size used in a study. Squares indicate the minimum grain size used.

5.1.4 Pressure and Temperature Conditions

The pressure and temperature conditions used for the active reaction experiments in this study were 10 bar or 100 bar CO_2 pressure and at 25°C or at 125°C temperature in a factorial design (Fig. 5.3). These conditions were chosen for several reasons: The difference between each set of pressure-temperature conditions is by the order of one magnitude greater, allowing paired comparison of the variables. The conditions used were distinct in pressure-temperature space from studies in the literature and no previously reported studies had carried out experiments at pressures and temperatures which fell within the CO_2 phase diagram, where the CO_2 was in a liquid phase.

Previous experiments in the literature (Table 5.1) appeared to have been carried out at either low pressures – high temperatures, or under conditions where pressure and temperature were roughly equivalent in magnitude. The minimum temperature of any experiment which required water in its liquid state was dictated by the saturation line of H_2O, which allowed water to become superheated at higher pressures. These conditions are frequently found in low temperature ore-deposits and in the shallow crust (Kazuba et al. 2006) and analogues of the natural systems may inform further research.

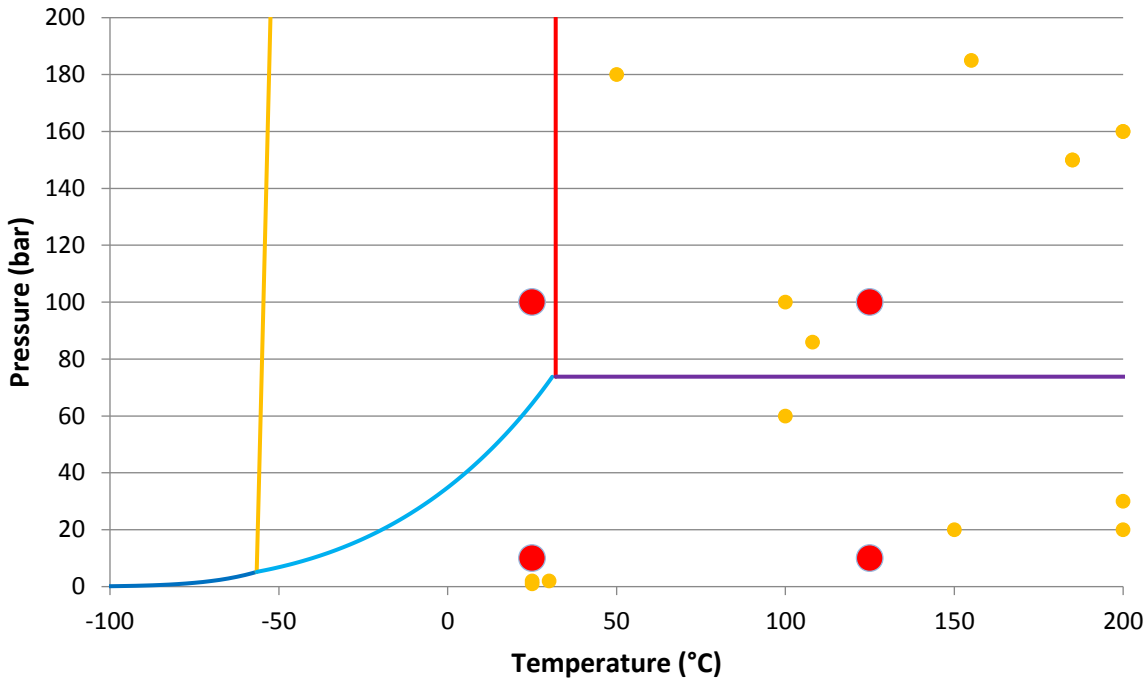

Figure 5.3: Pressure / Temperature conditions used within carbonation experiments taken from a sample of the literature (orange circles). P/T conditions used in this study are shown in red. $P_{(critical)}$ (purple) is the critical pressure, $T_{(critical)}$ (red) is the critical temperature. Light-blue – saturation line, Orange - melting line, dark-blue – sublimation line.

Reference	P (bar)	T (°C)
Bonenfant et al. (2008)	1	25
Huijgen (2007)	2	30
Wu et al. 2001	2	25
Huijgen (2007)	20	150
Huijgen (2006)	20	200
Huijgen et al. (2005)	30	225
Huijgen (2007)	30	200
Prasad et al. 2009	60	100
Tai et al. 2006	86	108
Lin et al. 2008	100	100
Summers et al. 2004	150	185
Rush et al. 2004	150	185
Regnault et al. 2005	160	200
Regnault et al. 2009	160	200
Loring et al. 2011	180	50
O'connor 2002	185	155
Dufaud et al. 2009	1000	500

Table 5.1: Pressure temperature conditions used by other studies for mineral carbonation experiments

The physical form of CO_2 within the reaction vessel did not affect the reaction directly (Fig. 5.4). Within geological and industrial systems the different phases do act as effective solvents, but as the fluids within the chamber were static, then the pure CO_2 was not able to reach the samples under excess water conditions, due to the surface of the water directly blocking the CO_2 from reacting with the samples. Therefore, CO_2 can only react with the samples if it dissolves into the reaction fluid through the surface of the water present. The dissolved CO_2 will generate HCO_3^- ions in a ratio according to the dissolution constants previously discussed in Chapter 3.

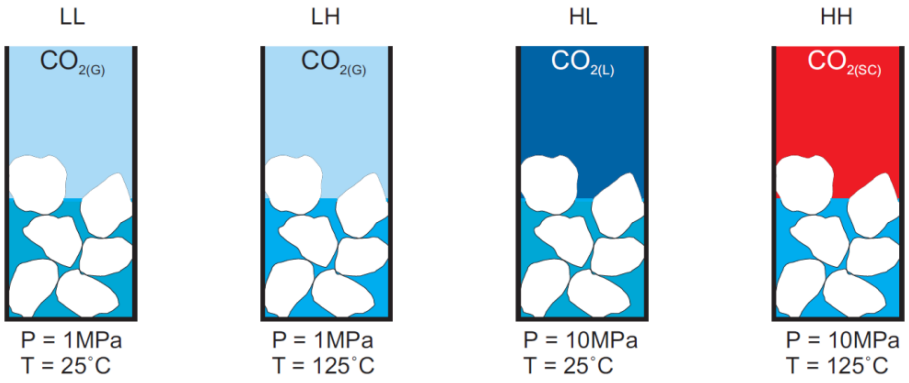

Figure 5.4: Phase relations between the fluids within the reaction chamber.

The concentrations of HCO_3^- ions for each set of experimental conditions are reported in Table 5.2 and are compared against each other in Table 5.3.

	Lt	Ht
Lp	1.42×10^{-07}	4.14×10^{-08}
Hp	1.43×10^{-06}	4.16×10^{-07}

Table 5.2: HCO_3^- concentrations theoretically present under different experimental conditions.

	Lt		Ht	
Lp	1	3.434	0.29	1
	0.099	0.35	0.029	0.099
Hp	10.07	34.54	2.93	10.05
	1	3.44	0.29	1

Table 5.3: HCO_3^- concentrations compared between experimental conditions.

Temperature affects the rate of reaction, which has a direct effect upon the formation or destruction of the porosity and/or permeability of a material and, as a result, on the growth of carbonate minerals into the interstitial spaces within the samples. If there is a rapid decrease in porosity and/or permeability then the reaction will stop before the carbonation potential of the material can be achieved and this will occur far more quickly than if the decrease in the porosity and/or permeability occurs more slowly.

5.2 Methods

5.2.1 Experimental Apparatus

A Parr Instruments 3.8 L batch pressure reactor was used to react the slag samples with gaseous, liquid and super-critical phases of CO_2. The whole control rig assembly consisted of a computer control system, a water cooling system, a heating element and a gas delivery and control system (Fig. 5.5). The computer system used the Thar SFC control software on a windows PC. This software communicated with a Siemens Mass Flow Reader to monitor flow at the start of the gas delivery system and a Thar SFC Automatic Back Pressure Regulator (ABPR) for pressure regulation at the back of the delivery system. The water cooling system comprised of a Julabo FL300 water cooler and pump, a Thar SFC High Pressure P-Series Pump and a heat Exchanger (HE1). The water within the system was cooled to 1°C to cool the CO_2 gas to a constant temperature in order to maintain the CO_2 in a liquid state and so allow it to be pumped into the gas-control system. The heating element was positioned around the Batch Reactor to allow both the gas and the samples to be heated within the reaction chamber. The heating element was controlled by a Parr 4834 Heater connected to UK mains electricity.

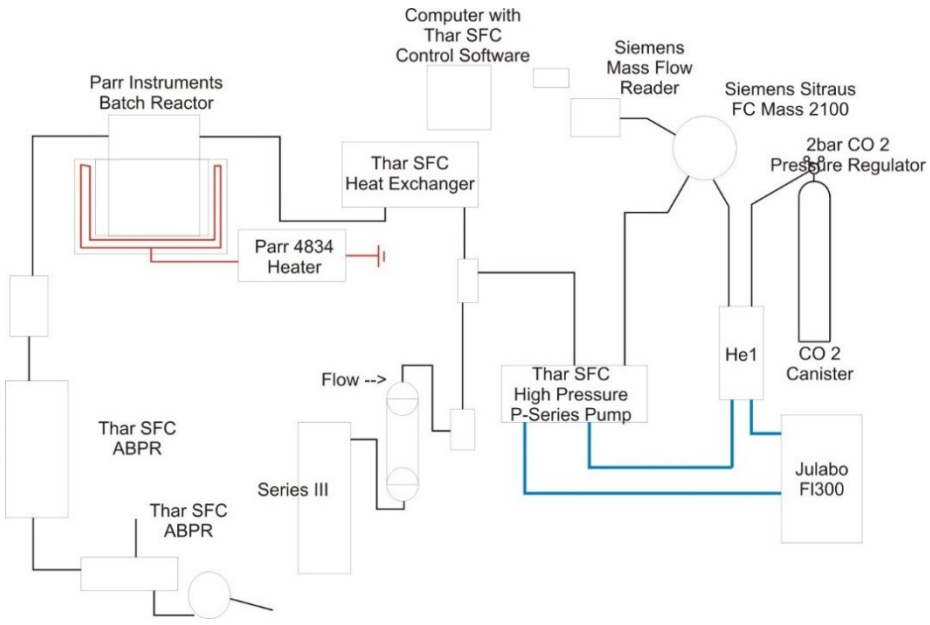

Figure 5.5: Schematic diagram of rig used to react slag samples under varying pressure and temperature.

The gas delivery system was supplied with CO_2 from a BOC liquid-withdrawal CO_2 canister (max 7.5 m^3 gas volume). The gas flowed into a heat exchanger (HE1) where it is chilled to 1°C and the flow was then measured by a Siemens Mass 2100 unit. The gas then flowed into a Thar SFC High Pressure P-Series Pump where it was cooled further. The gas then passed through a Thar SFC Heat Exchanger

before entering the Parr Instruments 3.8 L Batch Reactor fitted with a thermocouple attached to the Parr 4834 Heater. The pressure gauge and safety burst disc were rated up to 137 bar (2000 psi). The CO_2 pressure within the Batch Reactor was maintained using a Thar SFC ABPR. The CO_2 could be vented through the ABPR and then out of the system.

5.2.2 Experimental Conditions

The samples were reacted under different pressure and temperature conditions (Fig. 5.6) which allowed the slag samples to react with gaseous, liquid and supercritical CO_2. The amount of water used was also varied. The reaction time was kept constant at 19 hours throughout the experiments.

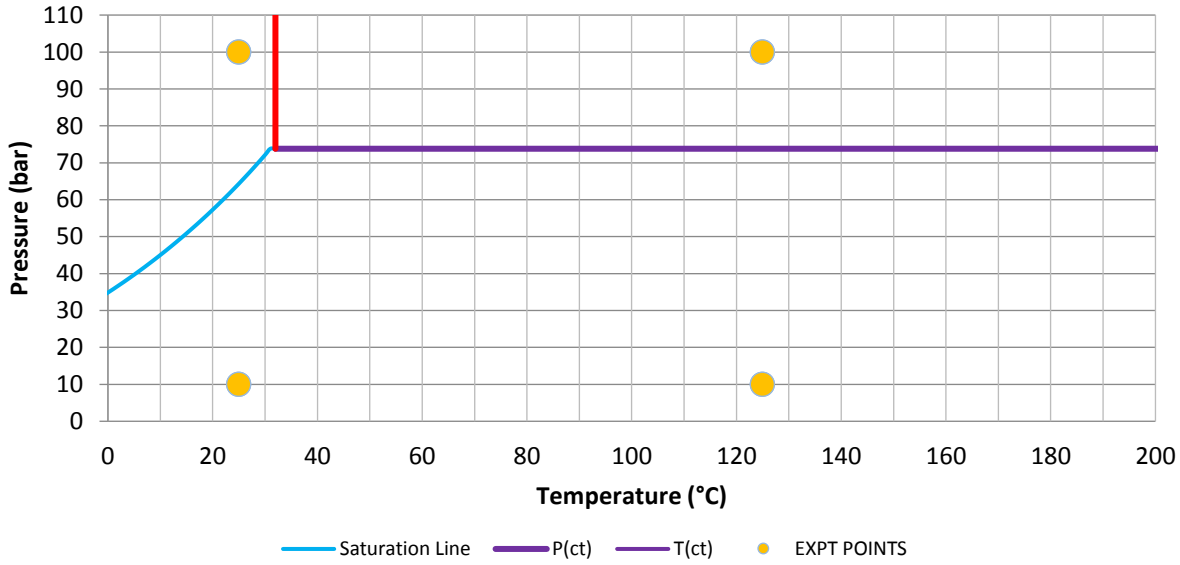

Figure 5.6: Pressure / Temperature conditions used in this study in relation to the maximum and minimum P/T conditions achievable with the apparatus. P(ct) is the critical pressure, T(ct) is the critical temperature.

5.2.2.1 Pressure

The operating pressure conditions were set either at 10 bar or 100 bar. The maximum operational pressure which could be used was dictated by the pressure rating of the FIKE Corporation safety burst disc (2000 psig / 137 bar ±5 %) and the local laboratory safety rules. Operational pressure could, therefore, be no more than 90% of the burst disc pressure rating (1900 psig / 123 bar). The laboratory safety pressure limit, as dictated by previous operational experience of using the pressure-rig setup, was set at 80% of the burst disc pressure (1600 psig / 109.8 bar). The minimum experimental operating pressure was set at 10 bar (1,000,000 Pa) CO_2, over four orders of magnitude greater than that of atmospheric pressure (CO_2 partial pressure in the atmosphere is 40 Pa). The maximum

experimental operating pressure was set at 100 bar CO_2, below the 109.8 bar local laboratory safety limit, but high enough to allow experiments to be run over several orders of magnitude.

5.2.2.2 Temperature

The temperature conditions used were 25˚C and 125˚C. The minimum experimental temperature of 25˚C was chosen to model the effects of higher than atmospheric pressures and concentrations of CO_2 at an easily maintainable temperature in the laboratory. A temperature of 25°C also realistically reflected general ambient environmental temperature conditions. The maximum experimental temperature of 125˚C was chosen to model temperature conditions which were of an order of magnitude larger than those of general ambient conditions, as well as to model the effects of superheated liquid water on the experimental material. Water at 10 bar and 100 bar pressure remains in a liquid state above 100˚C (vaporisation temperature of H_2O is 186.85˚C at 10 bar and 306.85˚C at 100 bar (Fig. 5.6).

5.2.2.3 Water availability

The moisture/water availability conditions used were either LOW (saturated to 15 wt. % of the material – the saturation point of 'Dust') or HIGH (excess water present). The LOW moisture content value used was based upon the saturation point of Dust as measured in the experiments carried out on 20 mm, 6 mm and Dust grain sizes (Chapter 2.5.3). HIGH moisture contents were attained by saturating the powdered samples until a visible layer of water covered the top of the sample. When experiments were carried out at conditions of 125˚C and HIGH water availabilities, a beaker containing 50 cm^3 of deionized water was placed into the reaction vessel to ensure that excess moisture was maintained within the reaction chamber preventing the samples from drying out.

5.2.2.4 Reaction Time

A reaction time of 19 hours was chosen as the maximum reaction length for both local laboratory health and safety reasons and for modelling a reasonable and economically viable length of time for an industrial process to occur. Local laboratory health and safety regulation meant that access to the laboratory was restricted during each experiment. Therefore, a reaction time of 19 hours was chosen to allow for the experiments to be run overnight (5pm -12 noon) minimising disruption to laboratory access. On an industrial basis, 19 hours was considered to be a short enough time length to be both economically viable and to allow for a quick turnover of material. Longer reaction times may hypothetically result in a higher yield of carbonate, but would necessarily be more expensive to operate and manage.

5.2.3 Experimental Materials

The materials used are detailed in Table 5.4. Steel slag has been shown to be a composite mixture of metals, metal oxides, metal-alumnide-oxides, olivines, assorted silicates, phosphides, hydroxides and carbonates. To investigate and mirror how the carbonation reactivity of some of these individual mineral families affected how the slag reacted, the following pure minerals were selected: Forsteritic Olivine to model the nesosilicate-family, Wollastonite to model short silicate-chain pyroxene-group silicates and Portlandite to model hydroxide minerals, initially identified within the Dust fraction of the steel slag. Further material details appeared in Chapter 2.

5.2.3.1 Olivine - $(Fe,Mg)SiO_2$

The olivine was sourced from lherzolite samples from the Peridot Canyon in San Carlos, Arizona. The olivine is present as gravity settled 'masses' within a basaltic lava flow. The spinel lherzolite masses are understood to have originated from the upper lithosphere and are Forsteritic in composition. Individual crystals ranged in composition from 75 to 85.82 % MgO (Frey et Prinz 1978). To obtain individual crystals of olivine, a lherzolite nodule was manually disaggregated with pure olivine phenocrysts <5 mm in size being manually picked to ensure a pure sample. The selected phenocrysts were then manually ground using an agate mortar and pestle to a size <250 µm.

This material had previously been studied as part of a carbonation reaction by Dufaud et al. (2009) at conditions of 1000 bar in an internally heated Ar-pressure vessel at 400-500°C. The reaction was run for 4 hours. The partial pressure of CO_2 was not reported. A conversion of olivine of 57% was reported.

5.2.3.2 Wollastonite – $CaSiO_3$

Wollastonite is a pyroxene mineral common within metamorphic rocks (DHZ 1992). It was chosen to model the pyroxene phase within steel slag, as steel slag contains several calcium silicates and has a high Ca-content (37.65 % CaO) (Chapter 2.3.4). The Wollastonite used in this study was bought from Fisher-Altec in a powdered form, with a grain size of <125 µm.

5.2.3.3 Portlandite – $Ca(OH)_2$

Portlandite was chosen due to the presence of hydroxide minerals in the slag products as identified by XRD (Chapter 2.5.5), which were also observed during the TGA analysis (Chapter 4.3) of passively weathered Dust. The Portlandite used in this study was bought from Fisher-Altec and displayed a grain size of <125 µm. Though only a minor component of the slag, hydroxide-minerals were predicted to form within the reaction fluid [Chapter 3.2].

5.2.3.4 'Dust'

The 'Dust' used in this study was the fine grained, steel slag fraction (<2 mm) derived by the crushing and screening of block steel slag into varying aggregate sizes. During the crushing process, the harder metallic blebs present in black steel slag are removed using an electromagnet. This results in the Dust fraction becoming 'depleted' in metallic-Fe in relation to other steel slag samples. Dust represented the smallest grain size fraction which was available for carbonation at the Redcar site. To date, it has proved to be by far the most reactive of all of the slag samples used, having a carbonation value of up to 17 Wt. % via passive weathering.

5.2.3.5 6 mm and 20 mm Steel Slag

The 6 mm and 20 mm grain size fractions are derived by the crushing and screening of block steel slag into its respective aggregate sizes. 20 mm steel slag aggregate represented the largest grain size aggregate fraction available for carbonation at the Redcar site.

5.2.3.6 Pellite and Pellite Powder

Pellite is produced by spraying molten blast furnace slag with water to produce a foaming pyroclastic material which is then pelletized by pouring the foamed material onto a water-cooled rotating drum. Pellite is similar to pumice in morphology. Pellite powder was prepared by hand-grinding a sample of Pellite to a <250 μm powder.

5.2.3.7 GBFS and GBFS Powder

Granulated Blast Furnace Slag (GBFS) is produced by pouring molten blast furnace slag onto a water-cooled rotating drum under conditions of excess water. This results in the instant solidification of the molten slag into shards. GBFS displays a glassy texture and is similar to Pele's hair in morphology. GBFS powder was prepared by hand-grinding a sample of GBFS to a <250μm powder.

Material	Composition	Locality	Grain Size	Treatment
Olivine	Mg-Rich (Frey et Prinz 1978)	Peridot Canyon, San Carlos, Arizona	Mixed size of picked Ol. Phenocrysts (<5 mm)	Ground to <250µm, no further treatment
Wollastonite	Ca_2SiO_3	Artificial	<125 µm powder	None
Calcium Hydroxide	$Ca(OH)_2$	Artificial	<125 µm powder	None
Dust	Mixed [Chapter 2.5.5]	Redcar	<2 mm [Chapter 2.5.2]	None
6 mm	Mixed [Chapter 2.5.5]	Redcar	6 mm	None
20 mm	Mixed [Chapter 2.5.5]	Redcar	20 mm	None
Pellite	Mixed [Chapter 2.5.5]	Redcar	4 mm-500 µm	None
Pellite Powder	Mixed [Chapter 2.5.5]	Redcar	<250 µm	Ground to <250µm, no further treatment
GBFS	Mixed [Chapter 2.5.5]	Redcar	1 mm-125 µm	None
GBFS Powder	Mixed [Chapter 2.5.5]	Redcar	<250 µm	Ground to <250µm, no further treatment

Table 5.4: Descriptions of the materials used in this study.

5.2.4 Experimental Method

Prior to the start of the experiment, the batch reactor was heated to the required experimental temperature. The pre-prepared samples of olivine, Wollastonite and Portlandite were weighed and placed into Pyrex test tubes in quantities of 0.7 g (due to the small number of grains picked), 5 g and 5g respectively. The pre-prepared samples of Dust, 6 mm aggregate and 20 mm aggregate were weighed and placed into Pyrex boiling tubes in quantities of 10 g each. A further Pyrex boiling tube containing mixed 6 mm and 20 mm aggregate was prepared to provide ample material for analysis by thin section, by SEM back-scatter imaging and elemental mapping after the experiment. Water was then added to the samples. For LOW water availability conditions, water was added in a volume equal to 15 wt. % of the weight of the initial sample. For HIGH water availability conditions an excess of water was added. The tubes containing the samples were then placed into a 500 cm^3 Pyrex beaker and placed into the centre of the batch reactor. The reactor was then sealed using bolt-tightened clamps. Gas inlet and outlet pipes were connected to the reactor from the Thar gas-control assembly. The gas supply-rate, maximum pressure value and emergency shutdown pressure values were input into the computer system and double checked.

The gas supply (industrial-grade CO_2 from a liquid-withdrawal canister) was then turned on. For experiments at 10 bar the gas supply was turned on until the reactor achieved a pressure of 15 bar. All connections were then tested using Snoop solution. The gas supply was then turned off and the pressure reduced to 10 bar by manual computerised-operation of the Automatic Back Pressure Regulator. The reactor was then sealed using the needle-valve taps at the top of the reactor gas lines. For experiments conducted at 100 bar the gas supply was turned on until the reactor achieved a pressure of 50 bar. All connections were then tested using Snoop solution. The pressure was then increased until the 100 bar pressure was achieved. All computerised systems were then checked for a further 30 minutes to ensure that experimental equilibrium had been reached and that all systems were operational before the experiment was left to run overnight.

5.2.5 TGA Analysis

A sub-sample of the crushed material was required for TGA analysis. The method of TGA analysis used was identical to that outlined in Chapter 4.2.2.

5.2.6 Petrographical Analysis

Thin-sections were produced for the suite of reacted steel slag aggregates to examine the 3D cross section of carbonation mineralisation. Samples of steel slag aggregate were also mounted onto steel stubs to enable SEM observations to be made.

5.2.7 SEM Analysis

Petrographical surface analysis of reacted 20 mm grains of steelmaking-slag was undertaken using a Hitachi TM-1000 Table-Top SEM with EDX data acquired using an Oxford-Instruments EDS Detector in the Department of Earth Sciences, University of Durham. Elemental mapping of samples was carried out using a Hitachi TM-3000 Table-Top SEM with EDX data acquired using an Oxford-Instruments EDS Detector in the Department of Archaeology, University of Durham. Data was acquired with varying scan times as stated. Optical Petrography was undertaken using a Zeiss Axio microscope with a Zeiss AxioCam ERc5s attachment for digital photography.

5.3 Results

5.3.1.1 Steel Slag Products

The results from the batch experiments of steel slags are displayed in Table 5.5. All active reaction experiments produced carbonation values higher than their initial fresh unreacted samples. All samples were run in duplicate.

	Mean Values (Wt. %)		
Expt. Conditions	DUST	6 mm	20 mm
FRESH	3.40	0.000	0.00
LpLtLs	8.05	1.01	0.10
LpLtHs	6.51	1.42	0.17
LpHtLs	12.16	1.09	0.31
LpHtHs	11.30	1.53	0.83
HpLtLs	8.01	1.296	0.84
HpLtHs	5.06	0.63	0.28
HpHtLs	12.73	0.63	0.29
HpHtHs	9.33	2.78	0.75

Table 5.5: The values for fresh unreacted samples and average Wt. % carbonation results for each experimental run. (Lp – 10 bar, Hp - 100 bar, Lt - 25°C, Ht - 125°C, Ls – LOW water availability, Hs – HIGH water availability)

20 mm Aggregate

The results from the 20 mm aggregate batch experiments ranged from 0.045 wt. % to 1.38 Wt. %, or 0.75-23.03 times that of the highest measured value for passive carbonation (0.06 wt. %). The highest average carbonation of any experimental run was 0.84 wt. % (14.11 times greater than that of the highest passive value) and was produced under conditions of 100 bar/25°C/LOW water availability (HpLtLs). This was closely followed by 0.83 wt. % (13. 94 times greater than the highest passive value) which was produced at conditions of 10 bar/125°C/HIGH water availability (LpHtHs). The data showed a trend towards higher carbonation with higher magnitude reaction conditions (Fig. 5.7).

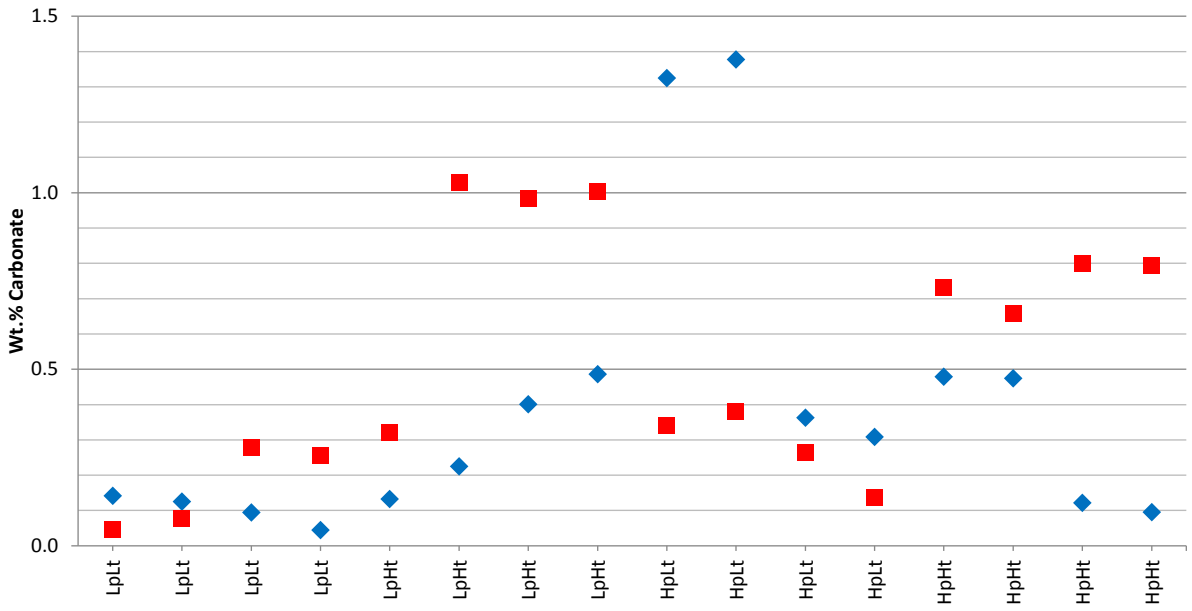

Figure 5.7: Graph showing the carbonation values achieved for 20 mm aggregate slag under the active reaction conditions. Blue diamonds – low water availability, Red squares – high water availability.

6 mm Aggregate

The results from the 6 mm aggregate batch experiments ranged from 0.50 wt. % to 2.96 wt. %, or 1.90 to 6.42 times that of the highest measured value for passive carbonation (0.46 wt. %). The highest average carbonation of any experimental run was 2.78 Wt. % (6.03 times greater than the highest passive value) and was produced at conditions of 100 bar/125°C/HIGH water availability (HpHtHs). The data showed a trend towards higher carbonation values with higher magnitude conditions. Higher pressures and higher water availability appeared to enhance the carbonation of the material (Fig. 5.8).

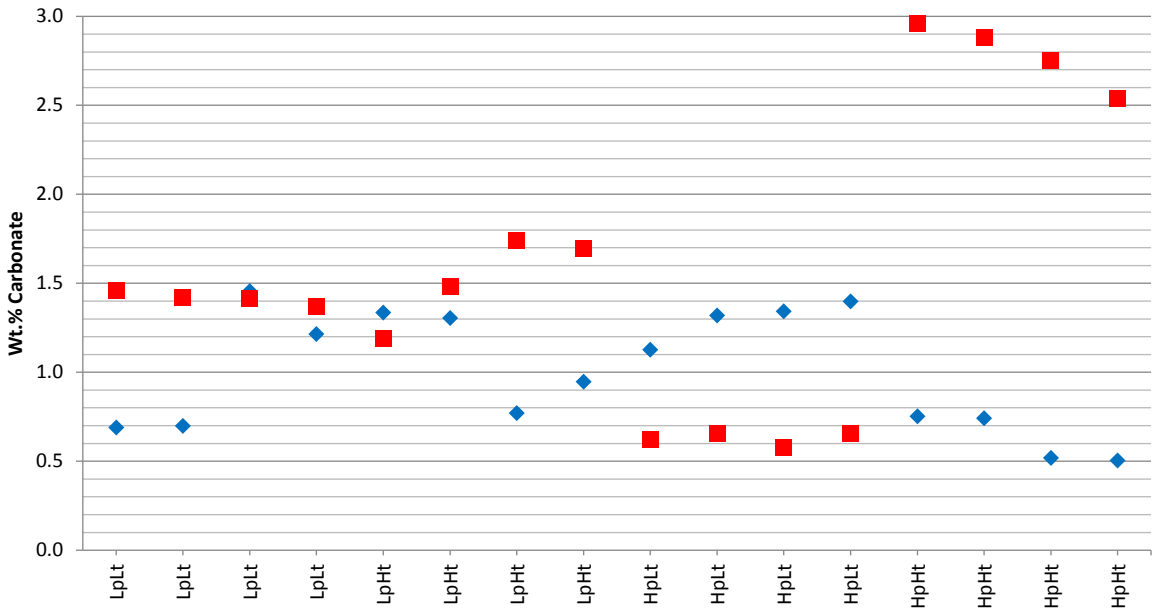

Figure 5.8: Graph showing the carbonation values achieved for 6 mm aggregate slag under the active reaction conditions. Blue diamonds – low water availability, Red squares – high water availability.

Dust

The results from the Dust batch experiments ranged from 4.65 wt. % to 12.97 wt. %, or 0.33 to 0.92 times that of the highest measured value for passive carbonation (14.05 wt. %). The highest average carbonation of any experimental run was 12.73 wt. % (0.72 times greater than the highest passive value) and was produced under conditions of 100 bar/125°C/LOW water availability (HpHtLs). The data showed a trend towards higher carbonation values with higher temperatures with no apparent pressure dependence. (Fig. 5.9).

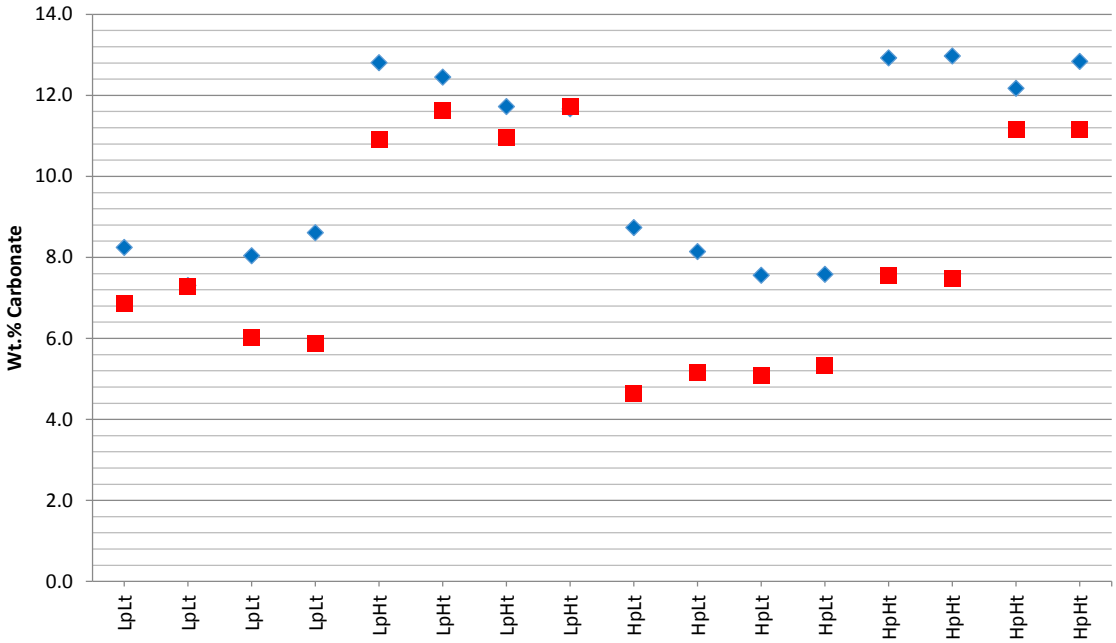

Figure 5.9: Graph showing the carbonation values achieved for Dust aggregate slag under the active reaction conditions. Blue diamonds – low water availability, Red squares – high water availability.

Steel Slag Carbonation vs. HCO_3^- Concentration and Water Availability

Fig. 5.10 shows the carbonation results separated by the water availability of each experiment and plotted alongside HCO_3^- Concentration.

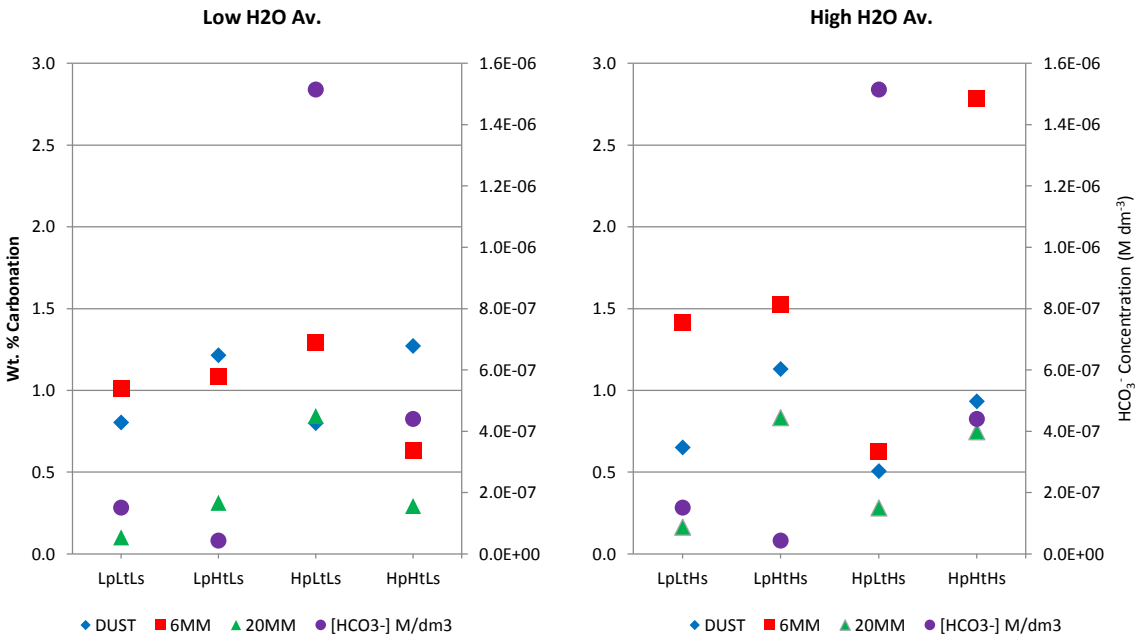

Figure 5.10: Carbonation values achieved by different materials in relation to the theoretical concentration of dissolved HCO_3^- present in the H_2O surrounding each sample.

Ideal Conditions

Based upon the data collected in this study the ideal conditions for carbonation can be tabulated for each material (Table 5.6, 5.7, 5.8).

20 mm aggregate - The carbonation of 20 mm aggregate steel slag appeared to be related to the variations in HCO_3^- concentration under low water availabilities and inversely related to the variations in HCO_3^- concentration with high water availabilities. Factors other than carbonation potential may be responsible for this. During high water availability, the increased kinetics of the carbonation reaction may result in a faster growth of precipitated carbonate crystals (than at lower temperatures) and this is a reflection of the reaction rate rather than of carbonation potential.

Apart from high pressure / low temperature conditions, all of the reactions produced higher carbonation values at higher water availabilities. This may be due to the precipitated crystals being able to grow out into the reaction fluid as opposed to being restricted to a thin film surrounding each grain. It was Interesting to note that LpHtHs and HpHtLs conditions produced similar carbonation values, as did HpLtHs and HpHtLs conditions.

20 mm	Low Temperature	High Temperature
Low Pressure	HIGH	HIGH
High Pressure	LOW	HIGH

Table 5.6: Table for 20 mm steel slag aggregate showing the order of carbonation values (red – 1st, orange - 2nd, green - 3rd, blue 4th) under different pressure and temperature conditions and the availability of water that yielded the highest carbonation values under those conditions.

6 mm aggregate - The carbonation of 6 mm aggregate steel slag appeared to be related to variations in HCO_3^- concentrations under low water availabilities and inversely related to variations in HCO_3^- concentrations with high water availabilities. As was the case for 20 mm aggregate, under high water availability the increased kinetics of the carbonation may have resulted in a faster growth of precipitated crystals and was a reflection of the reaction rate rather than of the carbonation potential.

Apart from High pressure / low temperature conditions, all of the reactions produced higher carbonation values at higher water availabilities. This, once again, may have been due to the precipitated crystals being able to grow out into the reaction fluid as opposed to being restricted to a thin film around each grain. It was noted that HpLtHs and HpHtLs conditions produced similar carbonation values and in a pattern similar to that of 20 mm aggregate.

6 mm	Low Temperature	High Temperature
Low Pressure	HIGH	HIGH
High Pressure	LOW	HIGH

Table 5.7: Table for 6 mm steel slag aggregate showing the order of carbonation values (red – 1st, orange - 2nd, green - 3rd, blue 4th) under different pressure and temperature conditions and the availability of water that yielded the highest carbonation values under those conditions.

Dust - The carbonation of Dust appeared to be directly related to HCO_3^- concentrations. When HCO_3^- concentrations were lower, the carbonation values were lower. This may be due to the effect of increased kinetics of carbonation under higher temperatures, which resulted in the formation of crusts above the 'paste-like' wetted dust at a quicker rate than at lower temperatures.

The preferred hydration conditions in all of the experiments were those of lower water availability. This was likely because lower water availability allowed the porosity and/or permeability to remain open for longer during the reaction, but the lower water availability also hindered the extent to which carbonation was possible. Agitation of the Dust + H_2O mixture would have been useful in reducing the effects of the paste rheology.

Dust	Low Temperature	High Temperature
Low Pressure	**LOW**	**LOW**
High Pressure	**LOW**	**LOW**

Table 5.8: Table for Dust showing the order of carbonation values (red – 1st, orange - 2nd, green - 3rd, blue 4th) under different pressure and temperature conditions and the availability of water that yielded the highest carbonation values under those conditions.

5.3.1.2 Blast Furnace Slags

The results from the batch experiments of the blast furnace slags (Pellite and GBFS) are displayed in Table 5.9 and are compared in Fig. 5.11. All active reaction experiments produced carbonation values higher than their initial fresh unreacted samples, with the powdered forms of each material achieving higher carbonation values than the granular forms. Individual differences are explained below.

	Average Values (Wt. %)			
Expt. Conditions	Pellite	Pellite Powder	GBFS	GBFS Powder
STANDARD	0.73	0.73	0.001	0.001
LpLtLs	0.36	1.35	0.007	0.13
LpLtHs	0.44	2.68	0.026	0.16
LpHtLs	0.38	1.49	0.075	0.72
LpHtHs	0.52	2.599	0.295	1.85
HpLtLs	0.37	2.996	0.022	0.16
HpLtHs	0.59	1.33	0.037	0.19
HpHtLs	0.87	3.096	0.32	1.43
HpHtHs	1.66	4.006	0.35	2.84

Table 5.9: The values for fresh unreacted Pellite and GBFS and average Wt. % carbonation results for each experimental run. (Lp – 10 bar, Hp - 100 bar, Lt - 25°C, Ht - 125°C, Ls – LOW water availability, Hs – HIGH water availability)

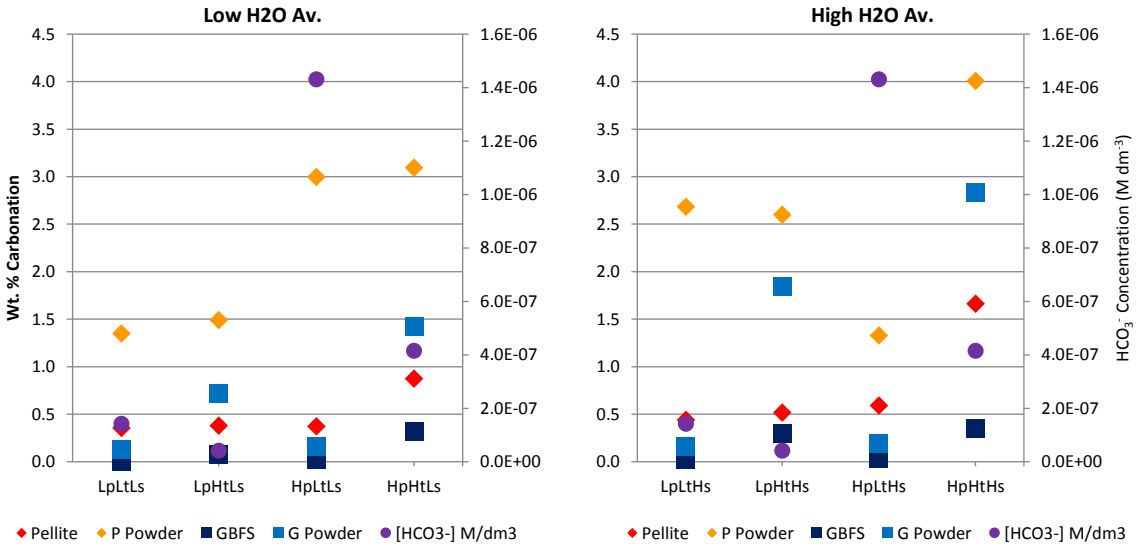

Figure 5.11: Comparison of the carbonation values achieved by samples of different blast furnace slag morphologies. Also plotted are the theoretical HCO_3^- concentrations present during each experiment.

Pellite

The results from the batch reaction of Pellite grains ranged from 0.15 wt. % to 1.83 wt. %, or 0.2 to 2.63 times that of the highest measured values for passive carbonation (0.69 wt. %). The highest average carbonation of any experimental run was 1.66 wt. % (2.39 times greater than that of the highest passive value) and was produced in conditions of 100 bar/125°C/HIGH water availability (HpHtHs). The data showed a trend towards higher carbonation values at higher magnitude pressures and temperatures and at high water availability (Fig. 5.12).

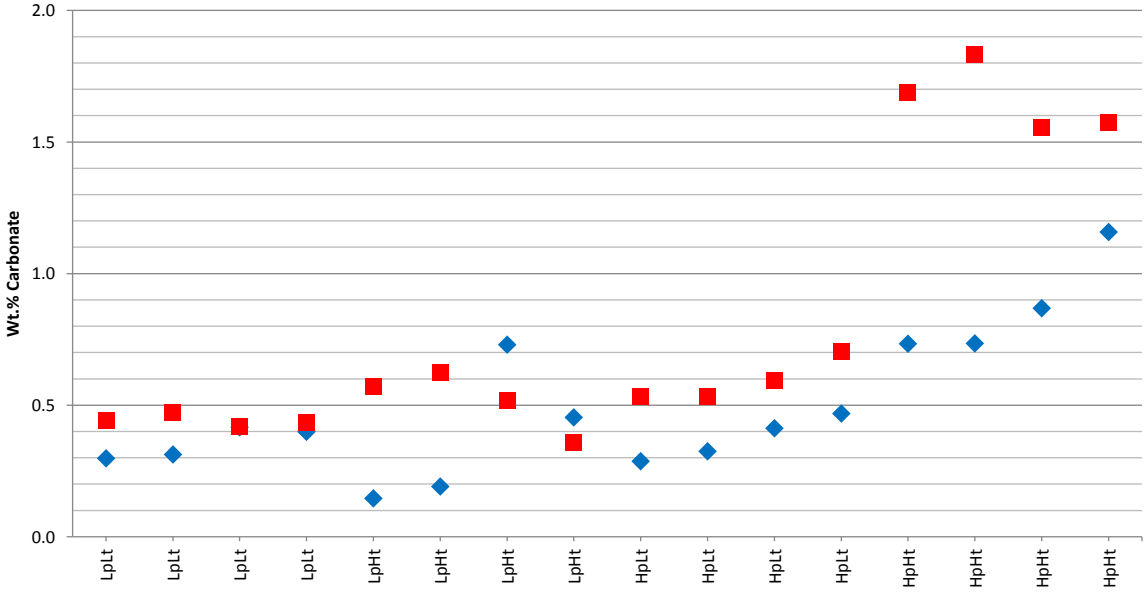

Figure 5.12: Graph showing the carbonation values achieved for grains of Pellite slag under the active reaction conditions. Blue diamonds – low water availability, Red squares – high water availability.

Pellite Powder

The results from the batch reaction of powdered (<250 µm) Pellite slag ranged from 1.31 wt. % to 4.025 wt. %, or 1.88 to 5.78 times that of the highest measured values for the passive carbonation of Pellite grains (0.6964 wt. %) this was likely due to the grain size of the material being a factor of four times finer than that of the material used in the passive study. The highest average carbonation of any experimental run was 4.006 wt. % (5.75 times greater than the highest passive value for granular Pellite) and was produced under conditions of 100 bar/125°C/HIGH and water availability (HpHtHs). The data showed a trend towards higher carbonation values with higher pressure and higher water availability (Fig. 5.13).

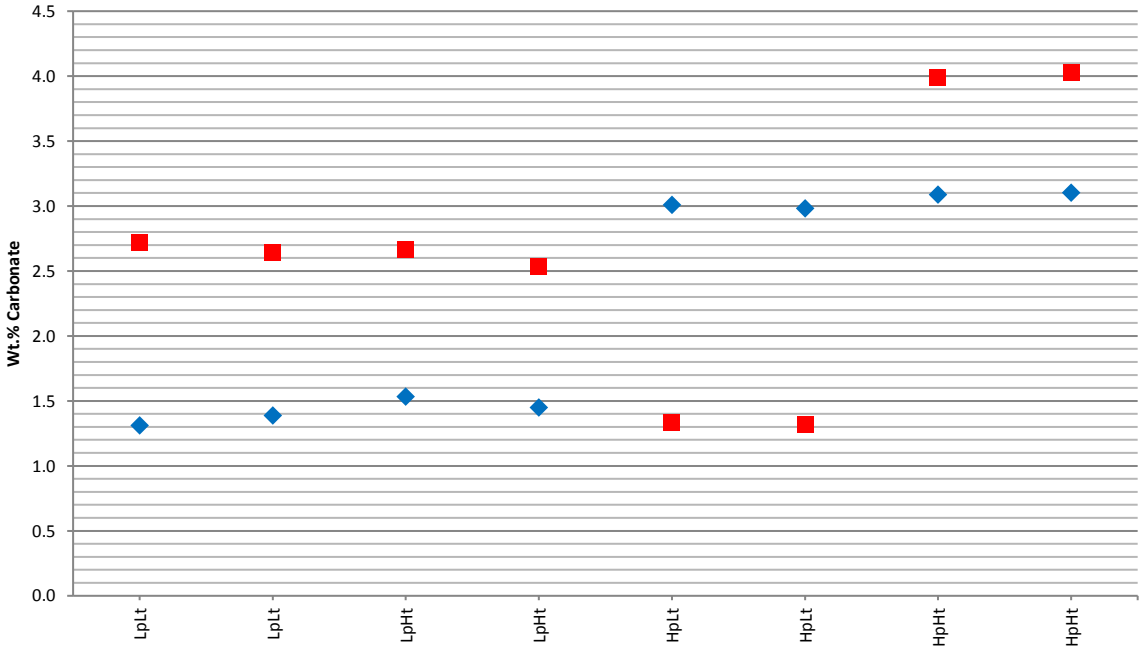

Figure 5.13: Graph showing the carbonation values achieved for powdered (<250 µm) Pellite slag under active reaction conditions. Blue diamonds – low water availability, Red squares – high water availability.

Pellite Carbonation vs. HCO_3^- Concentration and Water Availability

Fig. 5.14 shows the carbonation results as influenced by the water availability for each experiment and plotted alongside HCO_3^- Concentration.

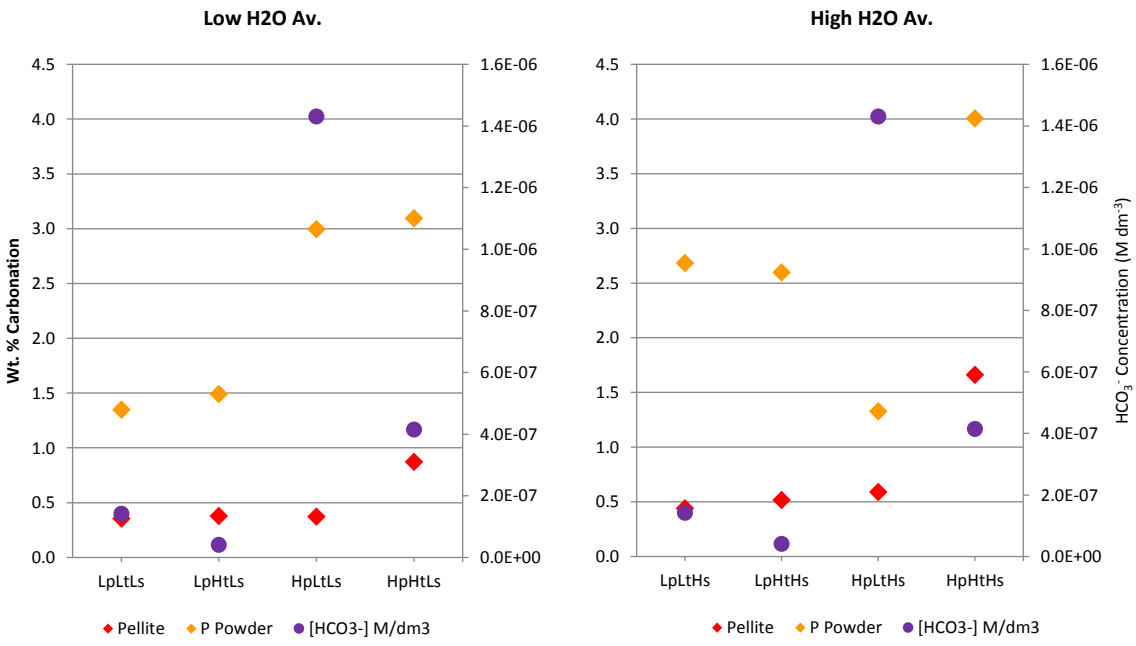

Figure 5.14: Pellite carbonation vs. the theoretical concentration of dissolved HCO_3^- concentration and water availability

Ideal Conditions

Based upon the data collected in this study the ideal conditions for carbonation can be tabulated for each material (Table. 5.10, 5.11).

Pellite	Low Temperature	High Temperature
Low Pressure	HIGH	HIGH
High Pressure	HIGH	HIGH

Table 5.10: Table for Pellite slag aggregate showing the order of carbonation values (red – 1st, orange - 2nd, green - 3rd, blue 4th) under different pressure and temperature conditions and the availability of water that yielded the highest carbonation values under those conditions.

Pellite Powder	Low Temperature	High Temperature
Low Pressure	**HIGH**	**HIGH**
High Pressure	**LOW**	**HIGH**

Table 5.11: Table for powdered (<250µm) Pellite slag aggregate showing the order of carbonation values (red – 1st, orange - 2nd, green - 3rd, blue 4th) under different pressure and temperature conditions and the availability of water that yielded the highest carbonation values under those conditions.

Interpretation

The carbonation values of both Pellite and Pellite powder showed a trend of increasing carbonation with higher magnitude reaction conditions, with there being no discernible correlation with HCO_3^- concentration. Under low water availabilities, there was a minor increase in carbonation with a decrease in HCO_3^- concentration within the low and high pressure data sets. Under conditions of high water availability there was a decrease in carbonation with a decrease in HCO_3^- concentrations between Low pressure and low temperature to Low pressure / high temperature conditions. However, there was an inverse relationship with HCO_3^- ion concentration between High pressure and low temperature to High pressure / high temperature conditions. The material, therefore, carbonated better under conditions of enhanced temperature. The data sets for granular Pellite and powdered Pellite approximately mirror each other. However, there was on average a 4.38 fold increase in carbonation due to the powdering (roughly approximating the decrease in grain size achieved by powdering the material). While several samples of powdered Pellite were well-cemented within the boiling-tubes after reaction. No samples appeared to develop the 'crusting' observed with Dust or calcium hydroxide samples. This indicated that there was still an appreciable amount of permeability within the samples and suggested that higher carbonation values may well be achieved with a longer reaction time, without necessarily requiring the material to be agitated.

GBFS

The results from the batch reaction of GBFS grains ranged from 0.0024 wt. % to 0.45 wt. %, or 0.012 to 2.209 times that of the highest measured values of passive carbonation (0.204 wt. %). The highest average carbonation of any experimental run was 0.35 wt. % (1.71 times greater than the highest passive value) and was produced under conditions of 100 bar/125°C/HIGH water availability (HpHtHs). The data showed a trend towards higher carbonation values with higher temperatures with no apparent pressure dependency. Higher water availability was more important at lower pressures, but there was no apparent effect of water availability at higher pressures (Fig. 5.15).

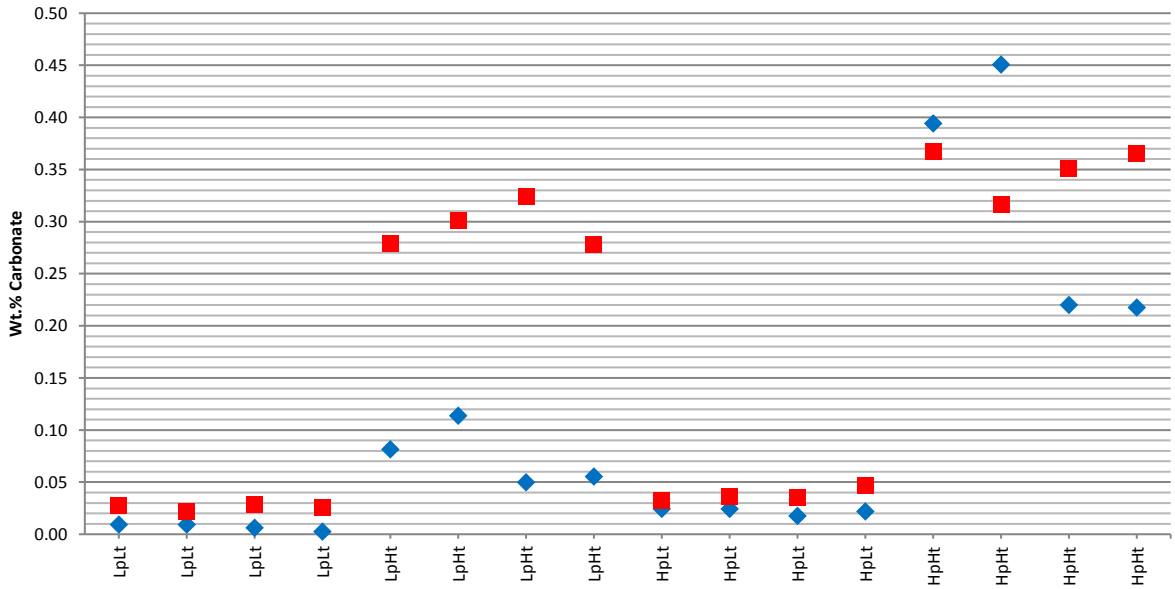

Figure 5.15: Graph showing the carbonation values achieved for grains of GBFS slag under the active reaction conditions. Blue diamonds – low water availability, Red squares – high water availability.

GBFS Powder

The results from the batch reaction of powdered (<250 µm) GBFS slag ranged from 0.12 wt. % to 2.91 wt. %, or 0.581 to 14.25 times that of the highest measured value for the passive carbonation of GBFS grains which was (0.204 wt. %) and was likely due to the grain size of the material being a factor of four times finer than that of the material used in the passive study. The highest average carbonation value for any experimental run was 2.84 wt. % (13.92 times greater than the highest passive value of granular GBFS) and was produced under conditions of 100 bar/125°C/HIGH water availability (HpHtHs). The data showed a trend towards higher carbonation values with higher temperatures, with no apparent change in carbonation values as a result of a change in pressure. Conditions of higher temperature and high water availability favour the reaction (Fig. 5.16).

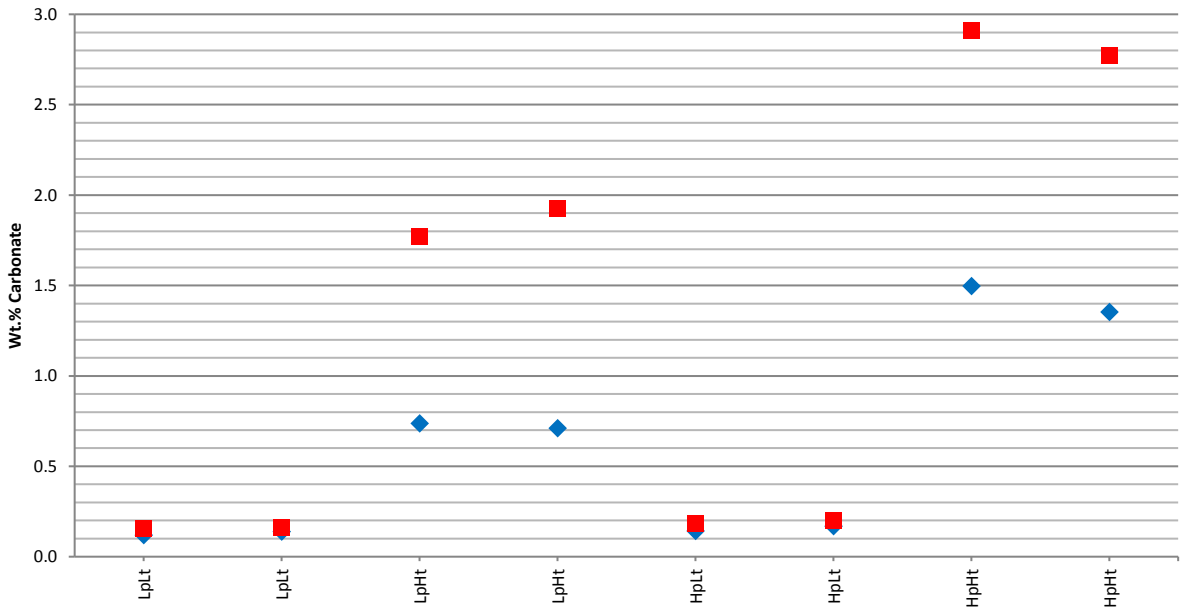

Figure 5.16: Graph showing the carbonation values achieved for powdered (<250 µm) GBFS slag under the active reaction conditions. Blue diamonds – low water availability, Red squares – high water availability.

GBFS Carbonation vs. HCO_3^- Concentration and Water Availability

Fig. 5.17 displays the carbonation results as influenced by water availability for each experiment and plotted alongside HCO_3^- concentration.

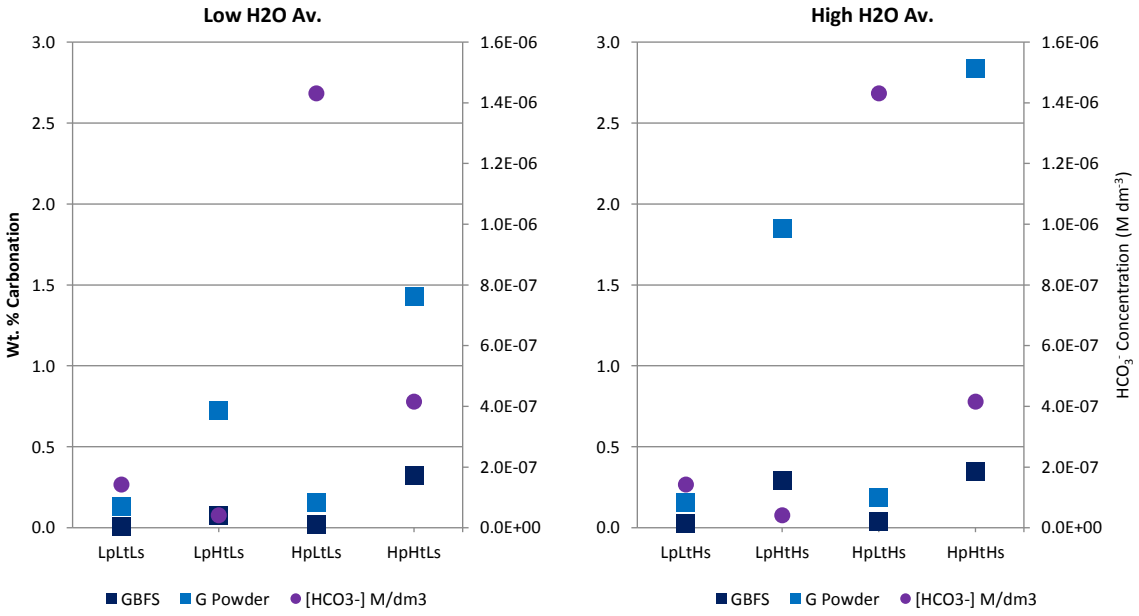

Figure 5.17: GBFS carbonation vs. the theoretical concentration of dissolved HCO_3^- concentration and water availability

Ideal Conditions

Based upon the data collected in this study the ideal conditions for carbonation can be tabulated for each material (Table. 5.12, 5.13).

GBFS	Low Temperature	High Temperature
Low Pressure	**HIGH**	**HIGH**
High Pressure	**HIGH**	**HIGH**

Table 5.12: Table for GBFS slag aggregate showing the order of carbonation values (red – 1st, orange - 2nd, green - 3rd, blue 4th) under different pressure and temperature conditions and the availability of water that yielded the highest carbonation values under those conditions.

GBFS Powder	Low Temperature	High Temperature
Low Pressure	**HIGH**	**HIGH**
High Pressure	**HIGH**	**HIGH**

Table 5.13: Table for powdered (<250µm) GBFS slag aggregate showing the order of carbonation values (red – 1st, orange - 2nd, green - 3rd, blue 4th) under different pressure and temperature conditions and the availability of water that yielded the highest carbonation values under those conditions.

Interpretation

The carbonation values of GBFS and GBFS powder showed that an increase in the pressure had only a minor effect on the carbonation value, with the carbonation of the materials increasing by only 1.8 to 2.2 times over a one-order-of-magnitude increase in CO_2 pressure. However, an increase in temperature significantly affected the carbonation of the materials by 9.9 to 12 times over a one-order-of-magnitude increase in temperature (Table 5.14).

LL	LH	**9.86**
HL	HH	**11.99**
1.76	**2.24**	**GBFS**

Table 5.14: Difference in carbonation due to temperature (LL/LH and HL/HH – right hand column), and pressure (LL/HL and LH/HH – bottom row).

The data sets for GBFS and powdered GBFS approximately mirrored each other. However there was, on average, an 8.17 fold increase in carbonation due to powdering (slightly greater than, but roughly approximating to, the decrease in grain-size achieved by powdering the material). While several samples of powdered GBFS were well-cemented within the boiling-tubes after reaction, no sample appeared to develop the 'crusting' observed with Dust or calcium hydroxide samples. This indicated that there was still an appreciable amount of permeability within the samples suggesting that higher carbonation values may well be achieved with a longer reaction time.

5.3.1.3 Standard Minerals

The results from the batch experiments on the mineral standards are displayed in Table 5.15. All active reaction experiments produced carbonation values higher than their initial fresh unreacted samples.

	Mean Values (Wt. %)		
Expt. Conditions	Olivine	Wollastonite	$Ca(OH)_2$
STANDARD	0.00	2.51	0.00
LpLtLs	0.016	13.45	32.08
LpLtHs	0.009	8.64	17.83
LpHtLs	0.027	20.13	38.24
LpHtHs	0.026	26.61	10.39
HpLtLs	0.008	13.16	42.027
HpLtHs	0.023	7.79	14.74
HpHtLs	0.095	20.24	40.77
HpHtHs	0.082	14.27	42.24

Table 5.15: The values for fresh unreacted mineral standards and average Wt. % carbonation results for each experimental run. (Lp – 10 bar, Hp - 100 bar, Lt - 25°C, Ht - 125°C, Ls – LOW water availability, Hs – HIGH water availability)

San Carlos Olivine - The carbonation results from the batch reaction of the samples of San Carlos Peridotite ranged from 0.0071 wt. % (HpLtLs) to 0.104 wt. % (HpHtLs) or (14.65 times difference). The highest average carbonation for any experimental run was 0.095 wt. % and was produced under conditions of 100 bar/125°C/LOW water availability (HpHtLs). The preferential conditions for carbonation were those of high pressure and high temperature (Fig. 5.18).

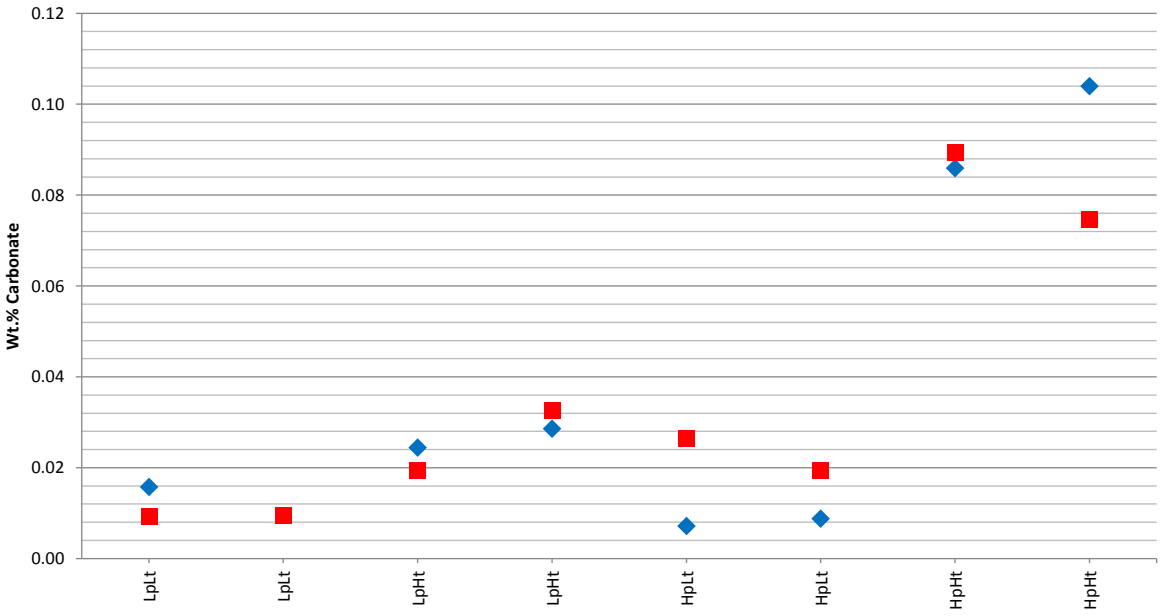

Figure 5.18: Graph showing the carbonation values achieved for San Carlos Olivine under the active reaction conditions. Blue diamonds – low water availability, Red squares – high water availability.

SCP Carbonation vs. HCO_3^- Concentration and Water Availability

Fig. 5.19 shows the carbonation results as influenced by water availability for each experiment plotted alongside HCO_3^- concentration.

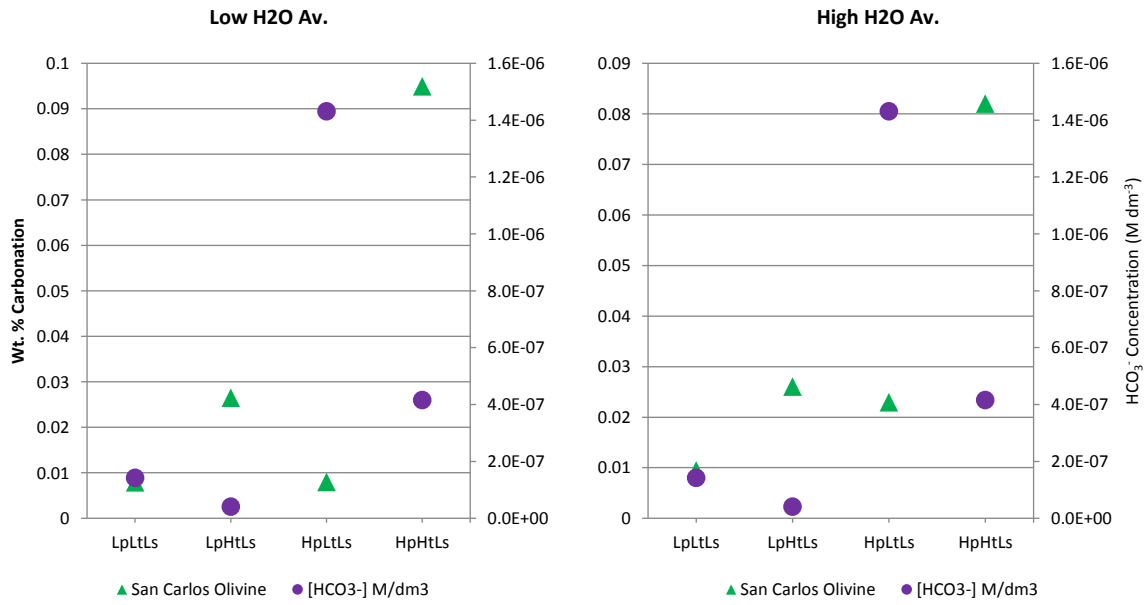

Figure 5.19: SCP carbonation vs. the theoretical concentration of dissolved HCO_3^- concentration and water availability

Ideal Conditions

Based upon the data collected in this study the ideal conditions for Olivine carbonation has been tabulated (Table 5.16).

SCP	Low Temperature	High Temperature
Low Pressure	HIGH	LOW
High Pressure	HIGH	LOW

Table 5.16: Table for powdered San Carlos peridotite derived olivine showing the order of carbonation values (red – 1st, orange - 2nd, green - 3rd, blue 4th) under different pressure and temperature conditions and the availability of water that yielded the highest carbonation values under those conditions.

The carbonation conditions for olivine appear to be inversely related to the HCO_3^- concentrations. When HCO_3^- concentration were higher the carbonation values were lower. Olivine appeared to carbonate most readily at higher temperatures. At low temperature conditions, higher water availability was the preferred condition, but at higher temperatures lower water availability was the preferred condition.

Wollastonite - The carbonation results from the batch reaction of the samples of artificial Wollastonite ranged from 7.63 wt. % (HpLtHs) to 26.67 wt. % (LpHtHs) or (3.49 times difference between the minimum and maximum values and between 3 to 10.6 times that of an initial unreacted sample). The highest average carbonation of any experimental run was 26.63 wt. %. This was produced under conditions of 10 bar/125°C/HIGH water availability (LpHtHs). Higher temperature conditions were preferential for carbonation (Fig. 5.20).

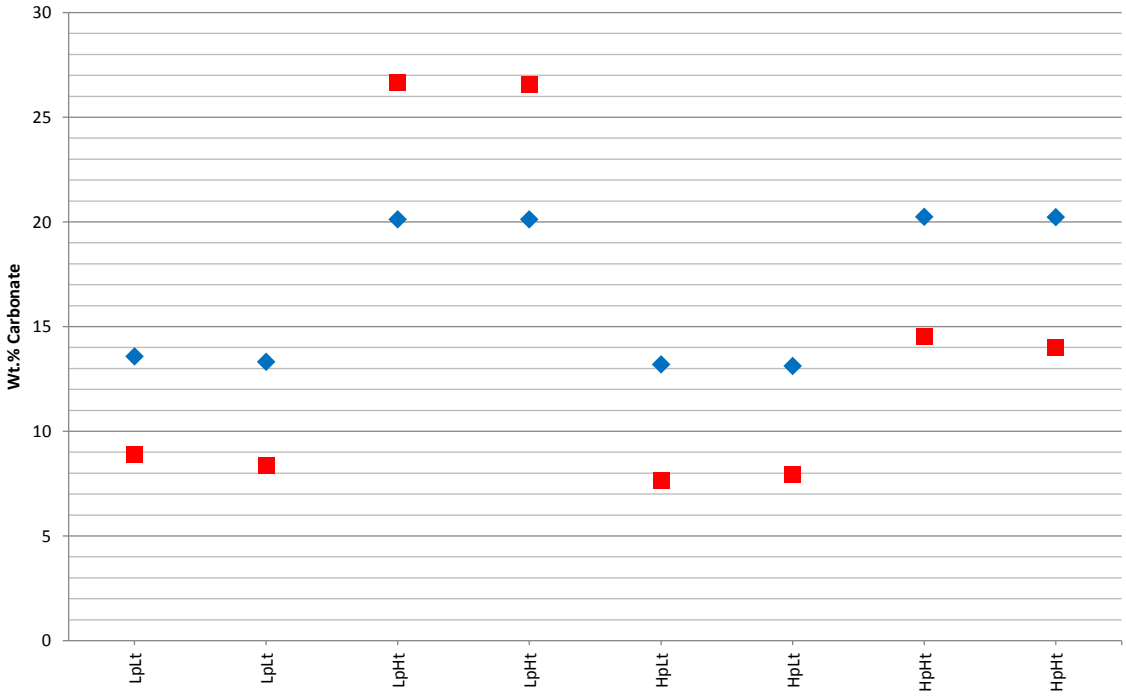

Figure 5.20: Graph showing the carbonation values achieved for Wollastonite under the active reaction conditions. Blue diamonds – low water availability, Red squares – high water availability.

Wollastonite Carbonation vs. HCO_3^- Concentration and Water Availability

Fig. 5.21 shows the carbonation results as influenced by water availability for each experiment and plotted alongside HCO_3^- concentration.

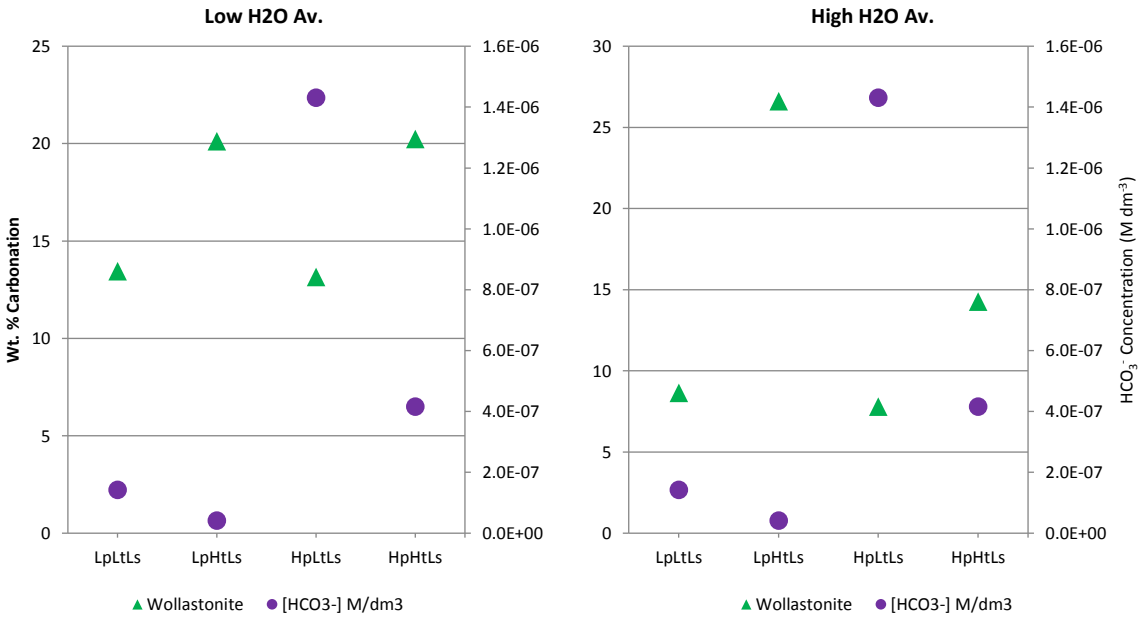

Figure 5.21: Wollastonite carbonation vs. the theoretical concentration of dissolved HCO_3^- concentration and water availability

Ideal Conditions

Based upon the data collected in this study the ideal conditions for Wollastonite carbonation have been tabulated (Table 5.17).

Wo.	Low Temperature	High Temperature
Low Pressure	LOW	HIGH
High Pressure	LOW	LOW

Table 5.17: Table for powdered Wollastonite showing the order of carbonation values (red – 1st, orange - 2nd, green - 3rd, blue 4th) under different pressure and temperature conditions and the availability of water that yielded the highest carbonation values under those conditions.

The carbonation conditions of Wollastonite appeared to be related inversely to the HCO_3^- concentrations. When HCO_3^- concentration were higher, carbonation values were lower. This effect was due to the increase in temperature of the reaction conditions. Wollastonite appeared to carbonate more readily at higher temperatures. At low temperature conditions, lower water availability was the preferred condition, but at higher temperatures higher water availability was preferred under low pressure. Lower water availability was also the preferred condition under higher pressure. This may be partly explained by the formation of crusts under such conditions which blocked the porosity and/or permeability of the sample in the test tube due to the rapid formation of carbonate minerals. Lower water availabilities allow the porosity and/or permeability to remain open for longer during the reaction, but this also hindered the extent of the carbonation possible. Agitation of the Wollastonite and water mixture would be required to reduce the effects of the paste rheology.

Calcium Hydroxide

The carbonation results from the batch reaction for samples of artificial calcium hydroxide ranged from 8.59 wt. % (LpHtHs) to 42.63 wt. % (HpHtHs) or (4.95 times difference between the minimum and maximum values, with the initial unreacted samples containing no carbonate). The highest average carbonation of any experimental run was 41.51 wt. % which was produced at conditions of 100 bar/125°C/LOW water availability (HpHtLs). Low water availability favoured the reaction (Fig. 5.22).

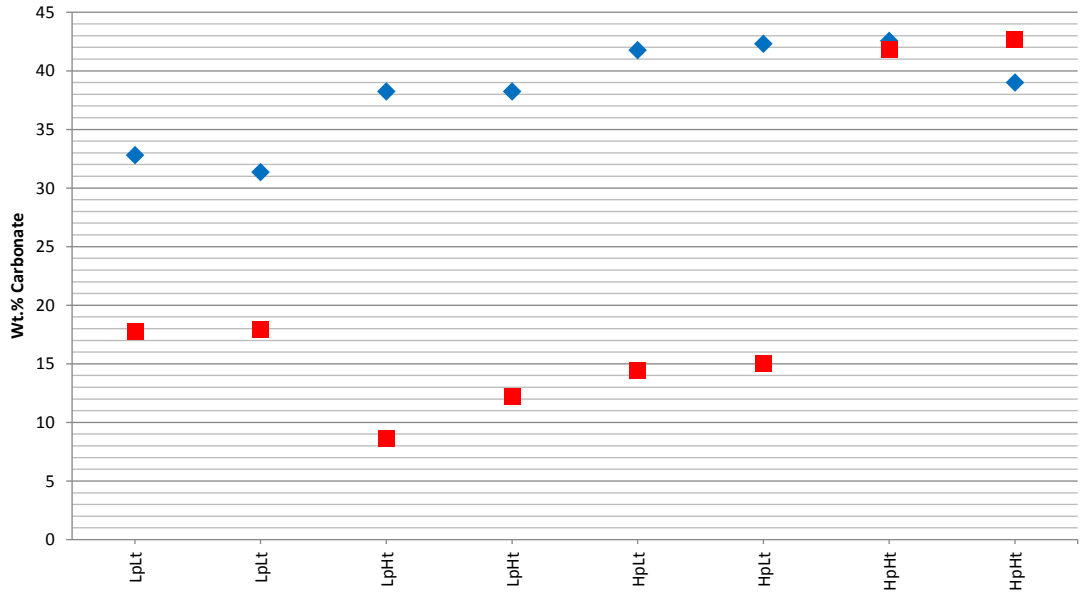

Figure 5.22: Graph showing the carbonation values achieved for calcium hydroxide under the active reaction conditions. Blue diamonds – low water availability, Red squares – high water availability.

Calcium Hydroxide Carbonation vs. HCO_3^- Concentration and Water Availability

Fig. 5.23 shows the carbonation results as influenced by the water availability for each experiment and plotted alongside HCO_3^- concentration.

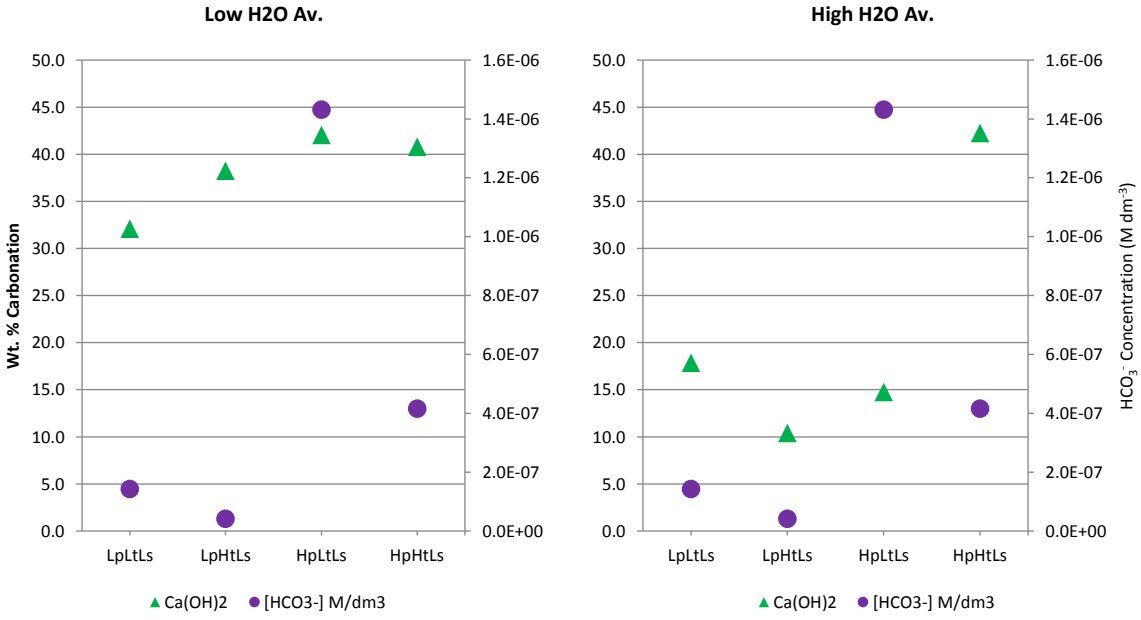

Figure 5.23: Calcium Hydroxide carbonation vs. the theoretical concentration of dissolved HCO_3^- concentration and water availability

Ideal Conditions

Based upon the data collected in this study the ideal conditions for calcium hydroxide carbonation have been tabulated (Table 5.18).

$Ca(OH)_2$	Low Temperature	High Temperature
Low Pressure	LOW	LOW
High Pressure	LOW	HIGH

Table 5.18: Table for powdered calcium hydroxide showing the order of carbonation values (red – 1st, orange - 2nd, green - 3rd, blue 4th) under different pressure and temperature conditions and the availability of water that yielded the highest carbonation values under those conditions.

Interpretation

The carbonation conditions for calcium hydroxide did not show a discernible trend with HCO_3^- concentration. However, there was a strong trend with regard to water availability. Higher water availabilities resulted in lower carbonation values, except for High pressure / high temperature conditions, while lower water availabilities resulted in higher carbonation values for all of the other conditions. This was likely due to the formation of a crust which blocked the porosity and/or permeability of the sample as a consequence of the rapid carbonate mineral formation. Lower water availability allowed the porosity and/or permeability to remain open for longer during the course of the reaction, but this also hindered the extent of the carbonation possible. Agitation of the $Ca(OH)_2$ and water mixture would have reduced the effects of the paste rheology and resulted in a higher degree of carbonation.

5.3.2 Petrographical Analysis

5.3.2.1 Descriptions of Surface Textures

Slag Aggregates

Low Pressure/ Low Temperature (10 bar / 25°C)

Experiments carried out at low pressure (10 bar) and low temperature (25˚C) generated surface textures with patchy carbonate coverage of 3-10µm grained, rhombohedral and flaky crystals. Material at LOW water availability conditions displayed patches of carbonate crystals approximately 100µm wide. Carbonate crystals ≈3µm in dimension were present in clusters. Most crystals were bladed. Material at HIGH water availability conditions produced crystals 5-10µm in dimension, which showed a more euhedral rhombohedral shape and were present in characteristic bladed-carbonate growth patterns (Fig. 5.24).

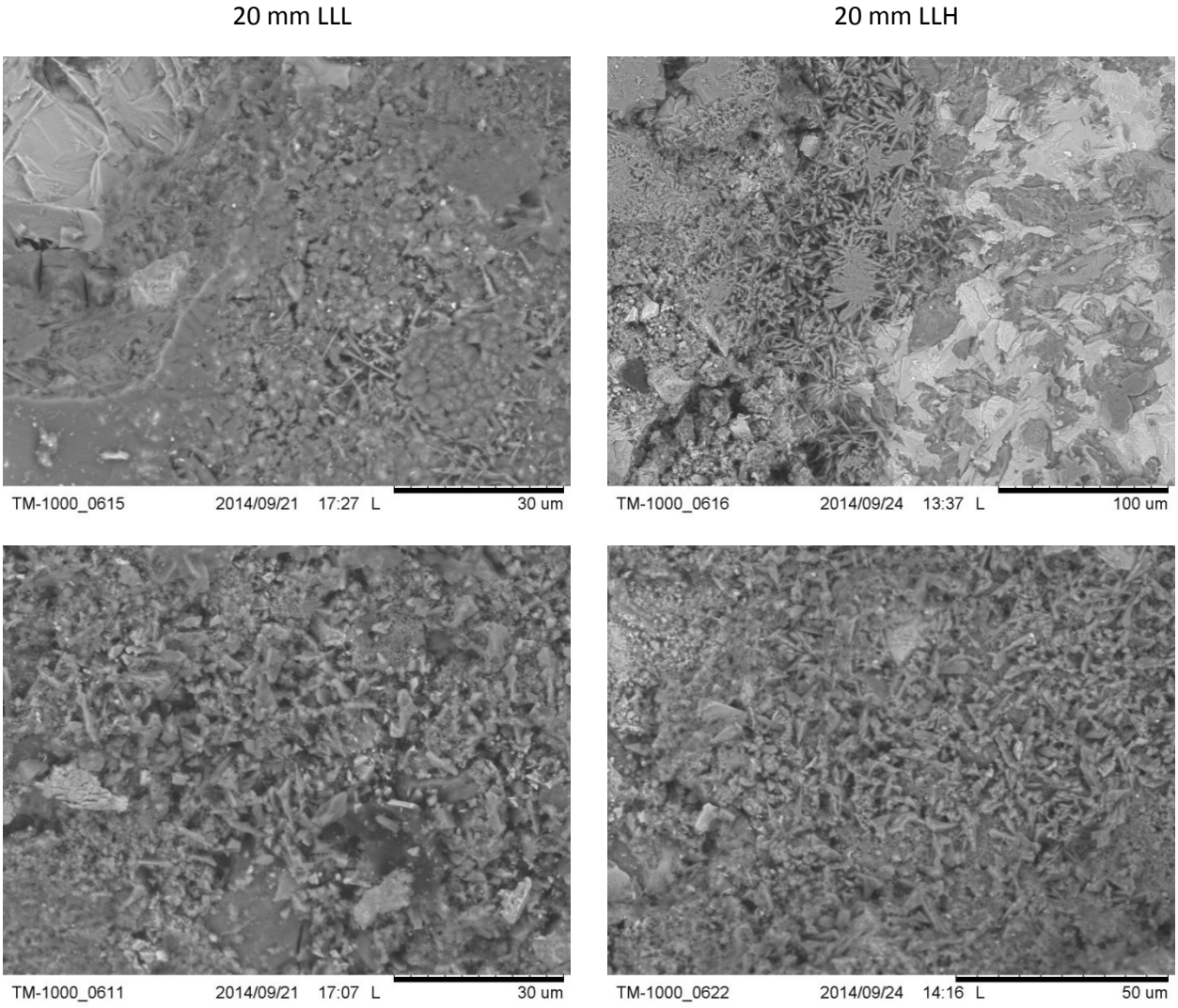

Figure 5.24: Back-scatter SEM image of carbonate minerals grown under low pressure/ low temperature (10 bar / 25°C) conditions. Left hand images were gown under restricted water availability, the right hand images were grown under excess water availability.

Low Pressure - High Temperature (10 bar / 125°C)

Experiments carried out at low pressure (10 bar) and high temperature (125˚C) generated surface textures with larger and fatter acicular-to-columnar textured crystals. Four crystal morphologies could be observed on the material: 30µm sized rhombohedral shaped bladed crystals, pseudo-triangular-based acicular crystals <100µm long, pseudo-hexagonal-based acicular crystals <100µm long and bladed inter-grown 'mats' of crystals that were <25µm long individually and >200µm wide as a cluster. Other spaces were in-filled with apparently amorphous crystals <5µm across. Material at LOW water availability conditions predominantly displayed rhombic and triangular-based-acicular crystal morphologies. There were occasional pseudo-hexagonal, acicular crystals present which were 20µm in length. The overall surface morphology consisted of rhombic and amorphous crystals on the surfaces of the grains with the acicular crystal morphologies only present within 'pits' on the surface, some of which appeared to have been formed as a result of carbonate precipitation. Material at HIGH water availability conditions displayed far coarser crystals. Generally, blockier crystals were present with well-formed, rhombohedral bladed nests formed by the overlap of many crystals. Acicular crystals were purely pseudo-hexagonal and appeared to radiate out from certain nucleation points. The overall surface morphology was of a mixture of bladed nests, thick pseudo-hexagonal crystals with rhombic crystals and amorphous crystals filling in the space between the dominant morphologies (Fig. 5.25).

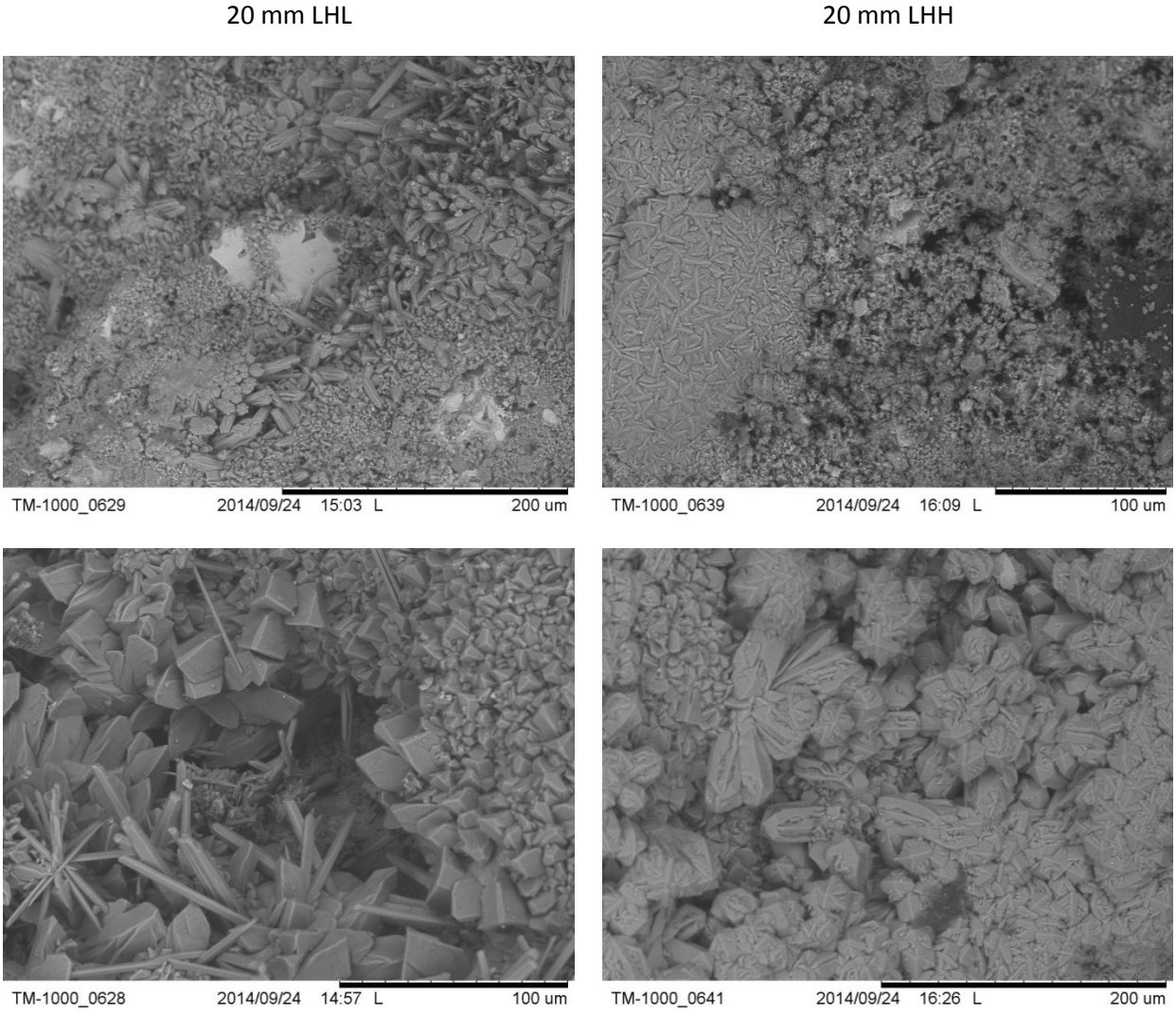

Figure 5.25: Back-scatter SEM image of carbonate minerals grown under low pressure/ high temperature (10 bar / 125°C) conditions. Left hand images were gown under restricted water availability, the right hand images were grown under excess water availability.

High Pressure - Low Temperature (100 bar / 25°C)

Experiments carried out at high pressure (100 bar) and low temperature (25˚C) generated generally 'flaky' surface textures with predominantly <5µm amorphous, spherical-to-oblong crystals being present. For 20 mm aggregate material, the LOW water availability conditions yielded higher carbonation values. Material at LOW water availability produced a wide coverage of small, approximately 1µm wide to 4µm long amorphous crystals. The overall surface morphology was one which was not entirely covered in crystals and the areas which did show mineral precipitation had no defined shape. Material at HIGH water availability conditions produced similar amorphous crystals which were <5µm in dimension. There were examples in which these crystals formed 'clumped' structures with a poorly defined bladed shape (Fig. 5.26).

20 mm HLL

20 mm HLH

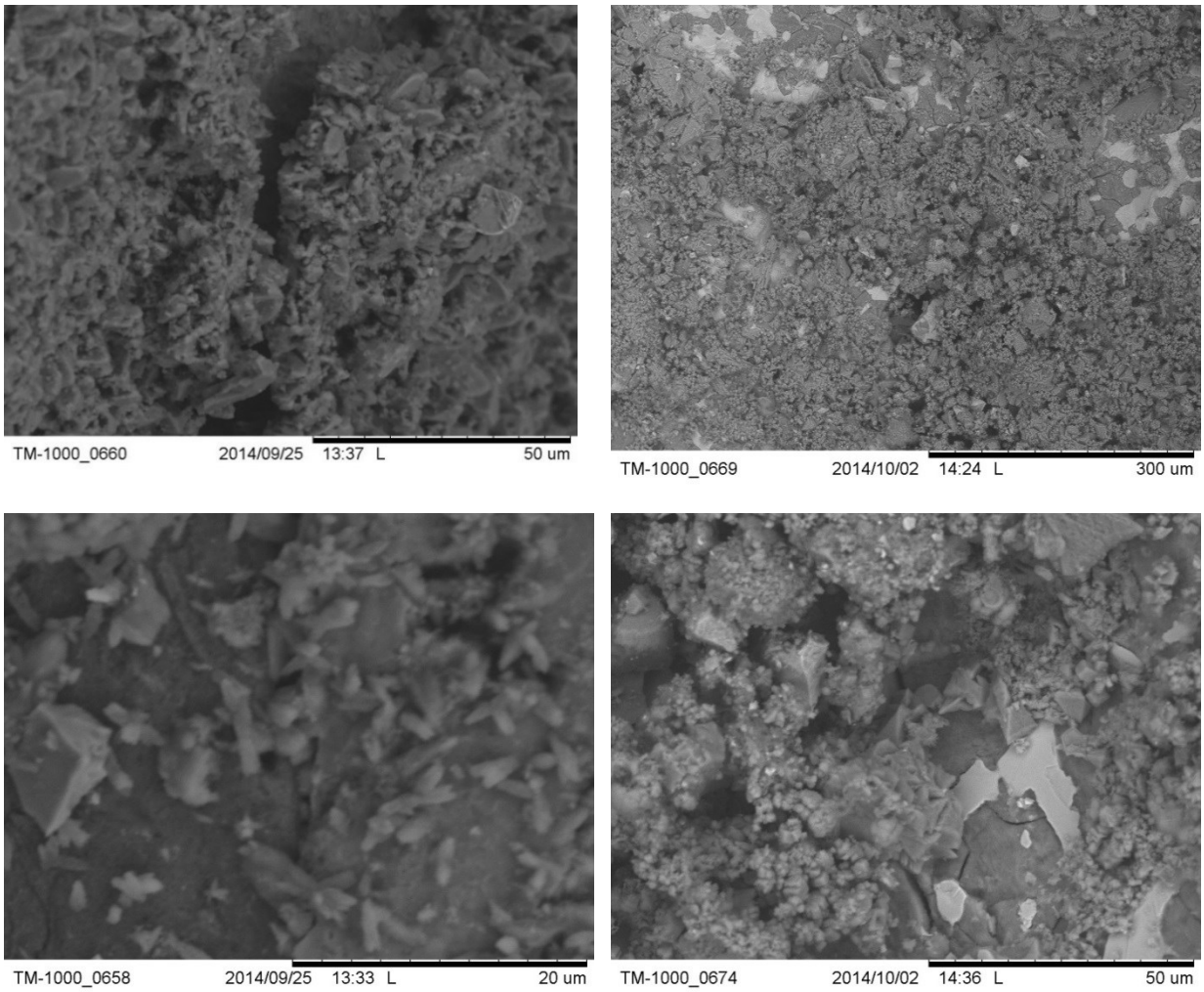

Figure 5.26: Back-scatter SEM image of carbonate minerals grown under high pressure/ low temperature (100 bar / 25°C) conditions. Left hand images were gown under restricted water availability, the right hand images were grown under excess water availability.

High Pressure -High Temperature (100 bar /125°C)

Experiments carried out at high pressure (100 bar) and high temperature (125˚C) generated surface textures which were covered in precipitated crystals with at least four crystal morphologies being present: 'rose bud' texture comprised of possible pseudo-hexagonal crystals up to 60µm in diameter with clusters of smaller crystals ≈10µm in diameter, longer acicular crystals which ranged up to 50µm long and 10µm wide, clusters of 'flaky' subhedral crystals ≈6µm long and 2µm wide. Rhombic forms were also seen. Material at LOW water availability conditions formed both coarse acicular textures and flaky subhedral crystals -some rhombic forms were also be present. The overall surface morphology was one which was entirely covered in precipitated crystals. Cementation textures were present as a consequence of the contact with other grains during the reaction. These contacts were on the scale of 100s µm. Material at HIGH water availability conditions displayed a 'rose bud' texture with the rest of the surface morphology taken up by the 'flaky' crystal texture. The 'rose buds' themselves appeared to be pseudo-hexagonal and appeared to comprise of crystals with dog-tooth-spar-like morphologies which all pointed towards the central axis of the growing crystal. This morphology occurred in 'mats' of crystals across the surface of the grains on the scale of 100s µm. At the edges of these 'mats' there were crystals with the same 'rose-bud' morphology, but on a smaller (≈10µm scale) (Fig. 5.27).

20 mm HHL 20 mm HHH

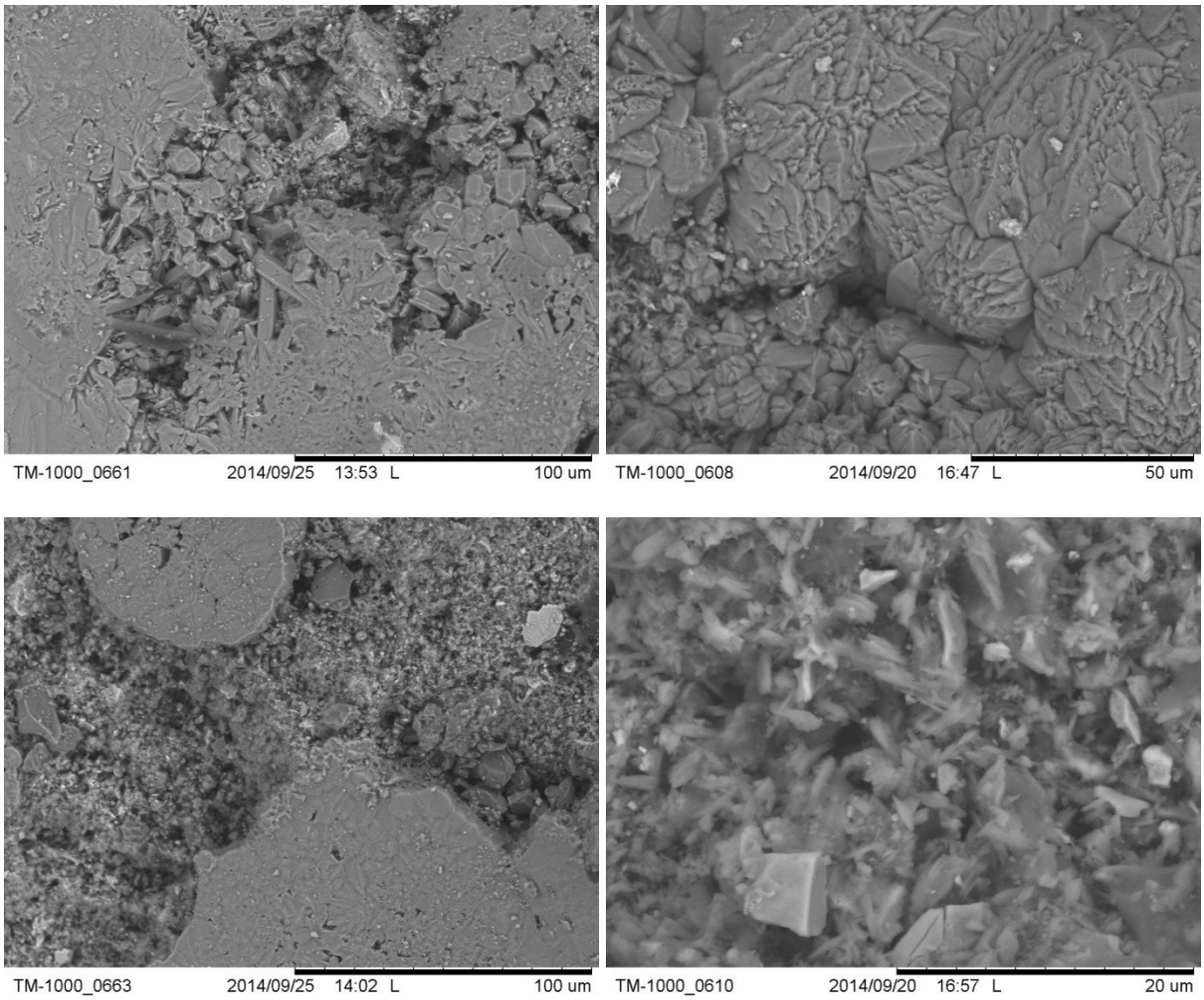

Figure 5.27: Back-scatter SEM image of carbonate minerals grown under high pressure/ high temperature (100 bar / 125°C) conditions. Left hand images were gown under restricted water availability, the right hand images were grown under excess water availability.

5.3.3 Descriptions of 2D thin Sections

Thin sections of reacted grains of slag were made in order to observe and investigate the cross sectional growth patterns of the carbonate minerals formed. The investigation was carried out by using both optical and SEM techniques. SEM-EDX was used to create element maps of several grains and to identify any mineral growths. The thicknesses of the mineral layers reported were based on the observed cross-sectional thickness in thin section. However, in all cases it was possible that the layer had been thinned during the sectioning process.

5.3.3.1 SEM Elemental Mapping

The element maps of reacted grain are shown in Fig. 5.28. The grains themselves showed a mix of calcium, iron and silicon signals. However, the mineral growths present on the perimeter of each grain

returned purely a Ca signal identifying them as a Ca-rich mineral phase. As a result of the TGA thermal composition data, the rhombic forms observed at the surface of the grains under SEM [Chapter 5.3.3], and the high order birefringence colour observed under XPL, these minerals were interpreted as being predominantly calcite.

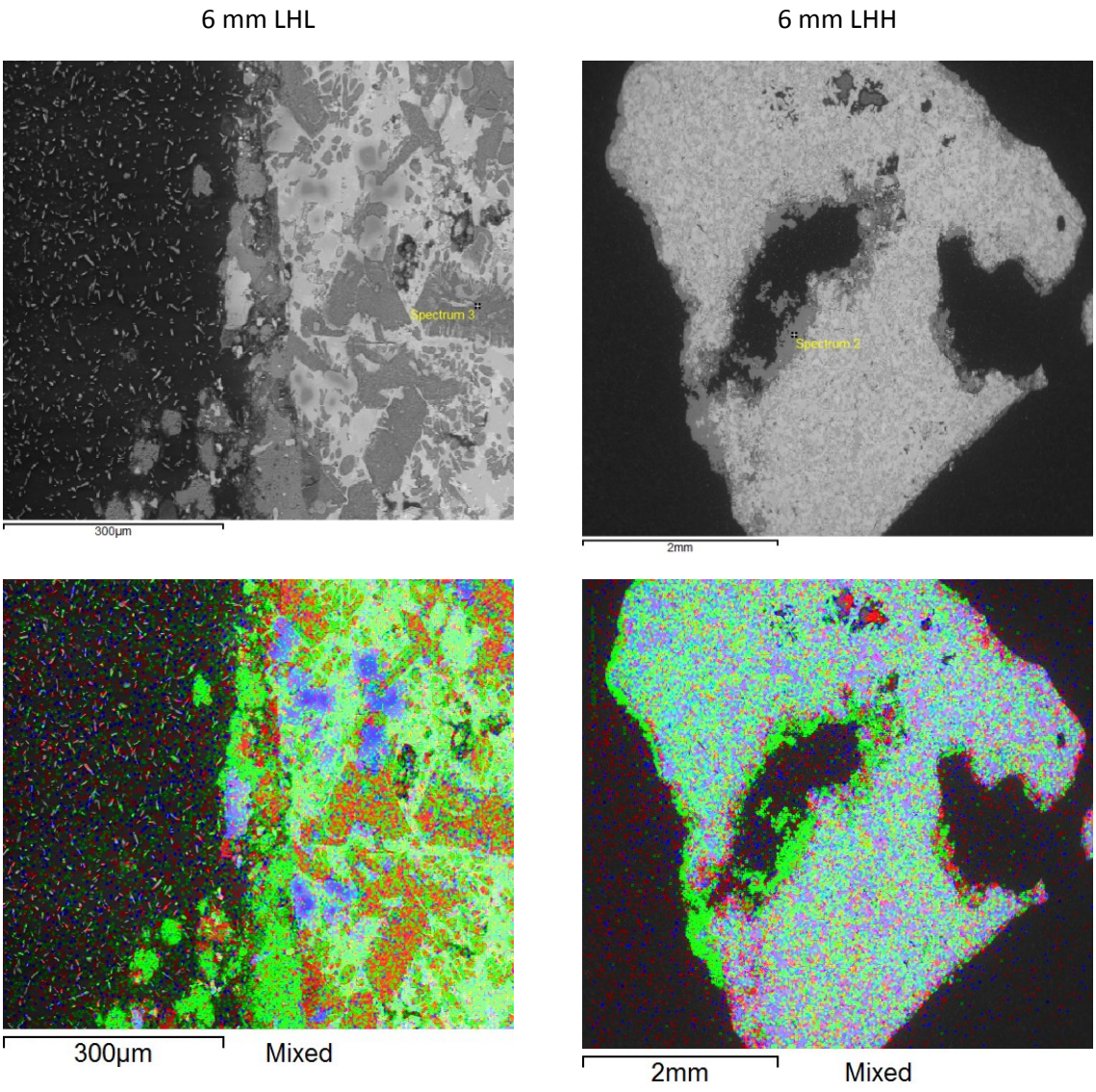

Figure 5.28: SEM images and EDX element-maps of thin-sectioned batch-reacted 6 mm aggregate samples

5.3.3.2 Thin Section Analysis

Steel Slag Aggregates

Low Pressure - Low Temperature (10bar / 25°C)

Experiments carried out at low pressure (10 bar) and low temperature (25˚C) generated surface growths of Ca-rich high-order-birefringent minerals up to 0.09 mm thick. In general, the mineralised layer covered the majority of the perimeter of each reacted grain as can be seen in the surface textures of Fig. 5.29. Overall, the mineralised layer was <0.06 mm thick, but the layer was highly variable in thickness generally varying between 0.032 – 0.064 mm. In hollows on the surface, the layer was observed to thicken to 0.07-0.08 mm. On slag grains containing olivine and/or pyroxenes (the 2nd-order birefringent minerals) the carbonate layer extended to its maximum thickness of 0.09 mm. There appeared to be little porosity present on the surface layer (Fig. 5.29).

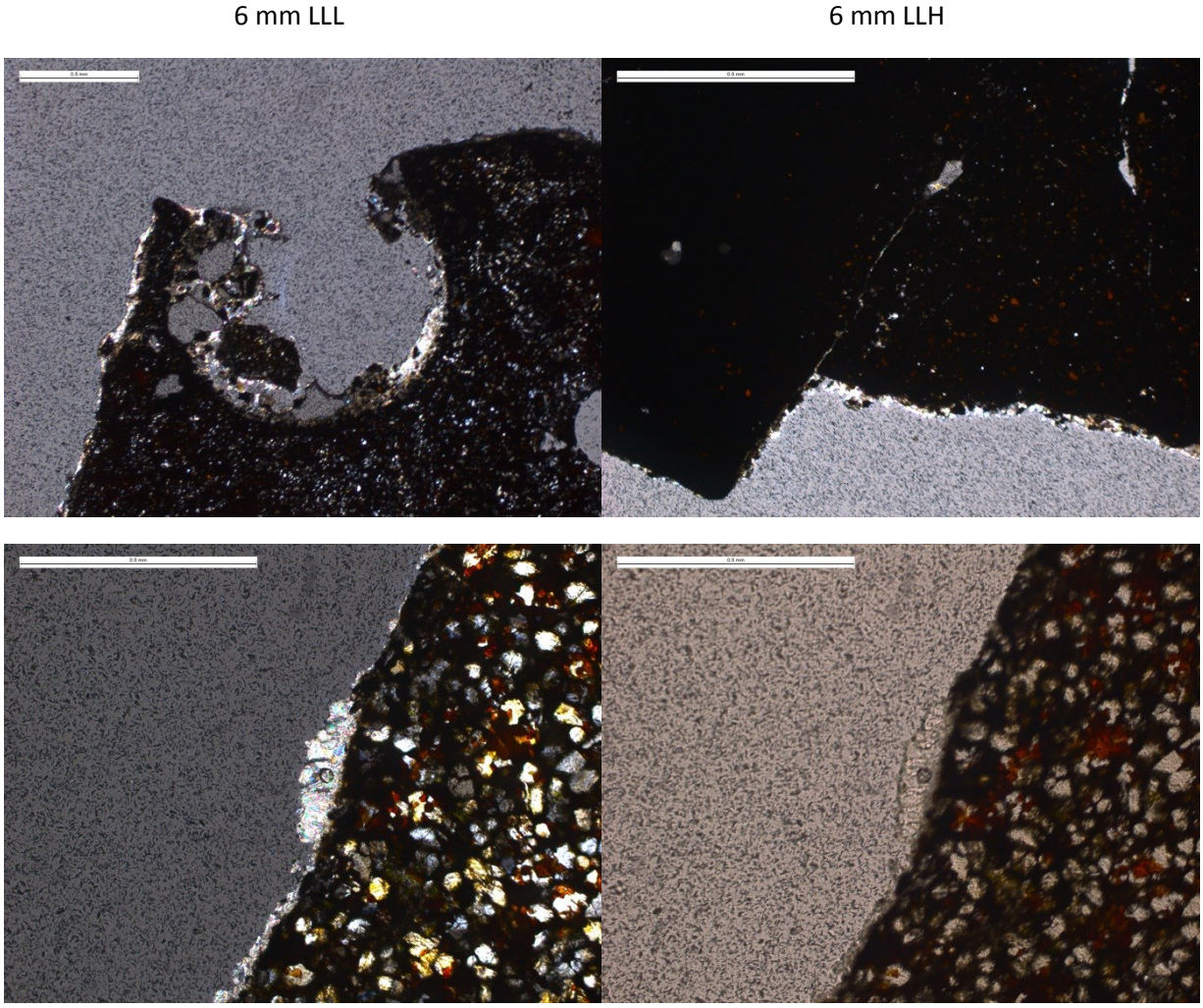

Figure 5.29: Thin section photomicrograph of carbonate minerals grown under low pressure/ low temperature (10 bar / 25°C) conditions. Left hand images were gown under restricted water availability, the right hand images were grown under excess water availability.

Low Pressure - High Temperature (10 bar / 125°C)

The experiments carried out at low pressure (10 bar) and high temperature (125˚C) generated surface growths of Ca-rich, high-order-birefringent minerals up to 0.120 mm in thickness. Under LOW conditions the surface thickness was between 0.032-0.064 mm and up to 0.125 mm in a 'divert' in the grain surface. Within the hollows of the grain, the thickness could reach 0.250 mm. In general, the majority of the perimeter of the grain had been mineralised. There appeared to be no mineral control of the thickness of the mineralisation and little to no porosity within the mineralised layer. Under HIGH conditions the thickness of the surface layer was <0.64 mm thick but was highly variable in thickness. The thickness increased up to 0.200 mm in hollows and the porosity within grains was mostly filled. There appeared to be no mineral control of the thickness of the mineralisation and little to no porosity within the mineralised layer (Fig. 5.30).

6 mm LHL 6 mm LHH

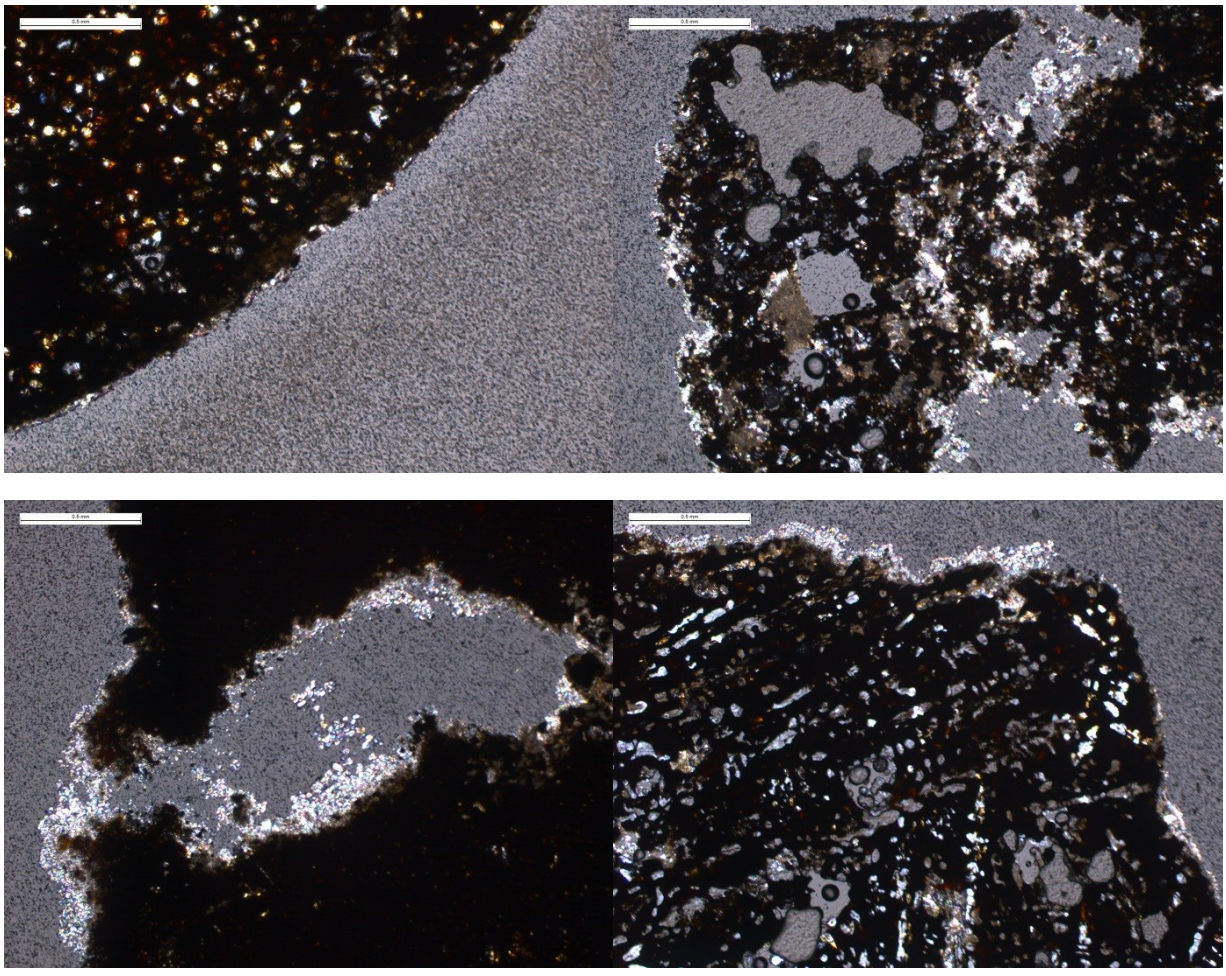

Figure 5.30: Thin section photomicrograph of carbonate minerals grown under low pressure/ high temperature (10 bar / 125°C) conditions. Left hand images were gown under restricted water availability, the right hand images were grown under excess water availability.

High Pressure - Low Temperature (100 bar / 25°C)

Experiments carried out at high pressure (100 bar) and low temperature (25˚C) generated surface growths of Ca-rich, high-order-birefringent minerals which were typically blocky in texture (Fig. 5.31). These reached a maximum surface thickness of 0.125mm. Under LOW conditions the mineralised surface generally varied between 0.032 – 0.064 mm in thickness. In hollows, the thickness could increase to 0.250 mm and could completely fill them. The internal porosity within the grain could be partially filled by a mineralised layer up to 0.032 mm thick. In general, the majority of the perimeter of the grain had been mineralised. There appeared to be little to no porosity within the mineralised layer. Under HIGH conditions the mineralised surface was generally 0.064 mm thick, though surfaces up to 0.125 mm thick were common. The mineralised layer was generally blocky in morphology and the majority of the grain perimeter had been mineralised. Thicker layers did appear to grow on grains which were opaque in XPL. There appeared to be little or no porosity within the mineralised layer.

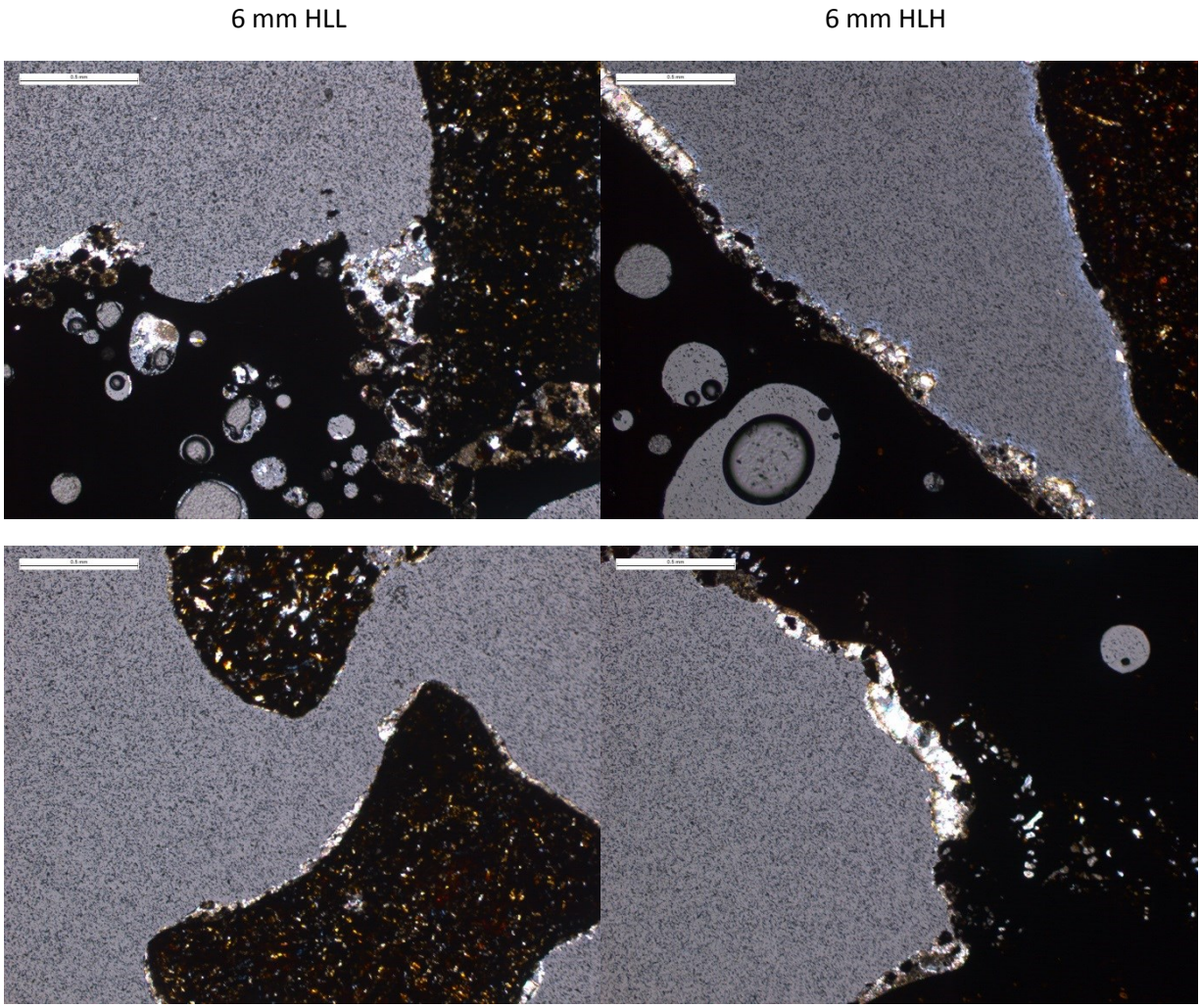

Figure 5.31: Thin section photomicrograph of carbonate minerals grown under high pressure/ low temperature (100 bar / 25°C) conditions. Left hand images were gown under restricted water availability, the right hand images were grown under excess water availability.

High Pressure -High Temperature (100 bar /125°C)

Experiments carried out at high pressure (100 bar) and high temperature (125˚C) generated surface growths of Ca-rich, high-order-birefringent minerals which varied between blocky and 'speckled' in texture and reached a maximum surface thickness of 0.320 mm. Under LOW conditions the mineralised surface generally varied between 0.032 – 0.125 mm in thickness. Thicknesses of 0.64 mm were common. Internal porosity within the grain could be partially filled by a mineralised layer of up to 0.032 mm thick. In general, the majority of the perimeter of the grain had been mineralised with a 'speckled' mineral morphology observable in XPL. There appeared to be no mineral control of the thickness of the mineralisation and little to no porosity within the mineralised layer (Fig. 5.32). Under HIGH conditions the mineralised surface was generally 0.125 – 0.250 mm thick. The maximum thickness observed was 0.320 mm. The majority of the perimeter of the grain had been mineralised, with a 'blocky' mineral morphology observable in XPL. Thicker layers did appear to grow on grains which were opaque in XPL. There appeared to be little to no porosity within the mineralised layer.

6 mm HHL 6 mm HHH

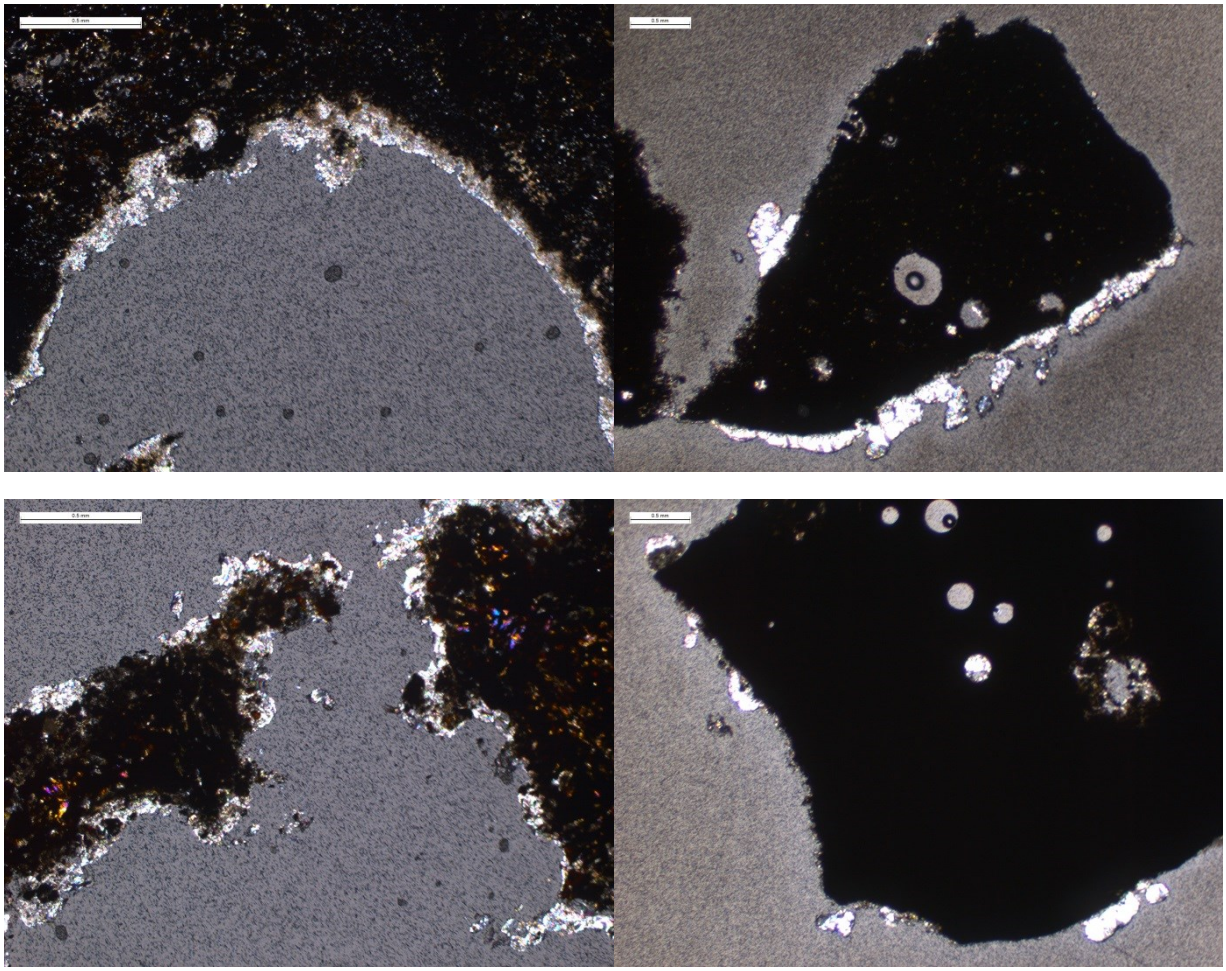

Figure 5.32: Thin section photomicrograph of carbonate minerals grown under high pressure/ high temperature (100 bar / 125°C) conditions. Left hand images were gown under restricted water availability, the right hand images were grown under excess water availability.

5.5 Discussion

The variables in the experiments were pressure (leading to a factor of 10 change between different HCO_3^- concentrations), temperature (leading to different kinetics and differences in dissolved CO_2 concentrations) and the availability of water (which had the potential to change the rheology of the reacting material). The variables within the materials themselves were the two different chemical types of slag (steel slags vs. blast furnace slags) and the grain sizes of these two chemical types. The different conditions in the study were secondary to the reactions which occurred under them, as the primary effects on the reaction were due to another factor: Pressure affects the concentration of HCO_3^- ions present, which directly effects the reaction. Temperature affects the rate of the reaction, which directly effects the rate at which porosity and/or permeability within a material is either formed or destroyed. The water availability dictated the concentration of HCO_3^- ions available for reaction and also influenced the physical properties of the material. An additional factor was the change in the dissolution behaviour of CO_2 with temperature, which changed the concentration of HCO_3^- ions and thereby affected the reactions.

Pressure

The variation of pressure from 10 bar CO_2 to 100 bar CO_2 did not appear to have a major effect on the baseline carbonation between the experiments. Changes in pressure appeared to have a limited effect on the carbonation observed. Within each set of experimental data, the effect of pressure on average ranged between 0.9 to 3 times the differences between Hp/Lp values between steel slags. Blast furnace slags showed 1.58 to 1.97 times the difference between Hp/Lp values in Pellite, and 1.48 to 2.52 times the difference between Hp/Lp values in GBFS.

Pressure conditions at 25°C did increase most of the carbonation values attained when compared to the highest passive carbonation achieved by the same material. The carbonation values of 20 mm and 6 mm aggregate slag were doubled by increasing the CO_2 pressure from atmospheric partial pressure to 10 bar CO_2 pressure. When the pressure was raised from 10 bar CO_2 to 100 bar CO_2 pressure, the carbonation value for 20 mm aggregate increased from the passive carbonation level by a factor of 9. However, 6 mm aggregate at 100 bar CO_2 pressure displayed an increased carbonation value of only a factor of 2. GBFS displayed a dramatic increase in carbonation values with increasing CO_2 pressure, with carbonation values increasing by a factor of 16.6 at 10 bar CO_2 pressure and by 29.7 at 100 bar CO_2 pressure. The carbonation values of Dust and Pellite followed a different trend displaying a decrease in carbonation value with higher pressure conditions when compared to the highest passive values achieved.

Overall, it can be concluded that by increasing the CO_2 pressure, the carbonation value attained by a material does increase, but the degree to which this increase occurs is limited and is material specific.

Temperature

The change in temperature from 25°C to 125°C appeared to enhance the carbonation values of the individual materials. Dust, Wollastonite, and GBFS appeared to be particularly sensitive to temperature increases and showed a noticeable trend of increasing carbonation values with higher temperature. The carbonation values for GBFS were between 10.34 to 11.52 times the differences between Ht/Lt suggesting a strong temperature dependence for the reaction for this material. However, the extent to which temperature influenced the carbonation values was limited, apart from in the case of GBFS. Within each set of experimental results the effect of temperature, on average, ranged between 1.67 to 2.78 times the differences between Ht/Lt values between steel slags. However, these effects were not uniform across the different materials. In the case of 20 mm aggregate, the variation in carbonation caused by the change in pressure and temperature individually were similar and it would be unreasonable to suggest one set of conditions was preferential to the other.

The effects of temperature when compared with pressure were also evident when the carbonate crystals grown during each experiment were examined. Under both 10 bar and 100 bar CO_2 pressure at 25°C the crystals formed were fine-bladed. Though these crystals displayed a good surface coverage on each individual sample, the crystals themselves were typically restricted in size, being up to 5 µm in dimension. Under the same pressure conditions, but at 125°C the crystals formed were euhedral and far larger than those which were formed under the lower temperature conditions. The rhombohedral carbonate crystals being up to 30 µm in dimension, and acicular and scalenohedral crystals being 10s of µm in length (but no longer than 100 µm). These textures gave an indication of the influence of temperature which resulted in greater amounts of sample (mineral) dissolution and the rapid attainment of metal-carbonate saturation, resulting in precipitation and crystallisation of carbonate crystals. Overall it can be concluded that increasing the temperature does increase the degree of carbonation attained by a material, but the effect appears to be highly material specific.

Water Availability

It was assumed that water was not lost as the reactions proceeded and thus the amount of water remained constant. The role of water in the reaction was to provide a medium in which ions could dissolve and the volume of water provided dictated the ion concentration present. The availability of water also determined the physical properties of the material. As shown in Chapter 3, 20 mm and 6 mm aggregates displayed very high hydraulic conductivities and porosities. However, powdered

materials, such as Dust and the 'pure' mineral specimens used in this study became 'pastes' when wet, collapsing the volume of the material when compared to the dry sample, and creating the potential for 'crusting' to occur. Thereby removing the potential for dissolved ions to move around the material.

The amount of water which was made available to the materials in the experiments was significant in changing the rheology of the materials. This resulted in important changes to the physical process of carbonation. Table 5.19 shows the rheology observably displayed by the different materials under different water availabilities (either LOW or HIGH).

	Water Availability	20 mm	6 mm	Dust	Pellite	PP	GBFS	GP
Rheology	Low	Granular	Granular	Funicular / Capillary	Granular	Funicular / Capillary	Granular	Funicular / Capillary
	High	Granular	Granular	Paste	Granular	Slurry	Granular	Slurry

Table 5.19: Rheology observably displayed by the different materials used in this study under different water availabilities.

The different growth environments which were produced as a result of controlling the amount of water available for reaction did affect how the carbonate crystals grew. Aggregate rheologies which were characterised by a network of open pore-spaces had a greater surface area over which the HCO_3^- rich fluid and the reacting material could interact. This network provided a larger surface area for the dissolution and transportation of ionic components around the system and also provided a greater surface area for nucleation. In turn, this enabled materials, which had granular properties to form an 'even' layer of carbonate upon their surfaces. Adding more water to the sample increased the volume in which these processes could take place and thereby increased the carbonation values achieved.

The same theory could be applied when considering slurries of material, but on a smaller-scale. The slurries formed by the ground (<250 µm) Pellite and GBFS still appeared to provide a suitably open framework in which carbonation could evenly occur. Adding more water to the reaction increased the volume in which the carbonation could occur and resulted in higher carbonation values. Slurries did form cohesive cemented masses, but not to the same extent as pastes. In pastes the network of porosity was restricted and their rheology was controlled by the cohesiveness caused by the presence of fine grain particles interacting with water. This resulted in the collapse of porosity and a reduction in the permeability of the material. As will be discussed in the Wollastonite and calcium hydroxide

experiments, pastes such as Dust, will form carbonate 'crusts' at the water-CO_2 boundary. This restricts the supply of HCO_3^- ions to the remaining sample beneath the crust, thus retarding carbonation. So, this results in carbonation values which are lower than would be normally be expected for fine-grained materials and explains why the carbonation values for dust were higher when water availability was low. Actively reacting Dust also achieved lower carbonation values than those obtained using passive weathering methods. This was despite the passive formation of similar crusts on the Dust slag-heaps. These problems can be overcome by restricting the availability of water to maintain a funicular or capillary state within the sample material, which will then produce a low degree of cohesion between particles. Any water present around the samples would be in the form of a meniscus around the particles and so the gas-filled pores would still be present and open. This open, albeit restricted, porosity framework would allow the movement of dissolved and gaseous CO_2 round the whole of the sample resulting in only localised carbonate crust formation which would not restrict the extent of carbonation.

The availability of water also affected the extent to which carbonate crystals could grow. The more water available, the more space there was for the crystals to form. This effect could be seen when the carbonate crystals grown under LOW or HIGH water conditions were compared. In all cases the crystals grown under excess water availability were more substantial than the crystals grown under conditions of lower water availability. The production of larger crystals resulted in the precipitation of greater volumes of carbonate, thus producing higher carbonation values.

Overall, it can be concluded that increasing the availability of water to a material will increase the carbonation value achieved *only* if the material displays an open network of porosity as can be determined by its rheological properties. Materials in which the porosity network collapsed under conditions of excess water had higher carbonation values when the availability of water was limited.

Chemical Composition, Grain Size and Type of Material

The experiments described in this chapter have provided data on how the different slag products responded to the external factors of pressure, temperature and water availability. However, an important variable to take into account is the reactivity of each of the materials used. The experiments did not provide any directly quantifiable measurements of the reactivity of each material, such as the rate of dissolution or the rate of the carbonation reaction and only an indirect qualitative assessment of the reactivity of each of the materials could be carried out. An analysis of 'reactivity' was further hampered by the lack of equivalent grain sizes available. However, there was enough data to make a judgement of the reactivity of the materials across several different grain sizes (Fig. 5.33).

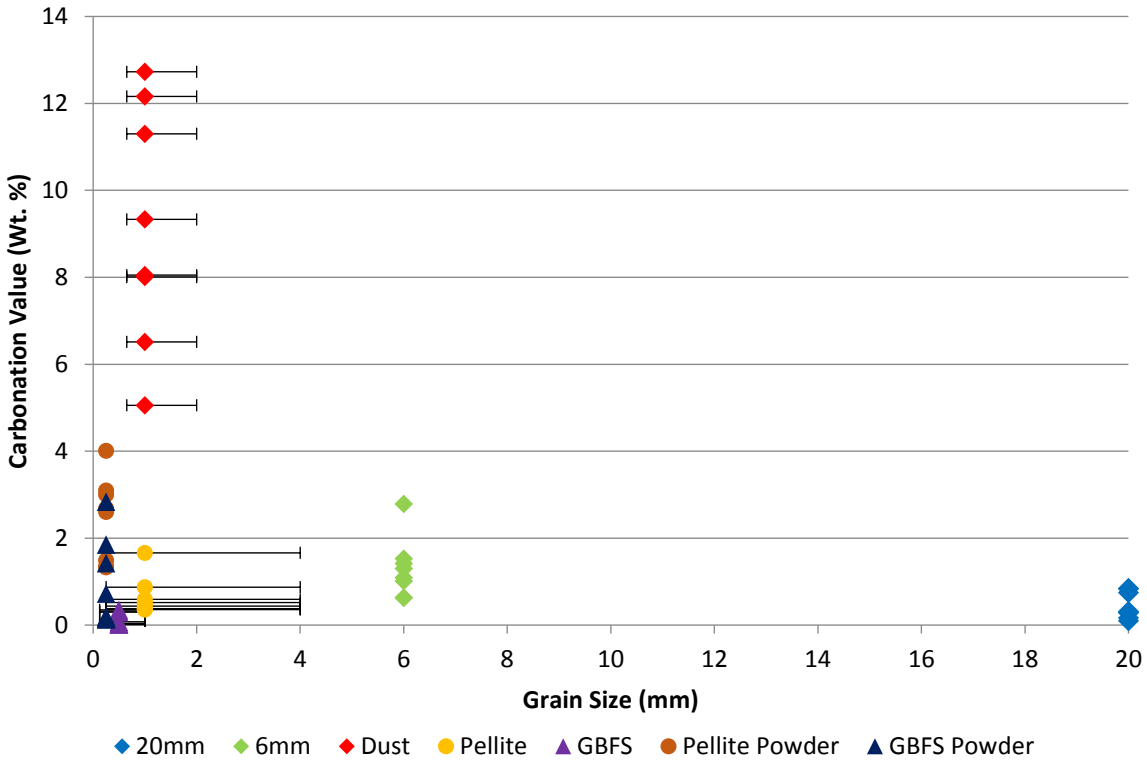

Figure 5.33: Carbonation values achieved by different slag materials in the study. All data was plotted to the grain-size at the 50% line of cumulative grain size [see Chapter 2]. Whisker lines indicate the range in the grain sizes present in each material.

It was apparent that steel slags were more reactive than blast furnace slags, even at coarser grain sizes. Pellite was the most reactive out of the blast furnace slags (Pellite and GBFS). However, both blast furnace slag samples achieved similar carbonation values when crushed to <250 µm suggesting that their surface crystallinity was an important factor in determining their reactivity.

Grain size was the biggest factor in establishing the carbonation value of a given material type. All three materials (steel slag, Pellite and GBFS) showed an exponentially increasing trend in carbonation with decreasing grain size.

5.5.2 Results Compared to Theoretical Potential

The slag samples used in this study were polymineralic and to understand their carbonation behaviour, samples of 'pure' standard minerals were reacted under the same conditions. The carbonation values achieved by the standard mineral samples used in this study were compared to their theoretical carbonation potential. This data was presented in 'triangle-diagram' form to illustrate the relative importance of each mineral species to the carbonation of the polymineralic slag samples. The effect

of the different variables in this study was explored in relation to the carbonation achieved by each mineral species, and a model was postulated.

Pressure - The variation in pressure affects the reaction of the silicate minerals (Olivine and Wollastonite) approximately by half as much as temperature. Calcium hydroxide was more responsive to the effects of pressure than to temperature (due to the effects of water availability) as will be shown below.

Temperature - An increase in reaction temperature increased the carbonation of the silicate minerals (Olivine and Wollastonite) by a greater factor than pressure. Calcium hydroxide was less influenced by temperature, as higher temperatures result in 'crusting' at the top of the sample which quickly terminated the reaction.

Water Availability - Controlling the availability of water to the materials in the experiments could change the rheology of the materials producing important changes in the physical process of carbonation. Table 5.20 shows the rheology observably displayed by the different materials under different water availabilities (either LOW or HIGH).

	Water Availability	Olivine	Wollastonite	$Ca(OH)_2$
Rheology	Low	Funicular / Capillary	Funicular / Capillary	Funicular / Capillary
	High	Slurry	Paste	Paste

Table 5.20 Rheology observably displayed by the different standard minerals in the study under different water availabilities.

As explained in 5.5.1 the water availability created different rheologies and therefore different porosity networks. 'Crusts' were observed in Wollastonite and calcium hydroxide samples which both formed pastes under conditions of high water availability, thereby limiting effective carbonation. This was evident when the carbonation values for calcium hydroxide were examined. Three out of four experiments resulted in far lower carbonation values for conditions of high water availability compared with those obtained under conditions of low water availability.

Olivine had high carbonation values with high water availability and at low temperature (25°C), but displayed higher carbonation values under conditions of low water availability at high temperature (125°C). This was possibly due to the faster rate of reaction as a result of the higher temperature and because at a faster reaction rate an open porosity is favoured.

Wollastonite and calcium hydroxide samples both formed pastes and again, due to the faster reaction rate, an open porosity was favoured in order to keep the reaction progressing for longer before the eventual formation of a 'crust' which terminated the reaction.

Theoretical Potential

Fig. 5.34 shows the %-carbonation potential achieved for each of the 'standard' minerals which were actively reacted under the same conditions as the slag samples. By combining the results of the three standard minerals, the theoretical carbonation value which could be achieved for a sample made up of a composition of olivine-structure minerals, pyroxenes and hydroxides could be predicted.

Under all conditions, olivine achieved less than 10% of its carbonation potential. Pyroxene achieved up to 70% to 90% of its carbonation potential under 10 bar CO_2 and 125°C conditions, but always achieved the second highest potential of the three minerals. Calcium hydroxide regularly achieved nearly 100% of its carbonation potential, only being hampered by the adverse effects of 'crust' formation as explained above.

Overall Fig. 5.34 shows that samples which comprised of hydroxides and pyroxenes achieved higher carbonation values than samples which were rich in olivine. The best conditions for carbonation of a mixed sample were either 10 bar CO_2, 125°C and low water availability, or 100 bar CO_2, 125°C and low water availability. These conditions correlated well with the ideal carbonation conditions for all of the slag samples within this study, apart from slight variations displayed by 20 mm steel slag aggregate (where these conditions were the 2nd and 3rd highest carbonating conditions), Pellite (1st and 3rd highest conditions) and Pellite Powder (1st and 4th highest conditions).

The pure minerals also reflected the behaviour of the mineralogy of the different slag samples. Pellite, which displayed a pyroxene-like mineralogy, produced some of the highest carbonation values and 'Dust', which contained hydroxide minerals, carbonated rapidly and also achieved high carbonation values.

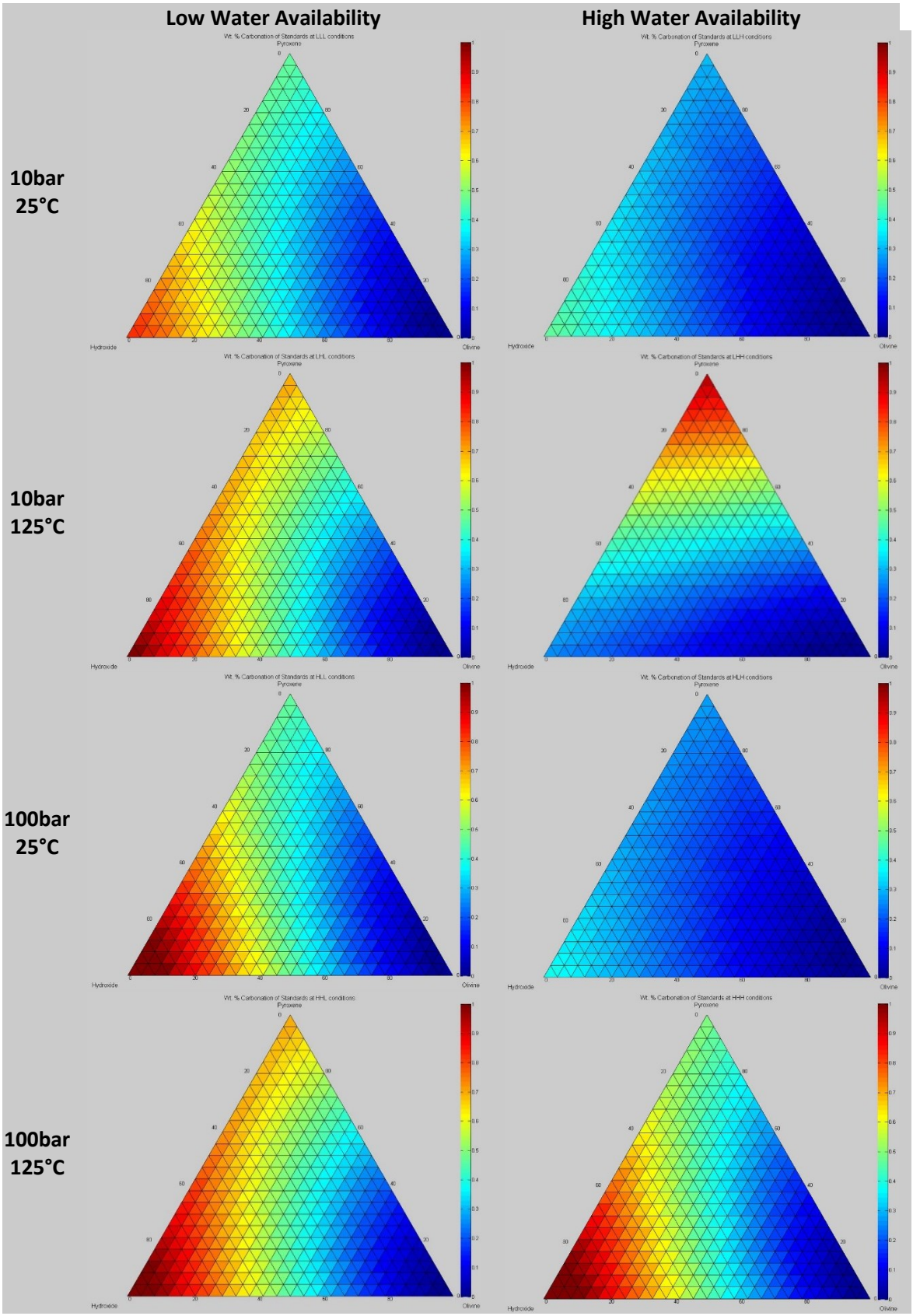

Figure 5.34: The theoretical carbonation potential of a material of mixed composition reacted under differing P/T/water conditions. The pure compositions are shown at the corners of each triangle- Mg-olivine (bottom right), Ca-pyroxene (top), Ca-hydroxide(bottom left). Colour scale between 0 to-1 (0% to 100% carbonation potential achieved)

5.5.3 Overall Conversion to Carbonate Achieved

The overall carbonation achieved by the different slag materials (the wt. % carbonation over total wt. % Ca+Mg+Fe cation content) in this study are shown in Table 5.21. The efficiency of cation carbonation increased with decreasing grain size across all material types. The maximum carbonation achieved by steel slags was achieved by Dust at HpHtLs conditions which resulted in a 14.98% conversion. The maximum value achieved for Pellite products was 3.33% for granular Pellite at HpHtHs conditions and 8.02% for powdered Pellite at HpHtHs conditions. The maximum achieved for GBFS products was 0.73% for granular GBFS under HpHtHs conditions and 5.94% for powdered GBFS at HpHtHs conditions. The conversion rate for all products was low. Therefore, the products were not carbonating effectively. A better understanding of the progression of the reaction front within the polymineralic material is required to engineer the conditions needed to improve the conversion rates.

	20 mm	6 mm	Dust	Pellite	Powder	GBFS	Powder
LpLtLs	0.12%	1.45%	9.47%	0.71%	2.70%	0.01%	0.27%
LpLtHs	0.20%	2.02%	7.67%	0.88%	5.37%	0.05%	0.33%
LpHtLs	0.38%	1.55%	14.32%	0.76%	2.99%	0.16%	1.52%
LpHtHs	1.02%	2.18%	13.30%	1.04%	5.21%	0.62%	3.87%
HpLtLs	1.03%	1.85%	9.42%	0.75%	6.00%	0.05%	0.33%
HpLtHs	0.34%	0.89%	5.95%	1.18%	2.66%	0.08%	0.40%
HpHtLs	0.36%	0.90%	14.98%	1.75%	6.20%	0.67%	2.98%
HpHtHs	0.92%	3.97%	10.98%	3.33%	8.02%	0.73%	5.94%
Average %	0.55%	1.85%	10.76%	1.30%	4.89%	0.30%	1.95%

Table 5.21: Degree to which the carbonation potential of a material has been achieved. % are reported as the degree of carbonation vs. the available cation content of each material.

5.5.4 Results Compared to Other Studies

The highest carbonation values achieved for each material in this study were compared to the carbonation values reported from other studies in the literature (Fig. 5.35).

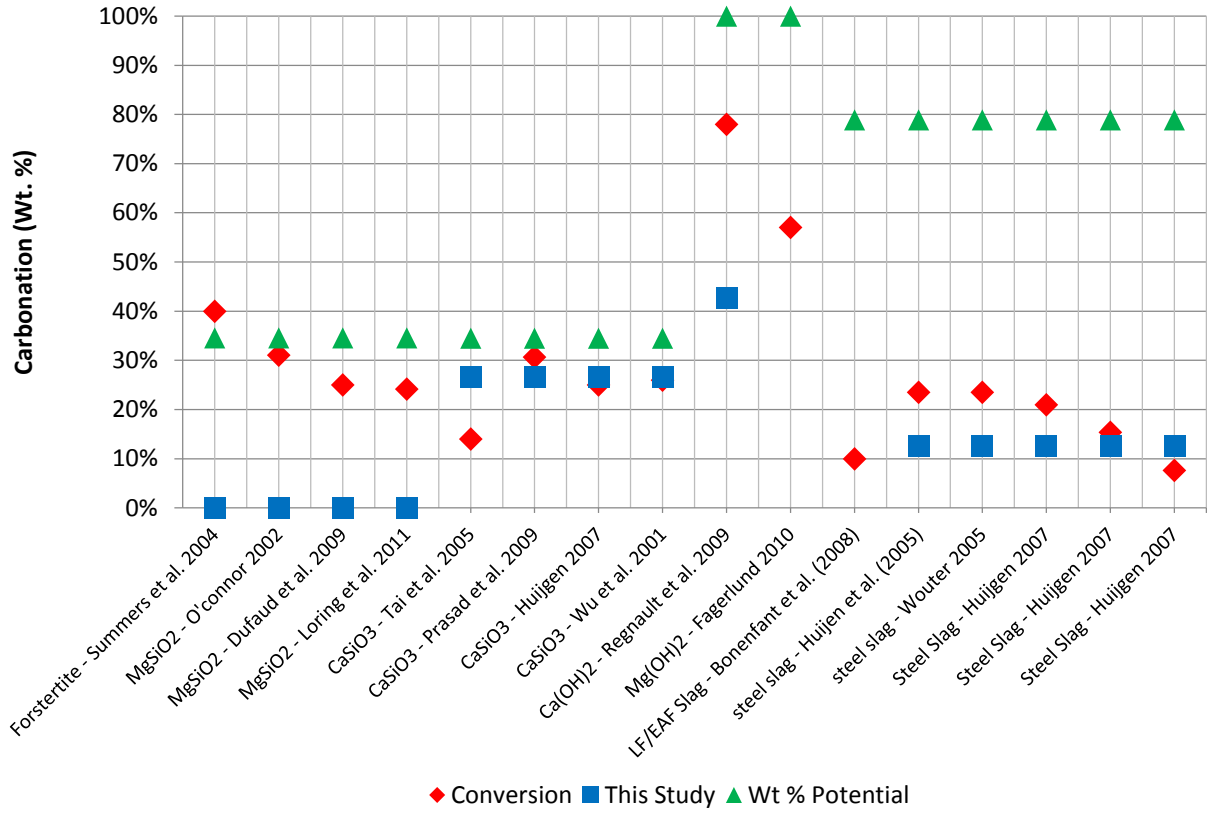

Figure 5.35: Comparison of the results from the carbonation experiments of this study compared to those from the literature and the theoretical carbonation potentials (in wt. %) for each substance.

Olivine - In comparison to other studies the carbonation results achieved in this study for olivine were poor. Dufaud et al. (2009) also used San Carlos Olivine in their study and they achieved a far higher carbonation value. Both Dufaud et al. (2009) and O'Connor (2002) achieved higher carbonations than were theoretically possible, but this was due both to their reporting style and to their use of additives. Dufaud et al. (2009) used a NaCl solution (at 100 g dm^{-3}) and oxalic acid under conditions of 1,000 bar pressure and 400-500°C, while Summers et al. (2004) used 1M NaCl solution with a $NaHCO_3$ additive (coupled with ultrafine grinding of their olivine sample) at conditions of 150 bar and 185°C. O'Connor (2002) and Loring et al. (2011) used conditions of 185 bar/155°C and 180 bar/50°C respectively, with Loring et al. achieving 10% Wt. conversion and O'Connor achieving 78% (Mg-Conversion). It is likely that O'Connor obtained higher carbonation values because of the much higher temperature and pressure conditions used (pressure approximately in the 150-160 bar range) assisted by the finer grinding of the sample. The addition of NaCl also appeared to enhance the reaction of olivine. Further work could involve adding NaCl or simply seawater to a sample of olivine.

Wollastonite - In comparison with other reported carbonation values, the carbonation results achieved for Wollastonite in this study compared favourably with other studies. Only Tai et al. (2005) achieved higher carbonation values as a result of using a 'slurry' made up of the material which was stirred in the reaction chamber – something the batch reactor used in this study was not equipped to do. Tai et al. (2005) also used similar reaction conditions (86 bar/108°C) to those used in this this study.

This study achieved higher carbonation values than Prasad et al. 2009 (60 bar/100°C – Wollastonite samples reacted for five months), Huijgen (2007) (20 bar/200°C – reacted 38 µm Wollastonite powder for 20 minutes) and Wu et al. 2001 (2 bar/ 25°C). From these studies it can be concluded that to efficiently carbonate Wollastonite, a temperature approaching 100°C is required together with a CO_2 pressure which is higher than atmospheric pressure. The porosity must also be kept open, either by using low water availability or by the formation of a stirred slurry. All of the studies used powdered Wollastonite, thereby benefiting from the enhanced reactivity inherent with smaller grain sizes. Achieving the maximum carbonation potential for Wollastonite is within reach and further work needs to be done to fine tune the reaction process to achieve the extra 5% required to meet the target carbonation.

Calcium Hydroxide - In comparison with other studies the carbonation results achieved for calcium hydroxide in this study compared favourably. Regnault et al. (2009) reacted $Ca(OH)_2$ at 160 bar and 200°C, but suffered from the same 'crusting' effect observed in this study. Fagerlund (2010) reacted $Mg(OH)_2$ (Brucite) at 28 bar and 500°C and achieved a similar level of carbonation in relation to the carbonation potential of Brucite. It can, therefore, be observed that hydroxide minerals will readily carbonate at low temperatures (25°C in this study), but do benefit from higher temperatures. The higher temperature does not necessarily have to be above 100°C. In terms of pressure - effective carbonation will take place at 10 bar CO_2 (this study) and may improve, up to a particular ceiling, at higher pressures.

The technique which will be key to unlocking the full potential of hydroxide mineral carbonation will be one which will result in a volume change within the material. This will open up the porosity and thereby eliminate the effect of 'crusting' which prevents the reactants from reaching into the core of the sample material.

Steel Slag - In comparison with other reported carbonation values, the carbonation results achieved for the 'Dust' steel slag in this study compared favourably with other studies. However, none of the

carbonation values in any of the studies compared favourably with the carbonation potential which theoretically could be achieved.

This study achieved lower, yet similar, carbonation values when compared to Huijgen et al. 2005 (19 bar / 100°C – using a slag grain size <32µm), Huijgen 2005 (1 bar partial pressure CO_2 under conditions of 30 bar pressure / 25°C to 225°C for 30 minutes - using a slag grain size <38µm) and Huijgen [Unpublished PhD Thesis 2007] using conditions of 20 bar / 150°C (for 30 minutes)and 30 bar / 200°C (for 60 minutes) and under conditions of excess water. No additives were used during the reactions, but the grain size used was finer than that of the Dust used in this study. It is important to note that the results from this study (12 wt. % Dust carbonation) were similar to the results from other studies, presented above, which were undertaken under higher temperatures and relatively lower pressures. The 20% carbonations (Huijgen 2005) are also similar to the passive carbonation values of 'Dust' at 17 wt. %. A technique which results in steel slag being carbonated through the 20% ceiling has yet to be found and this suggests that either additives and/or a better understanding of the progression of the reaction front conditions are needed.

Additionally, Bonenfant et al. (2008) studied the carbonation potential of Ladle Furnace (LF) and Electric Arc Furnace (EAF) slags, which were produced by a different furnace process to the Basic Oxygen Furnace (BOF) slags. These slags had a similar composition to BOF slags and achieved similar carbonation values to BOF slags, which suggests that slags produced by a variety of steel-making methods are behaving in the same manner geochemically. Bonenfant et al., however, did achieve their carbonation at atmospheric pressure and temperature, but additives were used to lower the pH.

5.5.5 Efficiency of CO_2 Use

Sources of CO_2 which could be used for carbonation experiments have their own CO_2 footprints. For atmospheric CO_2 the footprint is 0 g CO_2 / tonne. However, atmospheric CO_2 is not concentrated enough to be used for active carbonation as the partial pressure of CO_2 would remain at 0.04 Pa. The carbon footprint increases slightly for waste flue gas, if the gas is to be captured, pumped and possibly scrubbed from the nearby flues of the blast furnaces or BOF furnaces. British Oxygen Company (BOC) supplied CO_2 gas canisters, carry the carbon foot print of the capture of CO_2 from the atmosphere as well as the filling and transportation of the CO_2 cylinders. Therefore, it is necessary to calculate the waste CO_2 emitted from each batch reaction to ensure that the carbonation process was not a net 'CO_2 polluter'. Table 5.22 shows the efficiency of CO_2 calculated for a theoretical 1 m^3 volume of material to be carbonated. The volume of CO_2 present within the 1 m^3 volume is based upon the volume of pore space within each material and excludes any water which may have been present

within the pore spaces during any particular batch reaction. Despite this assumption, some of the efficiencies reported in Table 5.22 relied on data which was acquired from experiments which were conducted using conditions of excess water.

As is shown in Table 5.22 some materials did not achieve high efficiencies. GBFS and 20 mm steel slag aggregate displayed the lowest overall efficiencies. Dust and Pellite, however, required additional CO_2 to be provided to the system which resulted in very high carbonation efficiencies and no direct CO_2 waste from the batch reaction. There was a difference in efficiencies depending on the CO_2 pressure used. Table 5.23 shows that the highest CO_2 sequestration efficiencies were achieved at lower CO_2 pressures. This is further good news for industry as if this technique was to be commercially realised, it would make economic sense to use batch reactors which would operate under lower pressure, thereby making the plants safer and more economic to operate.

Efficiency of CO_2 Sequestration

Temp	**Saturation**					
		Lp (10 bar)				
		20 mm	6 mm	Dust	Pellite	GBFS
L	*L*	7.07%	87.78%	**1147.11%**	**105.82%**	0.38%
L	*H*	11.45%	**122.48%**	**928.43%**	**130.84%**	1.46%
H	*L*	21.64%	94.25%	**1733.24%**	**112.93%**	4.16%
H	*H*	57.93%	**132.07%**	**1610.87%**	**153.90%**	16.37%
		Hp (100 bar)				
		20 mm	6 mm	Dust	Pellite	GBFS
L	*L*	5.86%	11.22%	**114.09%**	11.09%	0.12%
L	*H*	1.95%	5.42%	72.08%	17.55%	0.21%
H	*L*	2.03%	5.44%	**181.37%**	25.96%	1.78%
H	*H*	5.19%	24.08%	**133.00%**	49.38%	1.94%

Table 5.22: Efficiency of CO_2 used within a theoretical batch carbonation process. Calculations were based upon the weight of CO_2 present within the pore space of a 1m^3 volume of material and the mass of CO_2 absorbed during each experiment.

Temp	Saturation	20 mm	6 mm	Dust	Pellite	GBFS
L	*L*	LP	LP	LP	LP	LP
L	*H*	LP	LP	LP	LP	LP
H	*L*	LP	LP	LP	LP	LP
H	*H*	LP	LP	LP	LP	LP

Table 5.23: Optimal pressure conditions which generate the highest efficiency of CO_2 per theoretical batch carbonation process. The optimal pressure conditions are based upon the values within Table 5.22.

5.6 Conclusion

In this study slag products and 'pure' mineral species were reacted at different temperatures, in enhanced CO_2 environments at different pressure. The relationship between water availability and the degree of carbonation was also examined. However, given that the water within the chamber was in a liquid state under all of the experimental conditions and that there was no agitation of the water/sample mixture, then the CO_2 could only dissolve into the reaction fluid via the top surface of the liquid water. Therefore, in these experiments the phase of the CO_2 had no effect upon the samples and only the pressure and temperature conditions which affected the dissolution of CO_2 were important. This study has produced results for much larger grain-sized material than had previously been reported in the literature and experiments were carried out on materials within the liquid-phase region of CO_2, which had also not previously been reported in the literature.

The study has concluded that active reaction does produce carbonation values higher than the carbonate content of the fresh material. However, passive weathering methods produced higher carbonation values for 'Dust' than in all of the active reaction experiments and similar results were found for granular Pellite in six-out-of-eight experiments.

The highest active carbonation values achieved for each sample of slag material are shown in Table 5.24:

Material	Carbonation Achieved	Under Conditions Of	Compared to Passive Method
20 mm aggregate	0.844 wt. %	100 bar/25°C/Low water availability	14.1 times higher
6 mm aggregate	2.783 wt. %	100 bar/125°C/High water availability	6 times higher
Dust	12.726 wt. %	100 bar/125°C/Low water availability	28% lower
Pellite	1.662 wt. %	100 bar/125°C/High water availability	2.4 times higher
Pellite Powder	4.006 wt. %	100 bar/125°C/High water availability	5.8 times higher
GBFS	1.714 wt. %	100 bar/125°C/High water availability	1.7 times higher
GBFS Powder	2.839 wt. %	100 bar/125°C/High water availability	13.9 times higher

Table 5.24: The highest carbonation value achieved by each material and the active reaction conditions this was achieved at compared to the carbonation achieved under passive conditions.

The variation of pressure from 10 bar CO_2 to 100 bar CO_2 did not appear to have a major effect on the baseline carbonation in the experiments. Higher pressure resulted in the increase of the concentration of HCO_3^- ions, but this did not appear to dramatically enhance the reaction conditions of the experiments. Rather, the initial increase from atmospheric CO_2 concentration to 10 bar CO_2 pressure had the greatest effect upon the reactions. It can, therefore, be concluded that with increasing pressure, the carbonation value attained by a material does increase, but the degree to which this increase occurs is limited and is material specific. Should this work find use in industry then it is recommended that, depending upon the source of CO_2 available, the lower pressure (10 bar CO_2 pressure) conditions should be utilised for carbonation. Thereby, making optimum use of any CO_2 supplied or captured from an industrial plant.

The variation in temperature from 25°C to 125°C did appear to enhance the carbonation values of the individual materials and Dust, Wollastonite, and GBFS appeared to be particularly sensitive to temperature increases, showing a noticeable trend of increasing carbonation values at high temperatures. The effect of temperature, on average, ranged between 1.67 to 2.78 times the difference between Ht/Lt values between steel slags. The difference was greatest for GBFS with the effect ranging, on average, from 9.86 to 11.99. Pellite though, displayed a more muted temperature reaction dependency and on average ranged from 1.53 to 1.85. In addition, the relationship between the increase in carbonation caused by the increase in HCO_3^- concentration and the increase caused by

temperature was highly material specific. Overall, it can be concluded that increasing the reaction temperature does increase the carbonation value attained by a material. Part of the effect which temperature had, was on the growth rate of minerals upon the surface of the materials. This, in turn, dictated the extent of stable mineral carbon sequestration and so the carbonation value for each material. Under higher temperatures, the carbonate crystals grew faster and higher. On a grain scale, this may have provided a larger surface area for the dissolution of the sample as opposed to the formation of numerous smaller crystals, which covered the surface of the sample, and thereby reduced the area of dissolution.

The effect of water availability was to predominantly change the rheological properties of the sample material and therefore the porosity network. Should the porosity network collapse, as the material formed a paste then the availability of HCO_3^- ions would be restricted within the sample volume. This is because the carbonation reaction produced 'crusts' of carbonate which blocked the supply of HCO_3^- ions into the deeper parts of the sample. Overall, it can be concluded that increasing the availability of water to a material will increase the carbonation value achieved *only* if the material displays an open network of porosity. This can be determined by its rheological properties. Materials which display a collapse of their porosity network under excess water forming a paste will have higher carbonation values under conditions of lower water availability.

Overall, it was apparent that steel slags were more reactive than blast furnace slags, even at coarser grain sizes. Pellite was the most reactive out of all the blast furnace slags (Pellite and GBFS). However, both blast furnace slag samples achieved similar carbonation values when crushed to <250 µm suggesting that their surface crystallinity was an important factor in determining their reactivity.

Grain size was the biggest factor in determining the carbonation value of a given material type. All three materials (steel slag, Pellite and GBFS) showed an exponentially increasing trend in carbonation with decreasing grain size.

The 'pure' standard mineral samples achieved the highest carbonation values at:

- Olivine - 0.095 Wt.% under conditions of 100 bar/125°C/Low water availability
- Wollastonite - 26.63 Wt.% under conditions of 10 bar/125°C/High water availability
- Calcium hydroxide - 41.51 Wt.% under conditions of 100 bar/125°C/Low water availability

When plotted against their theoretical carbonation potentials the best conditions for carbonation of a mixed sample was shown to be at either 10 bar CO_2, 125°C, or 100 bar CO_2, 125°C. These conditions correlated well with the ideal carbonation conditions for all slag samples within this study. The

optimum water availability for each reaction was highly material and grain-size specific and an overall optimum water availability for all materials could not be deduced from the pure mineral experiments. However, it is evident from the pure mineral experiments that composition is a major factor in the carbonation of minerals. When applied to polymineralic substances this is even more evident – if the mineralogy of a material is not reactive enough, then the level of carbonation will be restricted.

Across all slag materials the overall conversion to carbonate was poor. The following conversions were achieved:

- 20 mm aggregate – 0.55%
- 6 mm aggregate – 1.85%
- Dust – 1.76%
- Pellite – 1.30%
- Pellite Powder – 4.89%
- GBFS – 0.30%
- GBFS Powder – 1.95%

It is apparent that the majority of the carbonation potential of each material is not being achieved. The literature suggests that there is a '20%' carbonation achievement 'ceiling'. Currently the use of additives has not found a solution to breaching this ceiling and it may be that a better understanding of the mineralogy of the samples will be the key to creating the right 'mix' of conditions for optimum carbonation.

Chapter 6:

Mock Field Trial – Assessing the application of active carbonation

6.1 Introduction

A small-scale, mock field-trial was conducted in order to assess the effectiveness of introducing large volumes of pure CO_2 directly into a slag heap and to compare the sequestration values of CO_2 with the carbonation values achieved via the methods of passive weathering. Passive weathering being the natural process of carbonation which is achieved by the slag products over time when stockpiled in heaps at Redcar industrial site (Chapter 4), and active weathering being the carbonation achieved when the slag products react with CO_2 under pressures and temperatures higher than those of the natural environment (Chapter 5). Lafarge-Tarmac stockpiles iron and steel making slags at the Redcar industrial site and this study is applicable to the management of the slag-heaps as it aims to create conditions which promote the highest carbonation values possible. Values obtained in these experiments will also be compared in terms of CO_2 efficiency (the amount of CO_2 emitted vs. that sequestered).

6.2 Methods

The aim of the experiment was to carbonate a small volume of slag product in a recreated 'slag heap' scenario. This experiment was carried out under atmospheric conditions, with a set flow of CO_2 and by varying the amounts of water available to the reaction. To conduct this experiment, a water-tight apparatus was built at the Department of Earth Sciences, Durham, which would not only contain the sample of slag during the reaction but could also provide a means of sampling a vertical section. The experiment was run for a total duration of 10 hours. However, due to health and safety regulations the experiment could not be run over night – therefore the experiment was run for 5 hours per day over two working days.

6.2.1 Experimental Apparatus

A gas line was prepared using a CO_2 canister with a 2 bar CO_2 regulator attached. From this a 4 mm inner-diameter nylon-tube was attached to the regulator. To the downstream end of the tube a needle-valve was attached to control the flow. Onto this a triangular 'rose' was fitted to the downstream end of the CO_2 delivery line to diffuse the CO_2 gas away from the end of the gas line (Fig. 6.1). A 15 cm inner-diameter plastic pipe was glued to a flat plastic base which provided a water tight seal to contain the mixture of slag and water and into which the downstream end of the gas line was

inserted. A sample of slag was added on top to encase the gas line. The sample of slag was added until the tube was filled to a depth of 30 cm (containing approximately 5300 cm^3).

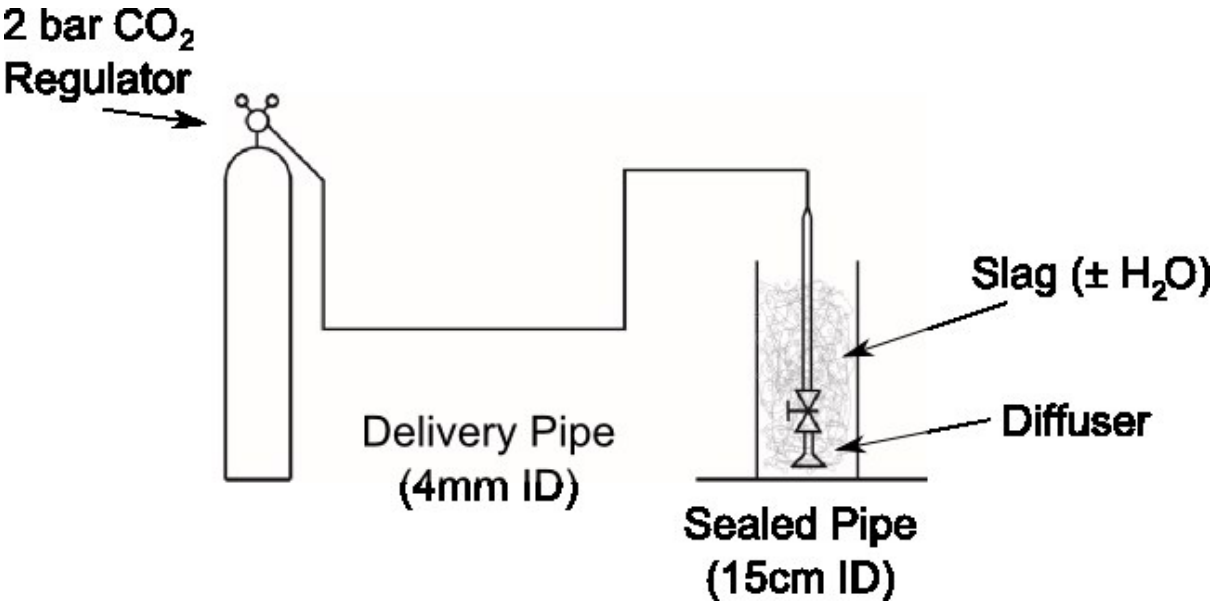

Figure 6.1: Apparatus used within the experiment

6.2.2 Experimental Conditions

Pressure

The experiment was conducted at a constant CO_2 pressure of 2 bar and a flow rate of 2 dm^3 min^{-1}. This flow rate was chosen as it provided a pressure which was high enough to deliver a constant stream of CO_2 gas. This flow rate was high enough to overcome the hydrostatic pressure of the water within the pipe, but was low enough to prevent the CO_2 from freezing. Freezing could occur due to the latent heat change associated with the continuous phase change from liquid-CO_2 from within the canister to gaseous- CO_2 upon exiting into atmospheric pressures.

Water Content

The water content of the pipe was varied from ambient levels of saturation - no water added (Pipe 1) - to 50% saturated (Pipe 2) and 100% (Pipe 3) of material saturated relative to the height of the pipe. This was done to study the effect of the availability of water on the carbonation reaction. Approximately, 0.0 dm^3 (Pipe 1), 1.25 dm^3 (Pipe 2) and 2.50 dm^3 (Pipe 3) of tap-water was added to the material in each experiment respectively.

Given that the reaction could not occur under dry conditions, it was hypothesised that if a larger volume of water was available for reaction then a greater degree of carbonation would be achieved as the increased concentrations of aqueous carbonic acid came into contact with the sample. The temperature of the tap water added to the slag column was approximately 16°C.

6.2.3 Experimental Materials

The material used within this experiment was 'Dust' (see Chapter 2 for a description). This was chosen as it consistently showed the greatest carbonation potential of all of the slag products available to this study as demonstrated in the experiments outlined in Chapters 4 and 5. The characteristics of the material have previously been described in Chapter 2.5.1. Due to the quantity of 'Dust' required for the experiment, further material was ordered from Lafarge-Tarmac. To compare the grain-size-distribution of the material supplied for this study with that supplied for the studies in Chapters 4 and 5, the Chapter 6 material was sieved using standard Endecott's sieves (4 mm mesh size to 32 µm mesh size) to ascertain the grain size distribution. Based upon the grain-size distribution for the material studied, Chapter 6 Dust (Fig 6.2, 6.3) it was expected that the carbonation potential identified in this study would be lower than that which would have been achieved had the Dust samples used in Chapters 4 and 5 been used. This difference was because the grain-size of Chapter 6 Dust was skewed towards a coarser grain size than that of Chapters 4 and 5 Dust.

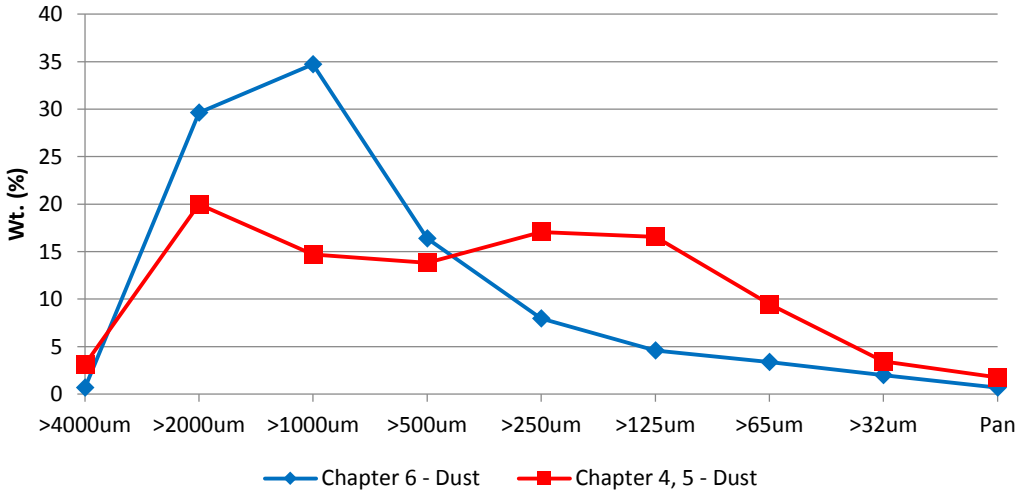

Figure 6.2: Grain-size distribution comparison between the Dust samples used in Chapter 6 compared to that used in Chapters 4 and 5

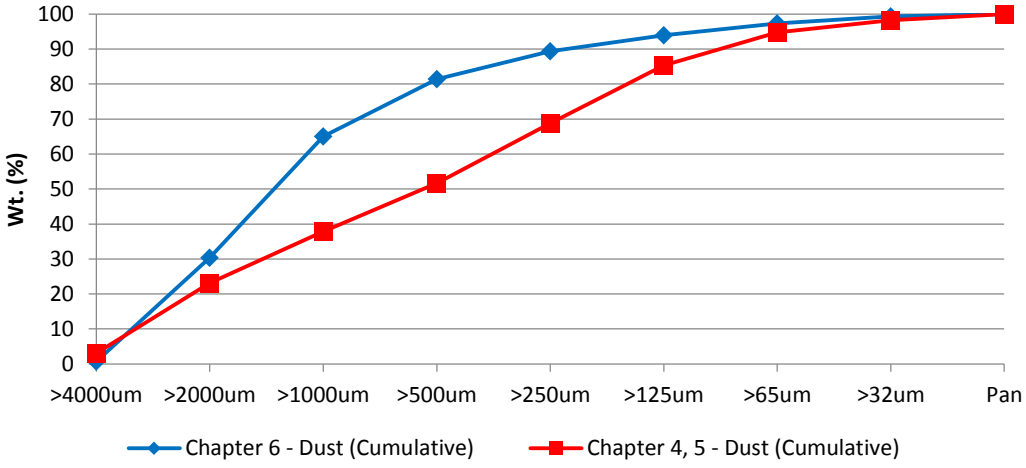

Figure 6.3: Cumulative grain-size distribution comparison between the Dust samples used in Chapter 6 compared to that used in Chapters 4 and 5

6.2.4 Experimental Method

Once the experimental apparatus had been prepared, the gas line was inserted into the retaining pipe and the sample was poured in around the diffuser. Due to the fine grain size of the 'Dust' the CO_2 supply was turned on at this point to prevent the diffuser from clogging with fine grained material, which could have been washed into it. For Pipe 1, the slag-material was added around the diffuser up to a height of 30 cm. For Pipe 2, the slag-material was added to a height of 15 cm at which point the sample was saturated with tap-water and further material was placed on top of this to complete the column height of 30 cm (thereby creating conditions of 50% saturation). For Pipe 3 slag-material was added to a height of 30 cm at which point the sample was saturated with tap-water (thereby creating conditions of 100% saturation) with further water being added to a height of 2 cm above the top of the samples to allow for the measurement of pH and conductivity of the water within the pipe. At the end of the experiment the top of the pipe was covered in plaster of Paris in order to 'seal' the sample into to pipe and to allow for the pipe to be sawn open.

In-situ Measurements

In situ temperature measurements were made with a 10 cm-long thermistor connected to an automatic pH meter. The pH measurements were taken using an electrode method, with attached temperature-probe. Conductivity measurements were also taken using an electrode. Although temperature was measured in the Pipe 2 and 3 experiments, it was only possible to measure pH and conductivity during the Pipe 3 experiment as only in this experiment was there sufficient water for the instruments to operate in.

Thermo-Gravimetric Analysis (TGA)

Duplicate samples were taken at 5 cm intervals from the base of each pipe and compiled to form a carbonation profile through the pipe. The method of TGA analysis used was identical to that of Chapter 4.2.3.

6.3 Results

The results from the Pipe experiments are outlined below. Visual observations were taken for each pipe (i.e. gas effervescence) and digital readings of temperature, pH and conductivity were taken every 2 minutes (or at shorter intervals if changes noted were rapid) for the first 30 minutes of the experiment, every 5 minutes for the next 30 minutes then after every 30 minutes for the remainder of the experiment. Temperature measurements were recorded for the Pipe 2 and Pipe 3 experiments. The pH and Conductivity measurements were taken only for the Pipe 3 experiment.

6.3.1 Pipe 1 – 10 hours, Ambient Saturation

The Pipe-1 experiment was run with a CO_2 gas flow rate into the pipe of 2 dm^3 min^{-1} without the addition of any additional water, apart from that present naturally upon the surface of the Dust aggregate slag grains. There was no visible sign of that a reaction had occurred. No noticeable gas was given off and there appeared to be no temperature change when the pipe was touched. No change in temperature was detected. The material within the pipe was poorly cemented throughout the height of the pipe and the material displayed little cohesion.

TGA Transect Taken Through the Pipe

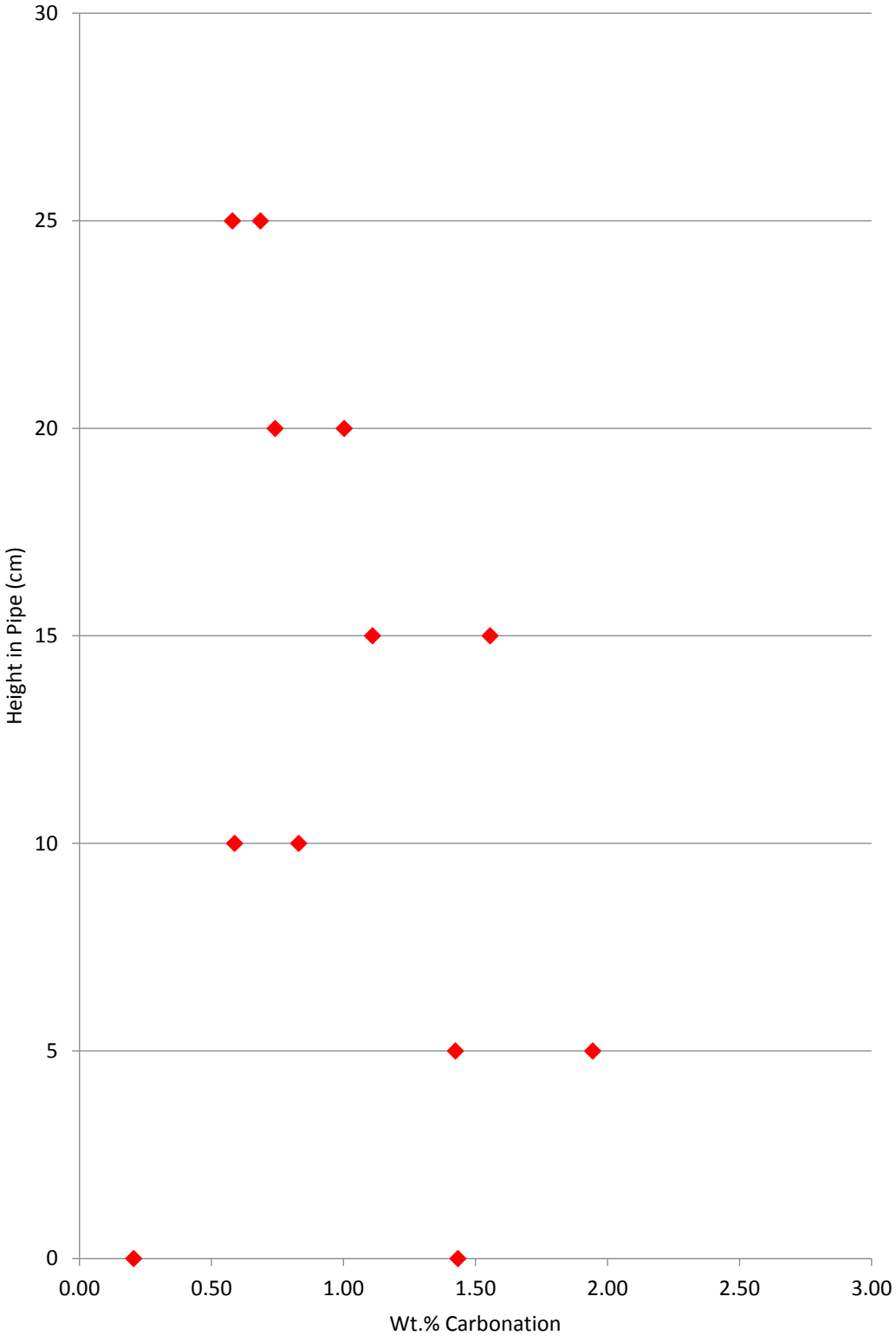

Figure 6.4: Wt. % carbonation values for samples taken from different height after the completion of the Pipe 1 experiment.

The carbonation values from Pipe 1 (Fig. 6.4) displayed a trend of decreasing carbonation with height, after a height of 5 cm, within the column of material. Carbonation values initially appeared to increase with a maximum of 1.94 wt. % reached at 5 cm from the base of the pipe. During the experiment no noticeable increase in temperature occurred. The trend of decreasing carbonation values with height indicated that the further away the sample was from the source of the CO_2 the lower the carbonation value achieved – possibly due to lower overall CO_2 pressures at the top of the pipe. The lack of moisture was likely to be a major factor in determining the carbonation values achieved. The flow of CO_2 gas may have driven out any moisture present, thereby limiting the reaction. Despite this Pipe 1 displayed the highest overall carbonation values.

6.3.2 Pipe 2 – 10 hours, 50% saturated

The Pipe-2 experiment was run with a CO_2 gas flow rate into the pipe 2 dm^3 min^{-1} with ½ the height of the column of Dust aggregate slag, saturated with approximately 1.25 dm^3 of tap water. Within ten minutes of the CO_2 supply being turned on, the smell of hydrogen-sulphide could be detected coming from the top of the pipe. The pipe began to heat up and the top of the column of the slag was warm to the touch. The temperature profile of the experiment with time is shown in Fig. 6.5, which shows that the reaction mainly occurred within the first two hours of the experiment before diminishing with time.

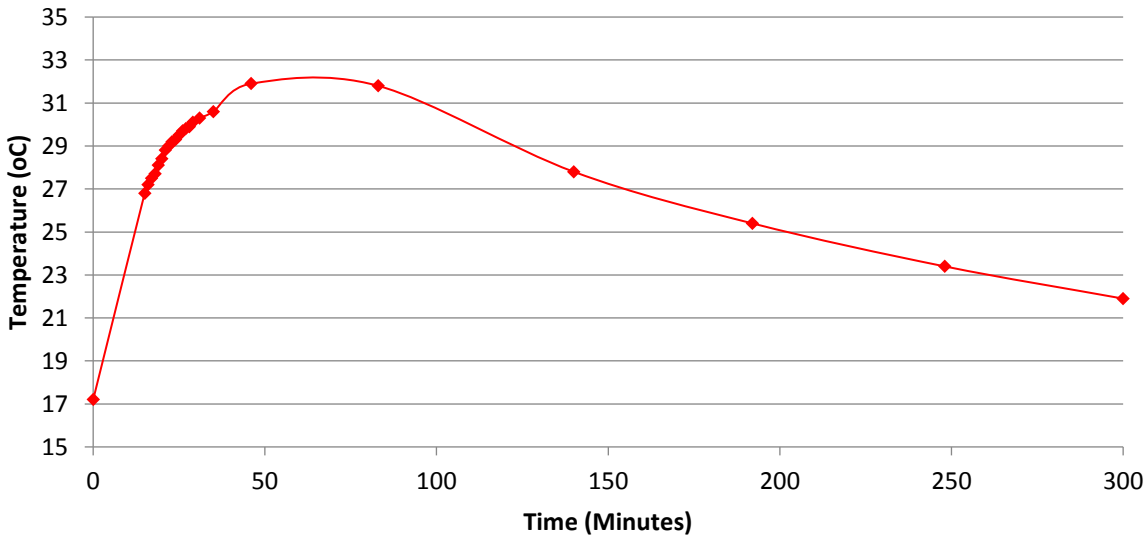

Figure 6.5: Temperature profile with time for the top 10 cm of sample-material during the first 300 minutes of the Pipe-2 experiment.

Textures within the pipe

The material within the pipe was weakly cemented up to a height of approximately 25 cm. Above 25 cm the top layer of material was poorly consolidated. An elutriation (gas-escape) pipe was visible within the cemented region from a height of 7 cm-15 cm from the base (Fig. 6.6). White Ca-rich crystals (Figures 6.7, 6.8) (confirmed by SEM-EDS) were present to a height of 5 cm within the material.

Fig 6.6: Cross-section of Pipe-2 after the experiment.

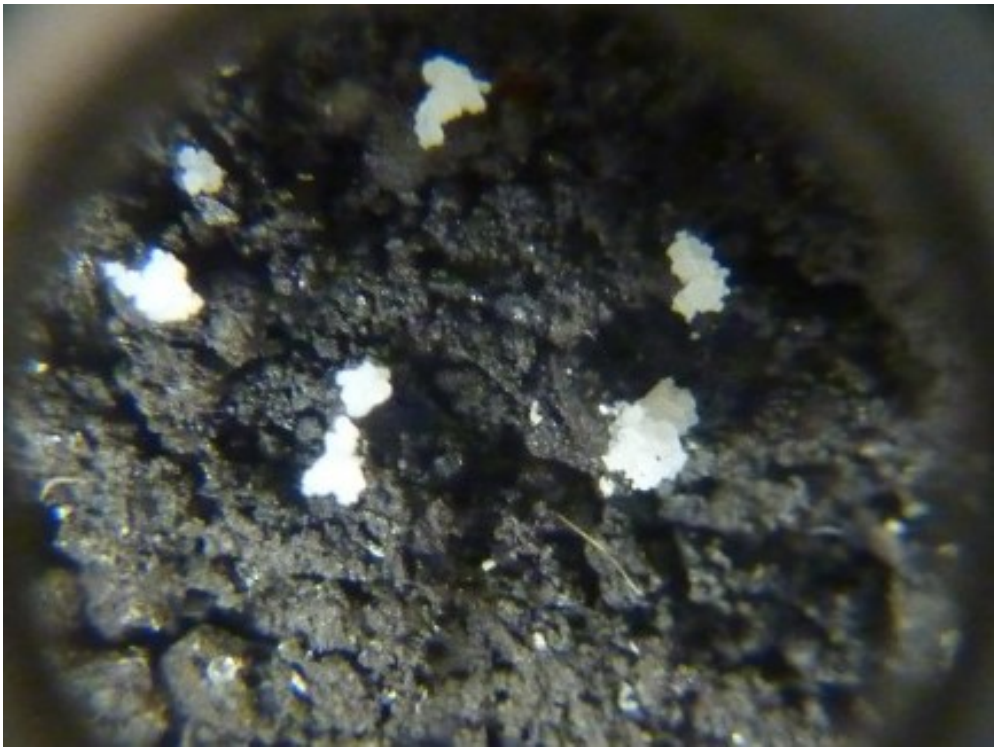

Figure 6.7: Ca-rich crystals precipitated from the CO_2-Slag-H_2O fluid at the base of Pipe-2.

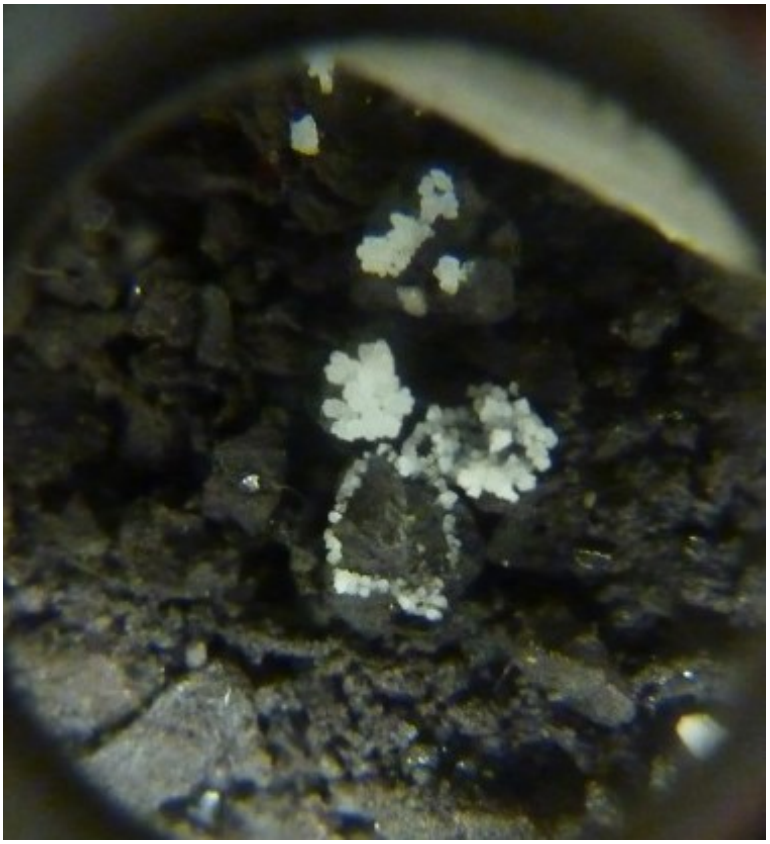

Figure 6.8: Ca-rich crystals precipitated from the CO_2-Slag-H_2O fluid at the base of Pipe-2.

TGA Transect Taken Through the Pipe

Samples of material were taken at 5 cm intervals from the base of the pipe and analysed in duplicate. The measurements at 22.5 cm from the base of the pipe were taken from a well-cemented area towards the centre of the pipe.

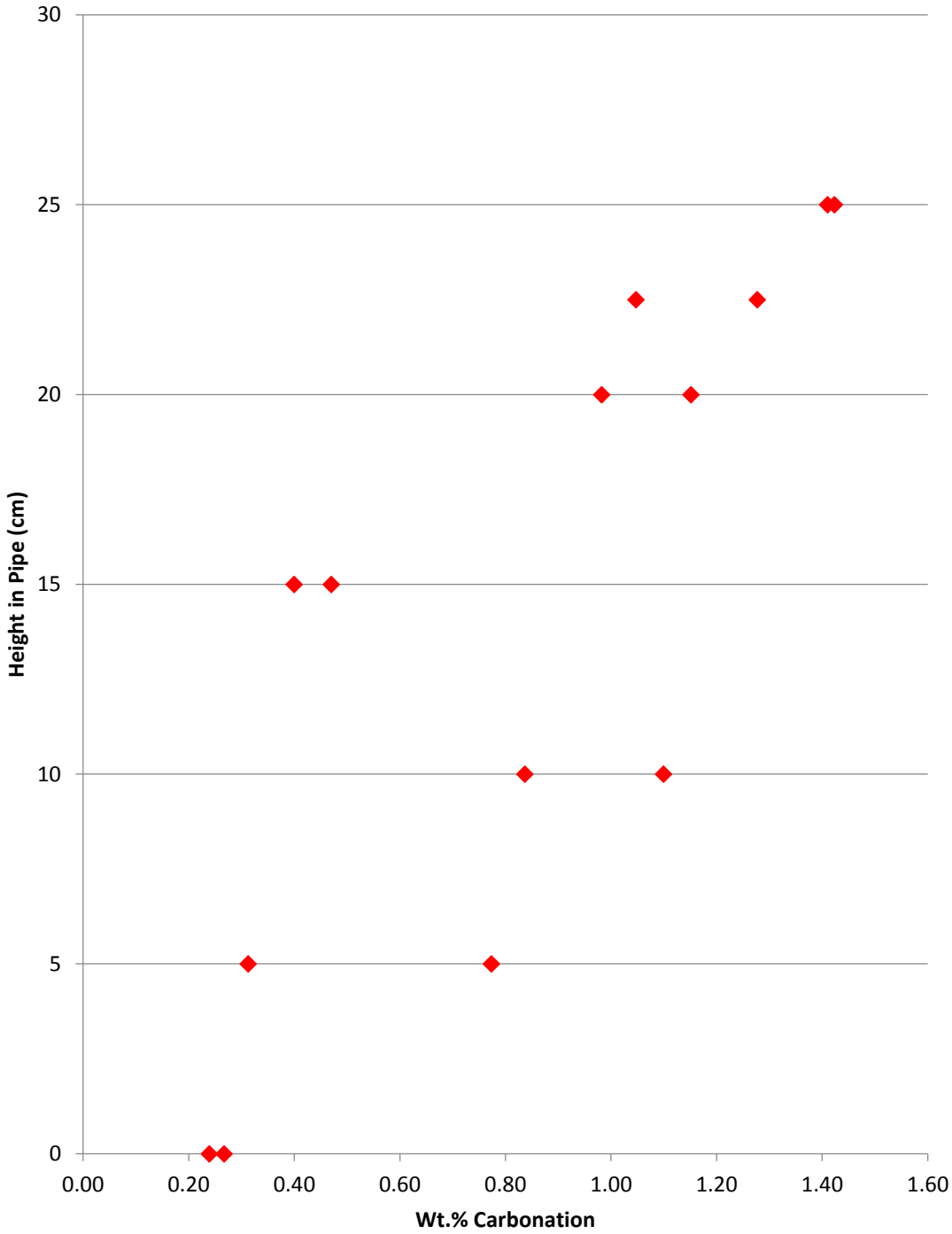

Figure 6.9: Wt. % carbonation values for samples taken from different height after the completion of the Pipe 2 experiment. The height of saturated material extends to 15cm.

The carbonation values from Pipe 2 displayed a trend of increasing carbonation with height within the column (Fig. 6.9), apart from a sample taken at 15 cm from the base of the pipe. Carbonation values do appear to be clearly divided above and below 15 cm into two separate trends. In the saturated region of the pipe, the carbonation values displayed by the samples were lower and demonstrated a greater variation than those from the 'non-saturated' region of the pipe. The 'non- saturated' region displayed a more even carbonation trend and higher values than those found within the majority of the saturated region.

During the experiment a temperature increase of 15°C was observed. Assuming a uniform temperature increase for the whole water content of the pipe (1.5 dm^3) then the total energy required to generate this increase was 94.21 kJ. This corresponds to the carbonation of 47.71g of Rankinite ($Ca_3Si_2O_7$) or 226.93g of Portlandite ($Ca(OH)_2$).

The top 50% of Pipe 2 also displayed higher carbonation values than any of the samples taken from Pipe 3 and any of the samples from the lower 50% of Pipe 2. It is possible that the higher temperature at the top of the pipe both increased the carbonation rate through reaction kinetics and provided a source of warm water vapour to the top of the pipe, thereby aiding the reaction by ensuring a sufficient distribution of moisture throughout the whole pipe. Though it was not possible to measure the pH of the fluid within the pipe, the noticeable smell of hydrogen sulphide supported the presence of a reducing environment within the pipe and suggested Eh conditions of at least -0.5 V. The lower part of the pipe may have been saturated to the point where the flow of CO_2 was confined to certain pathways within the lower part of the tube, which restricted the availability of CO_2 to other areas of the pipe. The low carbonation value at the base of the pipe showed that HCO_3^- and/or CO_2 was limited at the very bottom of the pipe below the level of CO_2 injection.

6.3.3 Pipe 3 – 10 hours, 100% saturated

The Pipe-3 experiment was run with a CO_2 gas flow rate into the pipe of 2 dm^3 min^{-1} with the height of the column of Dust aggregate slag saturated. Tap water was added to a height 2 cm higher than the top of the slag column to allow for measurements of pH and conductivity using a pH-probe and a conductivity-probe alongside a temperature-probe which was inserted into the material to a depth of 10 cm.

Description of the reaction

In contrast with Pipe-2 there appeared to be no hydrogen-sulphide given off and the temperature of the pipe did not noticeably increase. However, after the experiment was resumed at 276 minutes the temperature did increase by 5°C. The temperature profile of the experiment with time is shown in Figs. 6.10 and 6.11.

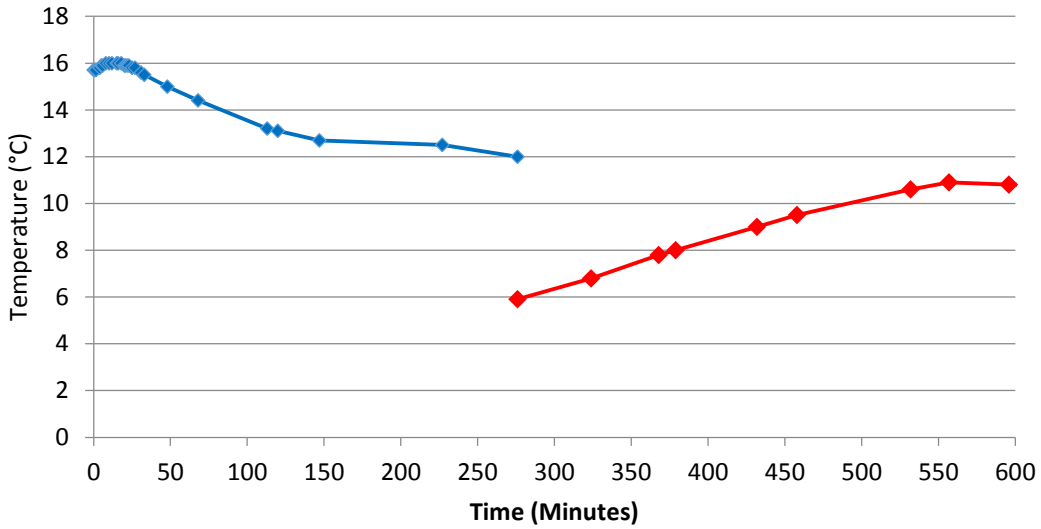

Figure 6.10: Temperature profile with time during the 10 hours of the Pipe-3 experiment. (Day 1 – up to 276 minutes (blue), Day 2 – from 276 minutes (red))

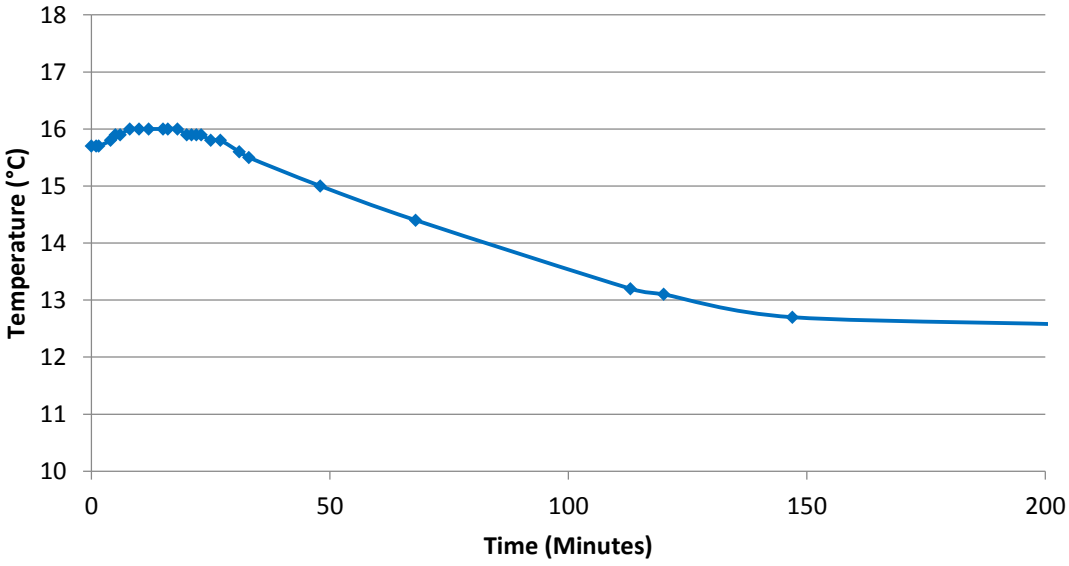

Figure 6.11: Temperature profile with time during the first 200 minutes of the Pipe-3 experiment.

The pH of the fluid at the top of the pipe remained between pH 6 to pH 6.5 throughout the experiment. A pH of 9.11 was recorded when the experiment was resumed for the second working day (at 276 minutes). This pH represented the equilibrium conditions of the fluid after resting overnight for 18 hours. The pH profile of the experiment with time is shown in figure 6.12.

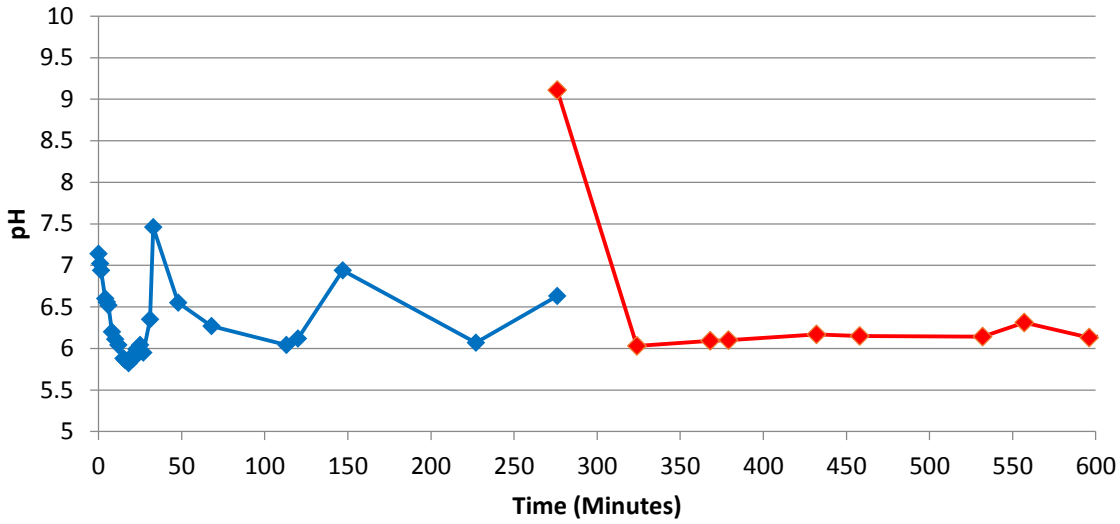

Figure 6.12: pH profile with time during the 10 hours of the Pipe-3 experiment. (Day 1 – up to 276 minutes (blue), Day 2 – from 276 minutes (orange))

The conductivity of the fluid at the top of the pipe lay between 500 µS/cm to 1000 µS/cm during the first working day of the experimental run. During the second working day, the conductivity fluctuated between 500 – 2500 µS/cm but largely remained at the higher end of the reading. The conductivity profile of the experiment through time is shown in figure 6.13.

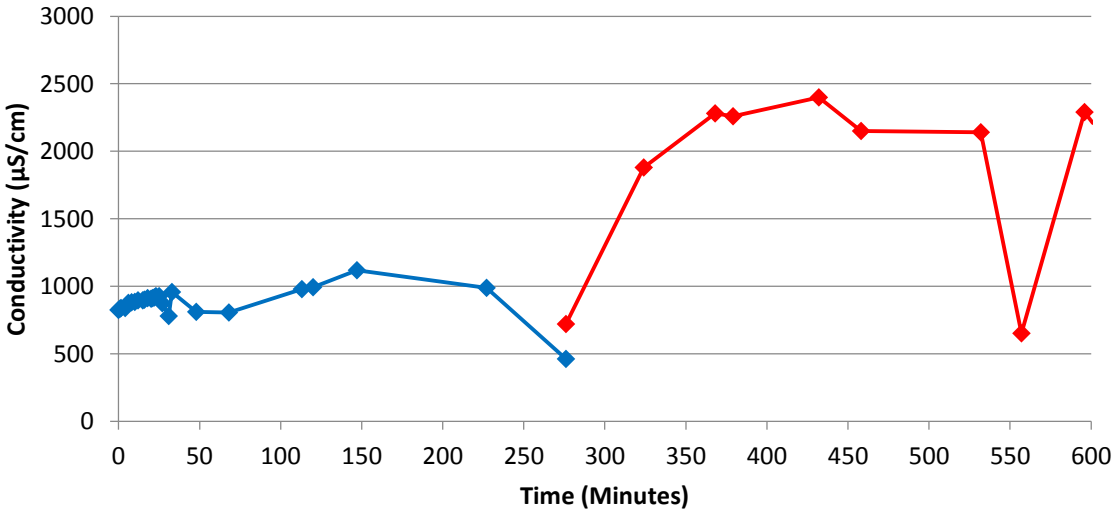

Figure 6.13: Conductivity profile with time during the 10 hours of the Pipe-3 experiment. (Day 1 – up to 276 minutes (blue), Day 2 – from 276 minutes (orange))

Textures within the pipe

The material within the pipe was well-cemented throughout the height of the column (Fig. 6.14). The samples were visibly whitened by the formation of carbonate between 5 cm to 20 cm from the base of the material. The material appeared to have become sorted into visibly finer and coarser layers of grains within the lower 17.5cm of the column.

Figure 6.14: Cross-section of Pipe-3 after the experiment.

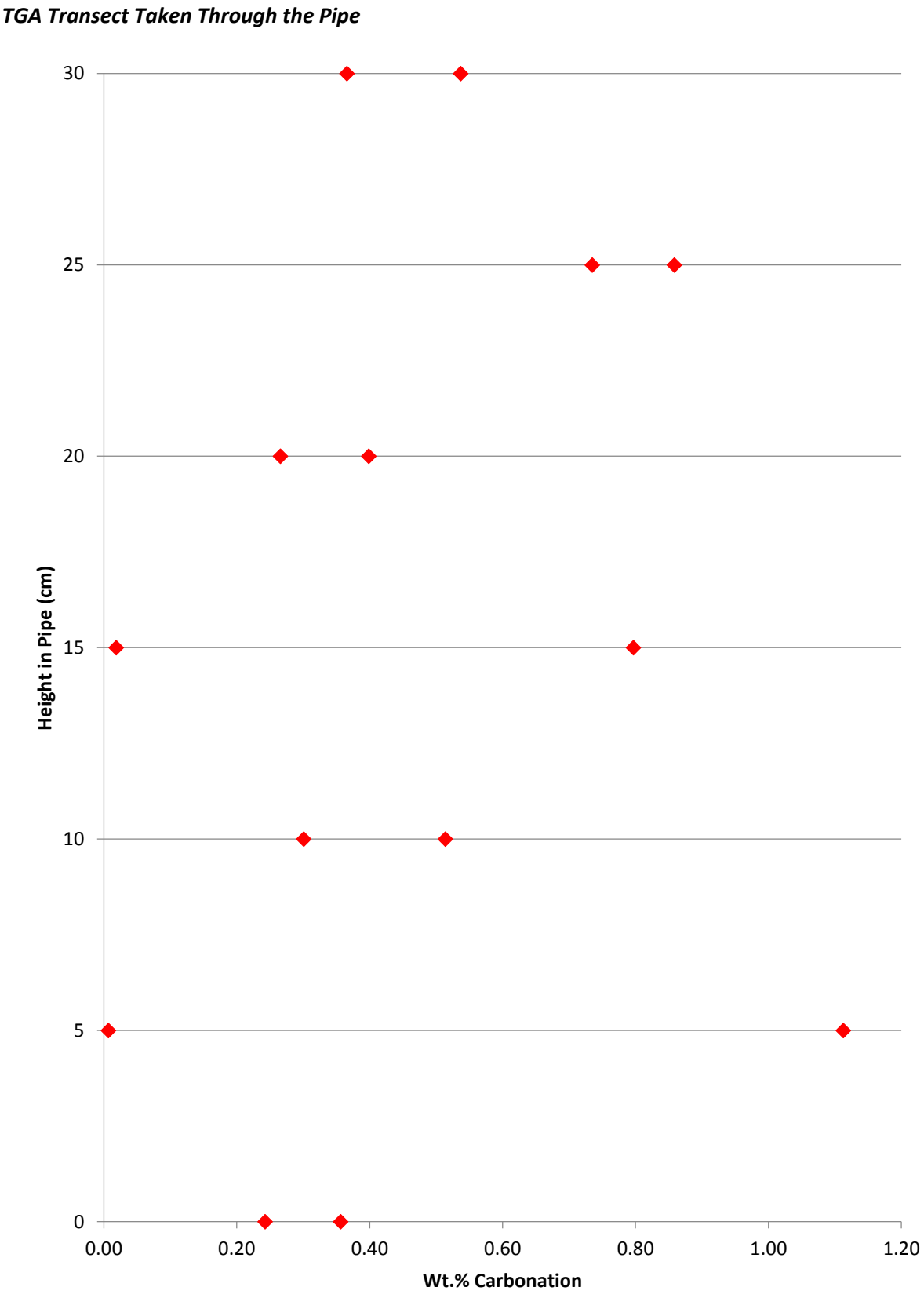

Figure 6.15: Wt. % carbonation values for samples taken from different heights after the completion of the Pipe 3 experiment.

The trend in carbonation values for Pipe 3 displayed a relative uniformity of carbonation (Fig. 6.15) suggesting that the saturated conditions may well have restricted the extent of carbonation within the pipe. This was supported by the lower carbonation values than those found in the non-saturated volume of Pipe 2. The highest carbonation values were recorded at 5 cm from the base, just above the height of the main point of CO_2 injection. The spread of data may represent the sampling of finer and coarser areas of the pipe material.

During the experiment a temperature increase of 5°C was observed over 5-10 hours. Assuming a uniform temperature increase for the whole water content of the pipe (1.5 dm^3) the total energy required for the increase was 62.8 kJ. This corresponds to the carbonation of 31.8g of Rankinite ($Ca_3Si_2O_7$) or 151.3g of Portlandite ($Ca(OH)_2$). The lower carbonation values in Pipe 3 may have been the result of the formation of preferred pathways for the flow of CO_2 within the pipe. The channelization of CO_2 through the pipe would carbonate only a small volume of the material. The rest of the carbonation would result from the diffusion of HCO_3^- ions through the water within the pipe. The flow of HCO_3^- ions through the volume of Dust would be achieved by the overturn of water within the pipe as it was disturbed by the upwards flow of the CO_2 gas.

The pH at the top of the pipe remained broadly between pH 6 and pH 7 for the duration of the experiment. A pH of 9.11 was recorded after the experiment was left overnight suggesting this was the equilibrium pH of the water-slag mixture within the pipe. This pH was reduced to pH 6 within 40 minutes of the flow of CO_2 resuming. This indicated that the CO_2 was rapidly disassociating the water to produce HCO_3^- ions and that this was the controlling factor in the reaction. Based upon the calculations in Chapter 3 it can be predicted that $CaCO_3$ would be directly precipitated as a result of the carbonation reaction. However, gypsum precipitation was also possible.

The conductivity measurements displayed two regimes. The first five hours of the experiment produced conditions which were predominantly between 500 – 1000 µS/cm while in the latter five hours of the experiment the conditions were predominantly between 2000 – 2500 µS/cm. As the experiment was left overnight this may reflect the dissolution of ions from the surface of the slag. These dissolved ions were then brought to the top of the pipe by the flow of water and gas around the pipe. Given that the conductivity was significantly raised within 40 minute, the overturn of the water around the pipe must be on the order of 30 cm hr^{-1} resulting in the water completely overturning 10 times during the Pipe 3 experiment and 20 times during the Pipe 2 experiment resulting in a homogenous distribution of ions around the saturated pipe volume.

6.4 Discussion

Table 6.1 shows the theoretically calculated weight (g) of carbonate formed in each pipe assuming an even carbonation for each 5 cm interval as derived by the amount of $CaCO_3$ understood to be present. The efficiency of this method of carbonation is also reported as the number of grams of CO_2 sequestered divided by 2359.13g of CO_2 (the number of grams of CO_2 that passed through the pipe during the 10 hours of the experiment duration at 2 dm^3 min^{-1} CO_2).

	PIPE 1	PIPE 2	PIPE 3
$gCaCO_3$	123.00	80.18	56.98
gCO_2	54.09	35.26	25.05
Efficiency	2.29%	1.49%	1.06%

Table 6.1: Table showing the gCaCO3 equivalent for the total wt. % carbonation achieved for the sum of all 5 cm carbonation intervals and the gCO_2 equivalent to this. Efficiency is reported as a percent of total CO_2 involved in the experiment that was theoretically sequestered.

The efficiency percentages show that this method of carbonation is not very efficient, even when the material used has been characterised in Chapters 4 and 5 as being the most reactive material within its chemical class. However, if it is assumed that the graphs of temperature increase (Fig. 6.5, 6.10) are an expression of the progress of the reaction then the majority of the reaction can be assumed to have occurred within the first five hours of the experiment. If this was the case then by reducing the length of the flow of CO_2 to 5 hours the efficiency could be doubled to a maximum of approximately 4.58%.

6.4.1 Comparison with Data from Chapter 4 and 5

It is evident that in relation to the carbonation values achieved by Dust in Chapters 4 and 5 the carbonation attained by Dust during this study was considerably lower (Table 6.2).

	PIPE 1	PIPE 2	PIPE 3
High	19.94%	13.00%	9.19%
Low	5.71%	3.72%	2.63%

Table 6.2: The maximum and minimum percentage carbonation achieved in the Chapter 6 study when compared to the results from the studies in Chapters 4 and 5.

The results from the passive study [Chapter 4] and active study [Chapter 5] were compared to the data (Fig 6.16, 6.17, 6.18).

Pipe 1

For Pipe 1 all carbonation values were lower than both the active and passive studies in Chapters 4 and 5.

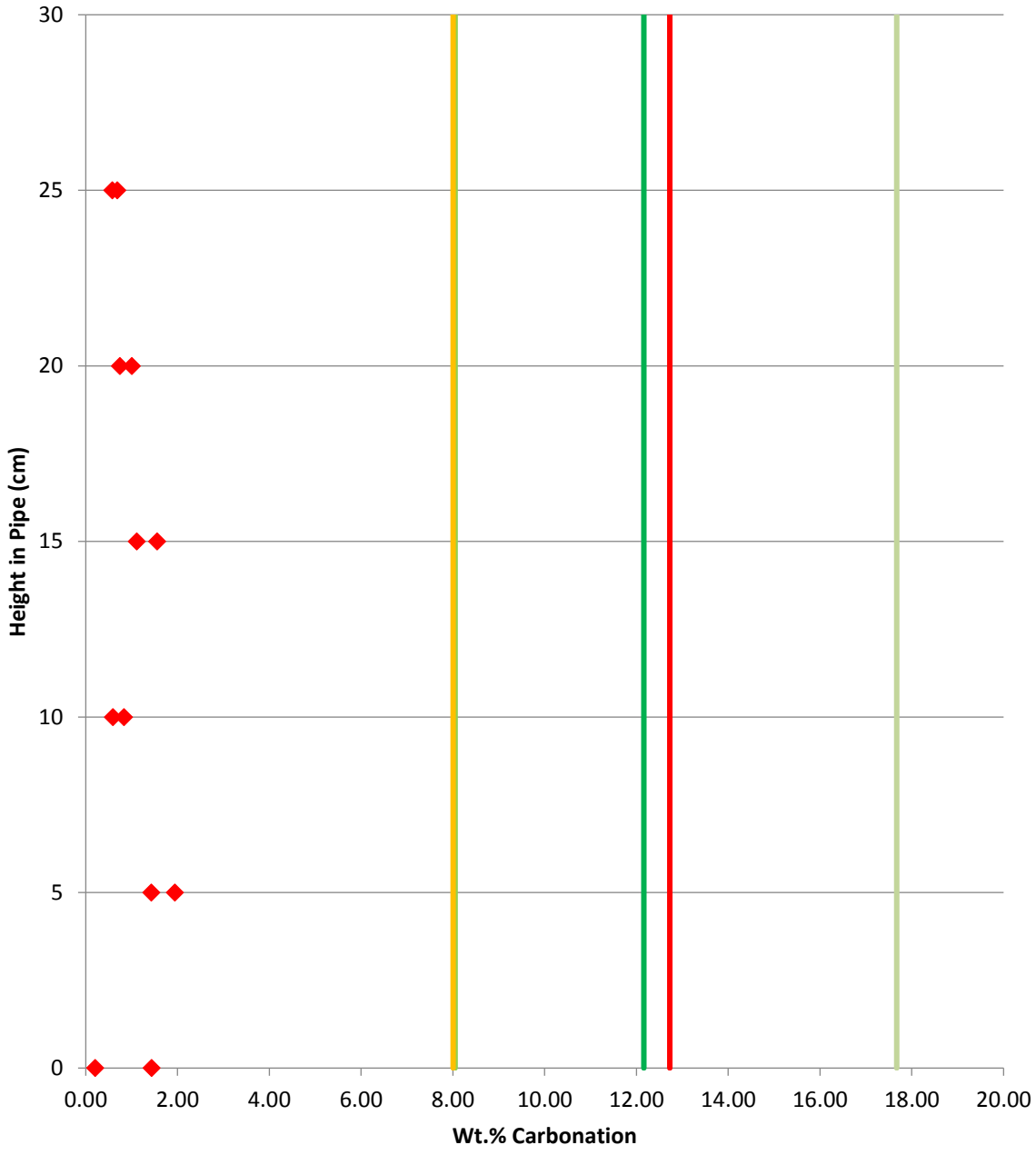

Figure 6.16: Carbonation values form the Pipe 1 experiment (from Figure 6.4) with the carbonation values achieved under passive and active reaction conditions. All carbonation values are compared to the active experiments under conditions of low water availability. The coloured lines on the graphs indicate the carbonation values achieved at the following conditions: Straw Green – Passive Conditions, Light Green – Low Pressure (10 bar) Low Temperature (25°C), Dark Green – Low Pressure (10 bar) High Temperature (125°C), Orange – High Pressure (100 bar) Low Temperature (25°C), Red – High Pressure (100 bar) High Temperature (125°C),

Pipe 2

For Pipe 2 all carbonation values are lower than both the active and passive studies in Chapters 4 and 5.

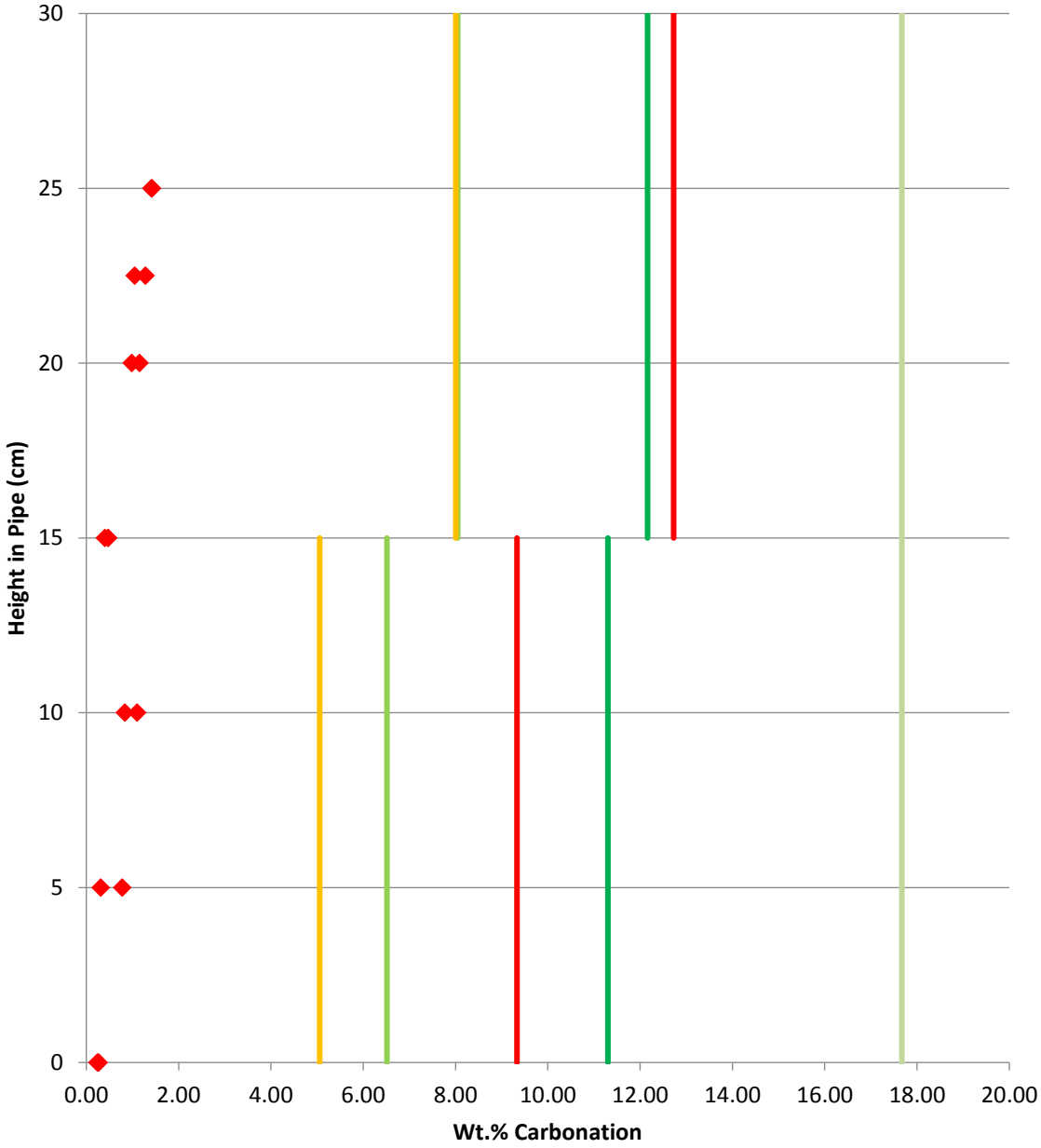

Figure 6.17: Carbonation values form the Pipe 2 experiment (from Figure 6.9) with the carbonation values achieved under passive and active reaction conditions. The lower 15 cm of the pipe is compared to the active experiments under conditions of high water availability. The top 15 cm of the pipe is compared to the active experiments under conditions of low water availability. The coloured lines on the graphs indicate the carbonation values achieved at the following conditions: Straw Green – Passive Conditions, Light Green – Low Pressure (10 bar) Low Temperature (25°C), Dark Green – Low Pressure (10 bar) High Temperature (125°C), Orange – High Pressure (100 bar) Low Temperature (25°C), Red – High Pressure (100 bar) High Temperature (125°C),

Pipe 3

For Pipe 3 all carbonation values are lower than both the active and passive studies in Chapters 4 and 5.

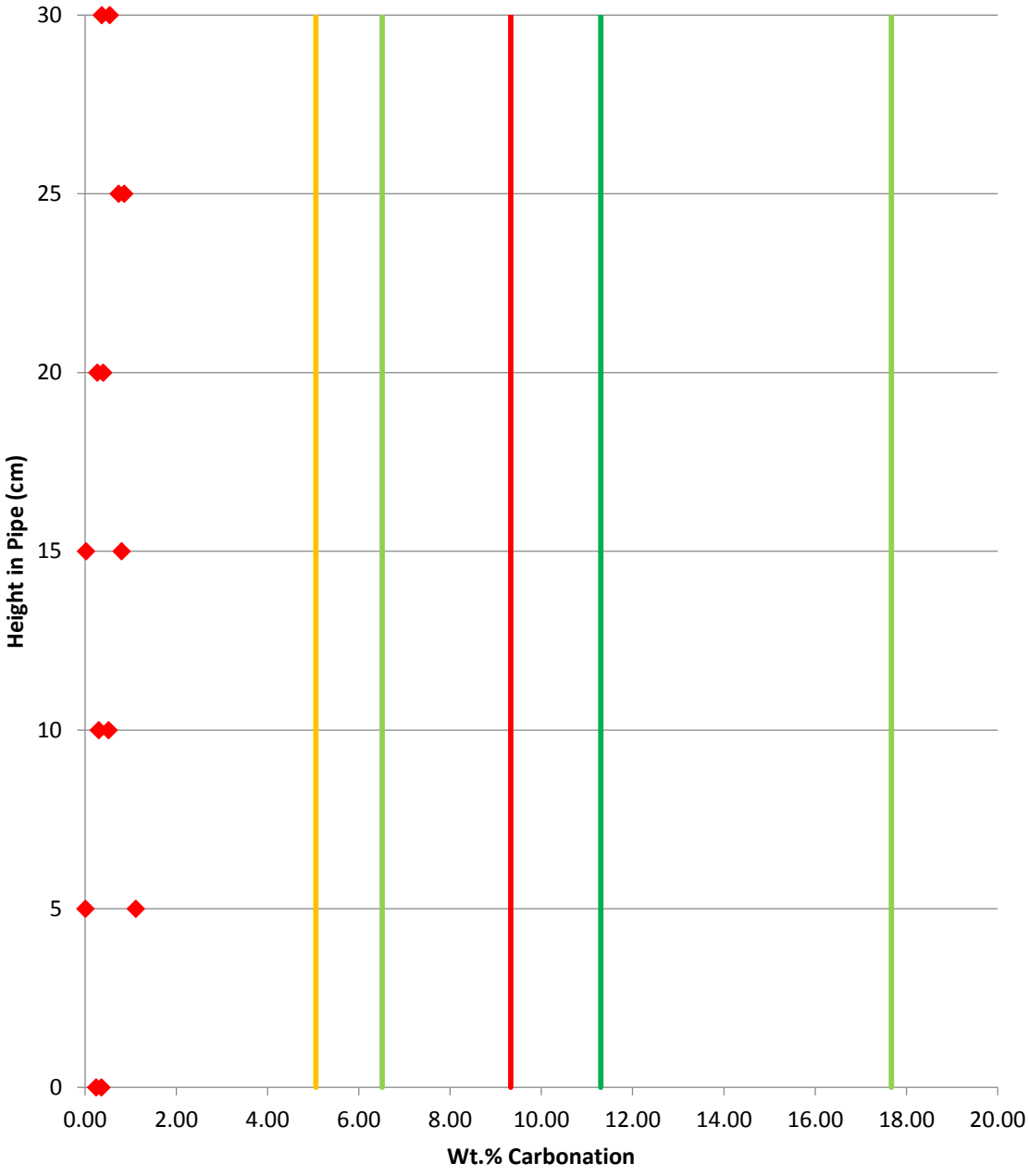

Figure 6.18: Carbonation values form the Pipe 3 experiment (from Figure 6.14) with the carbonation values achieved under passive and active reaction conditions. All carbonation values are compared to the active experiments under conditions of high water availability. The coloured lines on the graphs indicate the carbonation values achieved at the following conditions: Straw Green – Passive Conditions, Light Green – Low Pressure (10 bar) Low Temperature (25°C), Dark Green – Low Pressure (10 bar) High Temperature (125°C), Orange – High Pressure (100 bar) Low Temperature (25°C), Red – High Pressure (100 bar) High Temperature (125°C),

6.4.2 Overall Model

An overall conceptual model for the mock field trial can be constructed from the data collected in this study.

Eh, pH,

The equilibrium pH of water saturated slag appeared to be between pH 9.0-9.5. However, the pH of any moisture present within the pipe experiments would rapidly (within approximately 40 minutes) reach a pH of around 6-7 showing that the formation of carbonic acids had occurred resulting in carbonation. The strong smell of hydrogen sulphide signified the existence of a reducing environment within the pipe and suggests Eh conditions of at least -0.5V.

Conductivity

Conductivity depended upon the amount of time that the sample has been in contact with the moisture which surrounded it. Initially, the conductivity of the slag-water mixture was approximately 100 to 10 -times that of tap water, indicating that the water had rapidly dissolved available ions. When left for 24 hours the slag-water approximately doubled to quadrupled in terms of conductivity showing that the water had been able to dissolve a significantly higher concentration of ions with time.

The conductivity conditions within the moisture layer of slag grains is still unknown but may well follow a similar pattern to the results of the fully saturated slag.

Temperature

Temperature can be used as a proxy for understanding the progress of the carbonation reaction within the pipe experiments. Pipe 2 was able to display a larger temperature increase (15°C as opposed to 5°C) due to the lower volume of water into which the heat produced was absorbed. In comparison, the degree of carbonation and energy released by the reaction was similar once the volume of water had been taken into account.

The temperature profile for a pipe filled with material unsaturated with water is still unknown. However, if the water content of Pipe 3 resulted in all of the heat being transferred into the water within the pipe and thereby around the interior of the pipe via flow through the grains of slag. Likewise, if the water content of Pipe 2 allowed heat to be transferred within the lower 50% of the pipe via circulation via flow through the grains of slag and the top 50% via the movement of warm (31℃) moisture through the top of the pipe (thereby resulting in loss of energy from the system, cooling the pipe). Then by considering these processes the behaviour of heat within Pipe 1 can be

postulated. Pipe 1 did not have a high enough water content to facilitate the convection of heat via liquid flow or via a vapour phase, but it did display a higher degree of individual carbonation than Pipes 2 and 3 implying that heat must have been given off. However, the heat generated was not noticeable during the experiment, partly due to its transfer being controlled by conduction and partly due to the majority of carbonation occurring at the base of the pipe. This meant that the top of the sample column felt cool and the base of the column did not radiate an appreciable amount of heat.

Gas-Flow Conditions

The water saturation conditions within each of the pipes produced different gas-flow regimes in each of the experiments. The material within Pipe 1 contained open porosity and a lack of cementation and as a result the injected CO_2 gas passed through the sample column in an unrestricted manner. The 50:50 saturated/unsaturated conditions within Pipe 2 led to the formation of gas-escape pipes within the sample material below the level of 15 cm from the base of the pipe. Pipe 3 displayed structures of rhythmic layers of fine and coarse grained material with the flow of CO_2 gas envisaged as passing through the coarser grained layers due to their higher relative porosity. These layers were also found to be the most strongly cemented of all the sample material.

Carbonation

The carbonation trends for each pipe experiment are shown in Fig. 6.19. Three different trends are apparent within the data. Under unsaturated conditions there was a progressively decreasing trend in the degree of carbonation of the material. Under 50:50 conditions there was a progressively increasing trend in the degree of carbonation where up to 15 cm height in the column the carbonation values were similar to the results from Pipe 3 and above 20 cm in height the carbonation values were similar to the results from Pipe 1. In saturated conditions the results displayed a trend of even carbonation value, with the majority of the data points restricted to below 1 wt. % carbonation (approximately half the maximum carbonation value achieved under unsaturated conditions).

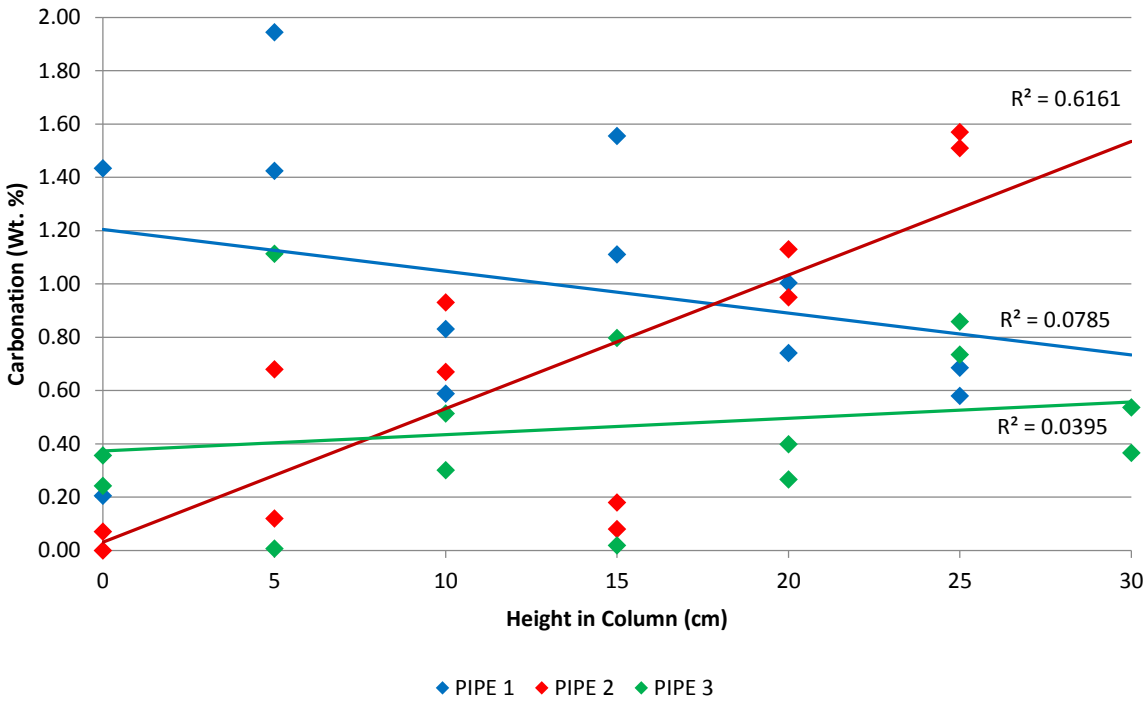

Figure 6.19: Graph showing all data points for the three pipe experiments.

The pH conditions of the reaction fluids tended to remain between pH 6-7, with the conductivity of the fluid increasing with time as ionic components were progressively dissolved into the reaction fluid. As the exothermic carbonation reaction progressed, heat was given out which may have enhanced the rate of carbonation. The distribution of heat around the sample material was dictated by the availability of water, which transported the heat either through the flow of water around the sample volumes or through the percolation of a warmed vapour phase throughout the sample volume. Under unsaturated conditions heat was transferred via conduction, possibly leading to localised areas of heating within the sample. Saturated sample conditions produced a more even spread in carbonation values throughout the pipe. However, this also appeared to restrict the maximum carbonation value which could be achieved. It is likely that adding a limited amount of water into the system (preferably as a warm vapour phase) would achieve the highest carbonation values. The flow of gas through a saturated, granular material leads to the formation of preferential flow paths localising direct carbonation, again a limited supply of water in a vapour phase allows the porosity to be kept open and allows diffuse gas flow through the column of material.

It is noted, however, that the above experiments have failed to reach the carbonation values attained via active and, in particular, passive weathering techniques. This was despite the assumption that due to a slightly coarser overall grain size within the experimental material the maximum carbonation value which could be achieved would be lower than in the other studies.

6.5 Conclusions

This study has concluded that:

- That a column of slag saturated with water will tend towards solution of pH 9-9.5. Addition of CO_2 gas can rapidly reduce this pH to between pH 6 and pH 7 and will create reducing conditions to at least Eh -0.5 V as indicated by the production of hydrogen sulphide gas.

- Temperature readings can be used to identify the progress of carbonation within a column of carbonating slag.

- The availability of water dictates the ways in which heat is distributed through a column of slag. Heat will be transported either through the flow of water around the sample volume in saturated conditions or under condition of restricted saturation through the percolation of a warmed vapour phase throughout the sample volume. Under unsaturated conditions heat will be transferred via conduction possibly leading to localised areas of heating within the sample.

- Each set of hydration conditions displayed its own trend. Under unsaturated conditions there was a progressively decreasing trend in the degree of carbonation of the material. This was possibly due to the increasing distance from the most concentrated source of CO_2. In saturated conditions the results displayed a trend of even carbonation values, with the majority of the data points restricted to below 1 wt. % carbonation (approximately half the maximum carbonation value achieved under unsaturated conditions) likely due to the even distribution of HCO_3^- due to diffusion through the water saturated material. Under 50:50 conditions there was a progressively increasing trend in the degree of carbonation caused partly by the carbonation of the lower saturated section of the pipe being controlled by the saturated conditions and the upper part of the pipe benefiting from the effects of warm water vapour which both kept the porosity open and enhanced the reaction conditions.

- The efficiency of this method of carbonation has been theoretically calculated to be between 1.06% (Pipe 3) and 2.29% (Pipe 1). The actual efficiency may be higher due to the restricted sample set for each experiment (n=12 or 14) and the broadly unknown reaction duration. If the reaction reached effective completion after 5 hours, as opposed to the 10 hour duration of the experiment then the efficiencies double.

- The ideal conditions proposed to maximise carbonation within the field trials are to add a limited amount of water (preferably as a warm vapour) and to avoid saturating the pore spaces to allow an even flow of CO_2 around the sample volume. However, this method of carbonation is less efficient and in the short term less effective than allowing the material to passively weather.

Chapter 7:

Acid and Alkali Treatments of Sample Material

7.1 Introduction

In this chapter the effects of reacting acidic and alkaline solutions with the different slag products is considered and the carbonation values achieved after active reaction with CO_2 under such enhanced conditions are reported. The experiments were conducted in order to determine how the pre-treatment of different slag products with either acid (1M HCl) or alkali (1M NaOH) affected the different slag products and whether this, in turn, affected their carbonation potential. It was hypothesised that these reactions could unlock the mineral phases within the slag, thus increasing the concentration of M^{n+} available for carbonation. The experimental reactions with CO_2 were conducted as a factorial experiment using conditions of 25°C / 125°C and 1 MPa / 10 MPa CO_2 pressure.

7.2 Methods

Slag samples were first reacted with 1M HCl or 1M NaOH for either 24, 48 or 72 hours and were then analysed by XRD, TGA and SEM analysis. After further reaction, under varying conditions of CO_2 pressure and temperature the samples were analysed using TGA and SEM methods.

7.2.1 Pre-Treatment Procedure

The samples were prepared by taking a weighed amount (100g of 6 mm steel slag aggregate, 50g of GGBFS, 50 g of Pellite) of sample material, which was then placed into 250 cm^3 stoppered bottles. The samples were then reacted with a pre-prepared 1 mol dm^{-3} solutions of either NaOH or HCl in a ratio of 50 cm^3 / 25g of sample. The bottles were then sealed and vigorously shaken for 30 seconds before the stoppers were released, but not removed, in order to equalise the pressure. The bottles were then placed into an oven at 50˚C and left for 24, 48 or 72 hours to react.

Once the prescribed time period had elapsed, the bottles were removed from the oven and left to cool to room temperature. The supernatant liquid was then decanted off. In order to prevent the NaOH and/or HCl reacting with the stainless-steel reaction chamber or the stainless-steel safety burst pressure disk, the samples were washed thoroughly with distilled water prior to reaction with CO_2 within the chamber. The washing method was to rinse the sample within the reaction bottle with distilled water with a volume 10-times that of the volume of NaOH or HCl used. To wash the samples

100 cm^3 of distilled-water was added, the bottle stoppered and then vigorously shaken for 30 seconds. The liquid was then decanted off. The procedure was repeated and the pH of the solution was noted. Once this procedure had been completed the bottles, with their stoppers removed, were returned to the oven at 50°C and left until they were dry. Once dry, a sub-sample of the material was crushed and ground to <250 µm. It was analysed using XRD analysis. Ground material was also analysed using TGA. Unground samples were also taken and observed under SEM.

7.2.2 XRD

Bulk XRD was undertaken on a number of samples to identify the mineral phases present. Slag samples were crushed using an agate pestle and mortar and sieved though a 125 µm mesh sieve. Powder X-Ray Diffraction (PXRD) data was collected from a sub-sample of the <125 µm powdered sample. Samples were analysed with CuKα1 radiation using a BRUKER D8 ADVANCE X-Ray Diffractometer (XRD) equipped with a BRUKER LYNXEYE Detector within a 10-90 2θ range with a step size of 0.02 over a period of 1 hour in a BB-Slit, V6-incident slit configuration.

All PXRD data was processed using EVA DIFFRAC. The identification of individual phases was achieved using the 'search/match' function of EVA DIFFRAC utilising the main 'slag-forming' elements identified using XRF analysis to narrow the search parameters. The initial phases identified by the computer programme was then observed and any duplicates removed. The remaining matches were then manually checked by comparison of the line spectra with the peak intensity of the possible phase matches.

7.2.3 TGA

Samples of the crushed material were required for TGA analysis. The method of TGA analysis used was identical to that of Chapter 4.2.3.

7.2.4 SEM

SEM images were acquired using either a Hitachi TM-1000 Table-Top SEM with EDS data acquired using an Oxford-Instruments EDS Detector in the Department of Earth Sciences, University of Durham or a Hitachi TM-3000 Table-Top SEM with EDX data acquired using an Oxford-Instruments EDS Detector in the Department of Archaeology, University of Durham.

7.2.5 Batch Reaction Process

After pre-treatment with acid or alkali the samples were reacted under elevated CO_2 pressures and temperatures using the batch equipment apparatus as described in Chapter 5.2.1. The pressure and

temperature conditions for this set of experiments was kept as in Chapter 5.2.2.1 (10 bar CO_2 or 100 bar CO_2 pressure) and Chapter 5.2.2.2 (25°C or 125 °C) respectively, as was the 19 hour reaction time Chapter 5.2.2.4. Unlike Chapter 5 the water availability was kept in excess and this was based on the conclusion, in Chapter 5, that the materials in this study (6 mm aggregate slag, Pellite and GBFS) responded better to carbonation under such conditions of high water availability.

7.2 Results

The slag products used were characterised after the initial chemical treatments and again after batch reaction under enhanced temperatures and CO_2 pressure. The results of these investigations are reported below.

7.3.1 Results of pre-treatments

An initial study was undertaken by adding 1M NaOH or 1M HCl to 50g of different slag products. The observed results are shown in Table 7.1.

Chemical Treatment	**NaOH**		**HCl**	
Reactant	t=0	t=7hr @55°C	t=0	t=7hr @55°C
San Carlos Peridotite	No immediate reaction	No clear difference, clear supernatant	No immediate reaction	No clear difference, green supernatant
Wollastonite	No immediate reaction	Clear supernatant, no obvious change	Immediate effervescence of gas (CO_2)	Possible viscous, gelatinous substance had formed
6mm Steel Slag	No immediate reaction	Clear supernatant with a film on top. Fine grained white/cream precipitate on top of slag	Strong sulphurous smell immediately given off	Clear supernatant with a film on top. Fine grained white/cream precipitate on top of slag

Table 7.1: Initial observations of the reaction of different slag products after the addition of 1M NaOH or 1M HCl, and further observation after 7 hours of reaction.

Further observations were taken after the materials had been reacting for 1 month:

- Alkali: After one month of reacting slag with the alkali solution the supernatant liquid was clear and there was a fine grained white/cream precipitate on top of the slag.
- Acid: After one month of reacting slag with the acidic solution the supernatant was red (Fe^{3+} rich) and there was a red precipitate on top of the slag.

7.3.1.1 Changes in Material Texture and Colour

Reaction of the different slag products with 1M NaOH or 1M HCl produced several changes to the slag material and/or the supernatant liquid over the 72 hours reaction time. These changes are outlined in Table 7.2.

Material	Acid Treatment	Alkali Treatment
6mm Steel Slag	The slag had turned a 'rust' coloured red-brown. The supernatant has turned green.	The slag had developed a white/cream precipitate. The supernatant was clear.
Pellite	The slag had turned black, the supernatant was clear.	The slag had developed a white/cream precipitate, the supernatant was clear.
GBFS	The slag had turned black, the supernatant was clear.	The slag had developed a white/cream precipitate the supernatant was clear.

Table 7.2: Changes in material texture and colour due to treatment with acid or alkali solution.

7.3.1.2 XRD Analysis

Fig. 7.1 shows the differences between untreated and acid-treated 6 mm steel slag aggregate. The differences in the peaks show that there was little to no change in the mineralogy of the sample over the 72 hours reaction time.

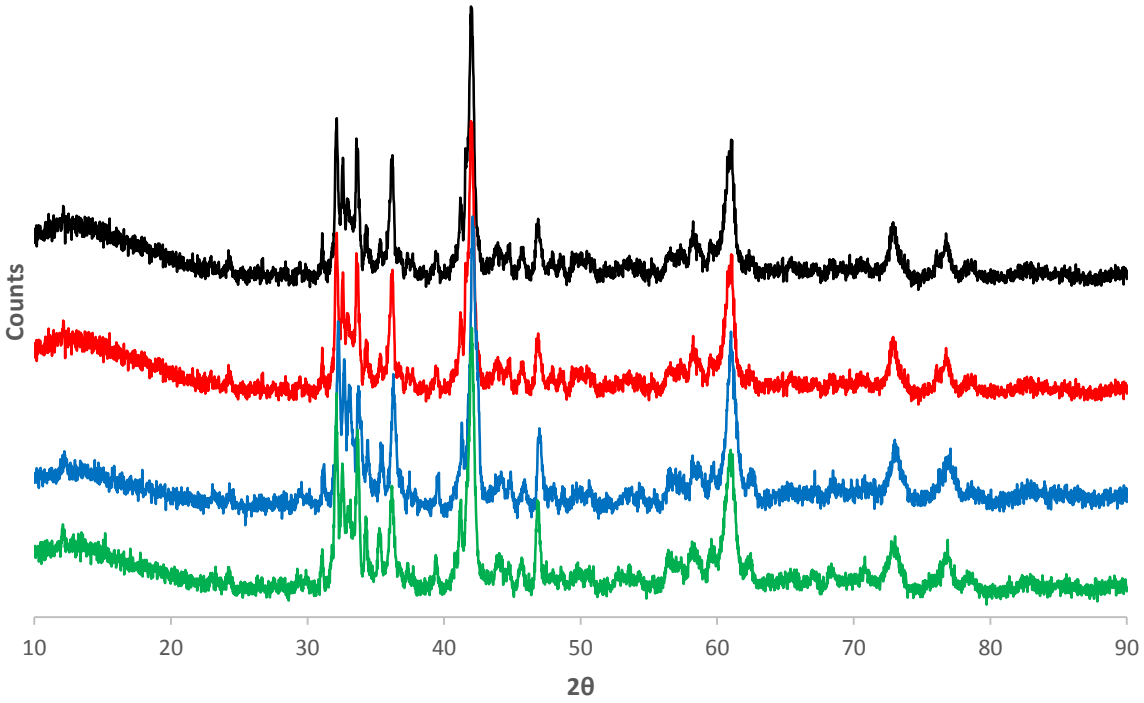

Figure 7.1: XRD traces for 6mm aggregate steel slag. Fresh sample (Black), samples reacted with 1M HCl for 24 hours (Red Trace), 48-hours (Blue Trace), 72-hours (Green Trace). The spectra have been offset for clarity.

Fig. 7.2 shows the differences between untreated and alkali-treated 6 mm steel slag aggregate. The differences in the peaks show that there was little to no change in the mineralogy of the sample over the 72 hours reaction time.

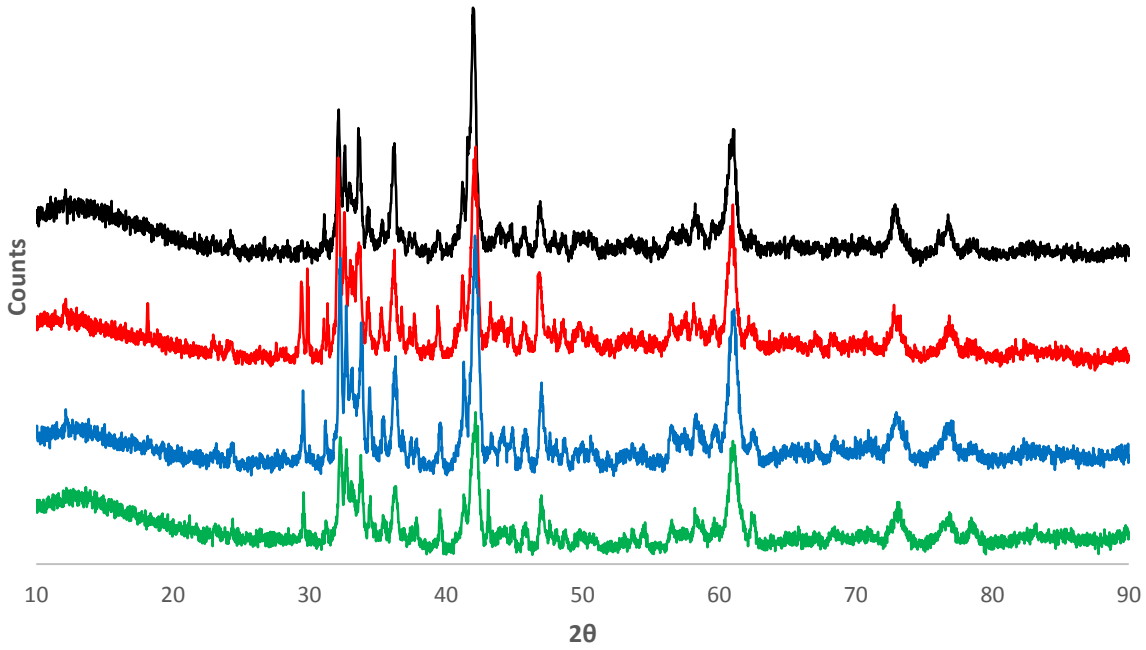

Figure 7.2: XRD traces for 6mm aggregate steel slag. Fresh sample (Black), samples reacted with 1M NaOH for 24 hours (Red Trace), 48-hours (Blue Trace), 72-hours (Green Trace). The spectra have been offset for clarity.

Pellite

Fig. 7.3 shows the differences between untreated and acid-treated Pellite. The differences in the peaks show that several crystalline minerals had been dissolved by the 1 M HCl solution leaving a glassy material with only one or two crystalline minerals present. Within 24 hours the majority of the crystalline materials had reacted into the solution and there was little change in mineralogy between 24 and 72 hours of reaction time.

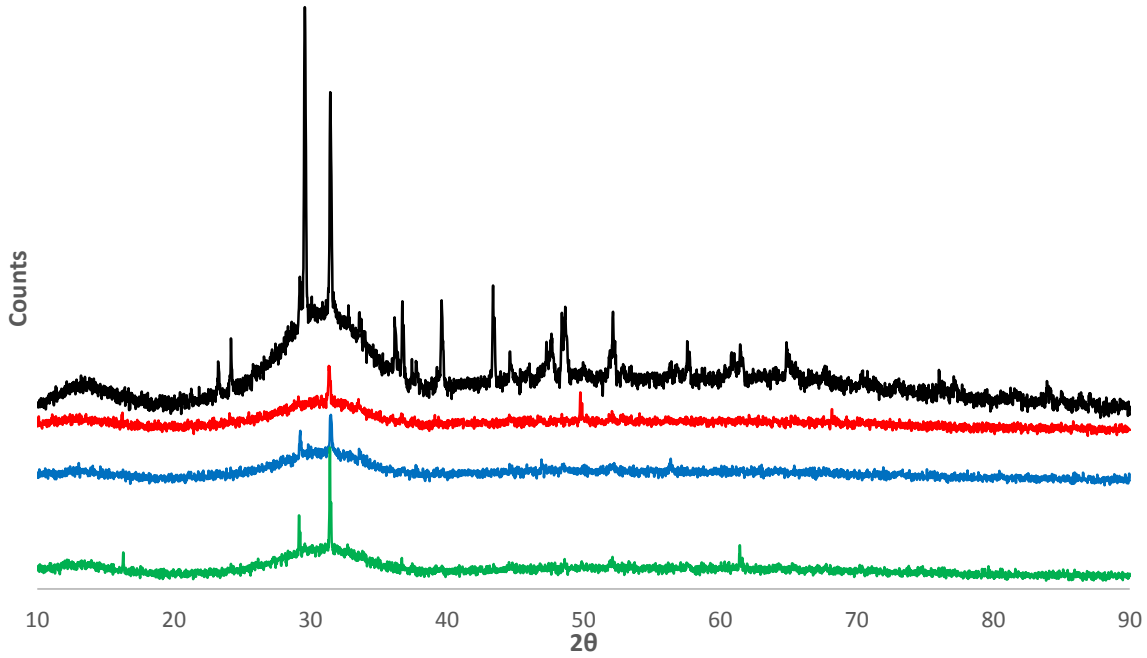

Figure 7.3: XRD traces for Pellite. Fresh sample (Black), samples reacted with 1M HCl for 24 hours (Red Trace), 48-hours (Blue Trace), 72-hours (Green Trace). The spectra have been offset for clarity.

Fig. 7.4 shows the differences between untreated and alkali-treated Pellite. The differences in the peaks show that there had been little change in the mineralogy of the samples over the reaction period of 72 hours with only minor evidence of reaction present.

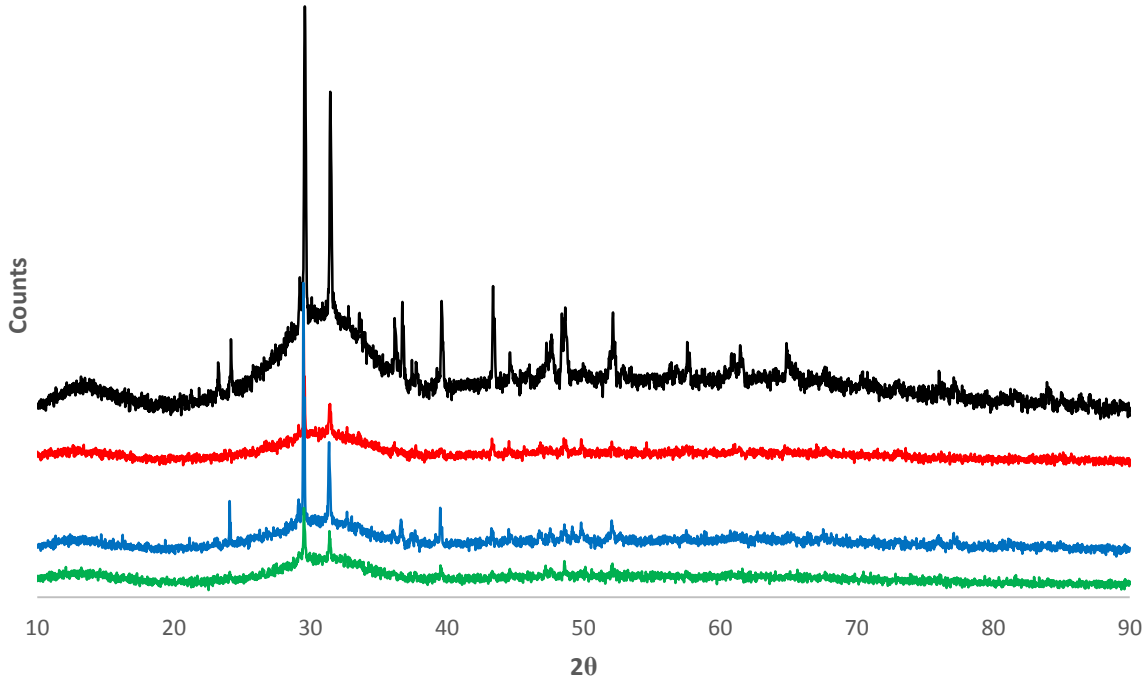

Figure 7.4: XRD traces for Pellite. Fresh sample (Black), samples reacted with 1M NaOH for 24 hours (Red Trace), 48-hours (Blue Trace), 72-hours (Green Trace). The spectra have been offset for clarity.

Granulated Blast Furnace Slag

Fig. 7.5 shows the differences between untreated and acid-treated GBFS. The differences in the peaks show that all the crystalline minerals had been dissolved by the 1 M HCl solution with only a glassy material remaining. Within 24 hours the majority of the crystalline materials had reacted into the solution with little change to the mineralogy between 24 and 72 hours of reaction time or the pH equilibrated pH.

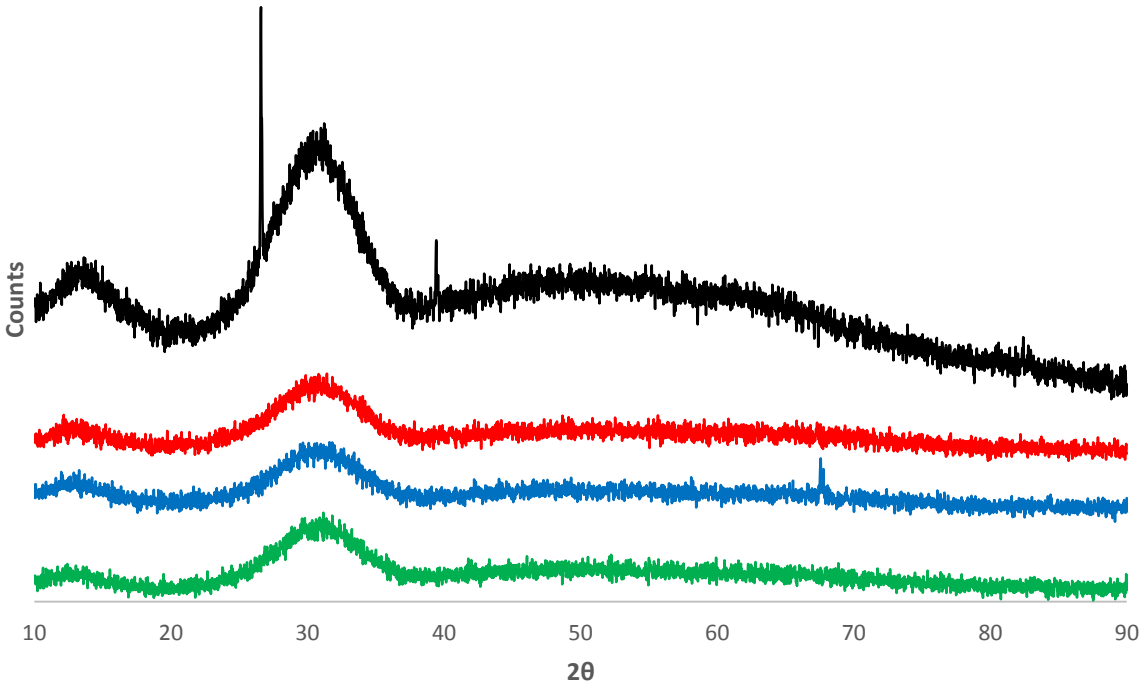

Figure 7.5: XRD traces for Granulated Blast Furnace Slag. Fresh sample (Black), samples reacted with 1M HCl for 24 hours (Red Trace), 48-hours (Blue Trace), 72-hours (Green Trace). The spectra have been offset for clarity.

Fig 7.6 shows the differences between untreated and alkali-treated GBFS. The differences in the peaks show that there had been little change in the mineralogy of the samples with only minor evidence of reaction present. There appeared to be little change in the mineralogy of the samples over the reaction period of 72 hours with only the possible precipitation of a new mineral at 29.5 2θ-angle.

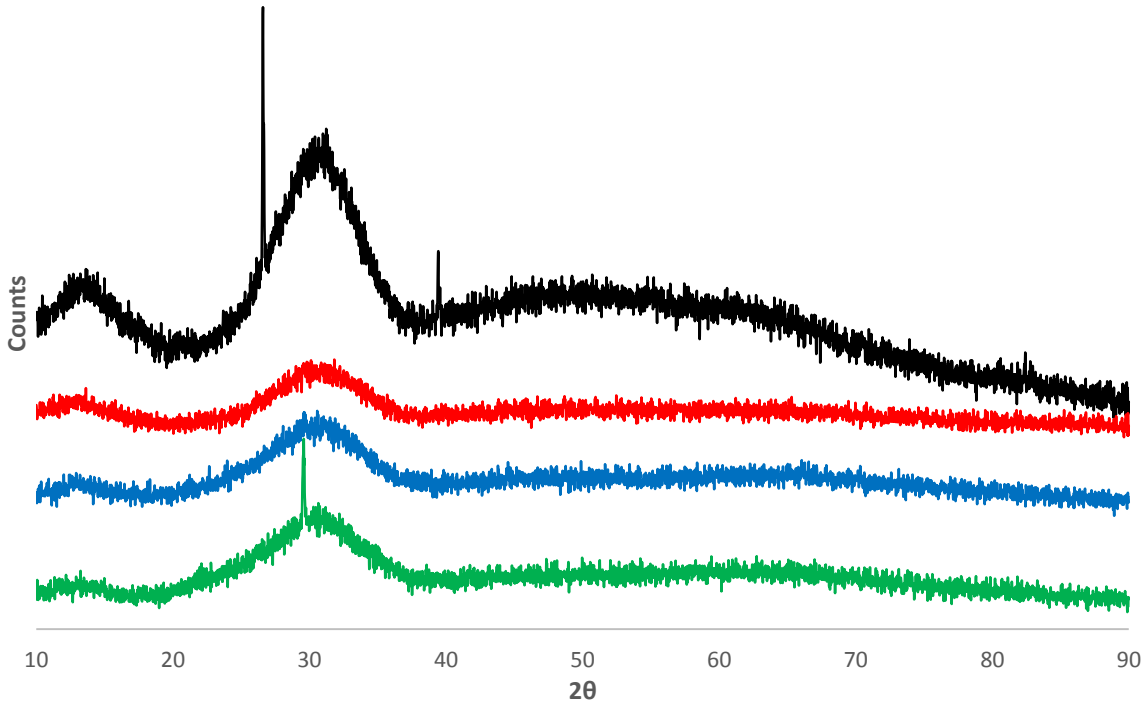

Figure 7.6: XRD traces for Granulated Blast Furnace Slag. Fresh sample (Black), samples reacted with 1M NaOH for 24 hours (Red Trace), 48-hours (Blue Trace), 72-hours (Green Trace). The spectra have been offset for clarity.

7.3.1.3 TGA

The TGA analysis of all of the slag samples reacted in 1M HCl for 24, 48 or 72 hours displayed no carbonate breakdown signal. Therefore, any carbonate generated during the subsequent batch reaction experiments was freshly formed under the conditions present within the reaction fluid.

The TGA analysis of the slag samples reacted in 1M NaOH for 24, 48 or 72 hours displayed minor amounts of carbonate. 6 mm steel slag aggregate displayed 0.11 wt. % to 0.12 wt. % carbonate after 24 hours, dropping to 0.02 wt. % to 0.05 wt. % after 72 hours. Pellite displayed 0.35 wt. % carbonate after 24 hours, 0.48 wt. % after 48 hours and 0.58 wt. % after 72 hours. GBFS displayed 0.02 wt. % carbonate up to 48 hours and 0.00 wt. % after 72 hours.

7.3.1.4 SEM

Backscatter SEM was using to observe the surface textures produced after reaction with either 1M HCl or 1M NaOH after 24, 48 and 72 hours. These textures are described below:

6 mm Steel Slag Aggregate – *Figure 7.7*

After 24 hours of reaction in 1M HCl, the surface of the 6 mm steel slag aggregate displayed etching and a 'ragged texture. From 24 hours to 72 hours this texture appeared to remain unchanged suggesting that the dissolution of the surface may have ceased.

After 24 hours of reaction in 1M NaOH the surface of the 6mm steel slag aggregate showed a possible mineral growth of fine 'bobbled' crystals upon the surface, probably caused by the increased pH leading to precipitation of hydroxides. After 48 to 72 hours the layer had thickened and µm-scale crystallites had formed.

Pellite – *Figure 7.8*

After 24 hours of reaction in 1M HCl the surface of the Pellite was smooth and appeared free of crystals and <10 µm dust grains could be seen. Between 24 to 72 hours the surface of the Pellite continued to etch, developed cracks and began to disintegrate.

After 24 hours of reaction in 1M NaOH the surface of the Pellite showed a 'speckled' surface with crystals growing upon the previously smooth surface. Between 24 and 72 hours these crystals continued to grow. However, individual grains displayed different degrees of crystal coverage.

GBFS – *Figure 7.9*

After 24 hours of reaction in 1M HCl the surface of the GBFS was cracked and observably etched, with glassy surfaces clear of crystals. From 24 hours to 72 hours the surface developed further cracks and fine fragments of disaggregated surface accumulated, particularly within vesicles.

After 24 hours of reaction in 1M NaOH the surface of the GBFS had developed a face-raised cube shaped mineral, otherwise the surface was clean. Between 24 and 72 hours the cubic minerals enlarged and the surface became 'speckled' with µm-scale crystals.

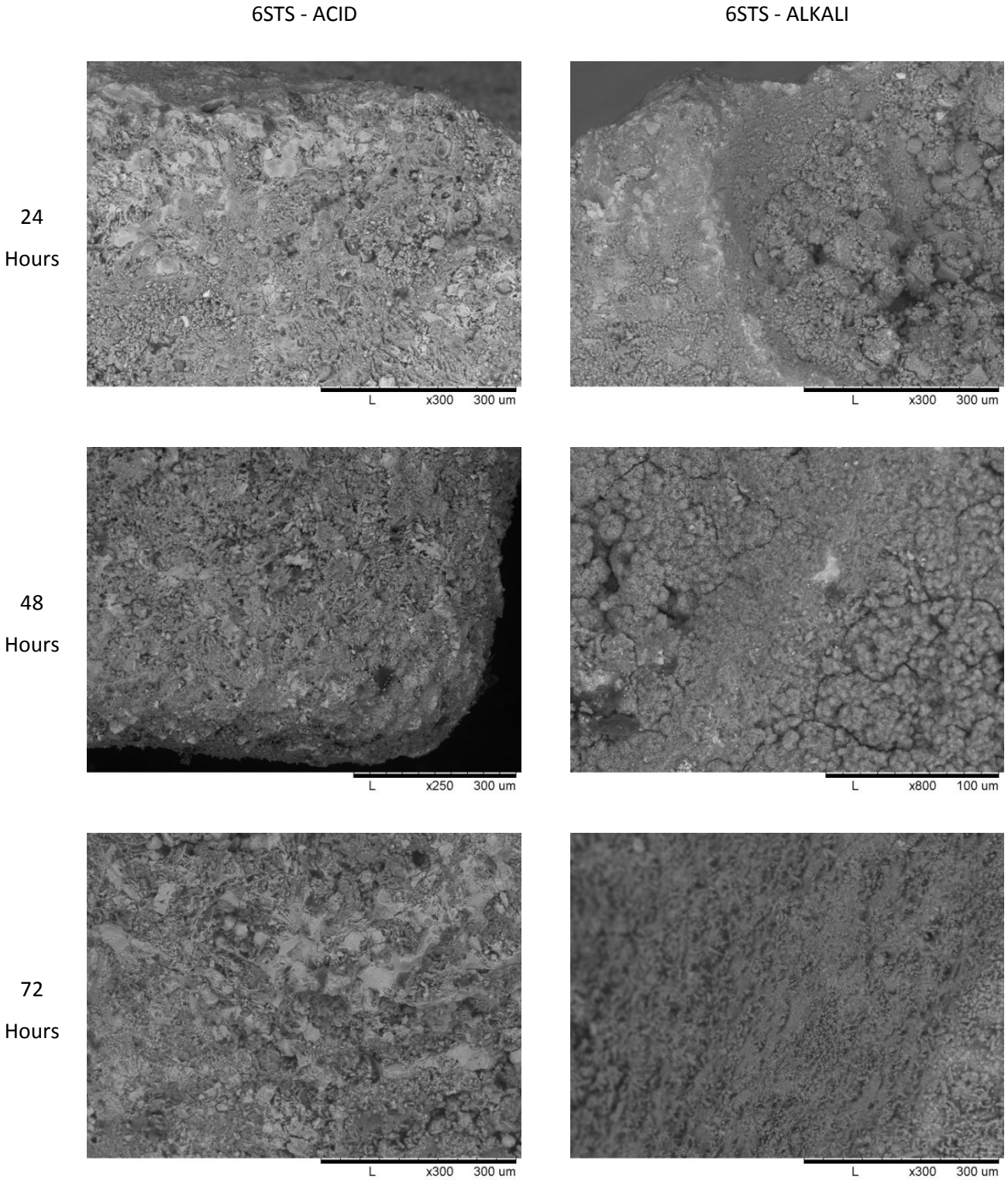

Figure 7.7: Backscatter SEM images of 6mm steel slag aggregate reacted for 24, 48 and 72 hours in either 1M HCl solution or 1M NaOH solution.

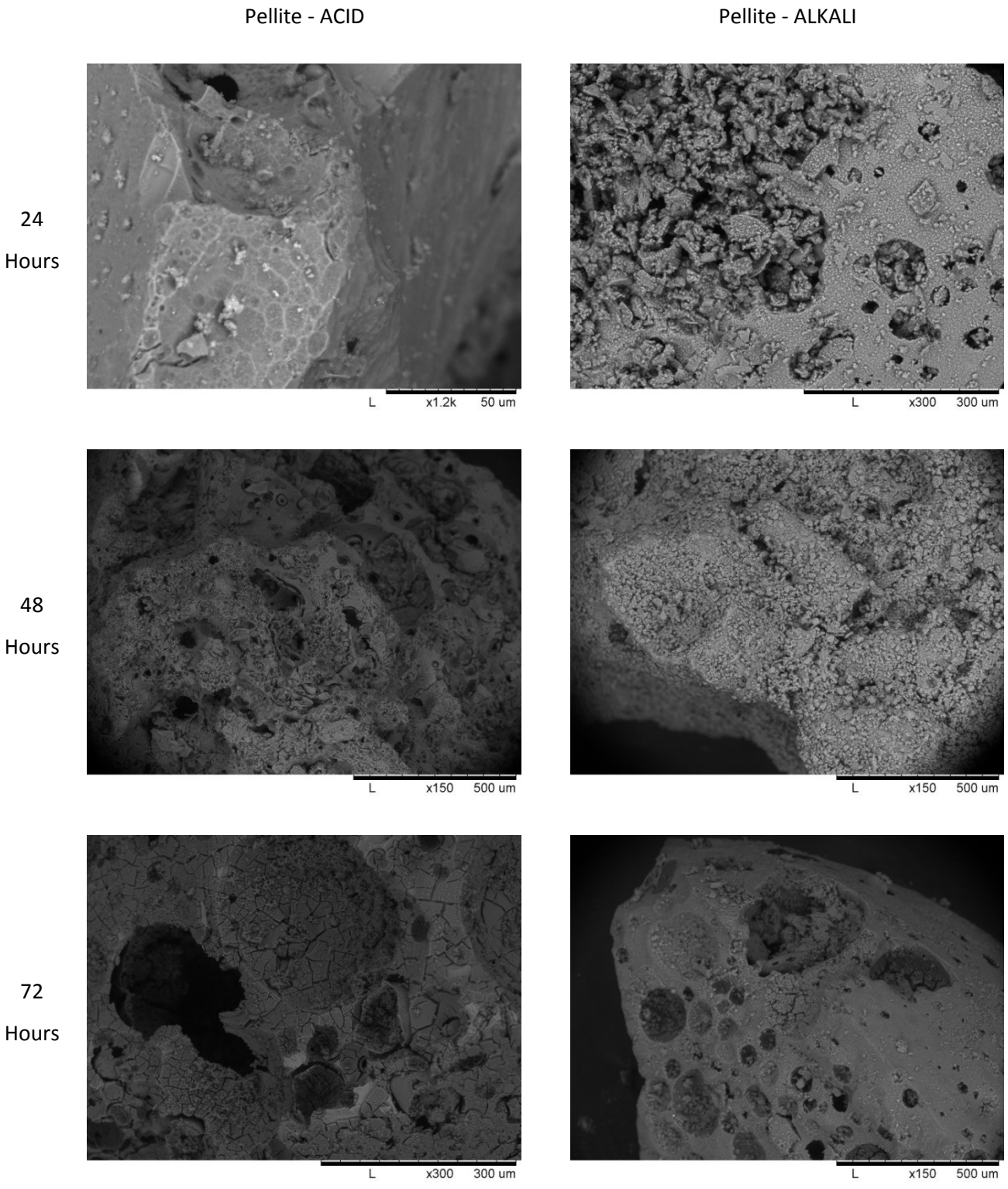

Figure 7.8: Backscatter SEM images of Pellite reacted for 24, 48 and 72 hours in either 1M HCl solution or 1M NaOH solution.

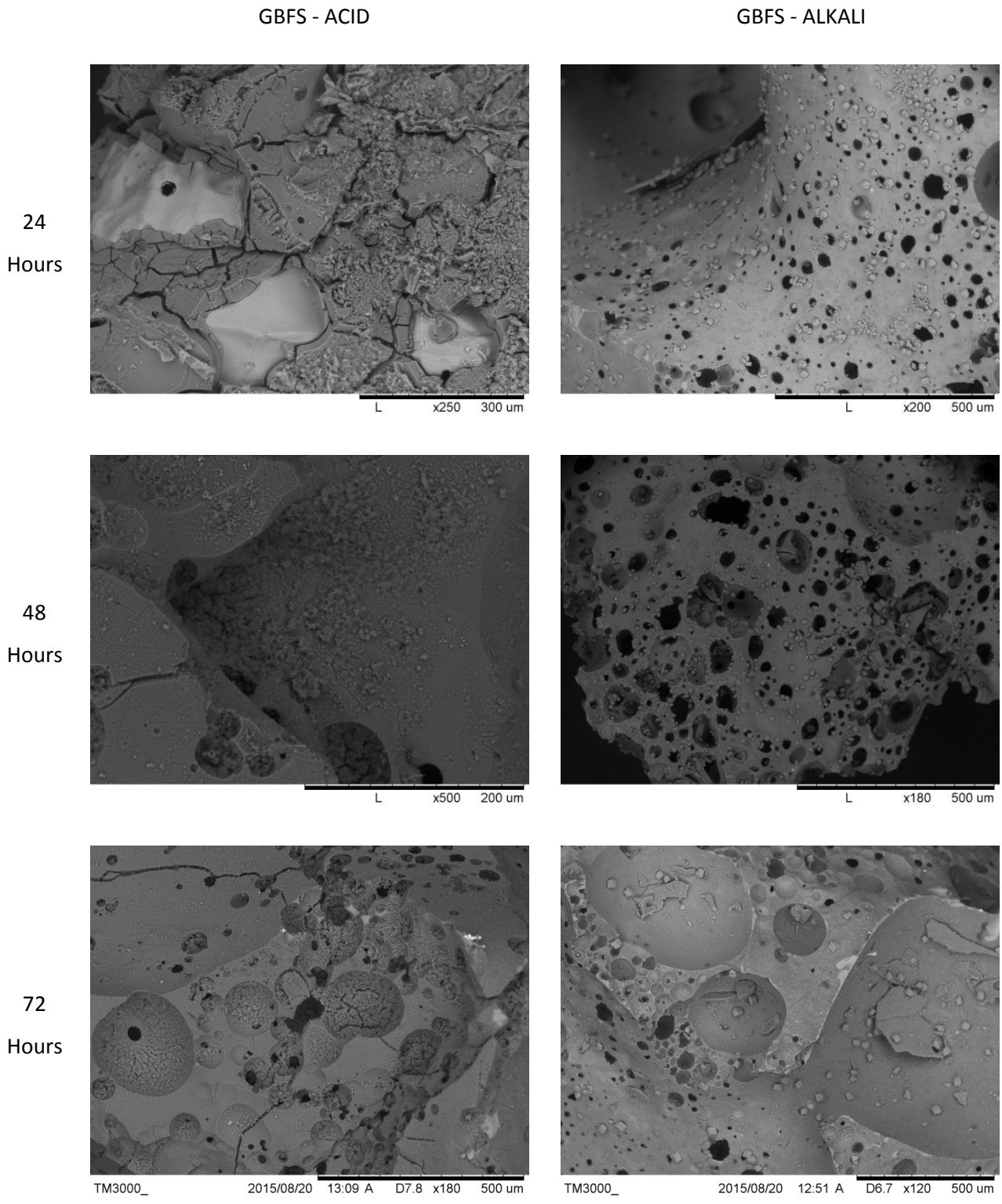

Figure 7.9: Backscatter SEM images of GBFS reacted for 24, 48 and 72 hours in either 1M HCl solution or 1M NaOH solution.

7.3.2 Post-Reaction Results

7.3.2.1 TGA

The wt. % carbonation results from the batch experiments for the different slag products are displayed in Table 7.3. All samples were run in duplicate and followed the TGA method outlined in Chapter 4.2.2.

	Average Values (Wt. %)					
Expt. Conditions	6 mm		Pellite		GBFS	
Highest Batch	HHH	2.783	HHH	1.662	HHH	0.350
	ACID	ALKALI	ACID	ALKALI	ACID	ALKALI
LpLtHs	0.000	0.007	0.002	0.703	0.005	0.079
LpHtHs	0.066	0.584	0.032	0.890	0.008	0.292
HpLtHs	0.094	0.666	0.038	0.369	0.019	0.030
HpHtHs	1.046	0.712	0.138	2.043	0.029	0.440

Table 7.3: The values for, and conditions of the highest untreated batch samples and average wt. % carbonation results for each treated experimental run. (Lp – 10 Bar, Hp - 100 Bar, Lt - 25°C, Ht - 125°C, Hs – HIGH water availability)

6 mm aggregate

Acid - The results from the batch reaction of acid treated 6 mm steel slag aggregate (Fig. 7.10) ranged from 0.0 wt. % to 1.52 wt. %, or 0 to 0.55 times that of the highest average untreated batch-reacted carbonation value. The highest average carbonation of any experimental run was 1.05 wt. % and was produced at conditions of 100 bar/125°C/HIGH water availability (HpHtHs). The data showed a trend of low average carbonation values with a strong preference for high pressure and high temperature conditions.

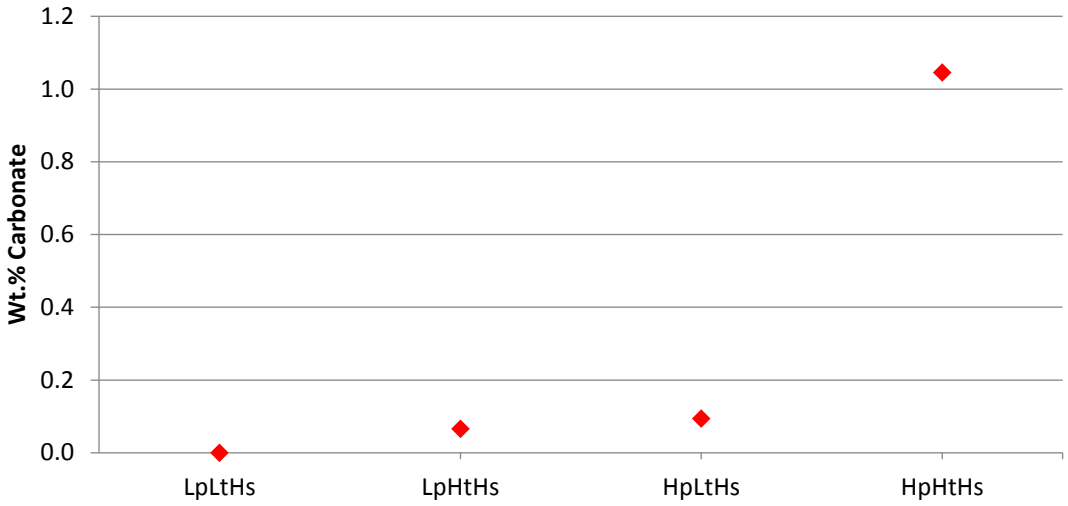

Figure 7.10: Graph showing the carbonation values achieved for 6 mm aggregate slag treated with 1M HCl under the active reaction conditions.

Alkali - The results from the batch reaction of 6 mm steel slag aggregate which was treated with alkali (Fig. 7.11) ranged from 0.0 wt. % to 1.33 wt. % or 0 to 0.48 times that of the highest average untreated batch-reacted carbonation value. The highest average carbonation of any experimental run was 0.712 wt. % produced at conditions of 100 bar/125°C/HIGH water availability (HpHtHs). The data showed a trend of relatively consistent carbonation values once the pressure / temperature conditions were greater than 10 bar/25°C.

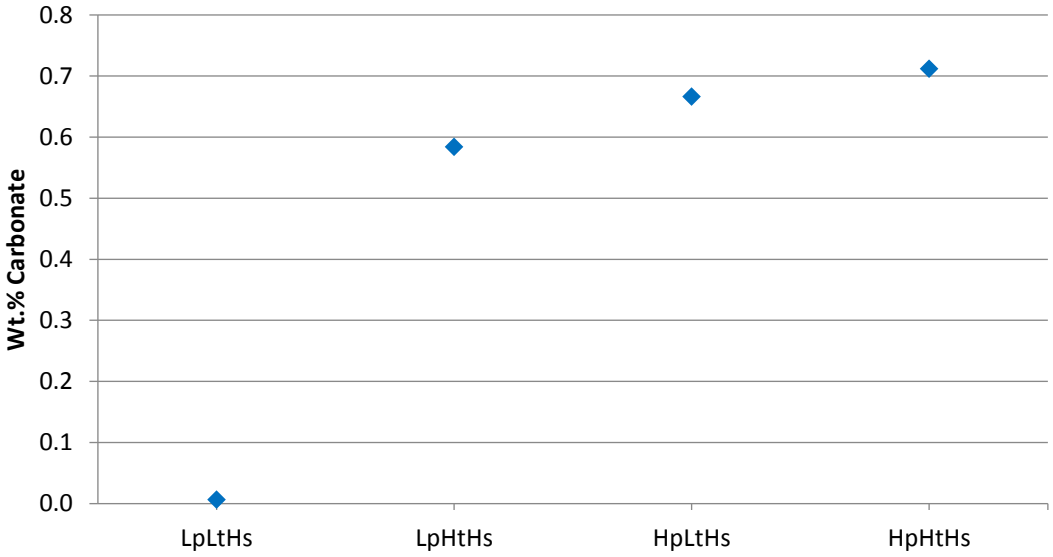

Figure 7.11: Graph showing the carbonation values achieved for 6 mm aggregate slag treated with 1M NaOH under the active reaction conditions.

Pellite

Acid - The results from the sample of Pellite, which was pre-treated with 1M HCl (Fig. 7.12) ranged from 0.00 wt. % to 0.14 wt. %, or 0 to 0.085 times that of the highest average value for untreated batch-reacted carbonation. The highest average carbonation value for any experimental run was 0.138 wt. % which was produced at conditions of 100 bar/125°C/HIGH water availability (HpHtHs). The data showed a trend towards higher carbonation values with higher pressures and particularly higher temperatures.

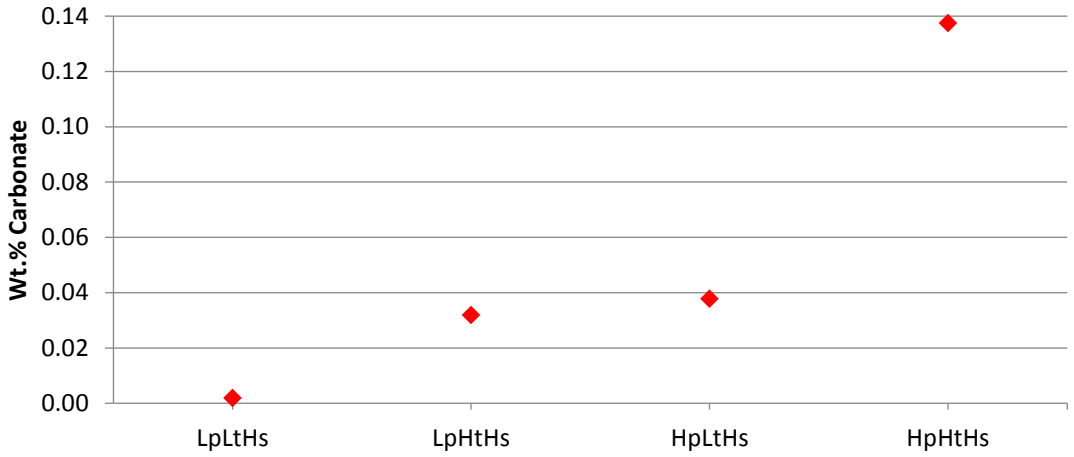

Figure 7.12: Graph showing the carbonation values achieved for granular Pellite treated with 1M HCl under the active reaction conditions.

Alkali - The results from the sample of Pellite, which was pre-treated with 1M NaOH (Fig. 7.13), ranged from 0.341 wt. % to 2.167 wt. %, or 0.21 to 1.3 times that of the highest average untreated batch-reacted carbonation value. The highest average carbonation value for any experimental run was 2.043 wt. % which was produced under conditions of 100 bar/125°C/HIGH water availability (HpHtHs). The data showed a trend towards increasing carbonation with increasing temperature.

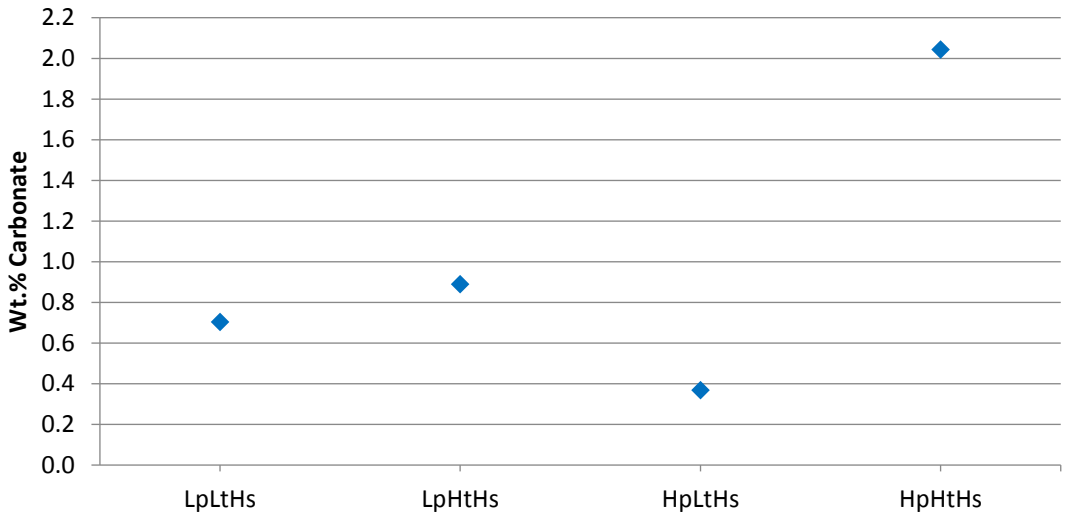

Figure 7.13: Graph showing the carbonation values achieved for granular Pellite treated with 1M NaOH under the active reaction conditions.

GBFS

Acid - The results from the sample of GBFS, which was pre-treated with 1M HCl (Fig. 7.14) ranged from 0.00 wt. % to 0.032 wt. %, or 0 to 0.091 times that of the highest average untreated batch-reacted carbonation value. The highest average carbonation value for any experimental run was 0.029 wt. % and was produced under conditions of 100 bar/125°C/HIGH water availability (HpHtHs). The data showed a trend towards higher carbonation values with higher pressures and particularly higher temperatures.

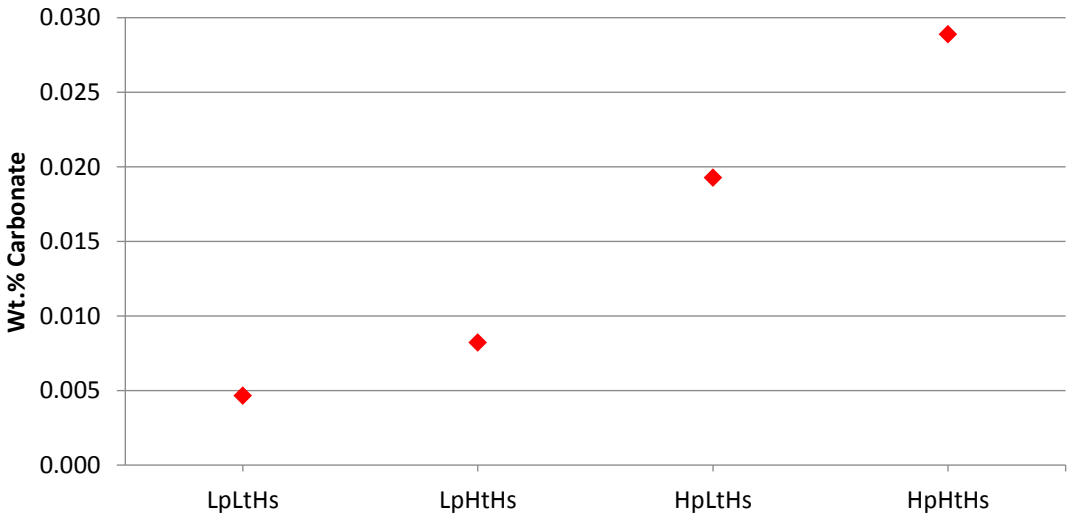

Figure 7.14: Graph showing the carbonation values achieved for granular GBFS treated with 1M HCl under the active reaction conditions.

Alkali - The results from the sample of GBFS, which was pre-treated with 1M NaOH (Fig. 7.15) ranged from 0.025 wt. % to 0.446 wt. %, or 0.0714 to 1.276 times that of the highest average untreated batch-reacted carbonation value. The highest average carbonation value for any experimental run was 0.44 wt. % which was produced under conditions of 100 bar/125°C/HIGH water availability (HpHtHs). The data showed a trend towards increasing carbonation with increasing temperature.

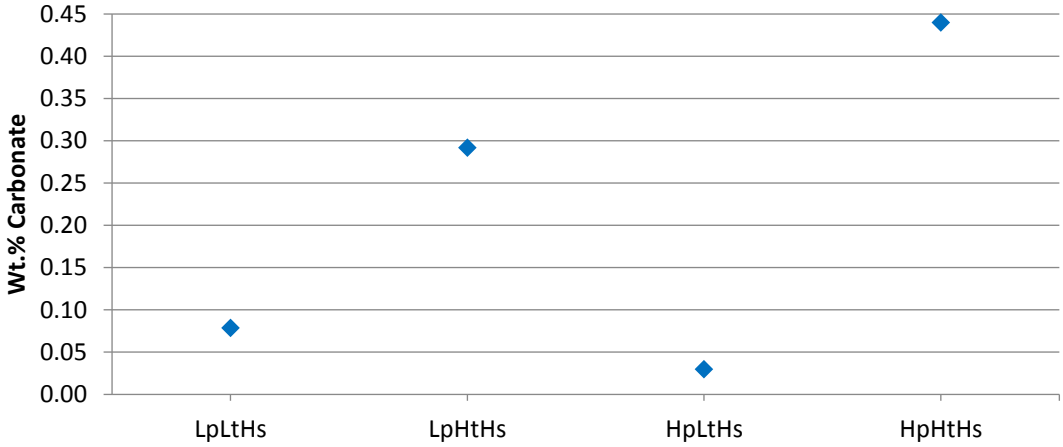

Figure 7.15: Graph showing the carbonation values achieved for granular GBFS treated with 1M NaOH under the active reaction conditions.

7.3.2.2 SEM Observation of Surface Textures

Backscatter SEM was used to observe the surface textures produced after active reaction with CO_2 under enhanced conditions. These textures are described below.

6mm Steel Slag Aggregate

Low Pressure - Low Temperature (10bar / 25°C)

Experiments carried out at low pressure (10 bar) and low temperature (25˚C) generated different surface textures and coverage depending upon the pre-treatment chemical. However, a similar 'fan'-like carbonate growth morphology was present on the surfaces of the grains (Fig. 7.16). Acid treated aggregate displayed a low surface coverage of carbonate minerals, with their growth restricted to 'patches' of up to 100 µm long and 50 µm wide. Alkali treated aggregate displayed a widespread surface coverage of carbonate minerals, which demonstrated one of two morphologies; either a 'bobbled' surface covering of very-fine carbonate or widespread areas of 'fan' morphology carbonate up to 50 µm long and 25 µm wide.

6STS – ACID - LLH

6STS – ALKALI - LLH

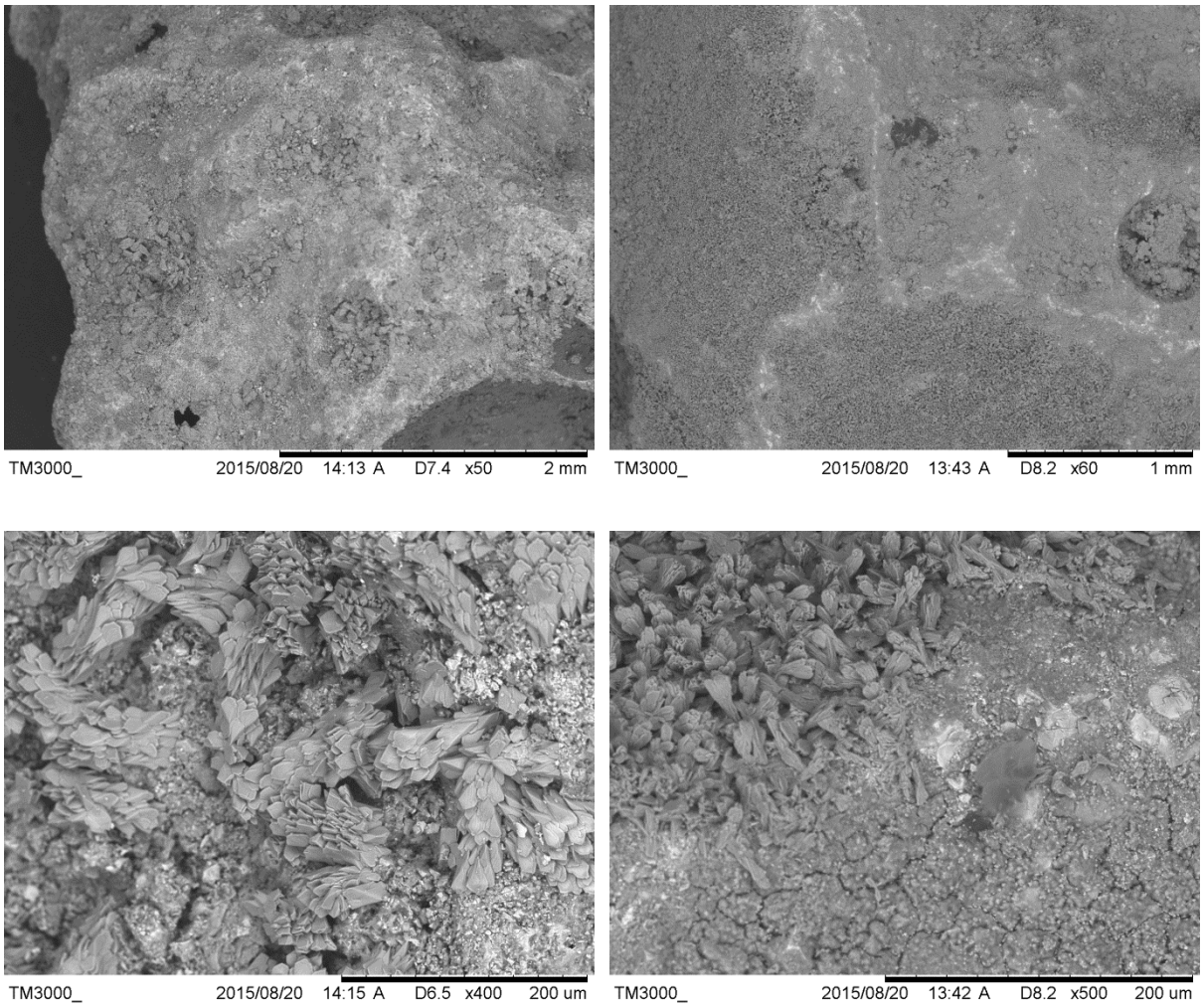

Figure 7.16: Backscatter SEM images of 6mm steel slag aggregate pre-treated with acid or alkali solution and reacted under 10bar CO_2 pressure at 25˚C

Low Pressure - High Temperature (10bar / 125°C)

Experiments carried out at low pressure (10 bar) and high temperature (125˚C) generated very different surface textures depending on the pre-treatment chemical used (Fig. 7.17).

Acid treated aggregate displayed a low surface coverage of coarse-grained, carbonate minerals with the crystals taking an observable monoclinic form, but with very poorly defined crystal faces. The crystals were approximately 400 µm long and up to 200 µm wide.

Alkali treated aggregate displayed a widespread surface coverage of carbonate minerals. Minerals showed clear crystals faces with observable triads-axes. The crystals were up to 40 µm long and 20 µm wide.

6STS – ACID - LHH

6STS – ALKALI - LHH

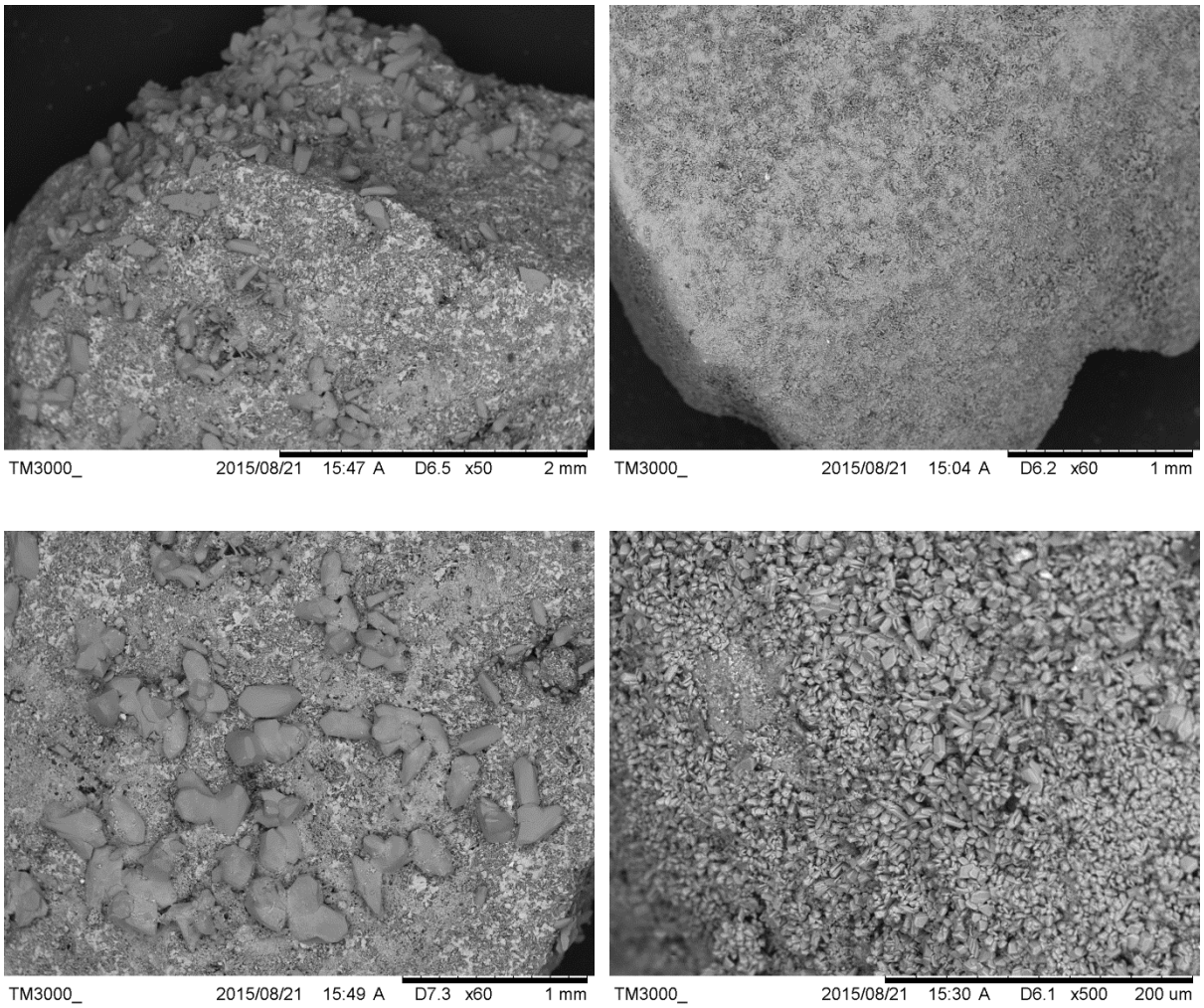

Figure 7.17:Backscatter SEM images of 6 mm steel slag aggregate pre-treated with acid or alkali solution and reacted under 10 bar CO_2 pressure at 125˚C.

High Pressure - Low Temperature (100 bar / 25°C)

Experiments carried out at high pressure (100 bar) and low temperature (25˚C) both generated similar 'flower' textures comprising of very fine grained crystals radiating from a nucleation point and growing out into the reaction fluid (Fig. 7.18).

Acid treated aggregate samples displayed a widespread surface coverage of carbonate minerals which showed 'spiky' flatter textured, carbonate growths up to 30 µm long and between 10 µm to 30 µm wide.

Alkali treated aggregate samples displayed a widespread coverage of carbonate minerals. These showed rounded pinnacoids and were approximately 10 µm in dimension.

6STS – ACID - HLH

6STS – ALKALI - HLH

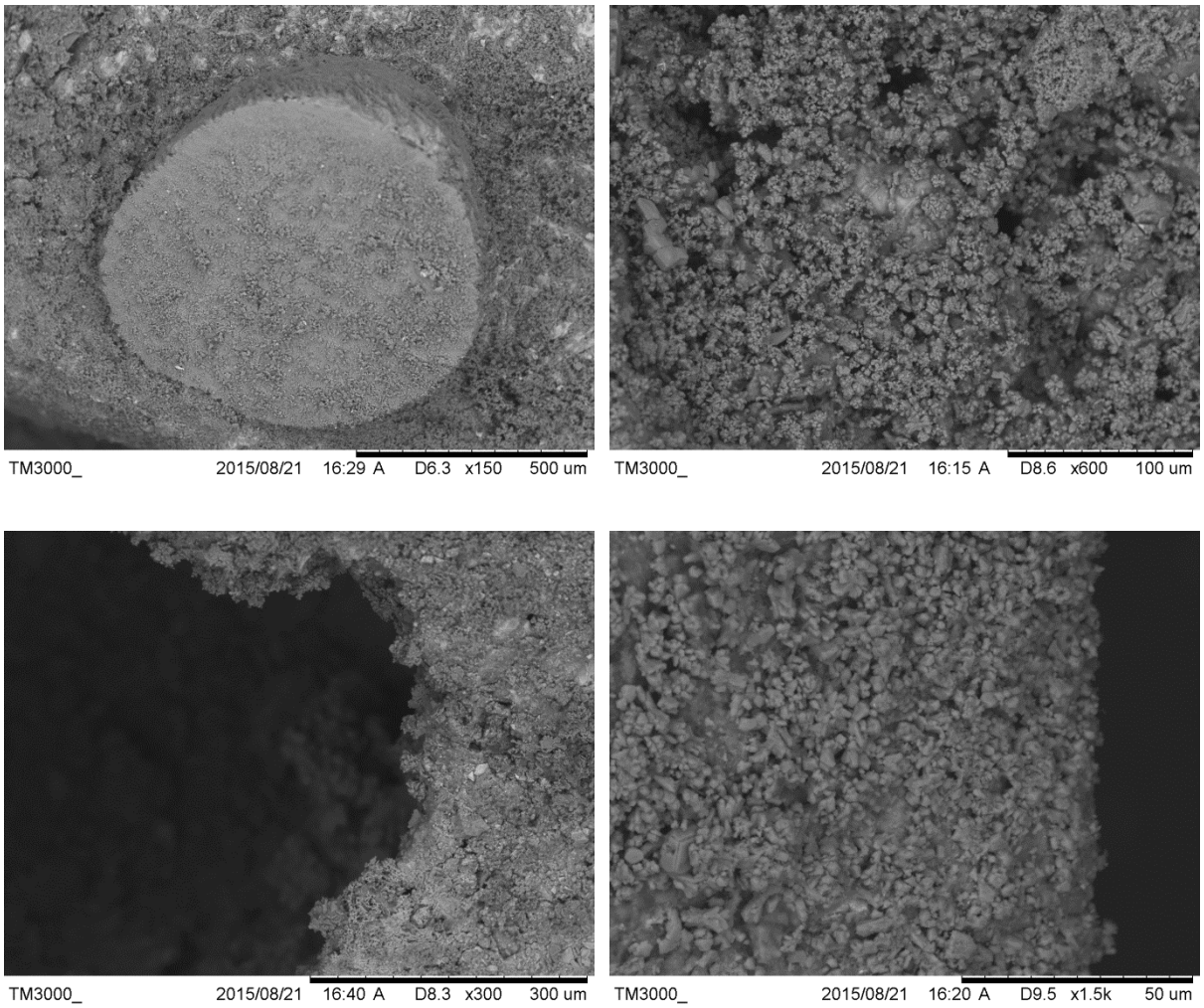

Figure 7.18:Backscatter SEM images of 6 mm steel slag aggregate pre-treated with acid or alkali solution and reacted under 100 bar CO_2 pressure at 25˚C

High Pressure -High Temperature (100 bar /125°C)

Experiments carried out at high pressure (100 bar) and high temperature (125˚C) both generated essentially similar 'rose bud' surface textures, which differed in size depending upon the pre-treatment chemical used (Fig. 7.19). Acid treated aggregate samples displayed a relatively wide surface coverage of carbonate crystals, but these radiated from only a few initial nucleation sites. On these samples the crystals had nucleated and then grown laterally to result in a wider coverage than could be achieved by nucleation alone. The 'mats' of 'rose bud' crystals were up to 350 µm in width and up to 300 µm in height. Alkali treated samples displayed wide surface coverage, carbonate crystals from many nucleation sites. These samples displayed surfaces with 'rose bud' growths approximately 200 µm in diameter and 30 µm in height, surrounded by smaller 'mats' of bladed crystals.

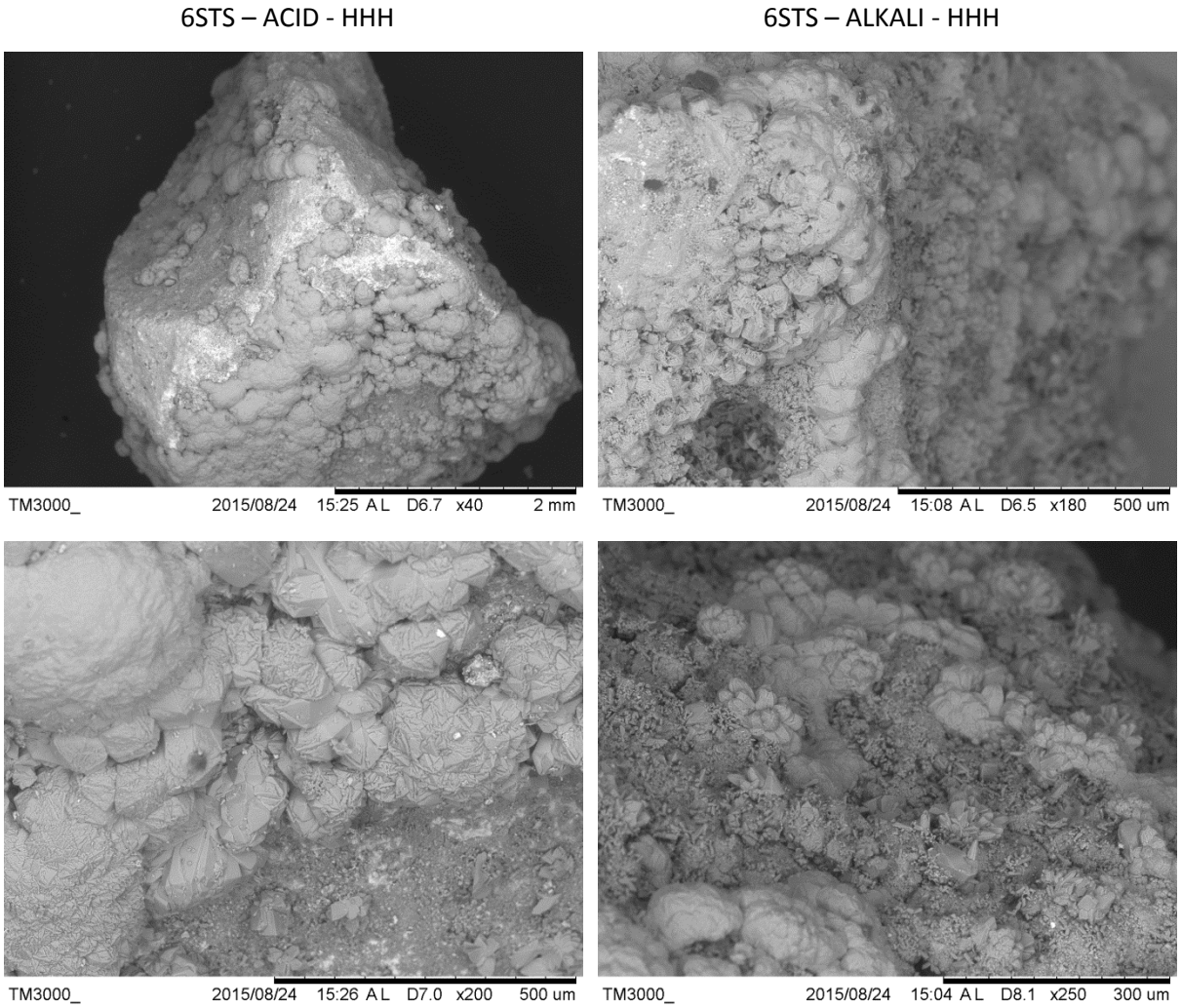

Figure 7.19:Backscatter SEM images of 6 mm steel slag aggregate pre-treated with acid or alkali solution and reacted under 100 bar CO_2 pressure at 125˚C.

Pellite

Low Pressure - Low Temperature (10 bar / 25°C)

Experiments carried out at low pressure (10 bar) and low temperature (25˚C) generated only sparse carbonate growth on both the acid or alkali treated samples (Fig. 7.20). Acid treated samples displayed no discernible difference when compared to unreacted acid-treated material and there appeared to be no distinct growth of carbonate minerals. Alkali treated Pellite displayed a 'granular' carbonate texture of fine grained crystals <20 µm in size.

Pellite – ACID - LLH

Pellite – ALKALI - LLH

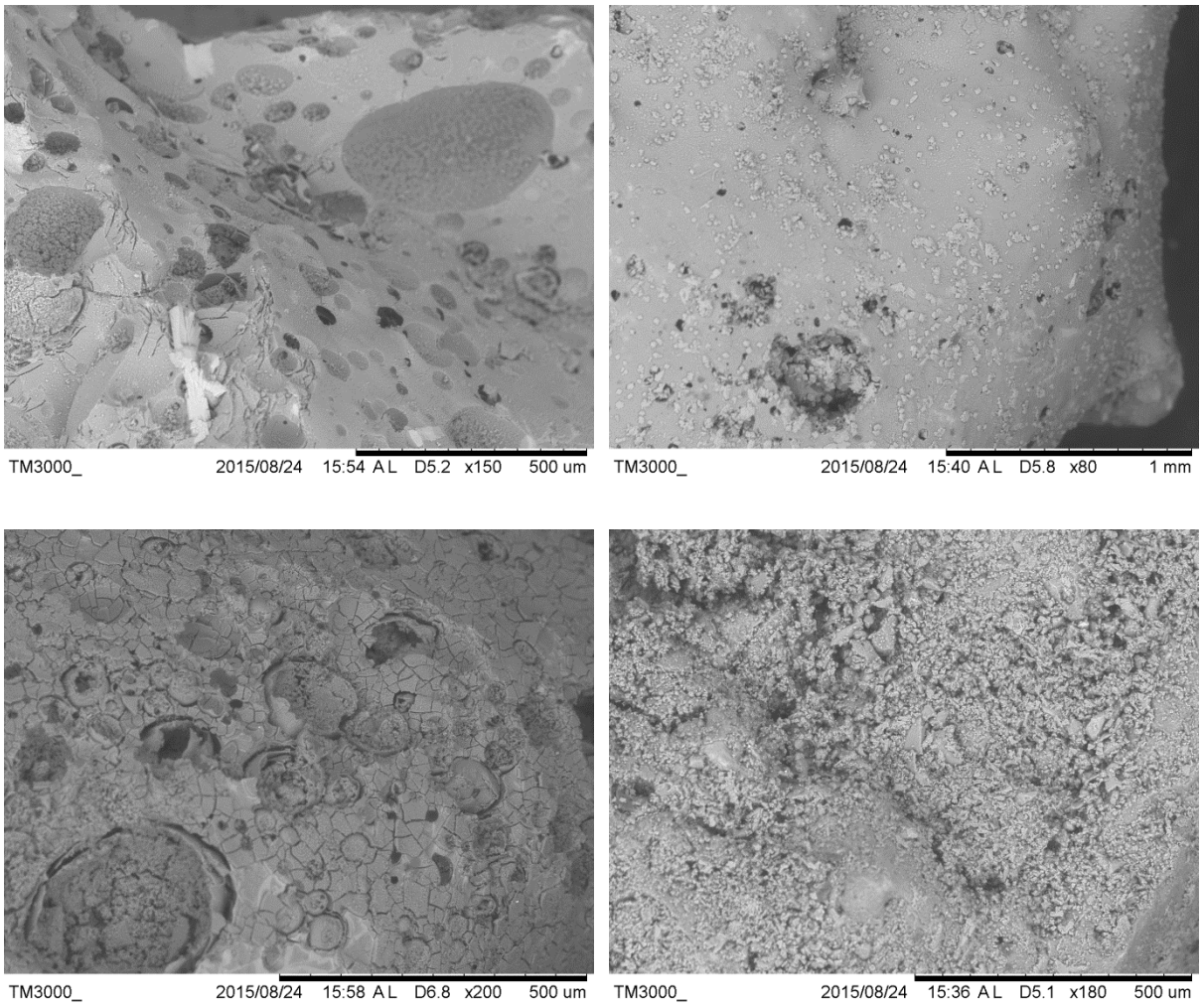

Figure 7.20: Backscatter SEM images of Pellite pre-treated with acid or alkali solution and reacted under 10 bar CO_2 pressure at 25˚C.

Low Pressure - High Temperature (10 bar / 125°C)

Experiments carried out at low pressure (10 bar) and high temperature (125˚C) generated different surface textures and coverage depending upon the pre-treatment chemical (Fig. 7.21).

Acid treated Pellite samples displayed no discernible difference when compared to unreacted acid-treated material and there appeared to be no distinct growth of carbonate minerals.

Alkali treated Pellite displayed relatively sparse carbonate coverage. The carbonates present were in the form of 'nodular' carbonate growths which were typically 10 µm in dimension, but could achieve sizes of up to 30 µm.

Pellite – ACID - LHH

Pellite – ALKALI - LHH

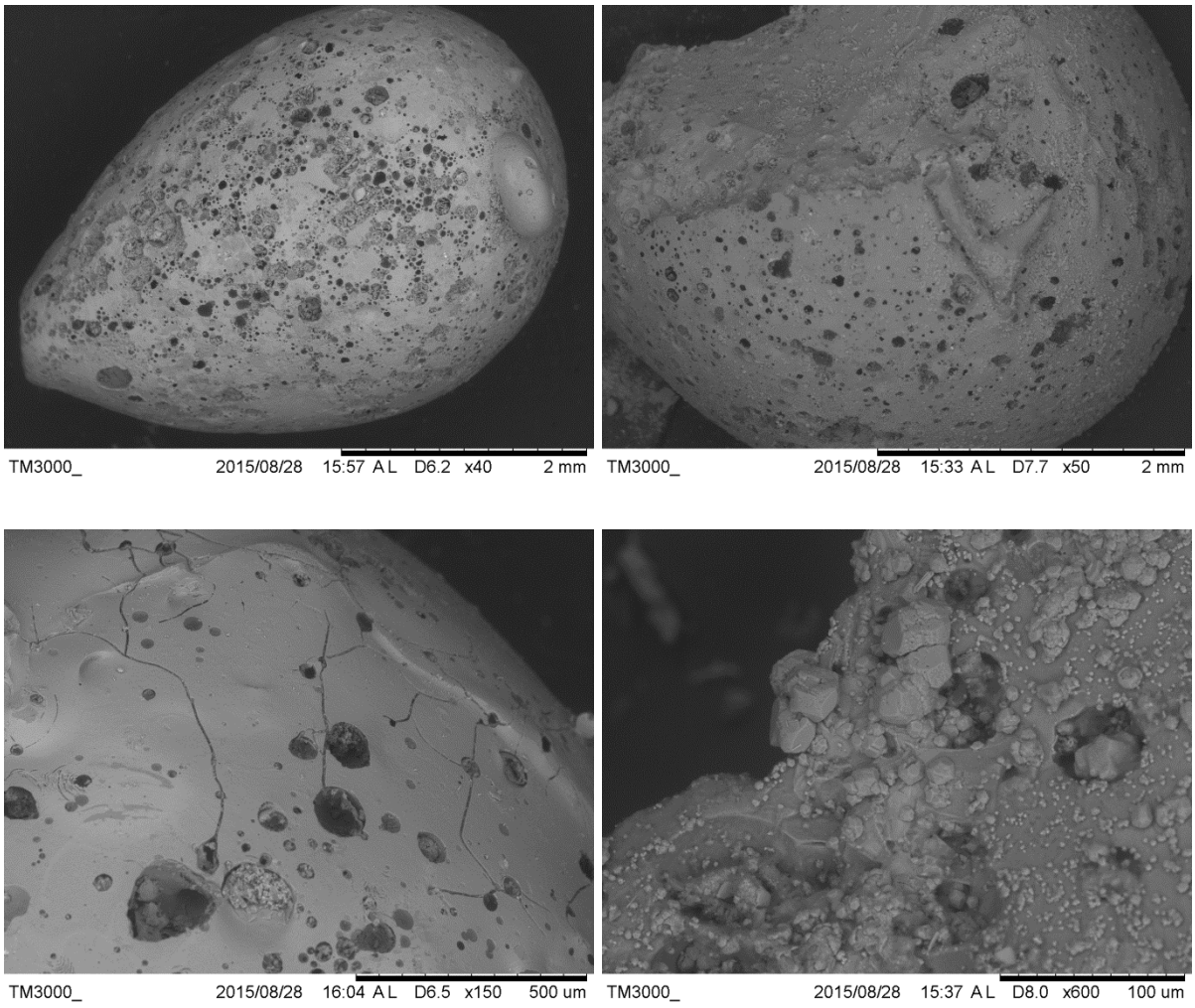

Figure 7.21: Backscatter SEM images of Pellite pre-treated with acid or alkali solution and reacted under 10 bar CO_2 pressure at 125˚C

High Pressure - Low Temperature (100 bar / 25°C)

Experiments carried out at high pressure (100 bar) and low temperature (25˚C) generated different surface textures and coverage depending upon the pre-treatment chemical (Fig. 7.22).

Acid treated Pellite displayed sparse, surface coverage of carbonate materials. The carbonate which had grown displayed a rhombic form up to 40 µm in width.

Alkali treated samples displayed widespread, yet patchy, carbonate coverage. The carbonate minerals present were either in the form of needles of up to 25 µm long and 5 µm wide or were rhombic in form and were approximately 40 µm in dimension.

Pellite – ACID - HLH

Pellite – ALKALI - HLH

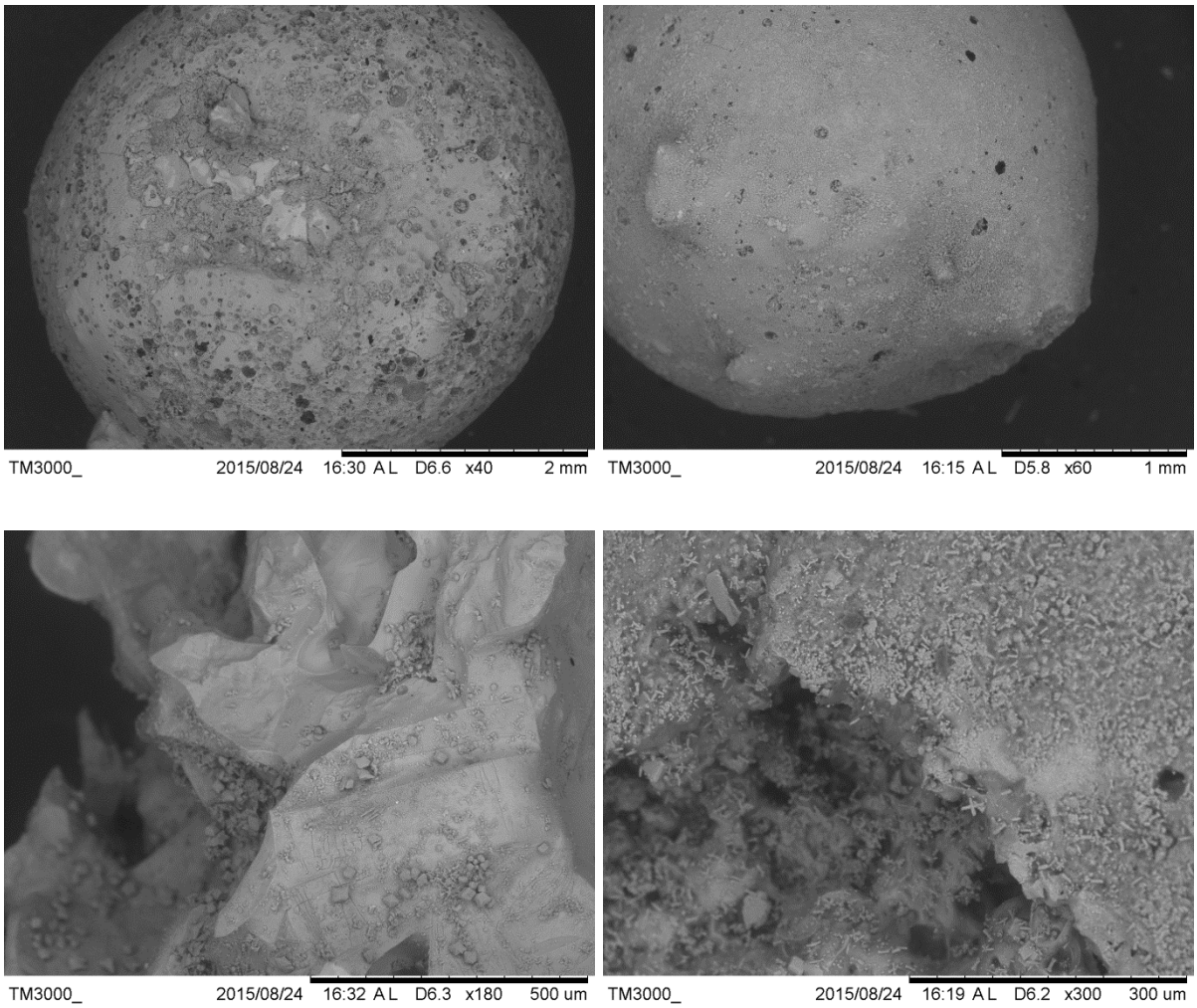

Figure 7.22: Backscatter SEM images of Pellite pre-treated with acid or alkali solution and reacted under 100 bar CO_2 pressure at 25˚C

High Pressure - High Temperature (100 bar / 125°C)

Experiments carried out at high pressure (100 bar) and high temperature (125˚C) generated different surface textures and coverage depending upon the pre-treatment chemical (Fig. 7.23).

Acid treated samples displayed sparse surface coverage of carbonate minerals with three different morphologies being present: crystals which showed a monoclinic form (but with very poorly defined crystal faces) up to 100 µm long and 50 µm; crystals which displayed a bladed form either as thin blades (60 µm long and <10 µm wide) or as sharp prism-ended forms 32 µm wide and 60 µm in height.

Alkali treated samples displayed a widespread coverage of carbonate minerals either as rectangular forms 30 µm long and 10 µm wide or as nodular' carbonate growths typically 20 µm in dimension.

Pellite – ACID - HHH

Pellite – ALKALI - HHH

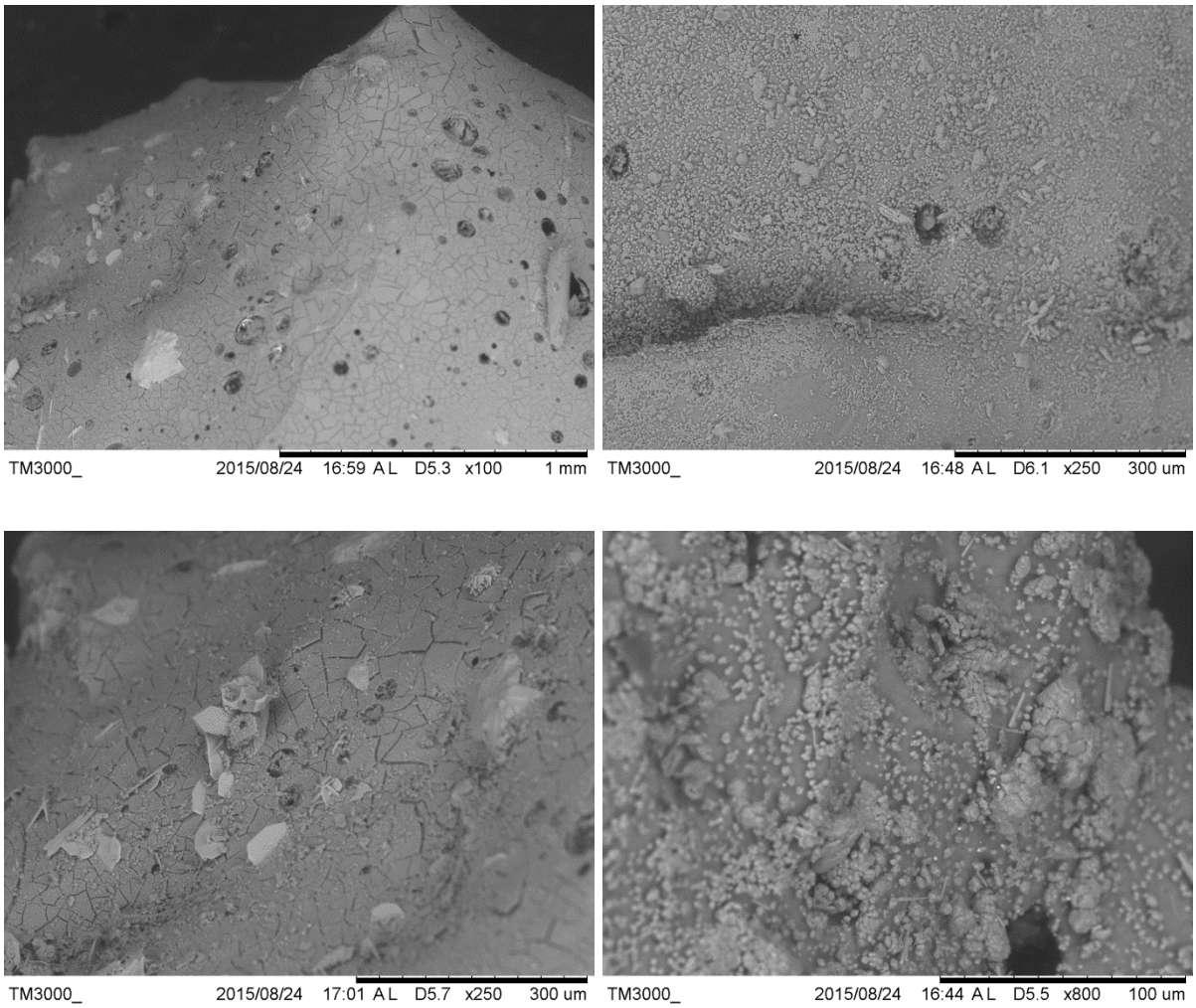

Figure 7.23: Backscatter SEM images of Pellite pre-treated with acid or alkali solution and reacted under 100 bar CO_2 pressure at 125˚C.

GBFS

Low Pressure - Low Temperature (10 bar / 25˚C)

Experiments carried out at low pressure (10 bar) and low temperature (25˚C) generated no observable carbonate minerals. Both acid and alkali treated GBFS samples displayed surface textures with no discernible difference when compared to the original unreacted material (Fig. 7.24).

GBFS – ACID - LLH

GBFS – ALKALI - LLH

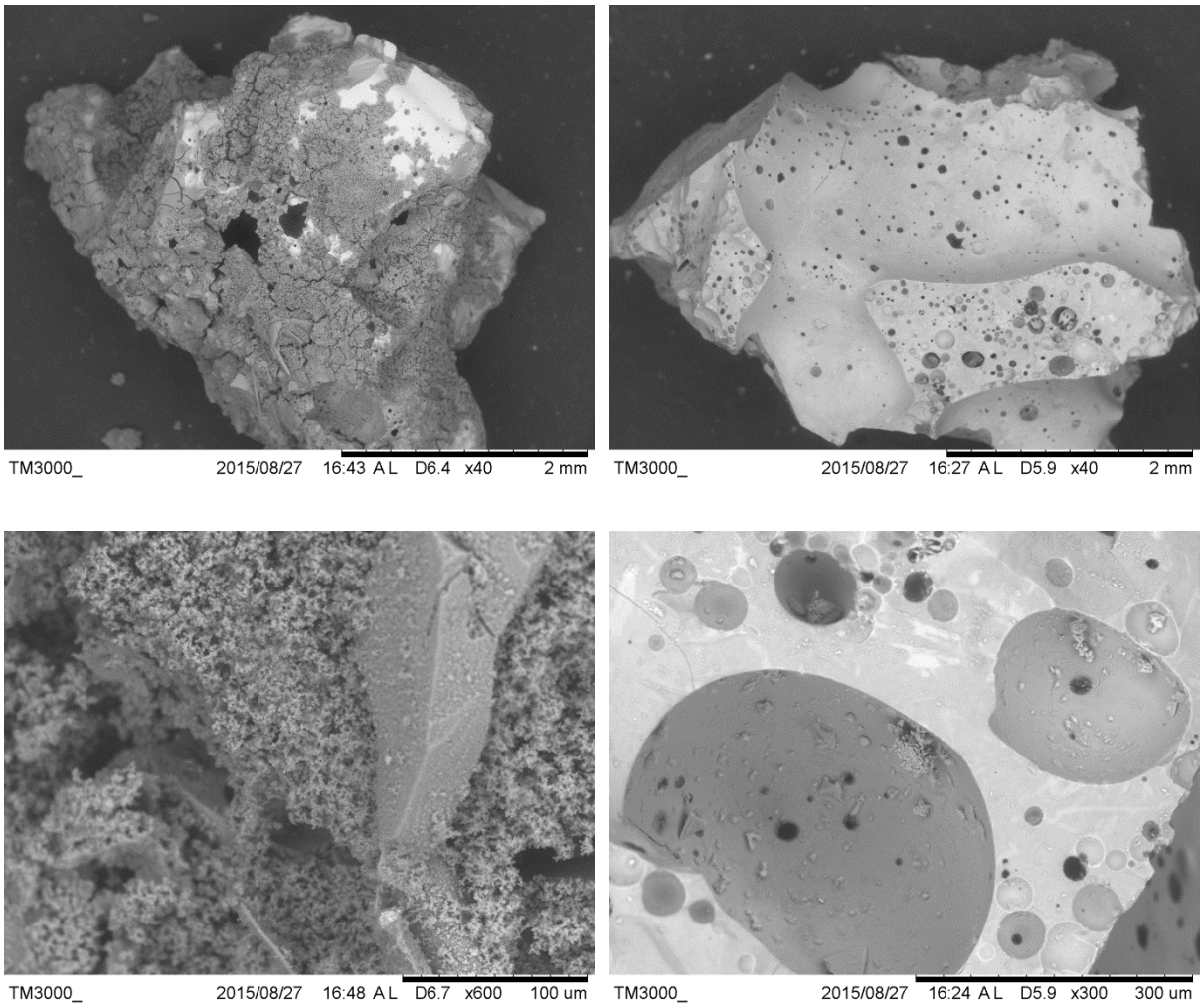

Figure 7.24: Backscatter SEM images of GBFS pre-treated with acid or alkali solution and reacted under 10 bar CO_2 pressure at 25˚C.

Low Pressure - High Temperature (10 bar / 125°C)

Experiments carried out at low pressure (10 bar) and high temperature (125˚C) generated different surface textures and coverage depending upon the pre-treatment chemical (Fig. 7.25).

Acid treated GBFS samples displayed no discernible difference when compared to unreacted acid-treated material and there appeared to be no growth of carbonate minerals upon the sample surface.

Alkali treated GBFS samples displayed patches of carbonate minerals which showed a 'nodular' morphology and were typically 20 µm in dimension, but could achieve up to 50 µm in size.

GBFS – ACID - LHH

GBFS – ALKALI - LHH

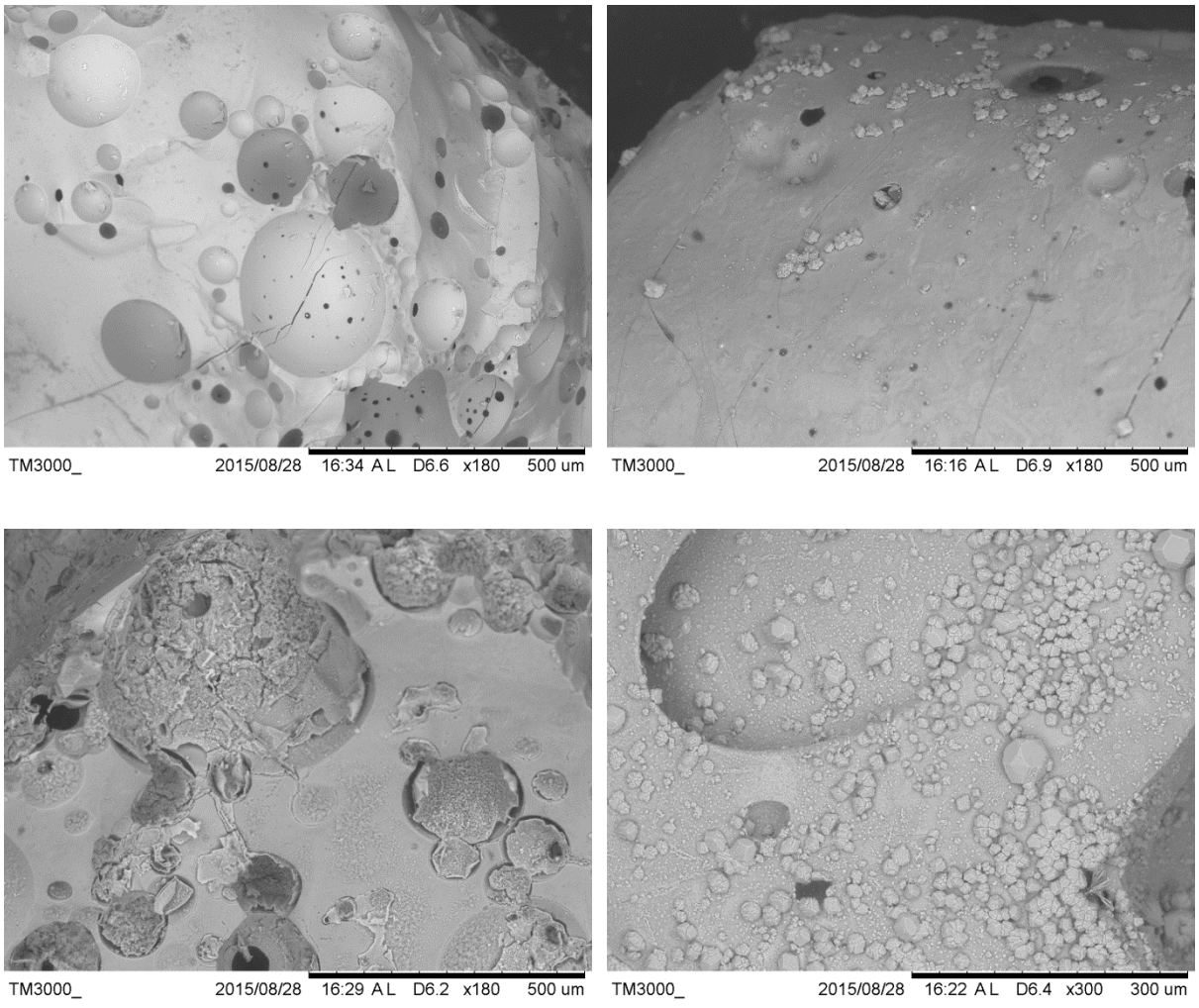

Figure 7.25: Backscatter SEM images of GBFS pre-treated with acid or alkali solution and reacted under 10 bar CO_2 pressure at 125˚C.

High Pressure - Low Temperature (100 bar / 25°C)

Experiments carried out at high pressure (100 bar) and low temperature (25˚C) generated different surface textures and coverage depending upon the pre-treatment chemical (Fig. 7.26).

Acid treated samples displayed a sparse surface coverage of carbonate minerals. Those that had formed, had grown as flat 'plates' approximately 20 µm in diameter and <5 µm in thickness.

Alkali treated samples displayed a poor surface coverage of pseudo-cubic carbonate minerals <10 µm in dimension.

GBFS – ACID - HLH

GBFS – ALKALI - HLH

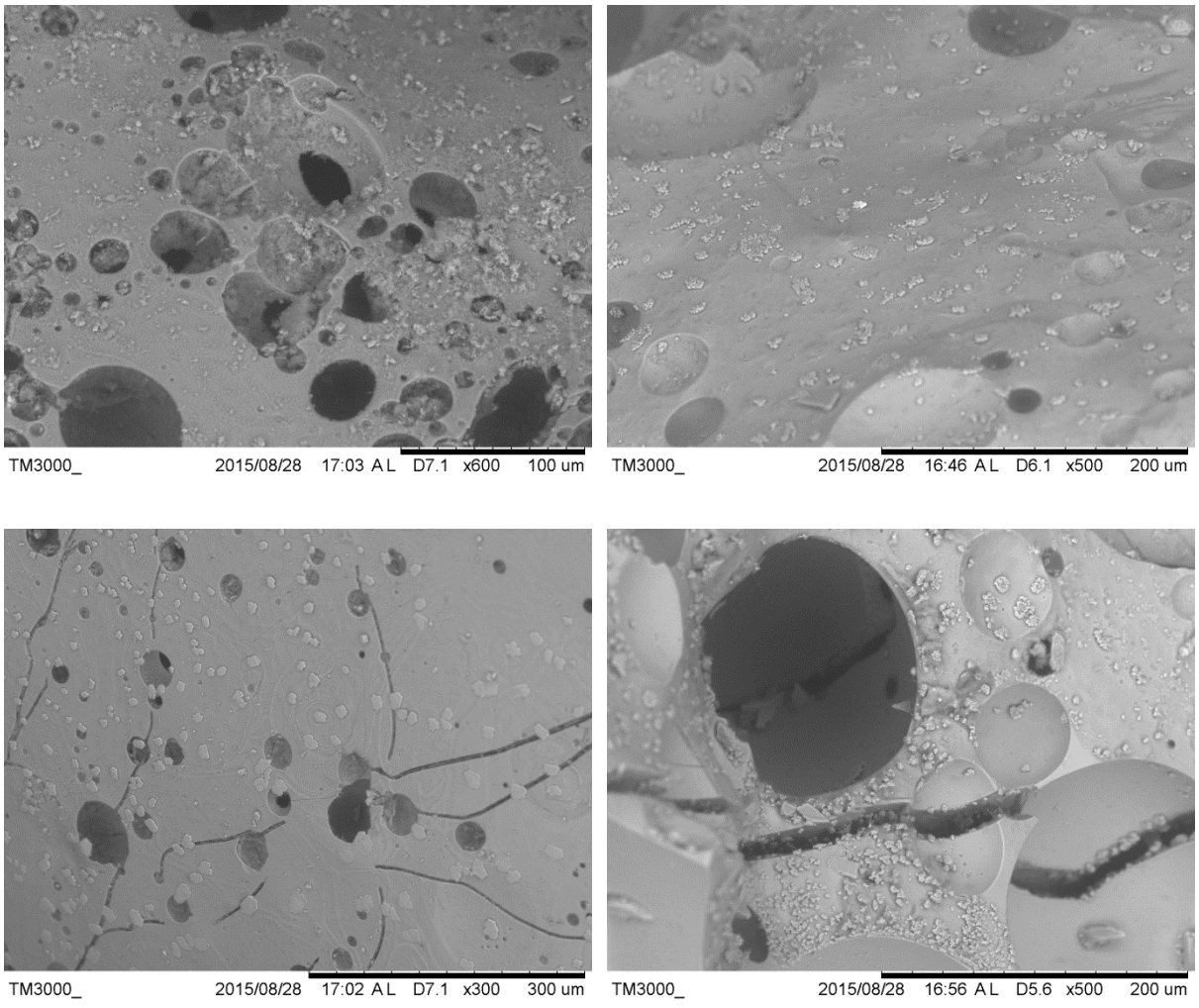

Figure 7.26: Backscatter SEM images of GBFS pre-treated with acid or alkali solution and reacted under 100 bar CO_2 pressure at 25˚C.

High Pressure - High Temperature (100 bar / 125°C)

Experiments carried out at high pressure (100 bar) and high temperature (125˚C) generated different surface textures and coverage depending upon the pre-treatment chemical (Fig. 7.27). Acid treated samples displayed no discernible difference when compared to unreacted acid-treated material and there appeared to be no distinct growth of carbonate minerals. Alkali treated samples displayed a poor surface coverage of monoclinic rhombs with well-defined crystal faces. These crystals were typically 20 µm long and 5 µm wide, but crystals up to 70 µm long and 35 µm wide were also seen.

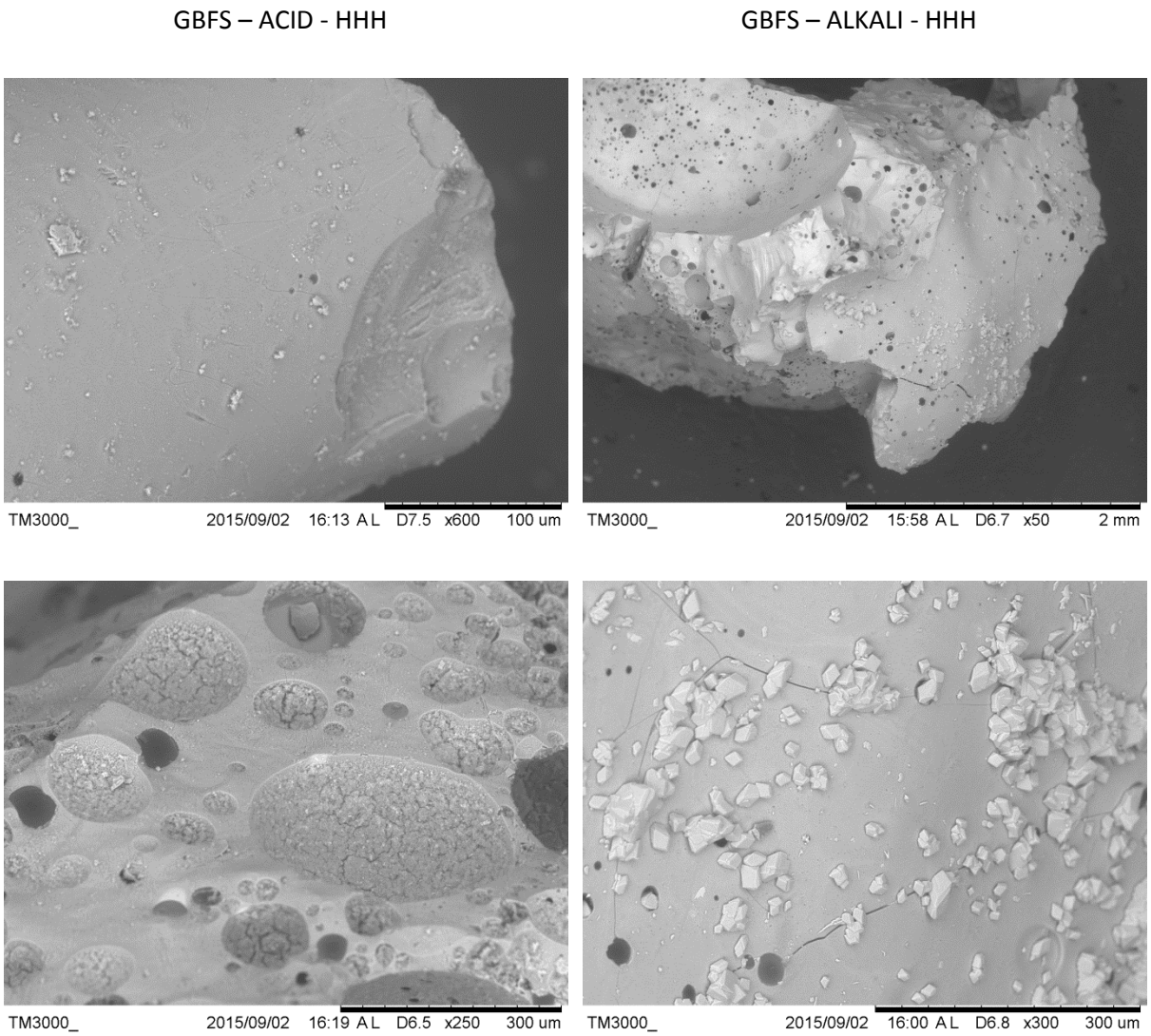

Figure 7.27: Backscatter SEM images of GBFS pre-treated with acid or alkali solution and reacted under 100 bar CO_2 pressure at 125˚C.

7.4 Interpretation

7.4.1 Steel Slags

The carbonation values achieved by untreated and treated samples of 6 mm steel slag aggregate are shown in Fig. 7.28.

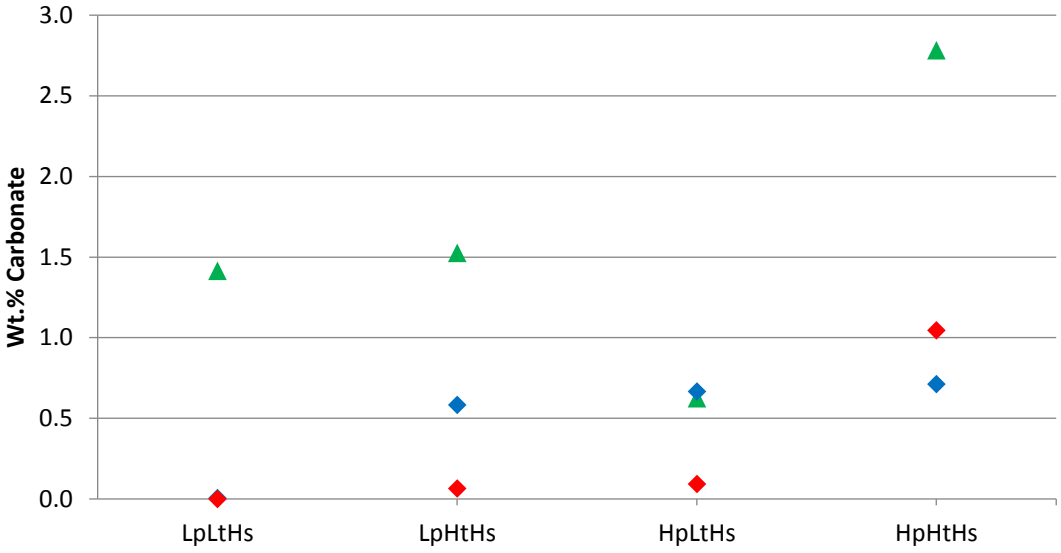

Figure 7.28: Graph showing the carbonation values achieved by treated and untreated samples of 6 mm steel slag aggregate. Green Triangles – Untreated aggregate [Chapter 5], Blue Diamonds – Aggregate treated with NaOH, Red Diamonds - Aggregate treated with HCl.

The acid treated samples showed very low degrees of carbonation, before achieving higher carbonation values (but still less than the untreated samples). The behavioural pattern was similar to that of untreated samples, albeit of a lower magnitude. The alkali treated samples displayed similar, but a lower magnitude pattern of carbonation values when compared to the untreated samples.

Given that the XRD analysis showed that there had been little to no change in the overall mineralogy of the samples as a result of treating them with either acid or alkali solutions, then any changes which did occur must have been too fine grained to detect. Evidence for the conditions within the reaction fluid can be derived from the petrological textures of the carbonate growths on the surface of the slag. The acid treated samples displayed carbonate morphologies which showed restricted nucleation sites and coarse growth textures. This suggested that it was difficult for crystals to grow in the hydrothermal environment present. When this was compared to the 'forests' of crystals grown upon the untreated samples, the retardation of crystal growth in the treated samples was particularly

noticeable. The only variable between the two experiments was the addition of the 1M HCl. Therefore, the reaction in HCl must have produced chloride bearing minerals which did not carbonate.

The alkaline treated samples displayed carbonate morphologies which were similar to those produced by untreated samples. This would indicate that the growth processes within the reaction fluid were similar, if not the same, to those within the reaction fluid surrounding the untreated samples. However, despite having similar morphologies and grain coverage, the carbonation values were still lower or similar to those produced by the untreated samples. The possible explanation is that the carbonation which took place on the surface of the grains occurred far more rapidly, reducing the surface area of the slag available for dissolution and, therefore, limiting the reaction due to a lessening supply of metal cations. This could have occurred as a result of the alkali treatment forming a thin layer of hydroxide which would readily react with the carbonate ions. This would, in turn. explain why the acid treated samples (which displayed retarded crystal nucleation textures) could achieve a higher degree of carbonation at HpHt conditions, as the acid treated samples retained a surface area from which dissolution could occu.r whereas the alkali treated samples did not.

7.4.2 Pellite

The carbonation values achieved by untreated and treated samples of Pellite are shown in Fig. 7.29.

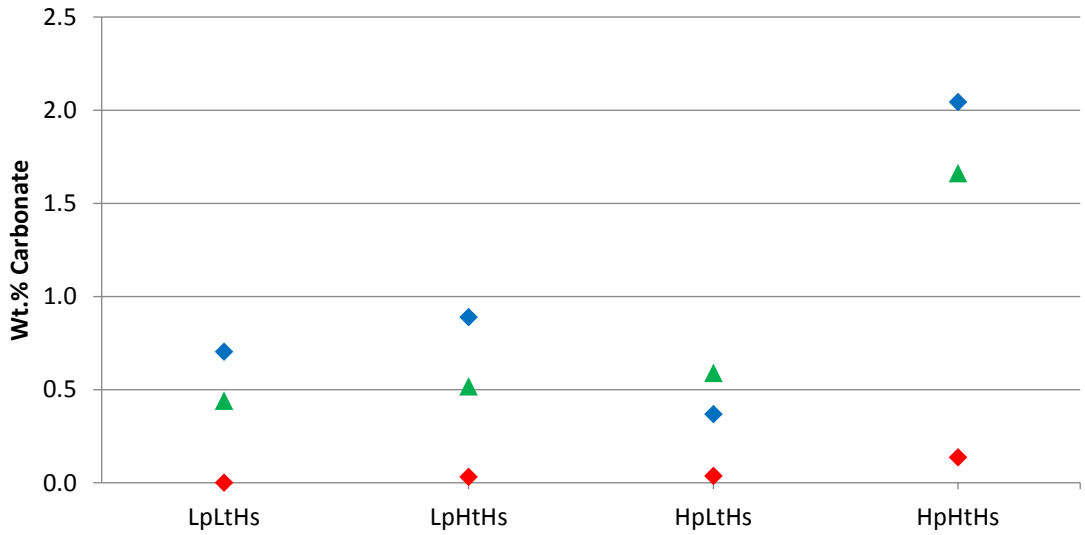

Figure 7.29: Graph showing the carbonation values achieved by treated and untreated samples of Pellite. Green Triangles – Untreated Pellite [Chapter 5], Blue Diamonds – Pellite treated with NaOH, Red Diamonds - Pellite treated with HCl.

The behaviour of the treated samples showed a similar behaviour to that displayed by the untreated samples. The acid treated samples followed the same carbonation trend, but of a lower magnitude, as the untreated samples. The alkali treated samples displayed a close match in carbonation trend to that of the untreated samples.

The XRD analysis of the acid treated samples showed that the samples had lost their crystalline phase, which may have been a factor in reducing the number of crystal-nucleation sites available on the material on which the carbonate minerals could form. The SEM images showed a lack of carbonate crystals on the grains as a whole, and those crystals which were present were of a smaller size to those precipitated upon the untreated grains. Again the formation of chloride bearing minerals, which did not carbonate could have played a part in retarding the growth of carbonate crystals within the reaction fluid. However, the lack of crystal nucleation sites may also have been a factor resulting in reduced carbonation values.

The XRD analysis of the alkali treated samples showed that there was little to no change in the mineralogy of the samples, which displayed higher carbonation values than the untreated samples. When compared to the carbonate textures on the reacted, untreated-samples there were few similarities between the two datasets despite the similar wt. % carbonate values. This suggests that there may have been a difference in the growth processes which occurred on the surface of the grains. These having been altered in some way resulting in the 'nodular' form of carbonate as opposed to the flatter forms.

The possible explanation is that the 1M NaOH solution had produced a layer of soluble hydroxides which rapidly dissolved under the acidic conditions into the reaction fluid beneath which the fresh Pellite material dissolved at a slower rate. This would result in a rapid saturation of the solution by metal ions and lead to rapid growth of carbonate crystals at nucleation sites on the surface of the grains. This would promote crystal forms which grew out into the reaction fluid instead of the component starved crystals which grew laterally across the surface. This rapid growth resulted in a less even carbonate mineralisation which allowed the dissolution of the Pellite surface into the reaction fluid for longer.

7.4.3 GBFS

The carbonation values achieved by untreated and treated samples of GBFS are shown in Fig. 7.30.

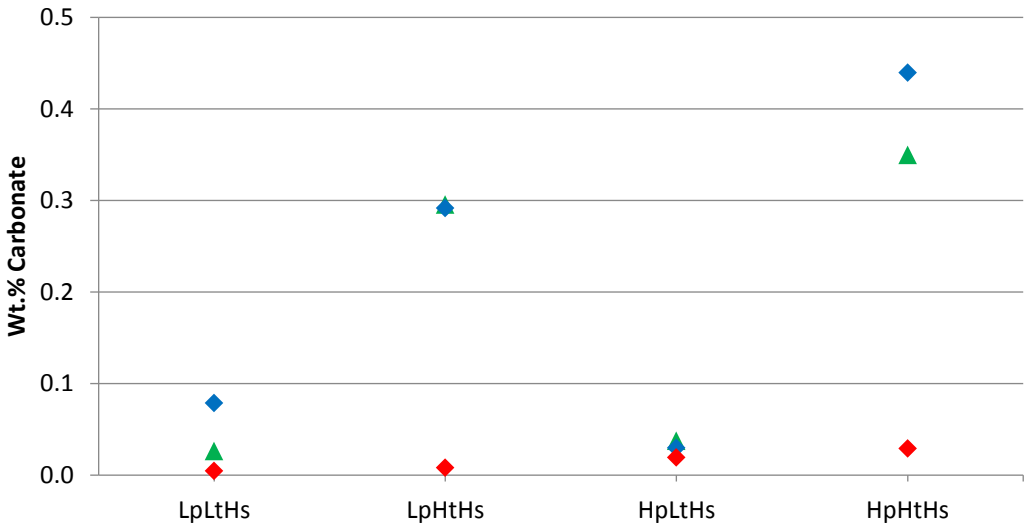

Figure 7.30: Graph showing the carbonation values achieved by treated and untreated samples of GBFS. Green Triangles – Untreated GBFS [Chapter 5], Blue Diamonds – GBFS treated with NaOH, Red Diamonds - GBFS treated with HCl.

The acid treated samples followed a trend of increasing carbonation with increasing pressure and temperature reaction conditions. However, the results for acid treated samples were up to two orders-of-magnitude lower than the results for the reacted alkali-treated or untreated samples. The alkali treated samples also displayed a similar carbonation trend to that of the untreated samples, while displaying higher or equal carbonation values than them.

The XRD analysis of the acid treated samples showed that the samples had lost their crystalline phase. This may be a factor in reducing the number of crystal-nucleation sites available on the material on which the carbonate minerals could form. The SEM images showed a lack of carbonate crystals on the grains. Again the formation of chloride bearing minerals may have played a part in retarding the growth of carbonate crystals within the reaction fluid. The fact that GBFS is a borderline inert material may have also played a part in the low carbonation values.

The XRD analysis of the alkali treated samples showed little change in the mineralogy of the samples. When the carbonate textures on the reacted untreated-GBFS samples were compared to the reacted alkali-treated samples there were few similarities between the two datasets despite alkali-treated samples displaying similar or higher wt. % carbonate values. This suggests that there may be a difference in the growth processes occurring upon the surface of the grains or the grains have been

altered in some way resulting in the growth of 'nodular' and 'granular' forms of carbonate rather than the rhombic forms. A similar process to that which was proposed to have occurred in the Pellite samples is also envisaged for the GBFS samples. Compared to the untreated samples, treatment with 1M NaOH produced larger carbonate crystals and more nucleation sites. The possible explanation for this was that the hydroxide layer rapidly reacts away under carbonated (acidic) conditions revealing areas upon which nucleation can occur. The alkaline conditions produced also promoted carbonate production leading to greater overall carbonation values. The face-raised-cube-shaped minerals which formed on the surface of the alkali-treated GBFS (Fig. 7.9) appeared not to have influenced the formation of carbonate. Though they may have provided some nucleation points, they were not observed on most of the mineral surfaces post-batch-reaction suggesting that they had dissolved into the reaction fluid.

Despite differences in physical morphology and mineralogy the different slag products displayed the same overall behaviour depending upon the pre-treatment chemical used. When samples were treated with HCl any available metal-oxides or metal-hydroxides reacted to form metal chlorides which would not carbonate (right-hand pathway in Fig. 7.31). This observation explained the lack of nucleation points on the surfaces of the slag grains and the lack of carbonate production overall. Although under certain conditions (such as high pressure, high temperature conditions for 6 mm steel slag aggregate) carbonate will form, it takes the higher magnitude conditions to enable this to occur. When samples were treated with NaOH any available metal ions reacted to form hydroxide minerals, which would readily carbonate (i.e. $Ca(OH)_2$ – Chapter 5.4.3) (left-hand pathway in Fig. 7.31). This explains how equal or greater degrees of carbonate can be formed on the slag grain surfaces, unless the reaction progresses rapidly enough to coat the surface of the grains with insoluble material (i.e. carbonate) and thereby limit the extent of material dissolution and thus terminating the carbonation reaction.

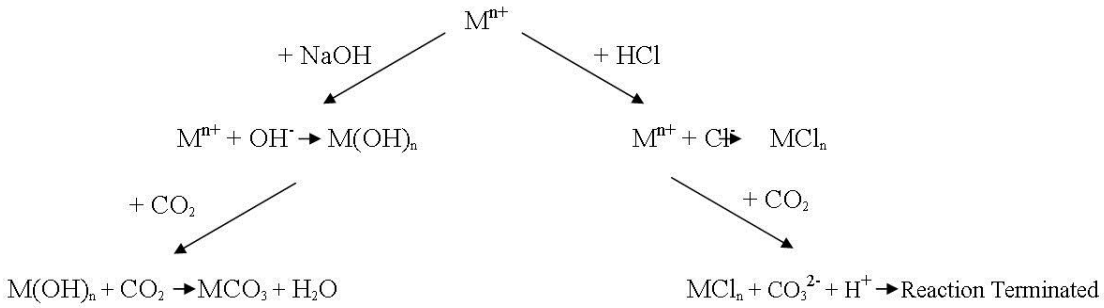

Figure 7.31: Reaction pathways for metal ions showing the products for slag treatment with HCl followed by reaction with CO_2 (right-hand pathway) and the products for slag treatment with NaOH followed by reaction with CO_2 (left-hand pathway)

7.5 Conclusions

In this study different slag products were reacted with 1M HCl or 1M NaOH and any resultant changes to the material were characterised using XRD, TGA and backscatter SEM analysis.

The chemically pre-treated slag products were actively reacted with enhanced CO_2 pressures and temperatures under excess water conditions. A comparison was made with the carbonation values achieved by un-treated samples (Chapter 5). It was hypothesised that this method should increase the carbonation observed due to reactions with the mineral phases comprising the slag allowing M^{n+} ions to be released into the reaction fluid. In the case of acid treated samples metal-chloride phases were produced resulting in lower carbonation than before. For alkali treated samples metal-hydroxide phases were formed, which then carbonated to higher carbonation values. This is summarised in Table 7.4.

	6 mm Aggregate	Pellite	GBFS
Acid	Lower	Lower	Lower
Alkali	Lower	Higher	Equal /Higher

Table 7.4: Table showing if the carbonation value for each slag product has increased or decreased due to the effects of the pre-treatment with acid / alkali solution.

This study has concluded that:

- Treating slag products with 1M HCl solution will etch the surface of the samples and result in disaggregation. Treating slag products with 1M NaOH solution will result in the formation of a layer, likely of hydroxide, on the surface of the slag material.

- Acid treatment results in fewer, but coarser crystals and may promote the lateral growth of crystals rather than growth out into the reaction fluid. Acid treatment of slag products produces lower carbonation values than those obtained for untreated material in all cases.

- Alkali treatment results in a wider surface area of a sample being covered in carbonate crystals, but these crystals are smaller than those crystals grown on acid or untreated samples. Alkali treatment also promotes the growth of crystals out into the reaction fluid. Alkali treated samples produced lower carbonation values then untreated Steel Slags, but produced results which were equal or surpassed the carbonation values of untreated Blast Furnace Slags.

Chapter 8: Economic Implications and Conclusions

8.1 Introduction

The understanding of the processes involved in the carbonation of slag products is important for the following reasons: Firstly, evaluating the extent to which iron and steel slag can act as a carbon sink could help the UK to attain its net CO_2 targets by reducing the net amount of carbon emitted by industrial Blast and Basic-Oxygen furnaces. Secondly, an understanding of how slag products carbonate will allow the carbonation process to be optimised, thus aiding the physical uptake and sequestration of CO_2 and allowing this by-product of the iron and steel making industry to be recycled more efficiently. To achieve this level of understanding, the behaviour of the materials and minerals involved in the process need to be researched in order to find the optimal conditions for carbonation.

8.2 Summary of Objectives

- In Chapter 2 the physical and chemical properties of the slag products used in this study were assessed. This then enabled the data in later chapters to be interpreted.
- In Chapter 3 a predicted chemical model of the H_2CO_3 concentrations present, in the experiments carried out in Chapters 4 and 5, was postulated, which enabled the data to be interpreted in terms of H_2CO_3 concentration. Eh-pH diagrams of the minerals, which were stable under the experimental conditions, were presented.
- Chapter 4 detailed the results of a study to measure the passive carbonation of slag products under environmental pressure and temperature conditions. New data was presented regarding the weathering characteristics of the slag products and a baseline was established against which the data from later chapters could be compared.
- Chapter 5 detailed how slag products were actively reacted with CO_2in the laboratory under varying conditions of pressure, temperature and water availability. New data, to expand the data set for the amount of carbonation achieved by different minerals and slag products under novel reaction conditions was reported.
- Chapter 6 detailed the results from a small-scale field trial of the active reaction of slag products under environmental conditions. This was conducted at a constant flow rate of CO_2 of 2 dm^3 min^{-1} and controlled water availability, in order to test the applicability of actively carbonating slag products under environmental conditions.
- Chapter 7 described the results of the active reaction of slag products which had previously been reacted with either 1M HCl or 1M NaOH.

8.3 Economic Applicability of the Results

This thesis has presented a range of data for the carbonation values displayed by different slag products under different conditions. The overall best carbonation conditions for each slag product are reported in Table 8.1.

Material	Best Technique Known	gCO_2-Seq. per tonne
20 mm	HpLtLs	8,440
6 mm	HpHtHs	27,830
DUST	Passive (H)	140,540
Pellite	HpHtHs (with Alkali)	20,430
GBFS	HpHtHs (with Alkali)	4,400

Table 8.1: Physical conditions required for optimal carbonation for each slag product. HpLtLs – 100 bar CO_2 pressure, 25°C, Low water availability, HpHtHs – 100 bar CO_2 pressure, 125°C, High water availability, Passive – outside environmental conditions.

Dust is best left to passively weather outside the laboratory. Steel-slag aggregate achieved optimal carbonation at high pressure conditions and blast furnace slag samples achieved their highest carbonations values at high pressure and temperature conditions, after first being pre-treated with an alkali solution. Although there are nuances to the data e.g. 20 mm aggregate displayed an almost equivalent carbonation at low pressure – high temperature conditions as it did under high pressure – low temperature conditions which would influence any decision made as to how or whether an industrial company would invest in new machinery or approaches to slag management. This study has shown that it is possible to enhance the carbonation achieved by most slag products.

However, there is a further layer of complexity, as each carbonation value was obtained as a result of additional CO_2 being emitted during the processing of the slag products. For passive weathering these were simply the CO_2 emissions produced as a result of the manufacturing process e.g. grinding the block steel-slag to aggregate, pelletiseation or granulation when processing blast furnace slags. For the active reaction experiments, further CO_2 emissions were generated as outlined in Chapter 5.5.5. If the slags were to be treated with chemicals then this would add extra cost and also create CO_2 emissions as a result of the manufacture the chemicals and their transportation. In which case, would the slag products become carbon positive, neutral or negative and by how much? A simple case of working out the net positive or negative CO_2 emissions from the process of grinding slag, which subsequently passively sequesters CO_2 was modelled. The model takes into account the use of different power sources necessary to grind the slags to determine the CO_2 savings.

The first step was to calculate the power required to grind 1 tonne of steel slag product using Bonds Law (Eq. 8.1) with the results given in Table 8.2:

$$Kw = m\,0.3162\,Wi\,\frac{1}{\sqrt{Dp}}$$

Kw – kilowatts (kw)

m - tonnes/hour

0.3162 - Constant

Wi – Work index of steel slag (30)

Dp – Final average size of crushed material (mm)

Equation 8.1

Material	Grain Size	kWh
20MM	20	2.121
6MM	6	3.873
DUST	2	6.708
Pellite	No Grinding Required	0
GBFS	No Grinding Required	0

Table 8.2: kWh required to grind one tonne of each slag product.

To compare the carbon emissions of different power sources which could be used to grind the slag products, the following values of gCO_2eq/kWh were used (Table 8.3):

Fuel Source	Coal	Oil	Gas	Solar	Nuclear	Wind
gCO_2eq/kWh	846	650	488	88	26	13

Table 8.3: Carbon emissions per kWh of electricity generation from a range of energy sources. Values from POSTNOTE 383 (2011).

The kWh energy required to grind each tonne of slag was multiplied by the carbon emissions generated per kWh from each energy source. This was then multiplied by the total tonnage of each slag product produced per year at Redcar. Finally, the total mean carbon sequestration achieved per year by passive weathering for each slag product was subtracted from this number. Table 8.4 shows the gCO_2 removed from the atmosphere per tonne of material, when the mean passive weathering carbonation value for the material had been achieved (i.e. how net-carbon-positive or net-carbon-negative a material is after grinding and passive weathering). While the stockpiled slag is carbon negative, when grinding is factored in some individual components are not.

Powered by	Coal	Oil	Gas	Solar	Nuclear	Wind
Material						
20 mm	**1701.7**	**1285.9**	**942.3**	**93.9**	**-37.7**	**-65.2**
6 mm	**2507.5**	**1748.5**	**1121.1**	**-427.9**	**-668.1**	**-718.4**
DUST	**-96235.8**	**-97550.4**	**-98637.1**	**-101320.1**	**-101736.0**	**-101823.2**
Pellite	**-2085.5**	**-2085.5**	**-2085.5**	**-2085.5**	**-2085.5**	**-2085.5**
GBFS	**-26.7**	**-26.7**	**-26.7**	**-26.7**	**-26.7**	**-26.7**

Table 8.4: How net carbon positive or negative in gCO_2 $tonne^{-1}$ each material is after grinding and passive weathering. Red indicates net carbon positive values, black indicates net carbon negative values.

Though Pellite and GBFS do not initially have to be ground, the CO_2 emissions from further grinding them to produce finer products would require the use of wind or nuclear energy in order to make the products carbon negative. Overall, the most economic option for the Redcar works would be to switch to electric grinding machines and to derive the power to drive these machines solely from a Redcar offshore wind farm (savings are shown in Table 8.5). If this was done, instead of using diesel driven grinding machines or deriving the power supply from the Drax coal-fired power station, an additional 667.28 tonnes of CO_2 could be saved per year at the Redcar site.

Material	20MM	6MM	DUST
gCO_2 saved $tonne^{-1}$ of slag	1766.9	3225.9	5587.4
gCO_2 per year of production	$52.1x10^6$	$285.5x10^6$	$327.9x10^6$

Table 8.5: CO_2 saved from switching from a coal-based power supply to a wind-based power supply.

8.4 Findings and Conclusions

8.4.1 Material Characterisation

Chapter 2 characterised the different slag products which were to be used in the various experiments in this study.

- Steel-slag products all displayed high CaO (37.65%) and Fe_2O_3 (32.673%) contents, with a mixed mineralogy (which included pyroxenes) potentially indicating that they could readily be carbonated and that they had a high carbonation potential.
- Aggregate steel-slags showed high hydraulic conductivities, indicating that any reaction fluids would flow through them easily. However, this property also meant that the material would dry out rapidly under certain environmental conditions restricting carbonation. Dust, however, formed a paste when wet which enabled it to retain moisture while under environmental conditions, but this property had the drawback of preventing reaction fluids from flowing through it.
- Pellite and GBFS products similarly displayed a high CaO (39.76%) content with appreciable MgO content (8.6%), but little to no Fe content. Also, Pellite and GBFS products were fine grained enough to retain water, but granular enough to allow it to pass through. The major difference between the two products was their mineralogy and physical texture.
- Pellite was dominated by pyroxenes and aluminide minerals and displayed a pumicious texture, whereas GBFS was dominated by quartz and alumno-silicates and displayed a glassy texture. These differences likely resulted in different magnitudes in carbonation.

8.4.2 Chemical Modelling

The results of the chemical modelling in Chapter 3 showed that of the active reaction conditions, 100 bar CO_2 at 25˚C produced the highest HCO_3^- concentrations at $1.43x10^{-6}$ mol dm^{-3}. The concentration of HCO_3^- ions under passive conditions was six orders of magnitude lower than this value, and four orders of magnitude lower than the lowest HCO_3^- concentration for the active conditions - 10 bar CO_2 at 125˚C being $4.14x10^{-8}$ mol dm^{-3}. The pH of the passive experiments will equilibrate at 5.61 while the active experiments will equilibrate to a pH between 2.91 and 3.68 (100 bar CO_2 at 25˚C and 10 bar CO_2 at 125˚C respectively). Geochemical Eh–pH plots showed that Ca and Mg will readily form carbonates under the conditions with Mn also showing potential to forma carbonates. Fe is more likely to form Fe-oxides rather than carbonate while any P or S in the system could form small amounts of phosphides or sulphides. However, if the lower theoretical pH's are attained then the carbonates

would not be stable though this may not happen due to the alkalinity of the slag products buffering the system to higher pH's thereby promoting carbonate precipitation.

- The modelling has shown that under passive conditions the pH will allow the precipitation of carbonates while under active conditions the pH will allow for the dissolution of metal ions into the reaction fluid and the precipitation of carbonates – predominantly Ca and Mg.

8.4.3 Carbonation via Passive Weathering

Chapter 4 measured the carbonation achieved via the natural passive weathering of the different slag products. The study showed that both the mineralogy and the grain size of the material was a major controlling factor in the carbonation rate, with carbonation values increasing with smaller grain sizes. In the case of steel-slag aggregate, carbonation rate doubled as grain size was halved. Dust produced the highest carbonation values at around 14 wt. % with all other carbonation values at least two orders of magnitude lower than this. The second highest was Pellite at 0.7 wt. %, then 6 mm aggregate (0.46 wt. %), 10 mm aggregate (0.16 wt. %), 20 mm aggregate (0.06 wt. %) with GBFS displaying the lowest carbonation values (0.02 wt. %).

Due to the high hydraulic conductivities displayed by the aggregate slags, it is possible that the carbonate formed on grains at the top of the slag heaps could be washed further down into the heap. This thereby prevented the top layer of grains from becoming sufficiently coated in carbonate to stop their weathering. If eluviation did occur, then the slag heaps were producing more carbonate than was measured on the grains in this study.

- Using the current measurements, the study showed that approximately 6,434 to 10,127 tonnes of CO_2 per year was passively being sequestered by the slag products located at the Redcar site.

8.4.4 Carbonation via Active Reaction

The experiments in Chapter 5 involved the reaction of slag products samples with CO_2 pressures and temperatures, which were higher than those found under environmental conditions. In this chapter results were reported for the carbonation of 20 mm aggregate slag – larger than any previously reported grain size in the literature. Experiments were also conducted on materials within the liquid-phase region of CO_2 - the first such reported occurrence in the literature. The highest mean material carbonation was achieved by Dust at 12.73 wt. % carbonation, followed by <250 µm Pellite Powder (4.006 wt. %), <250 µm GBFS Powder (2.839 wt.%), 6 mm aggregate (2.78 wt. %) , GBFS (1.71 wt. %), Pellite (1.66 Wt.%) while 20 mm aggregate displayed the lowest highest-mean carbonation at 0.84 wt.

% - all of the carbonation values reported here were the highest achieved by each material within this study and were all achieved at 100 bar CO_2 pressure and 125˚C.

It was noted that the variation of pressure from 10 bar CO_2 to 100 bar CO_2 pressure did not appear to have a major effect on the baseline carbonation in the experiments. However, the variation in temperature from 25°C to 125°C did appear to enhance the carbonation values of the individual materials in the study, particularly that of Dust, Wollastonite, and GBFS. Part of the effect of the enhanced temperature was to increase the growth rate of carbonate minerals upon the surface of the slag products, which in turn dictated the extent of stable mineral carbon sequestration and hence, the carbonation value for each material.

Varying the water availability to the samples, changed their rheological properties and therefore the porosity network. If the porosity network collapsed, forming a paste rather than a granular slurry, then the availability of HCO_3^- ions would be restricted within the sample volume. This was because the carbonation reaction produced 'crusts' of carbonate which blocked the supply of HCO_3^- ions to the deeper parts of the sample. So, increasing the availability of water to a material increases the carbonation value achieved only if the material displays an open network of porosity, which is determined by its rheological properties.

The mineral composition and grain size of the material used is a major factor in determining the carbonation of each material. All types of slag show an exponentially increasing trend in carbonation with decreasing grain size, but it is apparent that steel slags are more reactive than blast furnace slags (Chapter 4). When the carbonation of samples of pure Olivine, Wollastonite and $Ca(OH)_2$ was carried out, the optimum carbonation conditions were found to be at either 10 bar CO_2, 125°C, or 100 bar CO_2, 125°C, which correlated well with the conditions favoured by the slag samples.

- Across the whole range of slag material the conversion rate to carbonate was poor. When the conversion rates were compared to the %-metal-cation content of each material, conversion of 0.55% to 1.76% was achieved by steel slags and 0.3% to 4.89% for blast furnace slags. The literature currently suggests that there is a '20%' carbonation achievement 'ceiling' and it is apparent from this study that the majority of the carbonation potential of each material is not being achieved. A better understanding of the mineralogy of the samples and the carbonate mineral growth processes is likely to be the key in creating the right 'mix' of conditions to realise this untapped carbonation potential. In terms of industrial application, it is recommended that 10 bar CO_2 pressure is used as this makes optimum use of a supply of CO_2 (Chapter 5).

8.4.5 Effectiveness of the Field Trial

The results of a mock field-trial (Chapter 6) showed that the equilibrium pH of a slag-water mixture lay at pH 9-9.5 and that the addition of CO_2 rapidly reduced the pH to between pH 6- 7, producing reducing conditions within the column of material.

- The carbonation reaction within the column of material was sufficient to emit heat in measurable quantities. Therefore, temperature readings could be used to identify the progress of carbonation within a column of carbonating slag.

- The study concluded that while Dust can be carbonated in this manner, the method is inefficient (only 1.06% to 2.29% of CO_2 injected into the samples was absorbed) and in the short term less effective than allowing the material to passively weather.

8.4.6 Effects on Carbonation after Chemical Treatment

A further experimental study was carried out in Chapter 7 involving the reaction of the different slag products with either 1M HCl or 1M NaOH. The experiments used the same pressure and temperature conditions as were used in the Chapter 5 experiments. The study found that treating slag products with 1M HCl solution would etch the surface of the samples resulting in disaggregation and the growth of fewer, but coarser carbonate crystals. Prior treatment of the slag product with 1M HCl promoted the lateral growth of carbonate crystals. Treatment with 1M NaOH solution resulted in the formation of a layer of hydroxide upon the surface of the slag samples and, in turn, a wider surface area of the sample was covered in fine carbonate which grew out into the reaction fluid.

- The study concluded that acid treatment of slag products produced lower carbonation values than untreated material in all cases and that alkali treated samples produced lower carbonation values then untreated Steel Slags, but either equalled or surpassed the carbonation values for untreated Blast Furnace Slags.

8.4.7 Economic Implications

This study has shown that it is possible to make significant carbon savings by passively weathering the slag products at Redcar. Further savings could be made through the use of active reaction methods, as long as the process overall did not become carbon positive due to the use of pure CO_2 or through the use of chemical additives. This study has also shown that the current carbon savings can be enhanced through the use lower carbon energy sources for grinding, with the potential for an additional saving of 667.28 tonnes of CO_2 at Redcar via passive methods alone.

8.5 Recommendations for Further Work

As stated above the conversion rate of slag products into carbonate was poor. Comparing the %-metal-cation content of each material, conversion of 0.55% to 1.76% was achieved by steel slags and 0.3% to 4.89% by blast furnace slags. The literature suggests that there is a '20%' carbonation achievement 'ceiling' and it is apparent from this study that the majority of the carbonation potential of each material is not being achieved. Further work needs to be done to better understand the mineralogy of the samples and the carbonate mineral growth processes in order to create the optimum conditions needed to realise the untapped carbonation potential. Two further experiments could be conducted:

1. Reacting the materials under conditions which promote the growth of carbonate away from the surface of the material (as opposed to lateral growth) at a suitable rate. This would ensure that the material surface continued to react into the surrounding fluid, while sustaining an overall porosity and permeability, which allows the reactant fluids to migrate towards the centre of the material grain.

2. Flowing reaction fluid over the samples and precipitating the carbonate formed away from source of cations, thereby preserving the surface of the material for further reaction.

Bibliography

Alfredsson, H. A., Hardarson, B. S., Franzson, H., & Gislason, S. R. (2008). CO_2 sequestration in basaltic rock at the Hellisheidi site in SW Iceland: stratigraphy and chemical composition of the rocks at the injection site. Mineralogical Magazine, 72(1), 1-5.

Baciocchi, R., Costa, G., Di Bartolomeo, E., Polettini, A., & Pomi, R. (2010). Carbonation of stainless steel slag as a process for CO_2 storage and slag valorization. Waste and Biomass Valorization, 1(4), 467-477.

Baciocchi, R., Costa, G., Polettini, A., & Pomi, R. (2009). Influence of particle size on the carbonation of stainless steel slag for CO_2 storage. Energy Procedia, 1(1), 4859-4866.

Bates, L. 2015, 2013 UK Greenhouse Gas Emissions, Final Figures. A report to the Department for Energy and Climate Change. DECC - ONS. DECC, London

Bonenfant, D., Kharoune, L., Sauve, S., Hausler, R., Niquette, P., Mimeault, M., & Kharoune, M. (2008). CO_2 sequestration potential of steel slags at ambient pressure and temperature. Industrial & engineering chemistry research,47(20), 7610-7616.

Boone, M. A., Nielsen, P., De Kock, T., Boone, M. N., Quaghebeur, M., & Cnudde, V. (2013). Monitoring of stainless-steel slag carbonation using X-ray computed microtomography. Environmental science & technology, 48(1), 674-680.

Brown, M. E. (1999). Thermal Decomposition of Ionic Solids. Elsevier Science.

CCC 2016 - Meeting Carbon Budgets - 2016 Progress Report to Parliament Committee on Climate Change Presented to Parliament pursuant to Section 36(1) of the Climate Change Act 2008 June 2016

Chang, E. E., Chen, C. H., Chen, Y. H., Pan, S. Y., & Chiang, P. C. (2011). Performance evaluation for carbonation of steel-making slags in a slurry reactor. Journal of hazardous materials, 186(1), 558-564.

Chang, E. E., Pan, S. Y., Chen, Y. H., Chu, H. W., Wang, C. F., & Chiang, P. C. (2011). CO_2 sequestration by carbonation of steelmaking slags in an autoclave reactor. Journal of hazardous materials, 195, 107-114.

Doucet, F. J. (2010). Effective CO_2-specific sequestration capacity of steel slags and variability in their leaching behaviour in view of industrial mineral carbonation. Minerals Engineering, 23(3), 262-269.

Dufaud, F., Martinez, I., & Shilobreeva, S. (2009). Experimental study of Mg-rich silicates carbonation at 400 and 500°C and 1 kbar. Chemical Geology,265(1), 79-87.

Eloneva, S., Said, A., Fogelholm, C. J., & Zevenhoven, R. (2010, April). Feasibility study of a method utilizing carbon dioxide and steelmaking slags to produce precipitated calcium carbonate (PCC). In Proceedings of International Conference on Applied Energy (ICAE), Singapore, April 21e23 (pp. 169-178).

Eloneva, S., Said, A., Fogelholm, C. J., & Zevenhoven, R. (2012). Preliminary assessment of a method utilizing carbon dioxide and steelmaking slags to produce precipitated calcium carbonate. Applied Energy, 90(1), 329-334.

Fagerlund, J., Nduagu, E., Romão, I., & Zevenhoven, R. (2010). A stepwise process for carbon dioxide sequestration using magnesium silicates. Frontiers of Chemical Engineering in China, 4(2), 133-141.

Frey, F. A., & Prinz, M. (1978). Ultramafic inclusions from San Carlos, Arizona: petrologic and geochemical data bearing on their petrogenesis. Earth and Planetary Science Letters, 38(1), 129-176.

http://www.engineeringtoolbox.com/water-thermal-properties-d_162.html

Huijgen, W. J. (2007). Carbon dioxide sequestration by mineral carbonation. Wageningen, Netherlands: Wageningen Universiteit.

Huijgen, W. J., Comans, R. N., & Witkamp, G. J. (2007). Cost evaluation of CO_2 sequestration by aqueous mineral carbonation. Energy Conversion and Management, 48(7), 1923-1935.

Huijgen, W. J., Witkamp, G. J., & Comans, R. N. (2005). Mineral CO_2 sequestration by steel slag carbonation. Environmental science & technology, 39(24), 9676-9682.

Huijgen, W. J., Witkamp, G. J., & Comans, R. N. (2006). Mechanisms of aqueous wollastonite carbonation as a possible CO_2 sequestration process.Chemical Engineering Science, 61(13), 4242-4251.

Huijgen, W.J., 2007. Carbon dioxide sequestration by mineral carbonation. Feasibility of enhanced natural weathering as a CO_2 emission reduction technology Dissertation for the Doctoral Degree. Netherlands: University of Wageningen.

IPCC, 2005: IPCC Special Report on Carbon Dioxide Capture and Storage. Prepared by Working Group III of the Intergovernmental Panel on Climate Change [Metz, B., O. Davidson, H. C. de Coninck, M. Loos, and L. A. Meyer (eds.)]. Cambridge University Press, Cambridge, United Kingdom and New York, NY, USA, 442 pp.

IPCC. 2013: Summary for Policymakers. In: Climate Change 2013: The Physical Science Basis. Contribution of Working Group I to the Fifth Assessment Report of the Intergovernmental Panel on Climate Change [Stocker, T.F., D. Qin, G.-K. Plattner, M. Tignor, S.K. Allen, J. Boschung, A. Nauels, Y. Xia, V. Bex and P.M. Midgley (eds.)]. Cambridge University Press, Cambridge, United Kingdom and New York, NY, USA

John J. Carroll and Alan E. Mather, "The System Carbon Dioxide-Water and the Krichevsky-Kasarnovsky Equation," Journal of Solution Chemistry, vol. 21, pp. 607-621, 1992.

Kaszuba, J. P., Janecky, D. R., & Snow, M. G. (2003). Carbon dioxide reaction processes in a model brine aquifer at 200°C and 200 bars: implications for geologic sequestration of carbon. Applied Geochemistry, 18(7), 1065-1080.

Kaszuba, J. P., Williams, L. L., Janecky, D. R., Hollis, W. K., & Tsimpanogiannis, I. N. (2006). Immiscible CO_2-H_2O fluids in the shallow crust. Geochemistry, Geophysics, Geosystems, 7(10).

Kodama, S., Nishimoto, T., Yamamoto, N., Yogo, K., & Yamada, K. (2008). Development of a new pH-swing CO_2 mineralization process with a recyclable reaction solution. Energy, 33(5), 776-784.

Lekakh, S. N., Rawlins, C. H., Robertson, D. G. C., Richards, V. L., & Peaslee, K. D. (2008). Kinetics of aqueous leaching and carbonization of steelmaking slag. Metallurgical and Materials Transactions B, 39(1), 125-134.

Lekakh, Semen Naumovich, et al. "Investigation of a two-stage aqueous reactor design for carbon dioxide sequestration using steelmaking slag. "Metallurgical and Materials Transactions B 39.3 (2008): 484-492.

Lin, H., Fujii, T., Takisawa, R., Takahashi, T., & Hashida, T. (2008). Experimental evaluation of interactions in supercritical CO_2/water/rock minerals system under geologic CO_2 sequestration conditions. Journal of Materials Science, 43(7), 2307-2315.

Loring, J. S., Thompson, C. J., Wang, Z., Joly, A. G., Sklarew, D. S., Schaef, H. T., ... & Felmy, A. R. (2011). In situ infrared spectroscopic study of forsterite carbonation in wet supercritical CO2. Environmental science & technology, 45(14), 6204-6210.

Navarro, C., Díaz, M., & Villa-García, M. A. (2010). Physico-chemical characterization of steel slag. Study of its behavior under simulated environmental conditions. Environmental science & technology, 44(14), 5383-5388.

O'Connor, W. K., Dahlin, D. C., Nilsen, D. N., Gerdemann, S. J., Rush, G. E., Penner, L. R., ... & Turner, P. C. (2002). Continuing Studies on Direct Aqueous Mineral Carbonation of CO_2 Sequestration (No. DOE/ARC-2002-003). Albany Research Center, OR (US).

Pollok, Kilian, Christine V. Putnis, and Andrew Putnis. "Mineral replacement reactions in solid solution-aqueous solution systems: Volume changes, reactions paths and end-points using the example of model salt systems." American Journal of Science 311, no. 3 (2011): 211-236.

POSTNOTE Number 383, June 2011, Carbon Footprint of Electricity Generation,Prasad, P. S. R.

(2009). Geological sequestration of carbon dioxide in Deccan basalts: preliminary. Current science, 96(2).

Rawlins, C. H. (2008). Geological sequestration of carbon dioxide by hydrous carbonate formation in steelmaking slag.

Regnault, O., Lagneau, V., & Schneider, H. (2009). Experimental measurement of portlandite carbonation kinetics with supercritical CO_2.Chemical Geology, 265(1), 113-121.

Regnault, O., Lagneau, V., Catalette, H., & Schneider, H. (2005). Experimental study of pure mineral phases/supercritical CO2 reactivity. Implications for geological CO_2 sequestration. Comptes Rendus Géosciences, 337, 1331-1339.

Renforth, P., Washbourne, C. L., Taylder, J., & Manning, D. A. C. (2011). Silicate production and availability for mineral carbonation. Environmental science & technology, 45(6), 2035-2041.

Ringrose, P. S., Mathieson, A. S., Wright, I. W., Selama, F., Hansen, O., Bissell, R., Saoula, N., Midgley, J. (2013). The In Salah CO_2 storage project: lessons learned and knowledge transfer. Energy Procedia, 37, 6226-6236.

Rush, G. E., O'Connor, W. K., Dahlin, D. C., Penner, L. R., & Gerdemann, S. J. (2004). Laboratory tests of mafic, ultra-mafic, and sedimentary rock types for in-situ applications for carbon dioxide sequestration (No. DOE/ARC-2004-038). Albany Research Center (ARC), Albany, OR.

Said, A., Mattila, H. P., Järvinen, M., & Zevenhoven, R. (2013). Production of precipitated calcium carbonate (PCC) from steelmaking slag for fixation of CO_2. Applied Energy, 112, 765-771.

Stolaroff, J. K., Lowry, G. V., & Keith, D. W. (2005). Using CaO-and MgO-rich industrial waste streams for carbon sequestration. Energy Conversion and Management, 46(5), 687-699.

Summers, C. A., Dahlin, D. C., Rush, G. E., O'Connor, W. K., & Gerdemann, S. J. (2005). Grinding methods to enhance the reactivity of olivine. Minerals & Metallurgical Processing, 22(DOE/ARC-2005-095).

Sun, Y., Yao, M. S., Zhang, J. P., & Yang, G. (2011). Indirect CO_2 mineral sequestration by steelmaking slag with NH 4 Cl as leaching solution. Chemical Engineering Journal, 173(2), 437-445.

Tai, C. Y., Chen, W. R., & Shih, S. M. (2006). Factors affecting wollastonite carbonation under CO2 supercritical conditions. AIChE journal, 52(1), 292-299.

UK Government Policy Paper. 2010 to 2015 government policy: greenhouse gas emissions.GOV.UK - Updated 8 May 2015 (2010-2015 – Coalition Government Policy)

Warchulski, R., Gawęda, A., Kądziołka-Gaweł, M., & Szopa, K. (2015). Composition and element mobilization in pyrometallurgical slags from the Orzeł Biały smelting plant in the Bytom–Piekary Śląskie area, Poland. Mineralogical Magazine, 79(2), 459-483.

Waugh, D. (2000). Geography: an integrated approach. Nelson Thornes.

World Steel 2015 - http://www.worldsteel.org/dms/internetDocumentList/statistics-archive/production-archive/steel-archive/steel-monthly/Steel-monthly-2014/document/Steel%20monthly%202014.pdf

Wu, J. C. S., Sheen, J. D., Chen, S. Y., & Fan, Y. C. (2001). Feasibility of CO_2 fixation via artificial rock weathering. Industrial & engineering chemistry research, 40(18), 3902-3905.

Appendix 1 – Chapter 2 - XRD Results

Steel Slag

EVA-DIFFRAC selected 250 individual matches of 2000 possible matches to display. Of these results a total of 96 were present as selectable matches. The author then sorted these 96 matches to remove chemical duplicates. This left a total of 82 individual chemical matches. The author then removed those matches that did not fully match the XRD trace to leave a total of 57 matches which fitted into 8 different groups. The remaining matches are reported below in Table 2.7.

Metals	
$Mn_{2.99}Al_{9.68}$	Manganese Aluminium
$Ca_8 Al_3$	Calcium Aluminium
Fe	Iron
Metal Oxides	
$Ca_2 Mn0._{34} Fe_{1.66} O_5$	Calcium Iron Manganese Oxide
$Ca\ Fe\ O_3$	Calcium Iron Oxide
$Ca_2 Al._{138} Fe0._{62} O_5$	Calcium Manganese Iron Oxide
$Ca\ Mn_7 O_{12}$	Calcium Manganese Oxide
$Ca_{3.6} Fe_{14.4} O_{25.2}$	Calium Iron Oxide
$Mg\ Mn\ O_4$	Magnesium Manganese Oxide
Fe O	Wustite
$Mn_3 O_4$	Hausmannite
$Mn\ O_2$	Pyrolusite
Metal Alumnide Oxides	
$Al\ Fe\ O_3$	Aluminium Iron Oxide
$Ca_2 Al0._5 Mn0._5 Fe\ O_5$	Calcium Aluminium Iron Manganese Oxide
Ca_2 (Fe Al) O_5	Calcium Aluminium Iron Oxide
$Ca_2 Al_2 O_5$	Calcium Aluminium Oxide
$Ca\ Mg_2 Al_{16} O_{27}$	Calcium Magnesium Aluminium Oxide
Ca_2 (Fe0.$_8$ Mn0.$_2$ Al)O_5	Calcium Manganese Aluminium Iron Oxide
Mg (Al_2O_4)	Magnesium Aluminium Oxide
Olivine-Structure	
$Mg_{1.36}0\ Fe0._{64}0\ Si\ O_4$	Forsterite (Ferroan)
$Ca\ Fe0._4\ Si0._6\ O_{2.8}$	Calcium Iron Silicate
$Ca_2\ Si\ O_4$	Larnite
$Ca_3\ Mg(SiO_4)_2$	Merwinite

$Fe_{2.7}$ $Si0._3$ O_4	Iron Silicon Oxide
Silicates (Assorted)	
	Garnet Range of Solid Solutions
	Brownmillerite (Range of Soild Solutions)
	Srebrodolskite (Range of Solid Solutions)
Ca $Mg0._2$ Al $Fe0._6$ $Si0._2$ O_5	Calcium Magnesium Aluminium Iron Silicate
Ca_{54} Mg Al_2 Si_{16} O_90	Calcium Magnesium Aluminium Oxide Silicate
Ca_2 $Fe_{1.2}$ $Mg0._4$ $Si0._4$ O_5	Calcium Magnesium Iron Silicate
Ca_3 Si O_5	Calcium Silicate
Ca Si_2	Calcium Silicide
H $Al(SiO_4)$	Hydrogen Aluminium Silicate
Fe_3 Al_2 Si_3	Iron Aluminium Silicide
Ca Mn Si_2 O_6	Johannsenite
Mg_{14} Si_5 O_{24}	Magnesium Silicon Oxide
Mn_5SiC	Manganese Silicon Carbide
$Ca0._{96}$ $Mg0.0_1$ $Mn0._{56}$ $Fe_{2.43}$ $Al0.0_1$ $(Si_2O_7)O(OH)$	Manganilvaite
Ca_5 $(SiO_4)_2$ (CO_3)	Spurrite
Ca_{18} $Ca(Fe0._{84}$ $Al0._{16})$ $(Al_{7.4}0$ $Fe0._60)$ Al_4 $(SiO_4)_10$ $(Si_2O_7)_4$ $(OH)_2$ $((OH)_{6.44}$ $O_{1.56})$	Vesuvianite
Phosphides	
Fe_3 (PO_4) O_3	Grattarolaite
Fe_2 O (PO_4) aplpha-Fe_2O (PO_4)	Iron Oxide Phosphate
FeP_2	Iron Phosphide
Mg P_4	Magnesium Phosphide
Al PO_4 . $_2H_2O$	Variscite
Hydroxides	
$Ca(OH)_2$	Portlandite
Ca $_{12}$ $Al_{13.86}$ $Fe0._{14}$ O_{32} $(OH)_2$	Mayenite
Mg_6 $Al_2(OH)_{18}$. 2H2O	Meixnerite
Carbonates	
$CaCO_3$	Calcite
$(Mg0.0_3$ $Ca0._{97})(CO_3)$	Calcite, Magnesium
Fe CO_3	Siderite
$Ca_{0.845}$ $Mg_{0.155}$ (CO_3)	Dolomite

Pellite

EVA-DIFFRAC selected 156 individual matches of 1310 possible matches to display. Of these results a total of 96 were present as selectable matches. The author then sorted these 96 matches to remove chemical duplicates. This left a total of 43 individual chemical matches. The author then removed those matches that did not fully match the XRD trace to leave a total of 26 matches. The remaining matches are reported below in Table 2.8.

Metals	
Mg	Magnesium
Ca	Calcium
Al_2O_3	Corundum
Oxides	
Al_2O_3 6-Al_2O_3	Aluminum Oxide
Basic Silicates	
Ca Si	Calcium Silicon
Ca Si_2	calcium silicide $_1$ Calcium Silicon
Mg Si_3	Clinoenstatite syn
Mg (Si_3)	Clinopyroxene low
Ca $Si_{2\ 5}$	Calcium Silicate
Ca Mg (Si_3)$_2$	Diopside
$Ca_{0.2}$ $Mg_{0.8}$ Si_3	Clinoferrosilite calcian syn
Ca Mg $A_{10.5}$ $Si_{1.56}$	Pyroxene group
Mg Ca Si_4	Monticellite
Ca_3 Mg (Si_4)$_2$	Merwinite
Alumnides	
Ca $_{13}$ Al_{14}	Calcium Aluminium
Ca Mg $Al_{14\ 23}$	Calcium Magnesium Aluminium Oxide
$Mg0.4$ $Al_{2.4\ 4}$	Magnesium Aluminium Oxide
Mg Al_2	Magnesium Aluminium
Al_3 Mg_2	Aluminium Magnesium
$Mg0.36$ $Al_{2.44\ 4}$	Crawfordite
Feldspar-Affinity	
Ca_8 A_{16} Mg $Si_{5\ 28}$	Melilite
Ca_2 Al_2 Si_7	Gehlenite syn
2 Ca O • $Al_{2\ 3}$ • $Si_{\ 2}$	Gehlenite

Ca_2 ($Mg_{0.25}$ $A_{10.75}$) ($Si_{1.25}$ $A_{10.75\ 7}$)	Gehlenite magnesian syn
$Mg_{3.5}$ Al_9 Sil $0._5$ 20	Sapphirine-2M
Mg Al Si	Magnesium Aluminum Silicide

Granulated Blast Furnace Slag

EVA-DIFFRAC selected 144 individual matches of 1254 possible matches to display. Of these results a total of 63 were present as selectable matches. The author then sorted these 63 matches to remove chemical duplicates. This left a total of 27 individual chemical matches. The author then removed those matches that did not fully match the XRD trace to leave a total of 10 matches. The remaining matches are reported below in table 2.9.

Oxides	
$Al_{2\ 3}$	Aluminum Oxide
SiO_2	Quartz
Silicates	
$Al_{\ 2}$ ($Si\ O_4$) O	Silimanite
Mg (Si_3)	Clinopyroxene
Ca_3 Mg (Si_4)$_2$	Merwinite
Mg_2 Si_4	magnesium skate- model $_{111}$ model III syn I Magnesium Skate
Si	Silicon
Hydroxides	
$_{1196}$ $Al_2(OH)_{18}$ • 4 H_2O	Meixnerite
Mg_4 $Sib_{\ 15}$ $(O_{11})_2$ • 6 H_2O	Sepiolite
Mg_5 (O H)$_2$ (Si_4)$_2$	Hydroxykhondrodite

Table 2.9: XRD-identified minerals from a sample of fresh GBFS

The main metals and minerals present are metal oxides, Al- Mg- Ca-pyroxenes, and hydroxide minerals.

Appendix 2 – Chapter 3 – Passive Weathering Results

Sample Taken On		Fresh		Sample 1		Sample 2		Sample 3	
Name	Type	Start Day	Wt%	Days	Wt%	Days	Wt%	Days	Wt%
February/March 2013	*6mm Steel Slag*	**184**	0.160	191	0.096	198	0.011	205	0.370
March/April 2013	*6mm Steel Slag*	**183**	0.008	190	0.030	197	0.004	204	0.212
April/May 2013	*6mm Steel Slag*	**123**	0.055	130	0.112	137	0.082	144	0.050
May 2013	*6mm Steel Slag*	**123**	0.000	130	0.032	137	0.000	144	0.221
June 2013	*6mm Steel Slag*	**96**	0.027	103	0.017	110	0.000	117	0.033
June/July 2013	*6mm Steel Slag*	**92**	0.075	99	0.082	106	0.114	113	0.112
July 2013	*6mm Steel Slag*	**61**	0.026	68	0.000	75	0.035	82	0.086
September 2013	*6mm Steel Slag*	**0**	0.000	7	0.000	14	0.000	21	0.057
April 2013 [Bag A]	*10mm Steel Slag*	**168**	0.006	175	0.022	182	0.070	189	0.022
April 2013 [Bag B]	*10mm Steel Slag*	**168**	0.045	175	0.039	182	0.048	189	0.106
May 2013	*10mm Steel Slag*	**137**	0.000	144	0.000	151	0.013	158	0.076
June 2013	*10mm Steel Slag*	**96**	0.000	103	0.053	110	0.024	117	0.150
July 2013	*10mm Steel Slag*	**61**	0.000	68	0.000	75	0.000	82	0.000
August 2013 [Bag A]	*10mm Steel Slag*	**45**	0.000	52	0.000	59	0.000	66	0.006
August 2013 [Bag B]	*10mm Steel Slag*	**45**	0.000	52	0.000	59	0.000	66	0.000
June 2013	*20mm Steel Slag*	**96**	0.000	103	0.000	110	0.014	117	0.060
Dust	*Steel Slag*	**0**	3.352482	7	9.711098	14	9.65969	21	12.7393
Pellite	*Iron Slag*	**0**	0.047762	7	0.03613	14	0.696404	21	0.28831
GBFS	*Iron Slag*	**0**	0.000	7	0.000	14	0.000	21	0.000

Sample 4		Sample 5		Sample 6		Sample 7		Sample 8	
Days	Wt%	Days	Wt%	Days	Wt%	Days	Wt%	Days	Wt%
212	0.298	209	0.002	223	0.019	230	0.052	237	0.129
211	0.105	208	0.005	222	0.000	229	0.013	236	0.124
151	0.181	148	0.044	162	0.038	169	0.005	176	0.46
151	0.205	148	0.000	162	0.033	169	0.080	176	0.308
124	0.014	121	0.000	135	0.005	142	0.019	149	0.000
120	0.282	117	0.058	131	*0.000*	138	0.137	145	0.246
89	0.039	86	0.076	100	0.139	107	0.067	114	0.076
28	0.081	25	0.001	39	0.000	46	0.028	53	0.059
196	0.068	193	0.000	207	0.000	214	0.000	221	0.000
196	0.047	193	0.058	207	0.144	214	0.000	221	0.000
165	0.064	162	0.113	176	0.015	183	0.000	190	0.037
124	0.159	121	0.000	135	0.000	142	0.000	149	0.000
89	0.059	86	0.000	100	0.000	107	0.074	114	0.006
73	0.055	70	0.023	84	0.000	91	0.000	98	0.023
73	0.000	70	0.000	84	0.000	91	0.000	98	0.000
124	0.000	121	0.000	135	0.000	142	0.000	149	0.000
25	14.0542	28	11.57088	39	14.0542	46	7.20368	53	9.373814
25	0.102136	28	0.240352	39	0.142244	46	0.171242	53	0.152348
25	0.000	28	0.000	39	0.000	46	0.000	53	0.000